Quarterly Publication

ISSN 3572 - 2383

Global Journal of Environmental Science and Management

Volume 8, Number 4, Autumn 2022

Global Journal of Environmental Science and Management (GJESM)

(QUARTERLY PUBLICATION)

OPEN ACCESS

Publication authorization is certified by the Ministry of Culture and Islamic Guidance; No. 93/3629; 14 May 2014
Scientific-Research grade is accredited by the Ministry of Science, Research and Technology; No. 3/18/59975; 20 June 2015

Circulation: 500

***p*ISSN 2383 - 3572** ***e*ISSN 2383 - 3866**

Aims and Scope

Global Journal of Environmental Science and Management (GJESM) is an international scholarly refereed research journal which aims to promote the theory and practice of environmental science and management. A broad outline of the journal's scope includes; peer reviewed original research articles, case and technical reports, reviews and analyses papers, short communications and notes to the editor, in interdisciplinary information on the practice and status of research in environmental science and management, both natural and man-made. The main aspects of research areas include, but are not exclusive to; environmental chemistry and biology, environments pollution control and monitoring, transport and fate of pollutants in the environment, concentrations and dispersion and trace of wastes in air, water, and soil, point and non-point sources pollution, heavy metals and organic compounds in the environment, atmospheric pollutants and trace gases, solid and hazardous waste management; soil biodegradation and bioremediation of contaminated sites; environmental impact assessment, industrial ecology, ecological and human risk assessment; improved energy management and auditing efficiency and environmental standards and criteria.

Vision and Mission

Global Journal of Environmental Science and Management (GJESM) publishes original. Peer-reviewed and technical environmental articles serve those environmental science and management through the on time quarterly publication with reliable information. GJESM is an integral partner with the scientific and technical communities, delivering superior information products and services that foster communication, build insights and enables individual and collective advancement in environmental research. Providing environmental science and management information to the general public with descriptions of contemporary advances in environmental issues to be used in improving environmental protection and management.

Abstracting and Indexing

Web of Science (ESCI); Scopus; Scimago Journal Rank (SJR); ProQuest (Agricultural and Environmental Science + Natural Science Collection + Ulrichsweb); Chemical Abstract (CAS); CABI Abstract; Global Health Abstract; Agricola; Committee on Publication Ethics (COPE); PubMed-NCBI; DOAJ; Open J-Gate; Google Scholar; Academia.edu; Geomar; WorldCat; Academic Resource Index; Environmental XPRT; Information Matrix for the Analysis of Journals (MIAR); Bibliothek Humburg; ScienceMedia; JournalTOCs; MSRT; ISC; RICeST; SID; Civilica; Magiran.

Global
Journal of Environmental Science and Management (GJESM)

Editor-in-Chief
Professor J. Nouri

pISSN 2383 - 3572
eISSN 2383 - 3866

QUARTERLY FULL OPEN ACCESS PEER REVIEWED PUBLICATION

Journal Abbreviation: Global J. Environ. Sci. Manage.

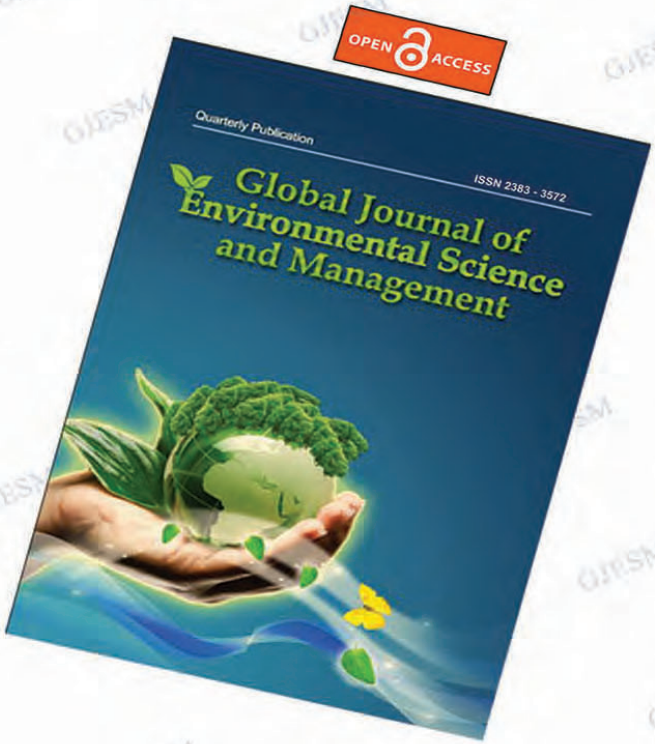

CALL FOR PAPERS

Publication benefits in
Global Journal of Environmental
Science and Management

- *Quarterly Publication journal*
- *Online submission and reviewing*
- *Online status inquiry*
- *Double blind peer reviewing*
- *Rapid evaluation and publication*
- *Immediate publication on the net*
- *Open access to all PDF full text of published articles*
- *No pay charge for publication*
- *Indexed and cited in well-known databases; particularly* Web of Science and Scopus

CLARIVATE ANALYTICS EMERGING SOURCES CITATION INDEX (Web of Science)

SCOPUS

www.gjesm.net
www.gjesm.org

editor@gjesm.net
global.jesm@gmail.com
gjesm.publication@gmail.com

Tel.: +9821 2610 5110
Fax: +9821 2610 5111

CONTENTS

Volume 8, Number 4, Autumn 2022

COVERING LETTER

Subject: **Submission of manuscript**

Dear Editor,

I would like to submit the following manuscript for possible evaluation

Manuscript Title:

Running Title (Short title):

Main Subjects:

Name and address of corresponding author:

Telephone #

Fax #

Email:

I affirm that the manuscript has been prepared in accordance with Global Journal of Environmental Science and Management guide for authors.

I have read the manuscript and I hereby affirm that the content of this manuscript or a major portion thereof has not been published in a refereed journal, and it is not being submitted fully or partially for publication elsewhere. The manuscript has been read and approved by all listed authors.

The source(s) of financial support of study (if any):

Type of Manuscript (check one):

- ☐ Original research paper
- ☐ Case report
- ☐ Research note
- ☐ Short communication
- ☐ Review paper

Name:

Corresponding Author Signature:

Date:

Global J. Environ. Sci. Manage. 8(4): 449-472, Autumn 2022, Serial #32

Global Journal of Environmental Science and Management
(GJESM)

Homepage: https://www.gjesm.net/

ORIGINAL RESEARCH ARTICLE

Water quality model-based methodology to assess assimilative capacity of wastewater discharges in rivers

F.M. Torres-Bejarano[1,*], M. Verbel-Escobar[2], M.C. Atencia-Osorio[2]

[1] *Department of Environmental Engineering, University of Córdoba, Carrera 6 No. 77- 305, Montería, Colombia*

[2] *Environmental Engineering Program, University of Córdoba, Carrera 6 No. 77- 305, Montería, Colombia*

ARTICLE INFO

Article History:
Received 19 September 2021
Revised 27 December 2021
Accepted 29 January 2022

Keywords:
Environmental modeling
Hydrodynamics
Pollutant transport
Self-purification
Water resource management

DOI: 10.22034/gjesm.2022.04.01

ABSTRACT

BACKGROUND AND OBJECTIVES: One of the negative impacts of polluting activities on aquatic ecosystems is the loss of its natural self-purification ability, for this reason, the purpose of this research was to evaluate the Sinú River capacity to assimilate wastewater discharges.
METHODS: Monitoring of several water quality parameters was carried out in the river at different seasons and a numerical method was used to simulate different scenarios through the Environmental Fluid Dynamics Code model. The model calibration process was tested applying the Root Mean Square Error and after calibrating the model, scenarios of increase and decrease of discharge concentrations and flows, and river flows were simulated. Finally, the results were compared to water quality reference limits.
FINDINGS: Results show that the model accurately represented the real conditions of the studied river section for all the evaluated parameters. Also, assimilative capacity was affected mostly by the scenario in which the river flow was decreased by 50%, and the flows and discharges concentrations were increased five times; causing parameters such as ammonia nitrogen, chemical oxygen demand, phosphates, and total nitrogen, to exceed the established reference limits with maximum concentrations of 2.7 mg/L, 30.9mg/L, 0.98 mg/L and 6.3 mg/L; respectively. Higher concentrations of water quality parameters were mostly found in the dry season since lower velocities and river flows promote less pollutants mixing and dilution processes.
CONCLUSION: The model spatiotemporal simulations showed the effect of the wastewater discharges on the Sinú River assimilative capacity and made it possible to find those scenarios where water quality parameters exceeded the reference limits, becoming an essential tool for water management and the development of strong water quality objectives by stakeholders and environmental authorities.

NUMBER OF REFERENCES	NUMBER OF FIGURES	NUMBER OF TABLES
58	10	6

*Corresponding Author:
Email: *franklintorres@correo.unicordoba.edu.co*
Phone: +573 0056 77648
ORCID: 0000-0003-3144-7289

Note: Discussion period for this manuscript open until January 1, 2023 on GJESM website at the "Show Article".

INTRODUCTION

Water quality is an issue that has been gaining importance for several years, mainly because water pollution is gradually becoming a significant problem in lakes and rivers (Yuceer and Coskun, 2016). According to the 2018 wastewater report published by the International Water Association (IWA), about 80% of all wastewaters is discharged into the world's waterways, where it creates health, environmental and climate risks, which can lead to changes in their assimilative capacity (AC). Knowledge of the impacts that wastewater discharges generate on water resources is essential for their proper management, and hydrodynamic and water quality models are essential tools for studying these impacts, generally based on the assimilation capacity of water sources (Villota-López *et al.,* 2021). Assimilative capacity refers to the natural ability of water bodies to self-purify and/or self-repair, either through dilution and/or dispersion of wastes and pollution without harming the aquatic environment. In addition, it can indicate the maximum dynamic capacity of the number of pollutants that can be accumulated, destroyed, transformed and transferred beyond the volume of the ecosystem without disturbing its normal activity, that is, the controllable pollutant input for each water flow in a river (Kulikova *et al.,* 2018). A negative impact of polluting activities on aquatic ecosystems is the loss of its natural self-purification and/or self-restoration ability, this translates in the decrease of its assimilative capacity (Lee *et al.,* 2017), since this ability allows a natural treatment of wastewaters in rivers (Egbe *et al.,* 2018), it's important to understand through this research how the discharges' flows and concentrations affect Sinú River assimilative capacity and under which conditions would the capacity become ineffective. Assimilative capacity can be determined through water quality studies and modeling; these have been used as a tool for assimilative capacity analysis in different water bodies. Dehghani *et al.* (2020) considered a one-dimensional pollutant transport model to calculate the assimilative capacity of a river. Hashemi *et al.* (2017) also implemented a one-dimensional model using two objective functions (pollutant concentrations and the distance the pollutants are in contact with the river water) to determine the assimilative capacity and dilution flux; finding that the variation of river flow in different seasons can change the assimilative capacity by up to 97%. Obin *et al.* (2021) applied the WASP model to calculate the water environmental capacity of the Lushui River (China) in normal, wet, and dry periods and Cely-Calixto *et al.* (2021) simulated water quality parameters of the Magdalena River (Colombia) with the mathematical model QUAL2K showing the river's tendency to be purified due to its great flow. Most common methods for assimilative capacity analysis include the design of monitoring programs in water bodies that involve statistical analysis of river and discharge flows with water quality parameters concentration and water quality simulation model configuration to estimate assimilative capacity (Gurjar and Tare, 2019; Quinn *et al.,* 2021). Another common method is the simulation of scenarios in which specific water quality limits are exceeded (Novo, 2017; Villota-López *et al.*, 2021); this method, implementing a two-dimensional hydrodynamic and water quality model, was mainly considered in this research as it can be a starting point to develop strong water quality objectives that can be fundamental in water resource management. According to the Environmental Diagnosis of the Sinú River Basin published in 2004 by the Environmental Authority: Regional Autonomous Corporation of the Sinú and San Jorge Valleys (CVS), domestic wastewater generated in the population centers has been identified as the main source of water pollution in the Sinú River basin. Although the natural conditions have changed due to anthropic action, the Sinú River self-purification capacity is able to recover acceptable quality levels for biota, but, due to the accelerated economic and demographic growth of the population, it is necessary to carry out more current studies on the dynamics of wastewater discharges into the river (CVS, 2004). Feria *et al.* 2017 simulated Sinú River water quality applying Streeter and Phelps model to determine its deoxygenation and re-aeration rates, however, there aren't assimilative capacity studies of this river, which is the third most important river in Colombia's Caribbean region. This study aims to assess the Sinú River capacity to assimilate wastewater discharges and its effects on this ability, analyzing through hydrodynamic and water quality modeling a section of the Sinú River, Colombia. This study has been carried out in a section of 11.06 km of the Sinú River, Montería City, Colombia using information from four monitoring campaigns in 2019.

MATERIALS AND METHODS

Description of the study area

Sinú River is the main water source in the Department of Córdoba and the third most important in Colombia on its Caribbean slope. It is born in the Nudo de Paramillo in the municipality of Ituango, Antioquia, and flows into the Caribbean Sea in the Tinajones delta area of San Bernardo del Viento, Córdoba. It has an extension of 437.97 km and about 13952 km^2 of watershed (CVS, 2004). In its course through the department of Córdoba, the Sinú River irrigates 16 municipalities, among which is the departmental capital, the city of Montería, which is crossed by the river in its middle reaches, where it becomes meandering with an alluvial plain composed of flood plains, with an average temperature of 27.17 °C (Valbuena, 2017). Monteria's total annual average rainfall is 1262 mm. The dry period goes from the beginning of December until mid- or late April. The wet period begins in May and ends in early December, with a tendency of decreasing rainfall in July and August (transition period); most of the rain falls in September, October, and November. The selected section of the Sinú River for this study has an extension of approximately 11.06 km, is located in Montería city (Colombia), and includes the route from Sierra Chiquita (8°44'11.16"N and 75°54'35.08"W) to the University of Córdoba (8°47'27.08"N and 75°51'47.10"W), as shown in Fig. 1. Along the study section, the Sinú River receives continuous discharges of domestic wastewater from communities settled along its banks, most of which are not authorized by the competent environmental authority. It also receives discharges from other informal activities (vehicle washing, among others) and authorized discharges from the treatment plants of Montería city (WWTP Northeastern and WWTP Southwestern).

Data collection

Information on hydrodynamic and climatic variables (flow rates, levels, precipitation, solar radiation, air temperature, wind speed and direction, and relative humidity) was downloaded from the Hydrology and Meteorology Data Management Information System (DHIME) developed by the Institute of Hydrology, Meteorology and Environmental Studies (IDEAM)

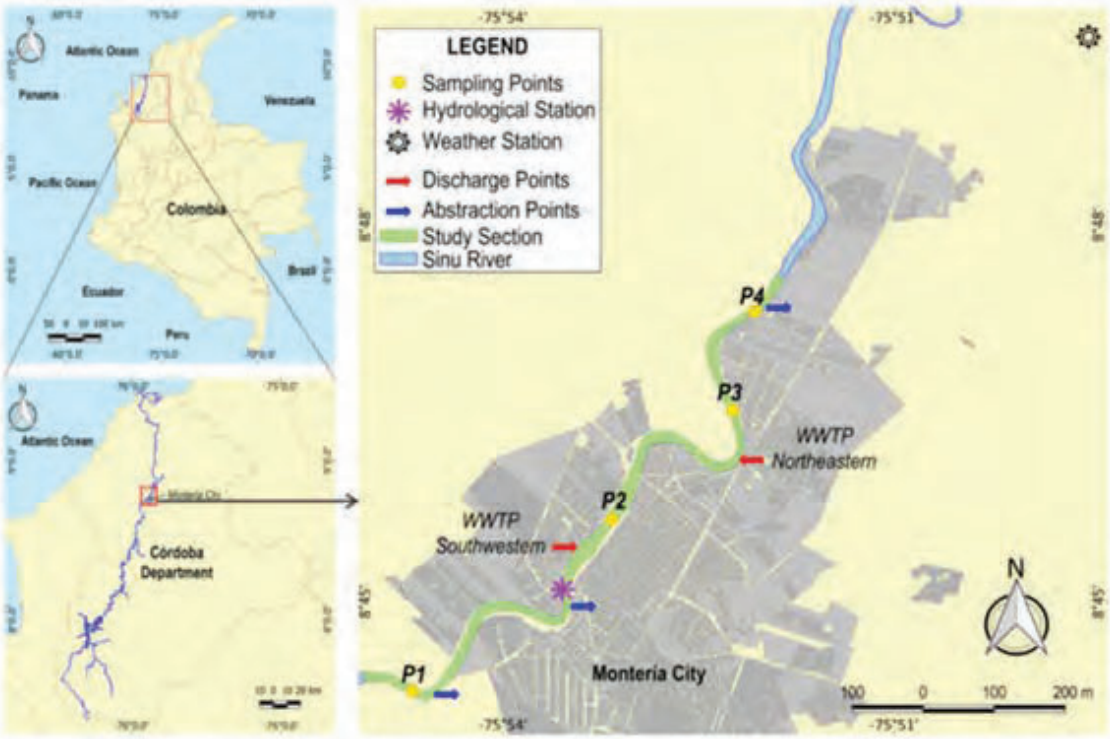

Fig. 1: Geographic location of the study area and sampling locations in the Sinú River section through Monteria city, Colombia

from the following stations:

1) Montería - Automatic (Aut) Station [13067020, Hydrological]: 8°45'05.8"N - 75°53'32.7"W.
2) Los Garzones Airport Station [13035501, Meteorological]: 8°49'33.0"N - 75°49'30.5"W.

In addition, the CVS provided information on the abstraction points (flow rates granted) and discharge points (flow rates and physicochemical characterization) within the study reach.

Water samples were collected during four monitoring campaigns in 2019 (March 18th, July 18th, September 25th and October 31st), for four points established along the study section (Fig. 1), collecting a total of 16 samples to obtain water quality data of the river and be able to carry out the model's calibration. Each point was defined considering the IDEAM (2017) Water Monitoring Protocol and was duly georeferenced with a Garmin GPS 60CSx. Temperature (T) and dissolved oxygen (DO) were measured *in situ* using a HANNAH Multiparameter Probe (model HI-929829), while water samples were studied taking into consideration the general techniques and preservation of sampling of the NTC-ISO 5667 for laboratory analysis of total nitrogen (TN) [SM 4500-Norg B; 4500-NH3 C], ammonia nitrogen (NH3-N) [SM 4500-NH3 B; SM 4500-NH3 C], phosphates (PO4-P) [SM 4500-P E], chemical oxygen demand (COD) [SM 5220 C] and total suspended solids (TSS) [SM 2540 D]. Furthermore, a monitoring campaign was carried out in May 2019 where depth data were taken along the study section to generate the river bathymetry utilizing a Garmin ECHOMAP 73sv bathymetric depth sounder.

Numerical model description

Initially developed at the Virginia Institute of Marine Science (VIMS) and subsequently sponsored by the United States Environmental Protection Agency (US EPA) and the National Oceanic and Atmospheric Administration (NOAA) Sea Grant Program, the Environmental Fluid Dynamics Code (EFDC) is a multifunctional surface water modeling system that can be used to simulate aquatic systems in one, two and three dimensions and includes hydrodynamic components, sediment contaminants and eutrophication. It can also simulate the transport of water quality constituents in geometrically and dynamically complex water bodies such as rivers, stratified estuaries, lakes, and coastal seas. It solves the motion (vertically hydrostatic) and free surface equations, along with the continuity and mass balance equations, i.e., with coupled hydrodynamics, salinity, temperature, sediment, and contaminant transport modules. It also allows drying and wetting in shallow areas employing a massive conservation scheme (Torres-Bejarano *et al.*, 2016; Ramos, 2018). Yiping *et al.* (2011) used it to study the impacts of water transfer on the transport of dissolved substances in Taihu Lake using the water age concept. Kim *et al.* (2017) used it to model algal bloom occurrence atterns in the lower part of this Han River to understand algal dynamics to better develop management alternatives. And Villota-López *et al.* (2021), to estimate the assimilative capacity of the Gallinas River. The water quality simulations and assimilative capacity was evaluated using the EFDC Explorer 10.2.2 modeling system, a commercial version of EFDC developed by DSI Company.

Hydrodynamics and water quality modules

EFDC Explorer applies hydrodynamic modeling based on the turbulent equations of motion and utilizing the Boussinesq approximation for variable density (variable density is a strictly mandatory analysis when dealing with equations for compressible flow), resulting in the momentum Eqs. 1 and 2, the continuity equation, the state equation and the transport equations for salinity and temperature, solved integrally in 2D and 3D. For more detailed information on these equations refer to DSI, (2020) and Torres-Bejarano *et. al.* (2020).

The momentum equation in the x direction:

$$\frac{\partial(m_x m_y H u)}{\partial t} + \frac{\partial(m_y H u u)}{\partial x} + \frac{\partial(m_x H v u)}{\partial y} + \frac{\partial(m_x m_y w u)}{\partial z} - m_x m_y f H v - \left(v \frac{\partial m_y}{\partial x} - u \frac{\partial m_x}{\partial y} \right) H v = -m_y H \frac{\partial(g\zeta + p + P_{atm})}{\partial x} - m_y \left(\frac{\partial h}{\partial x} - z \frac{\partial H}{\partial x} \right) \frac{\partial p}{\partial z} + \frac{\partial}{\partial x}\left(\frac{m_y}{m_x} H A_H \frac{\partial u}{\partial x} \right) + \frac{\partial}{\partial y}\left(\frac{m_x}{m_y} H A_H p d[u]y \right) + \frac{\partial}{\partial z}\left(\frac{m_x m_y}{H} A_v \frac{\partial u}{\partial z} \right) - m_x m_y c_p D_p u \sqrt{u^2 + v^2} + S_u \quad (1)$$

The momentum equation in the y direction

$$\frac{\partial(m_x m_y \mathrm{Hv})}{\partial \mathrm{t}} + \frac{\partial(\mathrm{m_y Huv})}{\partial \mathrm{x}} + \frac{\partial(\mathrm{m_x Hvv})}{\partial \mathrm{y}} + \frac{\partial(m_x m_y \mathrm{wv})}{\partial \mathrm{z}} - m_x m_y f H u + \left(\mathrm{v}\frac{\partial \mathrm{m_y}}{\partial \mathrm{x}} - \mathrm{u}\frac{\partial \mathrm{m_x}}{\partial \mathrm{y}}\right) H u = -m_x \mathrm{H}\frac{\partial(\mathrm{g}\zeta + p + P_{atm})}{\partial \mathrm{y}} - m_x \left(\frac{\partial \mathrm{h}}{\partial \mathrm{y}} - \mathrm{z}\frac{\partial \mathrm{H}}{\partial \mathrm{y}}\right)\frac{\partial \mathrm{p}}{\partial \mathrm{z}} + \frac{\partial}{\partial x}\left(\frac{m_y}{m_x} H A_H \frac{\partial v}{\partial x}\right) + \frac{\partial}{\partial y}\left(\frac{m_x}{m_Y} H A_H \frac{\partial v}{\partial y}\right) + \frac{\partial}{\partial z}\left(\frac{m_x m_y}{H} A_v \frac{\partial v}{\partial z}\right) + m_x m_y c_p D_p v\sqrt{u^2 + v^2} + S_v \quad (2)$$

Where, *u, v* are the horizontal velocity components in the curvilinear coordinates; *x, y* are the orthogonal curvilinear coordinates in the horizontal direction; *z* is the sigma coordinate; *t* is time; m_x, m_y are the square roots of the diagonal components of the metric tensor; P_{atm} is the barotropic pressure; $H = h+\zeta$, Total depth, is the sum of depth and free surface; *p* is the physical pressure in excess of the reference density hydrostatic pressure; *f* is the Coriolis parameter; A_H is the horizontal momentum and mass diffusivity; A_v is the vertical turbulent eddy viscosity; c_p is the vegetation resistance coefficient; D_p is the projected vegetation area normal to the flow per unit horizontal area S_u, S_v are the source/sink terms for the horizontal momentum in the *x* and *y* directions, respectively. In Eqs. 1 and 2, the first term from left to right represents the rate of change of velocity with respect to time; the next three are the advective components and represent fluid motion due to inertial forces; the one that follows is the Coriolis acceleration in the curvature and on the tangential stresses of the bottom, represented through the variation of the free surface; the one immediately after the equal sign is the pressure force, represented through the variation of the free surface, and the next two, the viscous forces that give rise to turbulence within the flow. Water quality structure managed by EFDC Explorer model is mainly composed of reactions that occur in water through organic and inorganic cycles, such as nitrogen, chemical oxygen demand, phosphorus, and algae. The governing mass-balance equation for each of the water quality state variables may be expressed as Eq. 3.

Advection-Diffusion-Reaction equation

$$\overbrace{\frac{\partial}{\partial t}(m_x m_y HC)}^{a} + \overbrace{\frac{\partial}{\partial x}(m_y HuC) + \frac{\partial}{\partial y}(m_x HvC) + \frac{\partial}{\partial z}(m_x m_y wC)}^{b} = \overbrace{\frac{\partial}{\partial x}\left(\frac{m_y H A_x}{m_x}\frac{\partial C}{\partial x}\right) + \frac{\partial}{\partial y}\left(\frac{m_x H A_y}{m_y}\frac{\partial C}{\partial y}\right) + \frac{\partial}{\partial z}\left(m_x m_y \frac{A_z}{H}\frac{\partial C}{\partial z}\right)}^{c} + \overbrace{m_x m_y H S_c}^{d} \quad (3)$$

As shown in Eq. 3, *C* is the concentration or intensity of transport constituent; *u, v* are the horizontal velocity components in the curvilinear coordinates; *w* is the vertical velocity component; A_H is the horizontal turbulent eddy diffusivity; S_c is the internal and external sources and sinks per unit volume; *H* is the total water depth. Eq. 3 comprises physical, advective and diffusive transport, together with kinetical processes; *a* is a temporal term, whereas *b* represents advection transport. On the right side, *c* represents the diffusive transport, and *d* is the reaction term which represents both the kinetic processes and external loads for each of the state variables (DSI, 2020; Villota-López *et. al.,* 2021).

Ammonia nitrogen reaction equation

$$\frac{\partial NH_4}{\partial t} = \sum_{x=c,d,g,m}(FNI_x BM_x + FNIP_x PR_x - PN_x P_x)\, ANC_x B_x + K_{DON} DON - K_{Nit} NH_4 + \frac{BFNH_4}{\Delta z} + \frac{WNH_4}{V} \quad (4)$$

In Eq. 4, FNI_x is the fraction of metabolized nitrogen by algal group *x* produced as inorganic nitrogen; *FNIP* is the fraction of predated nitrogen produced as inorganic nitrogen; PR_x is the predation rate of algal group *x;* PN_x is the preference for ammonium uptake by algal group *x*; P_x is the production rate of algal group *x;* ANC_x is the nitrogen-carbon ratio constant in algal group *x*; B_x is the algal biomass of algal group *x*; K_{DON} is the rate of dissolved organic nitrogen mineralization; *DON* is the dissolved organic nitrogen concentration; $BFNH_4$ is the water-sediment ammonium flux exchange, applied only to the bottom of the layer; WNH_4 are the external ammonium loads and K_{Nit} is the nitrification rate.

Reaction equation of total phosphate

Small concentrations of phosphate and other

phosphorus compounds can be found in natural water bodies. These substances leach from the terrain or result from organic pollution. Phosphates are directly linked to eutrophication (DSI, 2020). The equation employed by the model using Eq. 5.

$$\frac{\partial}{\partial t}(PO4t) = \sum_{x=c,d,g,m}(FPI_x(BM_x) + FPIP_x(PR_x) - P_x)APC_x(B_x) + K_{DOP}(DOP) + \frac{\partial}{\partial z}\left(WS_{TSS}(PO4p)\right) + \frac{BFPO4d}{\Delta Z} + \frac{WPO4p}{V} + \frac{WPO4d}{V} \quad (5)$$

Note that in Eq. 5, *PO4t* is the total phosphate concentration; K_{DOP} is the mineralization rate of dissolved organic phosphorus; *PO4p* is the particulate (sorbed) phosphate; *PO4d* is the dissolved phosphate; FPI_x is the fraction of metabolized phosphorus by algal group *x* produced as inorganic phosphorus; BM_x is the basal metabolism rate of algal group *x*; *FPIP* is the fraction of predated phosphorus produced as inorganic phosphorus; *APC* is the mean algal phosphorus-to-carbon ratio for all algal groups; K_{DOP} is the dissolved organic phosphorus mineralization rate; *DOP* is the dissolved organic phosphorus concentration; WS_{TSS} is the settling velocity of the suspended solid, provided by the hydrodynamic model; *BFPO4d* is the sediment-water exchange flux of phosphate, applied to the bottom layer only; *WPO4t* is the external loads of total phosphate, and *V* is the cell volume.

Dissolved oxygen reaction equation

$$\frac{\partial DO}{\partial t} = \sum_{x=c,d,g,m}\left[(1 + 0.3(1 - PN_x))P_x - (1 - FCD_x)\left(\frac{DO}{KHR_x + DO}\right)BM_x\right] + AOCR(B_x) - (AONT)(K_{Nit})(NH_4) - AOCR(K_{HR})(DOC) - \left(\frac{DO}{KH_{COD} + DO}\right) + K_{COD}(COD) + K_R(DO_s - D \frac{SOD}{\Delta z} + \frac{WDO}{V} \quad (6)$$

In Eq. 6, FCD_x is the fraction of basal metabolism exuded as dissolved organic carbon; KHR_x is the half-saturation constant of dissolved oxygen for algal dissolved organic carbon excretion for group *x*; *AOCR* is the dissolved oxygen-to-carbon ratio in respiration; *AONT* is the mass of dissolved oxygen consumed per unit mass of ammonium nitrogen nitrified; NH_4 is the ammonium nitrogen concentration; K_{HR} is the heterotrophic respiration rate of dissolved organic carbon; *DOC* is the concentration of dissolved organic carbon; KH_{COD} is the half-saturation constant of dissolved oxygen required for oxidation of *COD*; *DO* is the dissolved oxygen concentration; *COD* is the chemical oxygen demand concentration; K_R is the reaeration coefficient; DO_s is the saturated concentration of dissolved oxygen; *SOD* is the sediment oxygen demand, applied to the bottom layer only, and *WDO* is the external loads of dissolved oxygen.

Chemical oxygen demand reaction equation

$$\frac{\partial COD}{\partial t} = -\left(\frac{DO}{KH_{COD} + DO}\right)K_{COD}COD + \frac{BFCOD}{\Delta z} + \frac{WCOD}{V} \quad (7)$$

As shown in Eq. 7, KH_{COD} is the half-saturation constant of dissolved oxygen required for oxidation of chemical oxygen demand; K_{COD} is the oxidation rate of chemical oxygen demand; *BFCOD* is the sediment flux of chemical oxygen demand, applied to bottom layer only and *WCOD* is the external loads of chemical oxygen demand.

Suspended sediment transport equation

The water column equation for suspended sediment transport is derived from the generic transport Eq. 3 for a dissolved or suspended material. From which the physical terms of horizontal diffusion are omitted due to small inherent numerical diffusion encountered.

$$\frac{\partial}{\partial t}\left(mHC_j\right) + \frac{\partial}{\partial x}\left(PC_j\right) + \frac{\partial}{\partial y}\left(QC_j\right) + \frac{\partial}{\partial z}\left(mwC_j\right) - \frac{\partial}{\partial z}\left(mw_{s,j}C_j\right) = \frac{\partial}{\partial z}\left(m\frac{A_b}{H}\frac{\partial}{\partial z}C_j\right) + S^E_{s,j} + S^I_{s,j} \quad (8)$$

For Eq. 8, *Cj* represents the concentration of the j^{th} sediment class; A_b is the vertical turbulent eddy viscosity (m^2/s); w_s is the settling velocity of the sediment particles; $S^E_{s,j}$ is the external source-sink term, and $S^I_{s,j}$, is the internal source-sink term. The source term has been split into two terms so that the external source-sink term can include both point and non-point source loads. And the internal source-sink term can include the reactive decomposition of organic sediments or the exchange of mass between sediments classes (DSI, 2020).

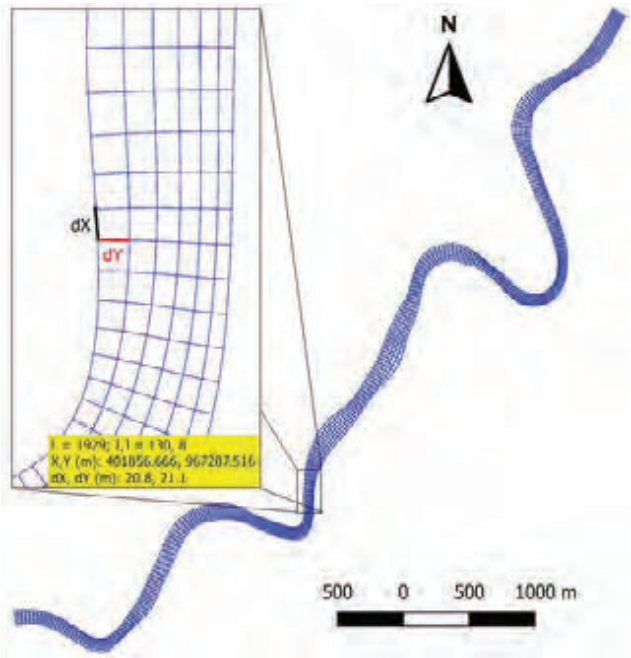

Fig. 2: Configuration of the generated grid

Modeling framework

For purposes of spatial discretization of the model in the study section, a numerical structured grid in a curvilinear and orthogonal system was generated, with a total of 6 rows, 360 columns and 2160 cells whose spacing varies in DX from 10.2 m to 58.3 m and in DY from 8.9 m to 47.03 m, since it presented the best computational times and greater stability during the model calculations (Fig. 2). The bathymetry was processed on this grid, and initial and boundary conditions were included to simulate hydrodynamics and water quality. Subsequently, the model was calibrated to obtain and guarantee reliable results. The simulation period was from February 28th to October 31st, 2019.

Initial and boundary conditions

Absolute depths obtained during the bathymetric campaign were transformed to river bottom elevations using the free water surface level of that day, obtained from the hydrological station Montería – Aut of IDEAM. Meteorological data (solar radiation, air temperature, wind speed and direction, precipitation, evaporation, and relative humidity) were obtained from IDEAM's Los Garzones Airport weather station. The initial water level was established based on the level reported by the Montería - Aut station for the starting day of the simulation (February 28th, 2019). From this same station, river flows were also obtained from a daily time series covering the entire simulation period (Fig. 3). The discharge and abstraction flows were provided by the environmental authority CVS. Dirichlet-type boundaries were defined as inflows referring to the upstream flow of the Sinú River and discharge flows, and outflows referring to abstraction flows. In addition, a free-flow outlet was established at the river's downstream boundary (Neumann-type boundary) (Fig. 3). Sinú River flow in the representative dry season month (March) varies between 125.1 m^3/s and 136.1 m^3/s; in October, the representative wet season month reaches flows up to 709.8 m^3/s. WWTP Northeastern and WWTP Southwestern have a discharge flow of 0.314 m^3/s and 0.099 m^3/s, respectively. Fig. 3 shows river flow input conditions for the whole simulation period.

Initial conditions for each water quality parameter (Fig. 3) were established from *in situ* measurements at the monitoring points (P1 and P4). The parameters concentrations at P1 (Fig. 1) were used as upstream conditions inflow of the Sinú River and the parameters concentrations at P4 (Fig. 1) were used as downstream free boundary conditions. Likewise, the

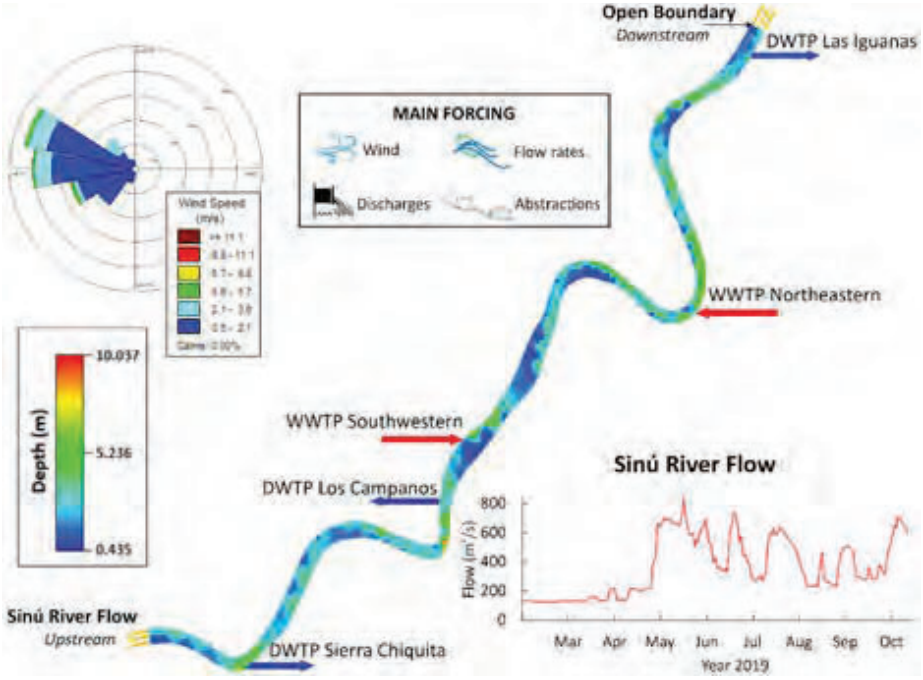

Fig. 3: Initial and boundary conditions

Table 1: WWTP parameters concentrations for water quality simulation

Parameters	WWTP Northeastern	WWTP Southwestern
Temperature (ºC)	30.2	36.2
COD (mg/L)	117.69	142.15
DO (mg/L)	1.9	1.9
NH_3-N (mg/L)	15	15
PO_4-P (mg/L)	3.5	3.5
TSS (mg/L)	68.17	43.56
Flow (m^3/s)	0.314	0.099

concentrations of each of the discharges' parameters were defined according to the information provided by the CVS (Table 1).

Model calibration

The hydrodynamic model was calibrated by gradually adjusting the hydrodynamics coefficients (bottom roughness, horizontal viscosity, etc.) and comparing the simulated water levels with the measured water level data in the river expressed as a time series obtained from the Montería - Aut station during the simulation period. The water quality model was calibrated using the time series generated for each analyzed physicochemical and biological parameter in P2 and P3 (Fig. 1), during the four measurement campaigns. Throughout the calibration process, coefficients and rates of the chemical reactions that govern the behavior of the physicochemical and biological parameters were gradually adjusted. In order to check the fit of the model simulated data with those measured *in situ*, the Root Mean Square Error (RMSE) was applied to measure the amount of error between the two data sets. RMSE ranges from 0 to ∞, where a value equal to 0 indicates a perfect fit using Eq. 9 (Ritter and Muñoz-Carpena, 2013).

$$RMSE = \sqrt{\frac{\sum_{i=1}^{n}(O_i - p_i)^2}{N}} \quad (9)$$

Where, O_i y p_i represent the sample (of size

Table 2: Evaluation criteria for RMSE (Ritter and Muñoz-Carpena, 2013)

Classification	Criteria
Very good	SD ≥3.2RMSE
Good	2.2RMSE≤SD<3.2RMSE
Acceptable	1.2RMSE≤SD<2.2RMSE
Unsatisfactory	SD<1.2RMSE

Standard Deviation (SD) of the measured data.

Table 3: Simulation scenarios applied in Sinú River

Scenario	Description	River	Discharges		
		F (%)	F (%)	Concentrations (%)	
				DO	Others
AS	Actual State of the river discharges and flows.	NC	NC	NC	NC
S1	Discharges' concentration modification.	NC	NC	↓80	↑400
S2	Decrease of river flow.	↓50	NC	NC	NC
S3	Decrease of river flow and discharges concentration modification.	↓50	NC	↓80	↑400
S4	Decrease of river flow and increase of discharges' flows.	↓50	↑400	NC	NC
S5	Decrease of river flow; increase of discharges' flows and modification of its concentrations.	↓50	↑200	↓66.67	↑200
S6		↓50	↑400	↓80	↑400

NC: No change; F: *Flow*; Others: T, COD, NH_3-N, TN, PO_4-P, TSS; ↑: *Increase*; ↓: *Decrease.*

Table 4: Modified coefficients in the hydrodynamic component

Hydrodynamic module	
Parameter	Value
Constant Horizontal Eddy Viscosity (m^2/s)	0.001
Horizontal Momentum Diffusivity (dimensionless)	0.150
Bottom roughness (m)	0.025

N) containing the measured and simulated data, respectively, for cell *i*. Table 2 shows the evaluation criteria for the RMSE.

Modeling scenarios formulation

The scenarios shown in Table 3 were formulated considering the National Water Resource Modeling Guide for inland surface waters. The concentrations of the discharges' parameters in the study section were modified to estimate under what conditions the river would not be able to assimilate the pollutants.

Assimilation capacity

To evaluate the assimilation capacity, the results obtained with the simulated scenarios were compared with the quality criteria applicable to any water body, which, for the case of Colombia, are regulated by the 1076 Decree of 2015 of the Ministry of Environment and Sustainable Development, in articles 2.2.3.3.3.9.2 to 2.2.3.3.3.9.12, and the 2115 Resolution of 2017 of the Ministry of Social Protection. However, these do not contemplate limit values for some parameters such as COD, TSS, NH_3-N, among others; therefore, legislation from countries such as Brazil (Resolution 357 of 2005) and the United States (EPA Standards) was consulted. Based on the current uses in the river, and the regulations and guidelines consulted, the quality criteria that would serve as a guide for the use of the water resource were consolidated.

RESULTS AND DISCUSSION

Hydrodynamic component calibration

The hydrodynamic model was calibrated by comparing the levels obtained from the Montería Aut. Station with the levels calculated by the model. During this process, some hydrodynamic coefficients were adjusted to obtain an optimal calibration (Table 4).

Fig. 4 shows the comparison between the observed

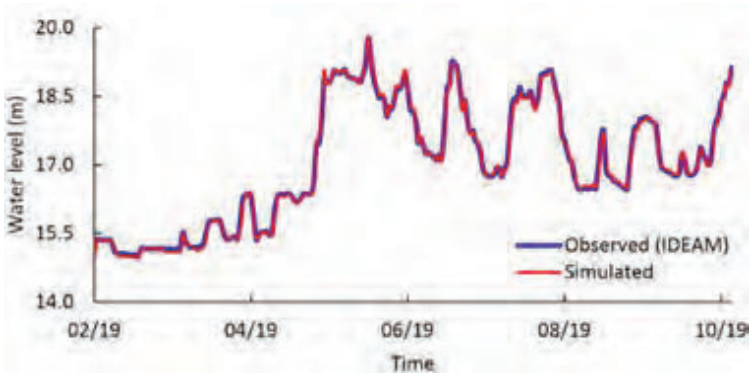

Fig. 4: Hydrodynamic component calibration

data and the simulated data. To verify the fit, the RMSE was calculated, resulting in a value of 0.089, which is in the very good fit category. This indicates that the simulated results are a good representation of the behavior and magnitude of the real levels in the study area during the simulation period.

Water quality component calibration and validation

Fig. 5 shows the results of the calibration of each parameter. The calibration of this module was performed with the concentrations obtained at points P2 and P3; it was necessary to adjust the water quality module coefficients with the values shown in Table 5.

To verify the calibration process, the RMSE was estimated for all simulated parameters (Temperature, COD, DO, NH_3-N, TN, PO_4-P, TSS) at points 2 and 3, considering the standard deviations of the data, the results are shown in Table 6. In P3, parameters such as temperature, PO_4-P and TSS were found in a very good fit category; COD, DO and NH_3-N in an acceptable category and TN in a good fit category. Considering all the calibration results, the EFDC Explorer model reached an accurate representation of the real conditions of the studied river section, which makes very acceptable the simulations of the hydrodynamic and physicochemical processes of the river. The comparison between simulated and measured data also shows that model results follow the seasonal trend seen in field data.

Hydrodynamic simulation

Once the calibration process was completed, the actual state of the study reach was simulated. The results for the dry season were obtained from the representative date of March 31st, and for the wet season, the representative date was October 26th, 2019. Water velocity in rivers can be affected by factors such as river geometry, roughness, slope zones and flow rate. Fig. 6 shows the velocity simulation results for dry and wet seasons. During the dry season (lower flows), velocities were below 0.61 m/s, while in the wet season (higher flows) velocities of up to 0.86 m/s were reached. The spatial changes in velocity in each season are not very significant, because the study section is in an alluvial plain area where slope variations are not representative (CVS, 2004; Acosta, 2013).

Water quality simulation

Results of the water quality simulations for the dry season were also obtained from the representative date of March 31st, and for the wet season the representative date was October 26th, 2019; the results for each parameter are observed in Fig. 7. Regarding the temporal variation, an increase in DO is observed during the wet season, this is consistent with what is reported in the literature, where precipitation has a positive effect on this parameter (Muñoz *et al.*, 2015; Liu *et al.*, 2020). In the case of parameters such as COD, NH_3-N, TN and PO_4-P the highest concentrations were found in the dry season; this occurs because the decrease in flow rates during this season generates a higher concentration of pollutant loads, which causes a decrease in DO and an increase in COD, due to decomposition processes (Liu *et al.*, 2020), additionally, Benjumea *et al.*, (2018) suggest that the high presence of organic matter at lower flow rates does not allow the dilution of nutrients. The highest concentrations of TSS occurred in the wet

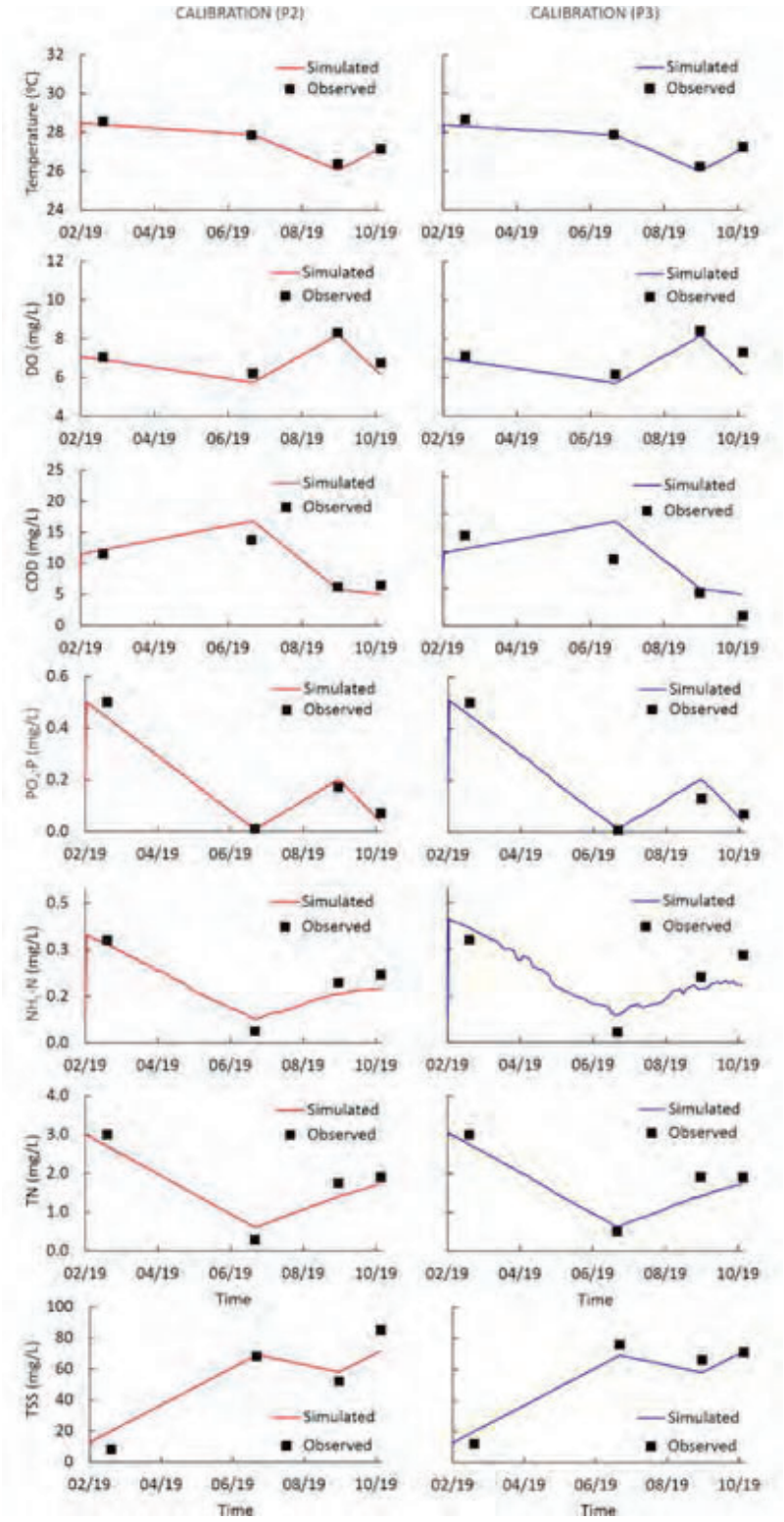

Fig. 5: Calibration and validation of physicochemical parameters at point 2 (red) and point 3 (blue)

Table 5: Main modified coefficients in the water quality component

Parameter	Reaction rates	(Value/d)
DO	Reaeration Rate (k_a)	1
	Nitrification Rate (k_n)	0.07
	Deoxygenation Rate (k_d)	1.5
COD	Oxidation Rate of the chemical oxygen demand (k_o)	0.03
TN	Nitrification Rate (k_n)	0.07
NH_3-N	Hydrolysis Rate of organic nitrogen (k_{hn})	0.08
	Nitrification Rate (k_n)	0.07
SST	Particle settling velocity (w_s)[a]	1.38×10^{-4}
	Sedimentation Rate of suspended solids (k_s)	-
PO_4-P	Hydrolysis Rate of organic phosphorus (k_{hPO})	0.08

[a] in m/d

Table 6: RMSE results for all parameters

Parameters	SD	RMSE	Fit category	SD	RMSE	Fit category
	P2			P3		
Temperature	0.815	0.177	Very good	0.891	0.202	Very good
COD	3.264	1.725	Acceptable	4.955	3.655	Acceptable
DO	0.770	0.38	Acceptable	0.800	0.623	Acceptable
NH_3-N	0.119	0.032	Very good	0.121	0.065	Acceptable
TN	0.964	0.298	Very good	0.887	0.299	Good
PO_4-P	0.189	0.038	Very good	0.191	0.047	Very good
TSS	28.613	9.604	Good	25.791	6.666	Very good

Fig.6: Dry and wet season velocity simulation

season since during wet periods there is a large influx of allochthonous materials into the river through surface runoff, i.e., the movement of rainwater and surface runoff promotes the detachment and entrainment of particles (sediments), increasing TSS (Jaya, 2017; Agustine *et al.*, 2018). Regarding the spatial distribution of concentrations, all parameters were negatively affected in the area immediately after the second discharge (WWTP Northeastern), where it was observed a slight decrease in DO and a significant increase in the other evaluated parameters (COD, NH_3-N, TN, and PO_4-P). This demonstrates the negative impacts that wastewater discharges have on the concentrations of physicochemical parameters in water bodies and their effect on the assimilative capacity of the receiving bodies (Cuesta-Parra *et al.*, 2018). Results relate to Aguilar and Solano, (2018) research regarding the river flow decrease in the dry season that also cause a decrease in de dilution capacity of pollutants from domestic wastewater,

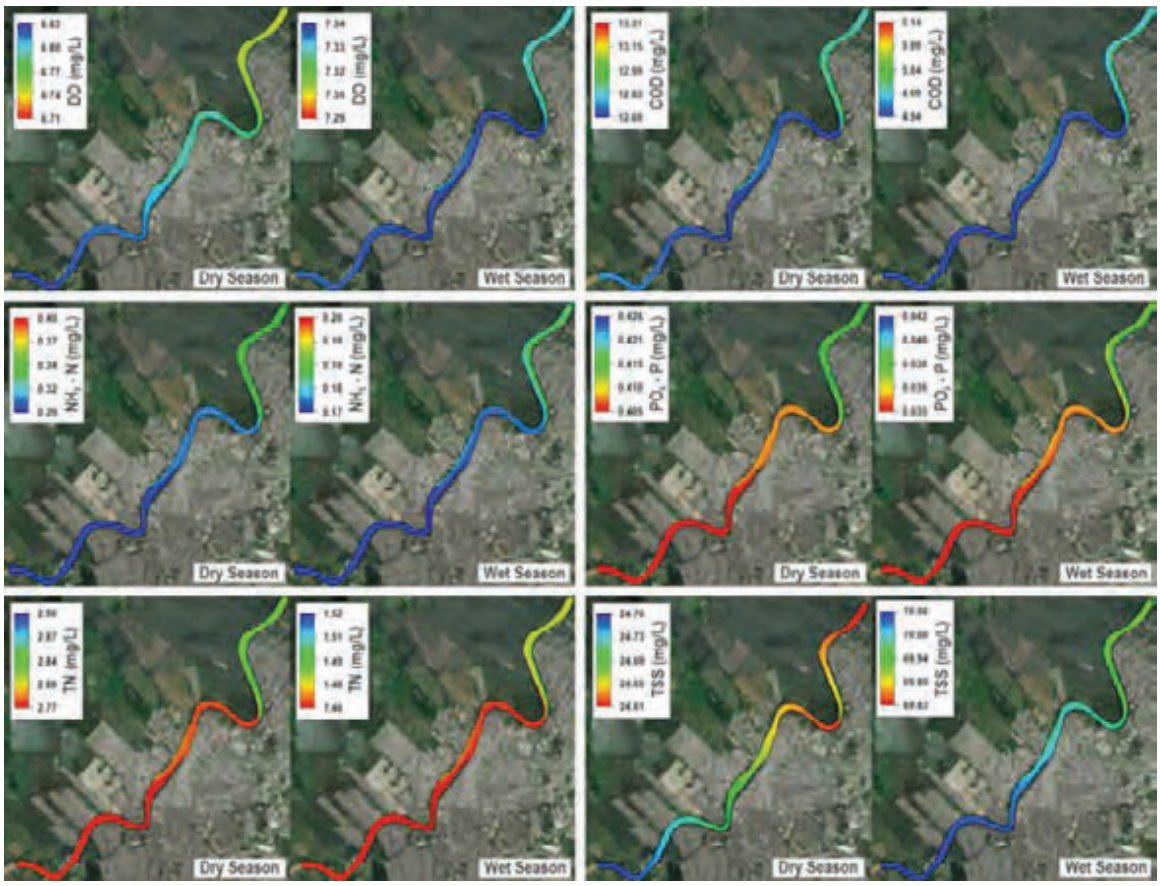

Fig. 7: Simulation results of physicochemical parameters in dry (March 31st) and wet (October 26th) seasons (Note the change of scale in the figures)

therefore affecting the assimilative capacity.

Simulated scenarios and assimilation capacity

Simulation results of the formulated scenarios are shown in Fig. 8. For the evaluation of the assimilation capacity, a comparison between the concentrations in the time series with the established reference limits was carried out.

Temperature

Temperature is a parameter of great importance in the analysis of water quality because its increase in water bodies can produce negative effects on the ecosystem and its fundamental processes, particularly, rivers temperature affects the availability of DO in the water column for fish and other aquatic organisms, it also affects the solubility of chemicals in the water and biological activity (Graham *et al.*, 2014; Zhen-Gang, 2017). Colombian regulations indicate that wastewater discharges must not cause an increase of more than 5 °C in the temperature of surface water bodies; the temperature time series in Fig. 8 shows that none of the scenarios exceeds the reference value, which indicates that the discharges evaluated in the study section do not significantly affect this parameter; however, it should be taken into account that even if the standard is met, the temperature fluctuations predicted in the different scenarios may influence the other water quality parameters studied. S6, which corresponds to a 50 % decrease in river flow and an increase of five times in discharge concentrations and flows, caused the greatest increase in river temperature, reaching 31.7 °C as the maximum value in the dry season; this could negatively affect the river's assimilative capacity since dissolved oxygen concentrations depend also on water temperature (Imam and El Baradei, 2006); an increase in the river's water temperature influences its oxygen metabolism which creates a decrease

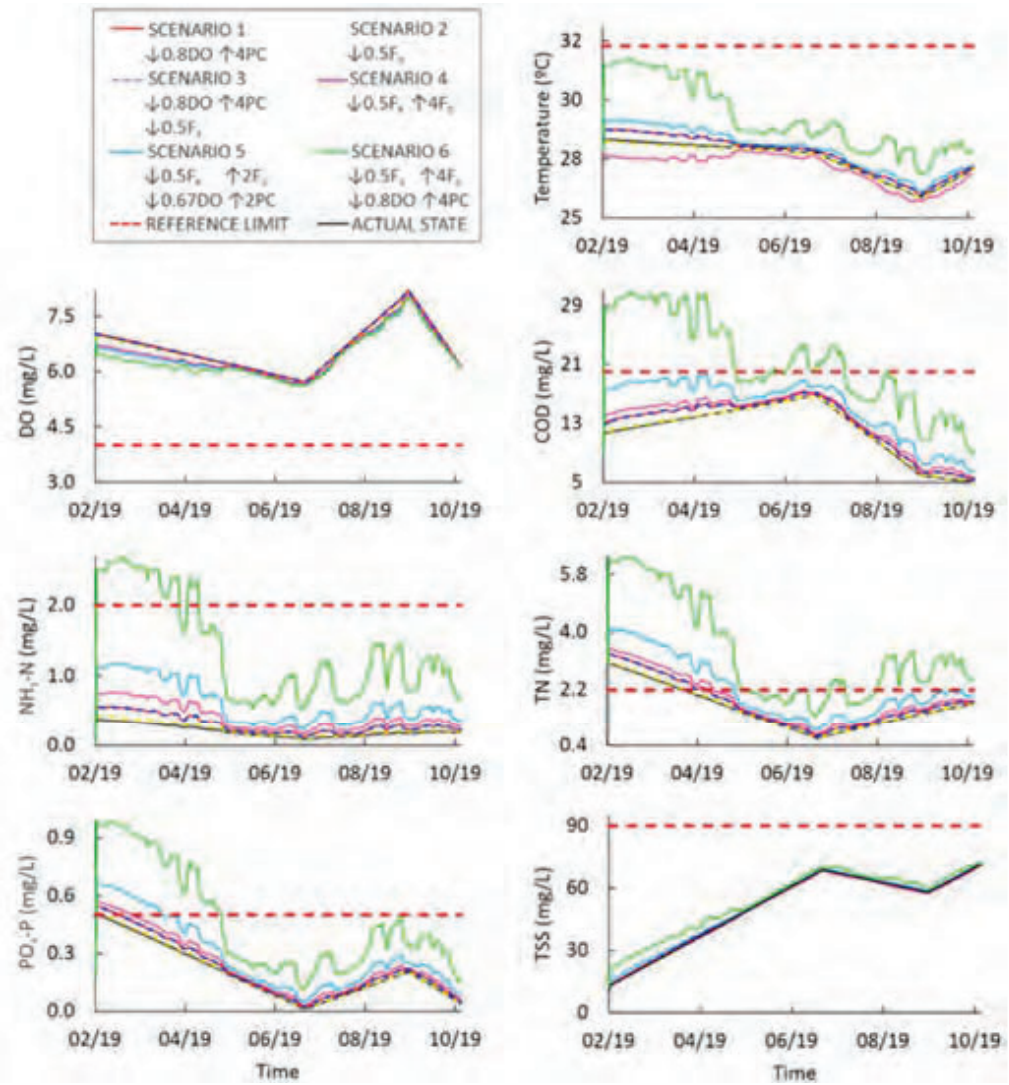

Fig. 8: Time series plots for each parameter

in its assimilative capacity due to rise biochemical processes that deplete oxygen (Chapra *et al.,* 2021).

Chemical Oxygen Demand

COD concentrations in the actual state are higher in March compared to those in October, but the highest concentrations occur between April and May (Fig. 8); however, the graph shows that S6 is the only one that exceeds the reference limit (20 mg/L), this occurs during the first months (March - May) and between June and July; during the dry season this parameter reaches a maximum concentration of 30.9 mg/L and water bodies that exceed the reference limit are considered polluted (Jingsheng *et al.,* 2006; Al-Badaii *et al.,* 2013). These results show that the river's assimilation capacity of this parameter is affected mainly when the river flow decreases by half and the concentrations and flows of discharges increase five times, which are the conditions in S6. In general, the change in flow rates, both in the river and in discharges, is the condition that affects assimilation capacity the most. S5 also shows a considerable increase in this parameter during the dry season, because in this scenario the river flow was reduced by half and the concentrations and flows of discharges increased three times. In all scenarios, a significant decrease

in COD was observed in October. This behavior is similar to the results obtained by Islam *et al.* (2015), where a decrease in COD was also observed during the wet period and an increase during the dry period. According to the results of their research, where there were higher concentrations of COD and NH_3-N in the dry season, Liu *et al.,* (2018) suggest that the reduction of the water assimilative capacity during the dry season showed that the pollution loads in this season were much more serious than the wet season and a reduction in pollutants loads must be done to meet its water quality protective goal.

Dissolved oxygen

Poor water quality is considered when DO concentrations are lower than the reference limit of 4 mg/L, thus it can be harmful to some fish and macroinvertebrate populations and have negative effects on chemical reactions of aquatic ecosystems (Patel and Vashi, 2015). As shown in Fig. 8, DO remains at good levels over this limit throughout the simulation time in all scenarios. Considering the above, it can be said that the river has the capacity to adequately assimilate current discharges without significantly affecting this parameter, therefore the river preserves its ability to assimilate oxygen demanding pollutants without disrupting the aquatic ecosystem (Chapra, 2018), even under the worst conditions represented by S6. In S6's dry season, there was a greater decrease in DO compared to its current state, which is associated with low flow values and less aeration of the medium (Liu *et al.,* 2020). DO decrease in water bodies due to the influence of discharges is consistent with what has been found in different studies (Graham *et al.,* 2014; Rubio *et al.,* 2017).

Ammonia nitrogen and total nitrogen

These parameters' variations are strongly related to both river flow and discharge concentrations and flows. This is evident when observing S2 in Fig. 8, where, although there was a decrease in half of the river flow, the discharge flows and concentrations were not altered, and as a result, concentrations very similar to those of the actual state were obtained. Most significant changes were observed in scenarios S5 and S6, where the flow of the river and the discharges' flow and concentrations were modified. S5 shows that the river can withstand a decrease in its flow by half and an increase of three times in discharge flow and concentrations without exceeding the reference limit for NH_3-N, while the same happens for TN only in the wet season. TN results show that although the reference limit of 2.18 mg/L was exceeded in all scenarios during the first months, by the end of the simulation in the wet season the limit was only exceeded in S6, reaching a maximum TN concentration of 6.3mg/L mg/L, which can accelerate eutrophication processes and generate negative effects on the aquatic ecosystem, as the necessary DO concentration for fish and vegetation could be depleted (Zhen-Gang, 2017). The S6 was the only one where the reference limit of 2 mg/L for NH_3-N was exceeded, and this only occurred in the first simulated months. NH_3-N reached a maximum concentration of 2.7mg/L. These parameters showed a tendency to increase during the dry season, which indicates that the river is not able to assimilate them when the flow is reduced by half and the discharge flow and concentrations increase five times. It is important to keep in mind that in high concentrations ammonia nitrogen can be toxic to aquatic life (Von-Sperling, 2007). These results contrast with those found by Husaini *et al.* (2007), where the highest concentrations were found in the wet season; while in the investigations of Girardi *et al.* (2016); Benjumea *et al.* (2018) and Villota-López *et al.* (2021), higher concentrations were found in the dry season, this is associated with the low dilution due to the decrease in flows during this season. Wang *et al.* (2015) also found that the assimilative capacity in terms of water environmental carrying capacity, tends to be lower for these parameters in the dry season because of the lower water level and degradation ability, while the larger water volume and good dynamic conditions in the wet season were positive to the assimilative capacity.

Phosphates

In general, it can be considered that the river assimilation capacity for this parameter is good because its degradation is observed over time, and at the end of the simulation, the phosphate concentrations are significantly lower than dry season concentrations; this coincides with the general notion that the increase of river flow can decrease the pollutant concentration over time because the dilution and self-purification effects increase;

this happens most frequently when the river's contaminants are mainly from point sources (Meng *et al.,* 2020). Phosphates time series show higher concentrations of this parameter in the dry season (Fig. 8) reaching a maximum concentration of 0.98 mg/L, this is attributed to the increase of pollutants and nutrients concentrations caused by reduced flows and decreased dilution capacity, this may also contribute to algal blooms and decay of DO levels (Montes *et al.,* 2013) especially if the river conditions are those of S6. The most detrimental scenario to the river is S6, since its conditions cause a very significant increase in phosphate concentrations during the dry season, when the reference limit of 0.5 mg/L is exceeded. Scenarios 1, 3 and 4 also show that during the first days of the simulation the limit is exceeded, which indicates that this parameter is sensitive to changes in discharge concentrations, since in scenario 2, where only the river flow decreased, the concentrations varied little compared to the actual state, and did not exceed the limit. During the wet season, phosphate concentrations do not exceed the limit in any of the simulated scenarios. Similar behaviors can be found in several investigations, higher concentrations in the dry season and lower in the wet season (Peña, 2019; Pan *et al*., 2020). Todorova *et al.,* (2017) studied phosphatases as a tool to assess self-purification effectiveness at different types of pollution in running waters since it has a positive correlation with phosphate concentrations and found its great value in terms of wastewater risk identification and evaluation of organic and nutrient loading in streams.

Total suspended solids

Fig. 8 shows that, unlike the other parameters, TSS tend to increase in most months. In the dry season, the concentrations of this parameter are significantly lower than in the wet season, this is associated with the increase of erosion processes during the wet season, this has been evidenced too in different investigations (Agustine *et al.,* 2018; Benjumea *et al.,* 2018). Although the increase of TSS is significant in the wet season, the quality standard of 90 mg/L is not exceeded in any of the scenarios which implies a good assimilation capacity in the river. The Sinú River can assimilate the most extreme conditions (S6), without exceeding the quality standard. On the contrary, in Zubaidah *et al.,* (2018) investigation, TSS loads were higher than the assimilative capacity value causing a detriment in the studied river water quality. TSS analysis is very important for water resource quality studies since it can influence the variability of other parameters. One of its main effects is photosynthetic activity reduction due to light passage loss (Rubio *et al.,* 2017; Cahyono *et al.,* 2019), in the same way, high TSS concentrations suffocate benthic habitats and interfere with feeding activities; additionally, suspended particles promote the absorption of nutrients, organic compounds and other potential pollutants (Graham *et al.,* 2014).

Longitudinal profiles

When analyzing the graphs in Fig. 9, it is found that none of the scenarios show a lower concentration than the reference limit (4 mg/L) for DO. Also, it is observed that in all scenarios DO concentrations during the wet season are higher than in the dry season, which matches with what is reported in the literature, where precipitation has a positive effect on DO (Muñoz *et al*., 2015; Liu *et al.,* 2020). The highest DO concentrations for all scenarios are found upstream of the first discharge (WWTP Southwestern) and the lowest downstream of the second discharge (WWTP Northeastern), with S6 being the scenario that makes oxygen availability vary the most in the two seasons, presenting values higher than 6.04 mg/L in the dry season and 6.79 mg/L in the wet season. DO and COD variability against distance was also investigated by Zubaidah *et al.,* (2019), the diffuse mixture of pollutant loads caused the dissolved oxygen concentration to decrease in downstream points, while the COD increased; however, the self-purification process could take place along the river, mainly in the middle zone of the studied section. Similar findings had Churun *et al.,* (2019) research, the assimilative process was observed in the location with the greater effluent concentration, DO decrease and then showed an increasing trend. Sinú River's results also show a slight decrease of DO immediately after each discharge, but over time, the concentration tends to be higher in the wet season, indicating once again a better assimilative capacity in this season Fig. 9.

In COD's case, none of the scenarios exceeds the established limit concentration (20 mg/L) in the wet season, but in the dry season it is exceeded after the second discharge in S6, presenting a maximum value

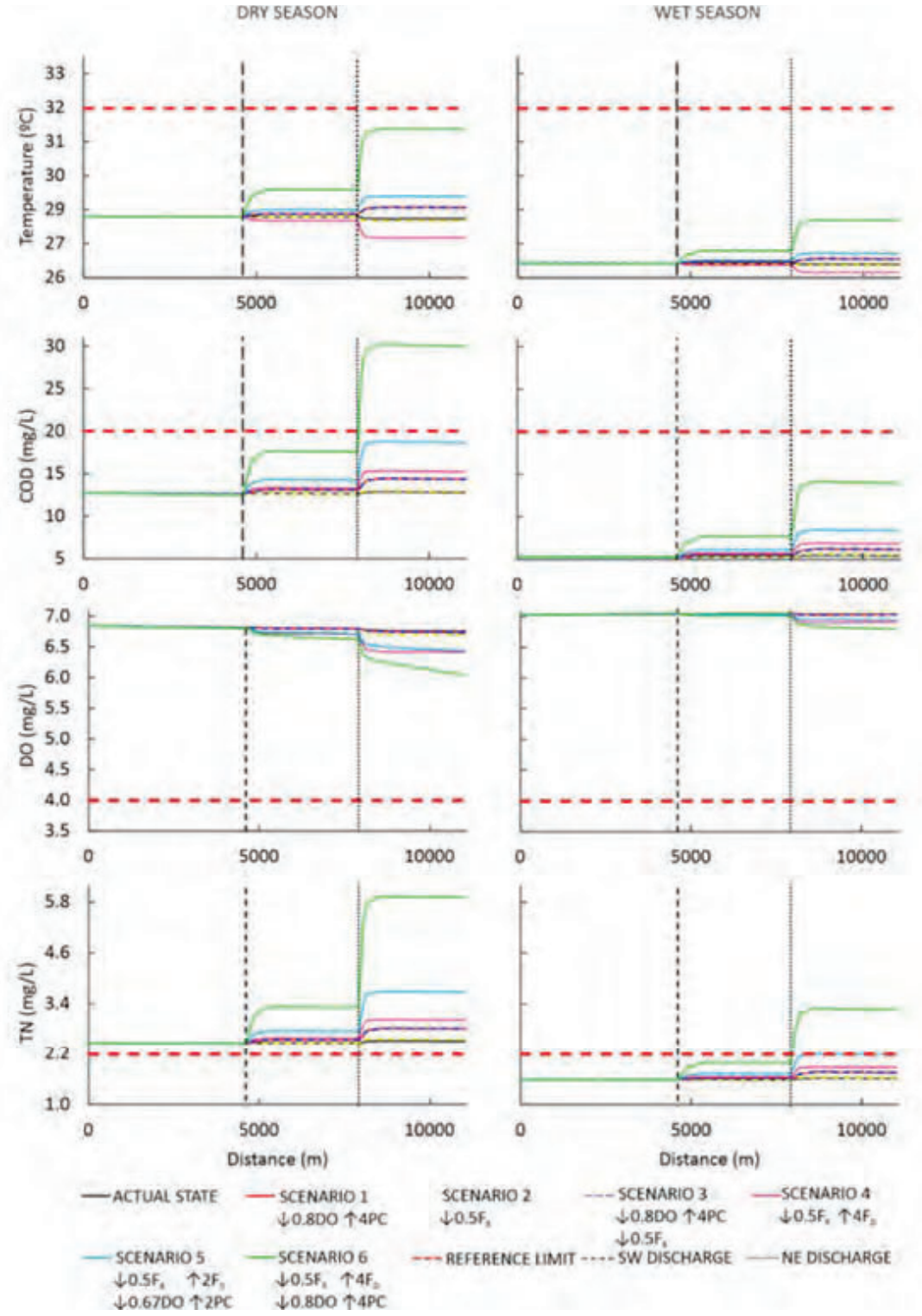

Fig. 9: Longitudinal profiles for temperature, COD, DO y TN

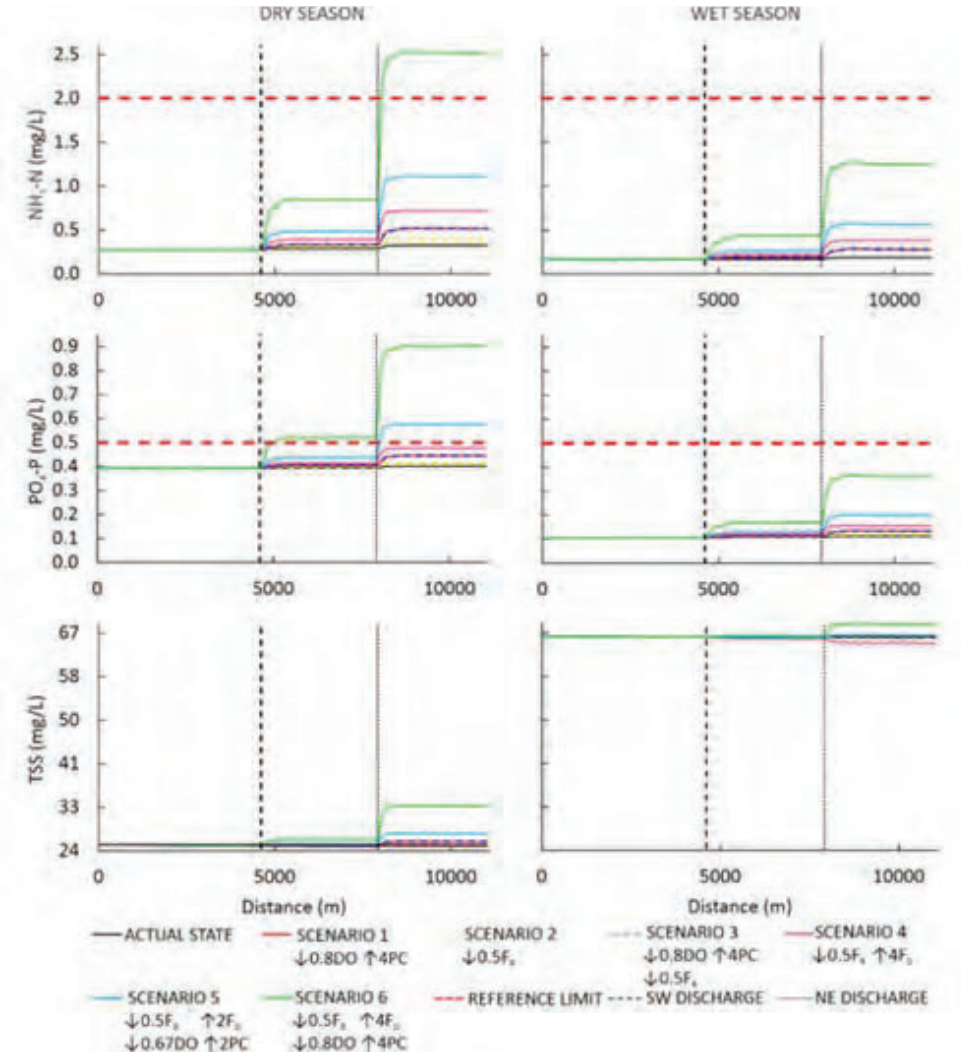

Fig. 10: Longitudinal profiles for PO_4-P, NH_3-N y TSS

of 30.9 mg/L, being this, as well as the DO, the scenario with the greatest variations in COD concentrations. For each scenario, the concentrations in the dry season are higher than during the wet season, as mentioned above, this is because the decrease in flows during the dry season generates a higher concentration of pollutant loads, which causes a decrease in DO and an increase in COD, due to decomposition processes (Liu *et al.,* 2020). It's important to understand that rivers' assimilative capacity is a complex process that also involves the simultaneous work of physical, chemical, and biological processes, and the water pollutants are reduced mostly through biodegradation processes (Taseiko *et al.,* 2016).

In the dry season, all the TN scenarios exceed the reference limit (2.18 mg/L), while in the wet season only S5 and S6 exceed it after the WWTP Northeastern discharge (Fig. 9), with a maximum value of 2.19 mg/L for S5 and 3.31 mg/L for S6. For all scenarios, TN concentrations are also higher during the dry season than the wet season, with greater variations after the wastewater discharges and especially after the second discharge (WWTP Northeastern). S6 is the scenario with the greatest variability in both periods. This situation also occurs for N-NH_3 and PO_4-P. Benjumea *et al.* (2018), found similar results for TN, NH_3-N and PO_4-P, and suggested that it was due to a high presence of organic matter and that the

low flow in the dry season does not allow dilution of these nutrients, in consequence, a lower assimilative capacity is shown. In addition, Toja *et al.* (2003) found higher concentrations of nitrogen and phosphates in low water levels in the Agrío and Guadimar rivers in Spain, attributing the low discharges dilution to the low rivers flow. Comparable results are shown in Meng *et al.,* (2020), rivers' concentration in their study area fluctuates during the research period, these parameters increase first and then decrease due to the pollutant assimilation, and this also happens in Sinú River. Temperature has higher concentrations during the dry season than during the wet season. Meanwhile, the TSS show higher concentrations in the wet season than in the dry season since rainwater movement and surface runoff promote sediments detachment and dragging. Like previous parameters, the greatest variations in concentration occur after the discharges, especially after the Northeastern discharge. Unlike the other parameters, which in all scenarios after the discharges there was only an increase (TN, NH_3-N, COD, PO_4-P) or only a decrease (DO) in the concentrations obtained in the simulations, this was not the case for temperature and TSS, because while in scenarios S1, S3, S5 and S6 their concentrations increased, in scenarios S2 and S4 their concentrations decreased after the discharges. It should be noted that for S2 and S4 there was no change in discharge concentrations, only in flow rates.

CONCLUSION

EFDC Explorer hydrodynamic and water quality model implementation showed an adequate fit of the measured data compared to those calculated by the model, especially for river water level, temperature, phosphates and total nitrogen, giving confidence in the model's adaptability to the river hydrodynamic and water quality conditions. For this reason, its use become one of the main tools for the Sinú River basin management and provide a bigger approach regarding Sinú River assimilative capacity. Model spatiotemporal simulations and the evaluated scenarios showed the discharges' effect on Sinú River's assimilative capacity since some parameters (TN, NH_3-N, COD, PO_4-P) exceeded the established reference levels and these are relevant to meet the necessary water quality criteria to keep a healthy aquatic ecosystem. It was possible to evaluate the assimilative capacity over time, observing a better assimilation for parameters such as COD, DO, PO_4-P, TN and NH_3-N during the wet season than the dry season. In general, it can be considered that Sinú River's assimilation capacity is good over time. In addition, it was found that Sinú River is more sensitive to changes in discharge flows than changes in discharge concentrations, the river was mostly affected by the decrease of its flow in half, and the 400% increase in current point sources flows; this notion can influence the river's planning and prevention programs in terms of wastewater flows that can be supported by the river without depleting its assimilative capacity; since this aspect is not currently taken into consideration for its management. Sinú River water quality modeling serves as a starting point for the competent environmental authorities to evaluate the river's self-purification ability under the current discharge conditions and predict which conditions this natural process gets affected; it constitutes a fundamental tool for the planning, design, and implementation of water resource pollution control programs and the development of effective water quality objectives.

AUTHOR CONTRIBUTIONS

F. Torres-Bejarano performed the experimental design, sampling campaigns, water quality analysis, and prepared the manuscript text. M. Verbel-Escobar performed the literature review and the model configuration and simulations, analyzed, and interpreted the data and results. M.C. Atencia-Osorio organized the methodology, analyzed, and interpreted the data and results, prepared the manuscript text, and manuscript edition.

ACKNOWLEDGEMENT

Authors are grateful to the University of Córdoba and especially to the Environmental Engineering Program for the support provided to carry out this investigation project.

CONFLICT OF INTEREST

The authors declare no potential conflict of interest regarding the publication of this work. In addition, the ethical issues including plagiarism, informed consent, misconduct, data fabrication and, or falsification, double publication and, or submission, and redundancy have been completely witnessed by the authors.

ABBREVIATIONS

^oC	Degree Celsius
AS	Actual state
A_b	Vertical turbulent eddy viscosity
AC	Assimilative capacity
A_H	Horizontal momentum and mass diffusivity
A_H	Horizontal turbulent eddy diffusivity
ANC_x	Nitrogen-carbon ratio constant in algal group *x*
AOCR	Dissolved oxygen to carbon ratio in respiration
AONT	Mass of dissolved oxygen consumed per unit mass of ammonium nitrogen nitrified
APC	Mean algal phosphorus-to-carbon ratio for all algal groups
Aut	Automatic
A_v	Vertical turbulent eddy viscosity
BFCOD	Sediment flux of chemical oxygen demand
$BFNH_4$	Water-sediment ammonium flux exchange
BFPO4d	Sediment-water exchange flux of phosphate
BM_x	Basal metabolism rate of algal group *x*
B_x	Algal biomass of algal group *x*
C	Concentration or intensity of transport constituent
C_j	represents the concentration of the j^{th} sediment class
COD	Chemical oxygen demand
c_p	Vegetation resistance coefficient
CVS	Regional Autonomous Corporation of the Sinú and San Jorge Valleys
d	Day
DO	Dissolved oxygen
DO	Dissolved oxygen concentration (equation)
DOC	Concentration of dissolved organic carbon
DON	Dissolved organic nitrogen concentration
DOP	Dissolved organic phosphorus concentration
DO_s	Saturated concentration of dissolved oxygen
D_p	Projected vegetation area normal to the flow per unit horizontal area
DWTP	Drinking water treatment plant
DX	Distance on the *X* axis
DY	Distance on the Y axis
EFDC	Environment Fluid Dynamics Code
F	Flow
f	Coriolis parameter
FCD_x	Fraction of basal metabolism exuded as dissolved organic carbon
F_D	Discharge flow
FNIP	Fraction of nitrogen produced and stripped as inorganic nitrogen
FNI_x	Fraction of nitrogen metabolized by algal group *x* produced as inorganic nitrogen

FPIP	Fraction of predated phosphorus produced as inorganic phosphorus
F_R	River flow
H	Total depth
h	Water depth bellow the vertical reference level
i	Cell
IDEAM	Institute of Hydrology, Meteorology and Environmental Studies
IWA	International water association
k_a	Reaeration Rate
K_{COD}	oxidation rate of chemical oxygen demand
k_d	Deoxygenation Rate
K_{DON}	Rate of dissolved organic nitrogen mineralization
K_{DOP}	Dissolved organic phosphorus mineralization rate
KH_{COD}	Half-saturation constant of dissolved oxygen required for oxidation of *COD*
k_{hn}	Hydrolysis Rate of organic nitrogen
k_{hPO}	Hydrolysis Rate of organic phosphorus
K_{HR}	Heterotrophic respiration rate of dissolved organic carbon
KHR_x	Half-saturation constant of dissolved oxygen for algal dissolved organic carbon excretion for group *x*
km	Kilometer
K_{Nit}	Nitrification rate
K_R	Reaeration coefficient
k_s	Sedimentation Rate of suspended solids
L	Liter
m	Meter
mg	Milligram
mm	Millimeter
m_x	Square roots of the diagonal components of the metric tensor
m_y	Square roots of the diagonal components of the metric tensor
N	North
N	Sample size
NC	No change
NE	Northeastern
NH_3-*N*	Ammonia nitrogen
NH_4	Ammonium nitrogen concentration
NOAA	National Oceanic and Atmospheric Administration
O_i	Measured data
p	Physical pressure in excess of the reference density hydrostatic pressure
P1	Monitoring point 1
P2	Monitoring point 2
P3	Monitoring point 3
P4	Monitoring point 4
P_{atm}	Barotropic pressure
PC	Physicochemical
P_i	Simulated data
PN_x	preference for ammonium uptake by algal group *x*
PO4d	Dissolved phosphate
PO4p	Particulate (sorbed) phosphate
PO_4-*P*	Phosphates
PO4t	Total phosphate concentration
PR_x	Predation rate of algal group
RMSE	The Root Mean Square
s	Second
S1	Scenario 1
S2	Scenario 2
S3	Scenario 3
S4	Scenario 4
S5	Scenario 5
S6	Scenario 6
S_c	Internal and external sources and sinks per unit volume
SD	Standard deviation
$S^E_{s,j}$	external source-sink term
$S^I_{s,j}$	Internal source-sink term

SOD	Sediment oxygen demand, applied to the bottom layer only
S_u	Source/sink term for the horizontal momentum in the x direction
S_v	Source/sink term for the horizontal momentum in the y direction
SW	Southwestern
T	Temperature
t	Time
TN	Total nitrogen
TSS	Total suspended solids
u	Horizontal velocity components in the curvilinear coordinate
US EPA	United States Environmental Protection Agency
v	Horizontal velocity components in the curvilinear coordinate
V	Cell volume
VIMS	Virginia Institute of Marine Science
W	West
w	Vertical velocity component
w_s	Particle settling velocity
WCOD	External loads of chemical oxygen demand
WNH_4	External ammonium loads
WOD	External loads of dissolved oxygen
WPO4t	External loads of total phosphate
WS_{TSS}	Sedimentation rate of the suspended solid
WWTP	Wastewater treatment plant
x	Orthogonal curvilinear coordinates in the horizontal direction
y	Orthogonal curvilinear coordinates in the horizontal direction
ζ	Water surface elevation above the vertical reference level
ρ	Water density

REFERENCES

Acosta, K., (2013). La economía de las aguas del río Sinú. Banco de la República - Center for Regional Economic Studies (CEER). Cartagena. 194: 17 -39 **(23 pages)**.

Aguilar, S.; Solano, G., (2018). Evaluación del impacto por vertimientos de aguas residuales domésticas, mediante la aplicación del índice de contaminación (ICOMO) en Caño Grande, localizado en Villavicencio-Meta. Bachelor's Thesis, Santo Tomás University, Colombia **(80 pages)**.

Agustine, A.; Wuana, R.A.; Silas, I., (2018). Seasonal variation in water quality parameters of river Mkomon Kwande local government area, Nigeria. Int. J. Recent Res. Phys. Chem. Sci., 5(1): 42-62 **(21 pages)**.

Al-Badaii, F.; Shuhaimi-Othman, M.; Gasim, M.B., (2013). Eater quality assessment of the Semenyih river, Selangor, Malaysia. J. Chem., 2013: 1–10 **(10 pages)**.

Benjumea Hoyos, C.A.; Suárez-Segura, M.A.; Villabona-González, S.L., (2018). Temporary and spatial variation of nutrients and total suspended solids in the basin of a high mountain tropical river. Rev. Academia Colomb. Cienc. Exactas, Fis. y Naturales. 42(165): 353–363 **(11 pages)**.

Cahyono, B.E.; Jamilah, U.L.; Misto; Nugroho, A.T.; Subekti, A., (2019). Analysis of total suspended solids (TSS) at Bedadung River, Jember District of Indonesia using remote sensing Sentinel 2A data. Singapore J. Sci. Res., 9: 117-123 **(7 pages)**.

Cely-Calixto, N.J.; Bonilla-Granados, C.A.; Carrillo Soto, G.A., (2021). A mathematical model for the simulation of the Magdalena River in the city of Barrancabermeja, Colombia. J. Phys. Conf. Ser., 1981: 012016 **(7 pages)**.

Chapra, S.C., (2018). Advances in river water quality modelling and management: Where we come from, where we are, and where we're going? Green energy and technology. Springer: 295–301 **(7 pages)**.

Chapra, S.C.; Camacho, L.A.; McBride, G.B., (2021). Impact of global warming on dissolved oxygen and BOD assimilative capacity of the world's rivers: Modeling analysis. Water, 13(17): 2408 **(20 pages)**.

Churun, A.; Siti, R.; Haeruddin; Heppi Puspita, S. (2019). Purification capacity and oxygen sag in Sringin River, Semarang. Int. J. Appl. Environ. Sci., 14(1): 1-16 (**16 pages**).

Cuesta-Parra, D.; Velazco-Rincón, C.; Castro-Pardo, J., (2018). Environmental assessment related to the sewage water discharge of a tannery company into Aburrá River. Rev. UIS Ing., 17(2): 141–151 **(11 pages)**.

CVS, (2004). Plan de ordenamiento y manejo de cuencas hidrográficas del río Sinú. Diagnóstico ambiental de la cuenca hidrográfica del río Sinú. Montería, Colombia **(88 pages)**.

Dehghani Darmian, M.; Khodabandeh, F.; Azizyan, G.; Giesy, J.P.; Hashemi Monfared, S.A., (2020). Analysis of assimilation capacity for conservation of water quality: controllable discharges of pollutants. Arabian J. Geosci., 13: 888 **(13 pages)**.

DSI, (2020). EFDC+ Theory Document. Version 10.2. Edmonds, United States **(284 pages)**.

Egbe, J.G.; Agunwamba, J.C.; Okon, E.E., (2018). Modeling and modification of the effect of self purification of Kwa river pollution. Int. J. Curr. Res. Acad. Rev., 6(9): 83-89 **(7 pages).**

Feria Díaz, J.J.; Náder Salgado, D.; Meza Pérez, S.J., (2017). Deoxygenation and re-aeration rates of the Sinu river. Ing. Desarrollo, 35(1): 1-17 **(17 pages)**.

Girardi, R.; Pinheiro, A.; Pospissil, L.; Torres, É., (2016). Water quality change of rivers during rainy events in a watershed with different land uses in Southern Brazil. Braz. J. Water Resour., 21(3): 514–524 **(11 pages)**.

Graham, J.L.; Stone, M.L.; Rasmussen, T.J.; Foster, G.M.; Poulton, B.C.; Paxson, C.R.; Harris, T.D., (2014). Effects of wastewater effluent discharge and treatment facility upgrades on environmental and biological conditions of Indian Creek, Johnson County, Kansas, June 2004 through June 2013: U.S. Geological Survey Scientific Investigations Report 2014–5187 **(92 pages).**

Gurjar, S.K.; Tare, V., (2019). Spatial-temporal assessment of water quality and assimilative capacity of river Ramganga, a tributary of Ganga using multivariate analysis and QUEL2K. J. Cleaner Prod., 222: 550–564 **(15 pages).**

Hashemi Monfared, S.A.; Dehghani Darmian, M.; Snyder, S.A.; Azizyan, G.; Pirzadeh, B.; Moghaddam, M.A., (2017). Water quality planning in rivers: assimilative capacity and dilution flow. Bull. Environ. Contam. Toxicol., 99(55): 531–541 **(11 pages)**.

Husaini, C.; Gbodi, A.; Orisakwe, O.; Ogbadoyi, E.; Ali, J.; Hussaini, M.; Garba, S.; Afonne, J.; Pam, H., (2007). Seasonal nitrate content of stream water, soil and some foodstuffs samples in Abuja municipal area of Federal Capital Territory, Nigeria. J. Health Sci., 53(4): 359–364 **(6 pages)**.

Imam, E.; El Baradei, S., (2006). Ecosystem and assimilative capacity of rivers with control structures. WIT Trans. Ecol. Environ., 95: 435 – 444 **(10 pages)**.

Islam, M.S.; Uddin, M.K.; Tareq, S.M.; Shammi, M.; Kamal, A.K.I.; Sugano, T.; Kurasaki, M.; Saito, T.; Tanaka, S.; Kuramitz, H., (2015). Alteration of water pollution level with the seasonal changes in mean daily discharge in three main rivers around Dhaka City, Bangladesh. Environ., 2(3): 280–294 **(15 pages).**

IDEAM, (2017). Protocolo de monitoreo del agua. Bogotá, D. C., Colombia **(587 pages).**

IWA, (2018). Wastewater Report 2018. The Reuse Opportunity. **(24 pages).**

Jaya, F., (2017). Estudio de los sólidos suspendidos en el agua del rio Tabacay y su vinculación con la cobertura vegetal y usos del suelo en la microcuenca. Bachelor's Thesis Cuenca University, Ecuador **(103 pages).**

Jingsheng, C.; Tao, Y.; Ongley, E., (2006). Influence of high levels of total suspended solids on measurement of COD and BOD in the Yellow river, China. Environ. Monit. Assess., 116: 321–334 **(14 pages)**.

Kim, J.; Lee, T.; Seo, D., (2017). Algal bloom prediction of the lower Han River, Korea using the EFDC hydrodynamic and water quality model. Ecol. Modell., 366: 27-36 **(10 pages).**

Kulikova, D.; Kovrov, O.; Buchavy, Y.; Fedotov, V., (2018). GIS-based Assessment of the Assimilative Capacity of Rivers in Dnipropetrovsk Region. J. Geol. Geogr. Geoecol., 27(2): 274-285 **(12 pages)**.

Lee, I.; Hwang, H.; Lee, J.; Yu, N.; Yun, J.; Kim, H., (2017). Modeling approach to evaluation of environmental impacts on river water quality: A case study with Galing River, Kuantan, Pahang, Malaysia. Ecol. Modell., 353: 167-173 **(7 pages)**.

Liu, G.; He, W.; Cai, S., (2020). Seasonal variation of dissolved oxygen in the southeast of the Pearl River estuary. Water. 12: 2475 **(18 pages)**.

Liu, Q.; Jiang, J.; Jing, C.; Qi, J., (2018). Spatial and seasonal dynamics of water environmental capacity in mountainous rivers of the Southeastern Coast, China. Int. J. Environ. Res. Public Health. 15(1): 99 **(21 pages)**.

Meng, Chunfang; Song, Xiaoyu; Tian, Kening; Ye, Bingxiao; Si, Tianxiu, (2020). Spatiotemporal variation characteristics of water pollution and the cause of pollution formation in a heavily polluted river in the upper Hai River. J. Chem., 2020: **(15 pages).**

Montes, R.; Navarro, I.; Domínguez, R.; Jiménez, B., (2013). Modificación de la capacidad de autodepuración del río Magdalena ante el cambio climático. Tecnol. Cienc. Agua, 4(5): 71-83 **(13 pages)**.

Muñoz, H.; Orozco, S.; Vera, A.; Suárez, J.; García, E.; Neria, M.; Jiménez, J., (2015). Relationship between dissolved oxygen, rainfall and temperature: Zahuapan River, Tlaxcala, Mexico. Tecnol. Cienc. Agua, 6(5): 59-74 **(16 pages)**.

Novo, P., (2017). Accounting for the assimilative capacity of water systems in Scotland. Water, 9(8): 559 **(13 pages)**.

Obin, N.; Tao, H.; Ge, F.; Liu, X., (2021). Research on water quality simulation and water environmental capacity in Lushui river based on WASP model. Water, 13(20): 2819 **(20 pages)**.

Pan, L.; Dai, J.; Wu, Z.; Wan, Z.; Zhang, Z.; Han, J.; Li, Z.; Xie, X.; Xu, B., (2020). Spatio-temporal dynamics of riverine nitrogen and phosphorus at different catchment scales in Huixian Karst Wetland, Southwest China. Water, 12(10): 2924 **(23 pages)**.

Patel, H.; Vashi, R.T., (2015). Chapter 2 - Characterization of textile wastewater. Characterization and treatment of textile wastewater, Elsevier Inc. 21–71 **(51 pages)**.

Peña, D., (2019). Diagnóstico de la calidad del agua de la Microcuenca quebradas las delicias cerros orientales de Bogotá a partir de los parámetros químicos de acuerdo con la normativa legal vigente. Bachelor's Thesis, Cooperative University of Colombia **(77 pages)**.

Quinn, N.W.T.; Tansey, M.K.; Lu, J., (2021). Comparison of deterministic and statistical models for water quality compliance forecasting in the San Joaquin river basin, California. Water, 13(19): 2661 **(32 pages)**.

Ramos, L.Á., (2018). Estudio de la dinámica del cromo en la cuenca alta del río Bogotá mediante la selección y aplicación de un modelo de calidad de agua para la representación de contaminantes conservativos en cuerpos de agua lóticos. Bachelor's Thesis, National Open and Distance University, UNAD Institutional Repository **(131 pages)**.

Ritter, A.; Muñoz-Carpena, R., (2013). Performance evaluation of hydrological models: Statistical significance for reducing subjectivity in goodness-of-fit assessments. J. Hydrol., 480: 33–45 **(13 pages)**.

Rubio, A.; Amézquita, L.; Martínez, E., (2017). Determinación de la capacidad de asimilación del vertimiento de la PTAR del municipio de Tenjo, Cundinamarca en la quebrada Churuguaco mediante el modelo QUAL2KW. Water Resources Specialization, Universidad Católica De Colombia **(161 pages)**.

Taseiko, O.; Spitsina, T.P.; Milosevic, H.; Radavanovic, D.; Valjarevic, A., (2016). Biochemical processes of self-purification model in small rivers. Math. Inf. Technol., 487 – 495 **(9 pages).**

Todorova, Y.; Schneider, I.; Yotinov, I.; Lincheva, S.; Topalova, Y., (2017). Potential of phosphatases for express assessment of self-purification at different types of pollution in running waters. Water Pract. Technol., 12(4): 953–963 **(11 pages).**

Torres-Bejarano, F.; Padilla Coba, J.; Rodríguez-Cuevas, C.; Ramírez-León, H.; Cantero-Rodelo, R., (2016). The hydrodynamic modelling for the water management of el Guájaro Reservoir, Colombia. Rev. Int. Metodos Numer. Calc. Diseno Ing., 32(3): 163-172 **(10 pages)**.

Torres-Bejarano, F.; Torregroza-Espinosa, A.; Martinez-Mera, E.; Castañeda-Valbuena, D.; Tejera-Gonzalez, M. (2020). Hydrodynamics and water quality assessment of a coastal lagoon using environmental fluid dynamics code explorer modeling system. Global J. Environ. Sci. Manage., 6(3): 289-308 **(20 pages)**.

Toja, J.; Alcalá, E.; Burgos, M.D.; Martín, G.; Plazuelo, A.; Schutter, T.; Prat, N.; Plans, M; Solá, C., (2003). Efecto del vertido tóxico en las comunidades de plancton y perifiton del río Guadiamar. Ministry of Environment. Regional Government of Andalusia **(16 pages)**.

Valbuena, D., (2017). Geomorfología y condiciones hidráulicas del sistema fluvial del rio Sinú. Integración multiescalar 1945 - 1999 - 2016. Master's Thesis, Colombia National University, Bogotá, Colombia **(21 pages)**.

Villota-López, C.; Rodríguez-Cuevas, C.; Torres-Bejarano, F.; Cisneros-Pérez, R.; Cisneros-Almazán, R.; Couder-Castañeda, C., (2021). Applying EFDC Explorer model in the Gallinas River, Mexico to estimate its assimilation capacity for water quality protection. Sci. Rep., 11(1): 13023 **(16 pages)**.

Von-Sperling, M., (2007). Wastewater Characteristics, Treatment and Disposal. IWA Publishing Volume 1 **(306 pages)**.

Wang, H.; Zhou, Y.; Tang, Y.; Wu, M.; Deng, Y., (2015). Fluctuation of the water environmental carrying capacity in a Huge River-Connected Lake. Int. J. Environ. Res. Public Health, 12(4): 3564–3578 **(15 pages)**.

Yiping, Li.; Kumud, Acharya.; Zhongbo, Yu., (2011). Modeling impacts of Yangtze River water transfer on water ages in Lake Taihu, China. Ecol. Eng., 37(2): 325-334 **(10 pages).**

Yuceer, M.; Coskun, M.A., (2016). Modeling water quality in rivers: A case study of Beylerderesi River in Turkey. Appl. Ecol. Environ. Res., 14(1): 383-395 **(13 pages).**

Zhen-Gang, J., (2017). Hydrodynamics and water quality: modeling Rivers, lakes, and estuaries. Second Edition, John Wiley & Sons Inc **(577 pages).**

Zubaidah, T.; Karnaningroem, N.; Slamet, A., (2018). Pollutant load and assimilation capacity in Martapura river, South Kalimantan, Indonesia. Built Environ. Sci. Technol. Int. Conf., 226-229 **(4 pages).**

Zubaidah, T.; Karnaningroem, N.; Slamet, A., (2019). The self-purification ability in the rivers of Banjarmasin, Indonesia. J. Ecol. Eng., 20(2): 177-182 **(6 pages)**.

AUTHOR (S) BIOSKETCHES

Torres-Bejarano, F., Ph.D., Associate Professor, Departament of Environmental Engineering, University of Córdoba, Carrera 6 No. 77-305, Montería, Colombia.
- Email: franklintorres@correo.unicordoba.edu.co
- ORCID: 0000-0003-3144-7289
- Web of Science ResearcherID: AAB-6324-2022
- Scopus Author ID: 22955027500
- Homepage: https://www.researchgate.net/profile/Franklin-Torres-Bejarano/

Verbel-Escobar, M., B.Sc., Environmental Engineering Program, University of Córdoba, Carrera 6 No. 77- 305, Montería, Colombia.
- Email: mverbelescobar73@correo.unicordoba.edu.co
- ORCID: 0000-0002-7350-9890
- Web of Science ResearcherID: NA
- Scopus Author ID: NA
- Homepage: https://38.academia.edu/MelanieVerbelEscobar

Atencia-Osorio, M.C., B.Sc., Environmental Engineering Program, University of Córdoba, Carrera 6 No. 77- 305, Montería, Colombia.
- Email: matenciaosorio39@correo.unicordoba.edu.co
- ORCID: 0000-0001-8482-0687
- Web of Science ResearcherID: NA
- Scopus Author ID: NA
- Homepage: https://unicordoba.academia.edu/MariaCamila97

HOW TO CITE THIS ARTICLE

Torres-Bejarano, F.; Verbel-Escobar, M.; Atencia-Osorio, M.C., (2022). Water quality model-based methodology to assess assimilative capacity of wastewater discharges in rivers. Global J. Environ. Sci. Manage., 8(4): 449-472.

DOI: 10.22034/gjesm.2022.04.01

url: https://www.gjesm.net/article_249277.html

Global J. Environ. Sci. Manage. 8(4): 473-484, Autumn 2022, Serial #32

Global Journal of Environmental Science and Management
(GJESM)

Homepage: https://www.gjesm.net/

ORIGINAL RESEARCH PAPER

Water resources carrying capacity before and after volcanic eruption

M. Dede[1], S.B. Wibowo[2], Y. Prasetyo[3], I.W. Nurani[2,4], P.B. Setyowati[5], S. Sunardi[1,6,7*]

[1] *Center for Environment and Sustainability Science, Universitas Padjadjaran, Bandung City, Indonesia*

[2] *Faculty of Geography, Universitas Gadjah Mada, Yogyakarta, Indonesia*

[3] *Department of Geodetic Engineering, Faculty of Engineering, Universitas Diponegoro, Semarang City, Indonesia*

[4] *Doctoral Program, Université Paris 1 Panthéon-Sorbonne, Paris, France*

[5] *Faculty of Agriculture, Universitas Brawijaya, Malang, Indonesia*

[6] *Environmental Sciences Program, Postgraduate School, Universitas Padjadjaran, Bandung City, Indonesia*

[7] *Department of Biology, Faculty of Mathematics and Natural Sciences, Universitas Padjadjaran, Sumedang, Indonesia*

ARTICLE INFO

Article History:
Received 04 September 2021
Revised 11 December 2021
Accepted 16 January 2022

Keywords:
Mount Merapi
Spatial-gridded model
Water availability
Water needs

DOI: 10.22034/gjesm.2022.04.02

ABSTRACT

BACKGROUND AND OBJECTIVES: Water resources carrying capacity is dynamic and can be influenced by catastrophic volcanic eruptions. The eruption of Mount Merapi in 2010 changed the landscape and community livelihoods due to the redistribution of a large volume of volcanic materials. This study aims to analyze water resources carrying capacity before and after the major 2010 eruption of Mount Merapi.

METHODS: The value of water resources carrying capacity is derived from that of water availability and the domestic water needs per capita per year. The model uses a grid of 100 x 100 meter cells to determine the spatial distribution of water resources carrying capacity in Krasak watershed, and this analysis considers the years 2008, before the eruption, and 2021, after the eruption. The population distribution data have been previously mapped by referring to statistical data and land use at the village level, while water availability is calculated considering rainfall, potential evaporation rate, and runoff.

FINDINGS: Water resources carrying capacity in Krasak watershed has undergone changes related to the distribution of volcanic material and human activities. The water resources carrying capacity for both periods experienced a surplus, although there has been an average decrease of 331.50 cubic meters per year for each grid cell. Water resources carrying capacity analysis shows a decline, especially in the midstream and downstream. Based on T-Test, there are significant changes in the water resources carrying capacity at 2008 and 2021 (p-value 0.047 and 95% confidence level).

CONCLUSION: Water resources carrying capacity increased only in some locations that occurred ecosystem succession after the eruption, although areas near the peak are decreased by sand and stone mining. The spatial-gridded model proved capable of analyzing this phenomenon.

NUMBER OF REFERENCES	NUMBER OF FIGURES	NUMBER OF TABLES
60	3	4

*Corresponding Author:
Email: *sunardi@unpad.ac.id*
Phone: +6281 1211 0064
ORCID: 0000-0001-9515-4608

Note: Discussion period for this manuscript open until January 1, 2023 on GJESM website at the "Show Article".

INTRODUCTION

Mount Merapi is an active volcano located in Central Java and the Special Region of Yogyakarta, Indonesia. Its volcanic edifice is surrounded by 10 rivers flowing to Indian Ocean in the south (Ville *et al.*, 2015; Anna *et al.*, 2016; Gob *et al.*, 2016). Merapi acts as a rain catchment area and contributes to surface water and shallow groundwater resources that meet the various needs of the surrounding community. Merapi is the most active volcano in Indonesia. Its "Merapi type" eruption is characterized by dome creation and destruction producing Pyroclastic Density Currents (PDCs) (Priatna and Kadarsetia, 2007). Basaltic-andesite lava of Merapi volcano was formed next to the subduction zone of Eurasian and Indo-Australian plates. The Eurasian plate is a continental plate type predominately composed of silica-aluminium (Si-Al) material, whereas the Indo-Australian plate is an oceanic plate with a composition of primarily silica-magnesium (Si-Mg) (Verstappen, 2010; Wang *et al.*, 2019). The interaction between these plates causes Merapi's eruptions to be divided into effusive and explosive phases, occurring alternately (Carr *et al.*, 2020). The last major eruption of Mount Merapi occurred in 2010 when volcanic ash spread up to thousands of kilometres from its crater through the air (long-range transport) (Wu *et al.*, 2019). The surrounding landscape changed drastically due to the sedimentation of pyroclastic materials and post-eruptive lahars. The Indonesian government made structural mitigation strategy to manage the cold lahar material using the 264 Sabo Dams, on the main rivers originating from Mount Merapi (Sukatja and Alfianto, 2017). The volcanic ash carried by the wind generally did not receive much attention in term of disaster mitigation because government focused on evacuating as many people as possible. Therefore, volcanic ash deposited on top soil, which damaged vegetation and caused changes in land use/cover through ecosystem succession. This phenomenon was classified as a post-disaster impact (Sutomo, 2013; Yudistira *et al.*, 2020). Ecosystem changes have a further impact, especially by decreasing the water resources carrying capacity (WRCC). Population growth and landscape changes, as signs of rural-to-urban transformation (urbanization–industrialization), have caused a decline in WRCC, thus worsening water crises (Sunardi *et al.*, 2020). The downward trend of WRCC is linearly related to socioeconomic structural changes that encourage increased water consumption and the release of wastewater into the environment. Ecosystem degradation amid the threat of climate change has become a barrier to recover water resource provisions (Cheng *et al.*, 2018; Yang and Yang, 2021). Declining WRCC is an implication of reduced vegetation cover and an increase in uncontrolled bare land, especially in areas close to population growth centres (Bangyou *et al.*, 2011; Dede and Widiawaty, 2020). Therefore, analysis of WRCC associated with Merapi can provide an important lesson about ecosystem dynamics and their impact on disaster-prone communities. WRCC analysis generally uses non-spatial approaches based on population, weather and climate, and socioeconomic and environmental data (Widodo *et al.*, 2015). Using geospatial approaches, WRCC study can surpass administrative boundaries from local scale to national scale (Lv *et al.*, 2021). The WRCC is obtained from the difference in values of water availability and the annual population's water demand in the study area based on spatial grids, especially in 2008 (pre-eruption) and 2021 (post-eruption). Few WRCC studies ignore geospatial aspects. It is only formulated by tabular data and even if using geospatial analysis, the analysis does not refer to ecoregions (eg. watersheds) and spatial grids. This study aims to analyse the WRCC in the Krasak watershed before and after the major eruption of Mount Merapi of Indonesia in 2010. This study would be useful for disaster mitigation, especially for determining new settlements and quantifying the socioeconomic activities of relocated population in detail.

MATERIALS AND METHODS

Study area and data acquisition

This study is based on a hypothesis that WRCC may change due to massive volcanic eruptions. Krasak watershed located at southwest of Mount Merapi, Indonesia. Administratively, Krasak watershed belonged to two provinces, i.e. Central Java and the Special Region of Yogyakarta in which there were three regencies, eight sub-districts, and 21 villages covering an area of 35.48 km^2. Krasak watershed was chosen as an appropriate location for WRCC research because it was an affected area

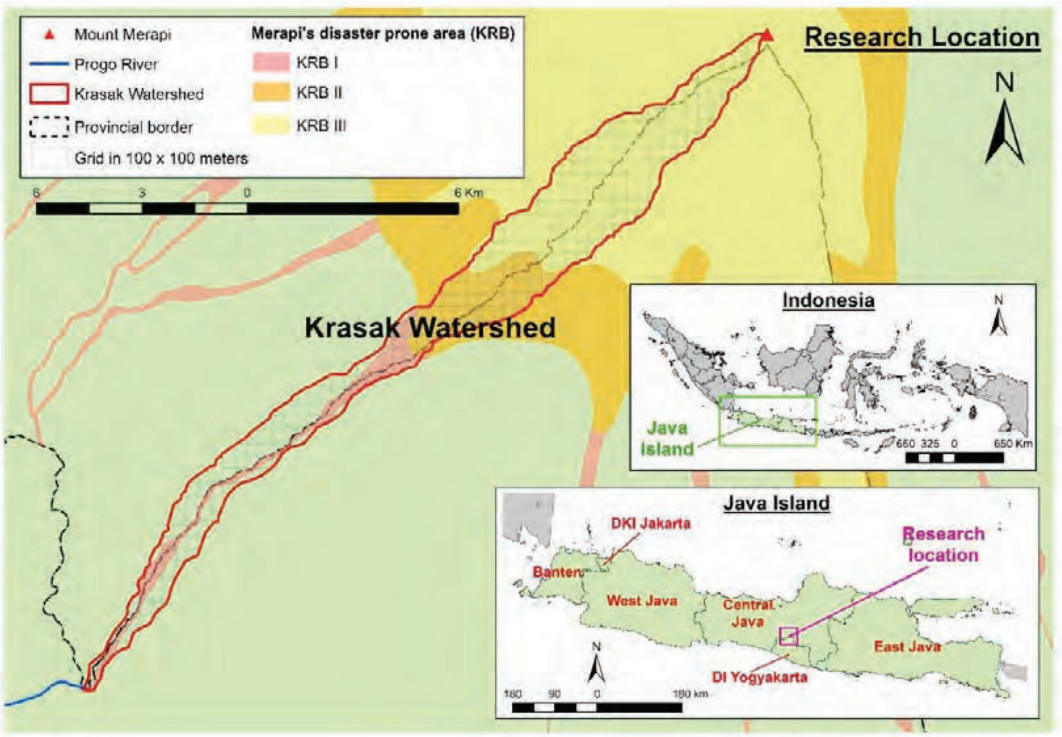

Fig. 1: Geographic location of the study area of Krasak watershed, in Indonesia (Mount Merapi is upstream and Kali Progo where is downstream of the watershed in Indonesia)

Table 1: Parameters for water resources carrying capacity

Variable	Parameter	Data source
Water availability	Rainfall	Annual rainfall
	Runoff	Rainfall intensity, land use-runoff capacity, and slope
	Potential evaporation	The geographical latitude and average temperature
Water needs	Population distribution	Population and land use data

covering three level of volcanic prone areas (KRB) during Merapi eruption in 2010 (Utami *et al*., 2018). Krasak watershed was inhabited by 28,081 people as of 2021 and possessed a complete database from previous studies (Umami *et al*., 2015; Maharani *et al*., 2016; Ikhsan *et al*., 2019b). Krasak watershed was divided by grids of 100 x 100 m to facilitate the analysis and aggregation of various parameters, as shown in Fig. 1. This analysis used the entire area of Krasak watershed, thus sample data refers to the population sample design. The grid size actually would refer to the unit of population density calculation in person per square kilometer, but the regulation of spatial data in Indonesia (Regulation of the Head of the Indonesian Geospatial Information Agency Number 3 of 2016 concerning Technical Specifications for the Village Maps) has required WRCC analysis to becomes more detailed – from 1 x 1 km to 100 x 100 m. The spatial-gridded approach differs from previous WRCC studies that were based on administrative regions of different sizes, even though the units were uniform in the legally formal context (Hastoyuando *et al*., 2020). The WRCC analysis used four parameters, i.e. rainfall, runoff capacity, potential evaporation rate, and spatial distribution of population. These parameters contributed to form variables for water availability and annual water demand (Table 1).

WRCC data processing and analysis

The WRCC calculation considered the water availability and the individual consumption per year. The WRCC value used volumetric units (m^3), with positive values indicating a surplus and negative values indicating a water resource deficit (Brontowiyono *et al.*, 2009; Tariq *et al.*, 2015; Yang *et al.*, 2019; Nikiel and Eltahir, 2021). This water requirement was not classified for agricultural activities because farmers generally provided their irrigation water from rivers and historical Mataram ditches coming from adjacent watersheds. Rainfall was derived from spatial interpolation using observational data from Governmental agencies such as Meteorology, Climatology and Geophysics Agency of Indonesia (BMKG), Indonesian Ministry of Public Works and Public Housing, and Indonesian Ministry of Agriculture. Furthermore, the runoff data were used as coefficient values for each land use type (Kodoatie and Sjarief, 2010; Tarigan, 2018; Asdak, 2020), shown in Table 2. Potential evaporation for the WRCC model was obtained from Blaney–Craddle method (Gotardo *et al.*, 2016; Mendoza and Peña, 2021). Calculation for the WRCC was presented using Eq. 1, and the analysis of the water availability was governed by Eqs. 2 to 4.

$$WRCC = WA - NW \quad (1)$$

Where WRCC is the water resources carrying capacity, WA is water availability, and NW represents the water needs per capita. This equation uses metres as international standard units using Eqs. 2 to 4.

$$WA = P - R - ET - \Delta S \quad (2)$$

$$R = 0.278 \times C \times P \times A \quad (3)$$

$$ET = p(0.46 \times T + 8.13) \quad (4)$$

Where, P is precipitation, R is runoff capacity, E is evapotranspiration, and S is the change in water storage. The parameter S for Krasak watershed was neglected because there is no significant surface reservoir in this area. Moreover, C is the runoff coefficient for each land use type, A is the catchment area, p is the annual average daytime percentage, and T is the annual average temperature.

Water needs were strongly influenced by the population and regional development characteristics, i.e. rural, urban, and peri urban. The spatial distribution of the population was useful in this analysis to understand the details. Therefore, a grid model as part of spatial approaches should be considered (Raju, 2004; Siljander, 2010; Widiawaty, 2019). In the case of Krasak watershed, land use data from the Indonesian Ministry of Environment and Forestry and population data from the Indonesian Central Statistics Agency were used for this model. Population distribution was tied to land use and regional characteristics, which required weighting (Bielecka, 2005; Mennis, 2009; Khomarudin *et al.*, 2010), as shown in Table 3. A spatial water needs analysis was performed using Eqs. 5 and 6. T-Test is used to compare the WRCC changes due to Merapi's eruption (Lohe *et al.*, 2015; Medina and Toledo-Bruno, 2016; Widiawaty *et al.*, 2020).

$$NW = Pop \times Wy \quad (5)$$

$$Pop_i = (Si / \sum ASi) \times Wi \times Pop \quad (6)$$

Where NW is the water needs per capita, Pop is the population, Wy represents the annual water needs per capita, Pop_i is the population in polygon i, Si is the area of polygon i, $\sum$ ASi is the total area of land use type i and Wi is the weight of land use type i.

RESULTS AND DISCUSSION

Merapi is an active stratovolcano in Indonesia

Table 2: Runoff coefficient (C) for land use types

Land use	C	Land use	C
Secondary forest	0.15	Bare land	0.60
Industrial forest (plantation)	0.47	Dryland farming	0.40
Bushes and shrubs	0.22	Dryland farming mixed with shrubs	0.20
Settlement	0.70	Rice field	0.52

Table 3: Weight (W) for land use types

Land use	W	Land use	C
Secondary forest	0.00	Bare land	0.00
Industrial forest (plantation)	0.03	Dryland farming	0.05
Bushes and shrubs	0.01	Dryland farming mixed with shrubs	0.02
Settlement	0.79	Rice field	0.10

Table 4: Land use in 2008 and 2021

Land use	Area (km^2)		Gain and loss	
	2008	2021	Km^2	%
Secondary forest	0.14	2.70	2.56	1826.04
Industrial forest (plantation)	3.38	0.53	−2.85	−84.37
Settlement	7.79	7.92	0.12	1.56
Dryland farming	13.33	7.28	−6.04	−45.34
Dryland farming mixed with shrubs	0.11	6.08	5.98	5649.67
Rice field	4.03	3.69	−0.33	−8.30
Bushes and shrubs	0.30	3.33	3.04	1022.07
Bare land	6.41	3.95	−2.47	−38.48

with its highest peak reaching 2930 m above sea level. Statictically, small eruptions occur every 2–3 years and larger eruptions occur every 10–15 years (Hapsari *et al.*, 2020). During its major eruption in 2010, Krasak watershed received 10.8 million m^3 of pyroclastic materials. This was the third largest after those of the Gendol watershed (24 million m^3) and Pabelan watershed (20.8 million m^3) (Kusumawardani *et al.*, 2017). Krasak watershed, located to the southwest of Mount Merapi, has been affected by 21 eruptions between the 18th and 21st centuries AD (Umaya *et al.*, 2020). The succession of ecosystems in Krasak watershed is a recurring event. The community continues to live in harmony with Mount Merapi, illustrated in part by its consistent population growth. WRCC analysis in Krasak watershed is important because it is related to the sustainability of water resources management in volcanic areas. Krasak watershed has an average elevation of 732.92 m above sea level (min: 114.48 m; max: 2871.34 m). Eleven years after Merapi's 2010 eruption, the changes in land use are characterized by increased scrub and reduced industrial forest (plantations) (Table 4). These changes are related to the pyroclastic flows (*Wedus Gembel* in Javanese), sand mining, and ecosystem succession initiated by pioneer vegetation (Utami *et al.*, 2021a, 2021b). Although Krasak watershed has a very high annual rainfall (2332–3102 mm/year), changes in land use have an impact on runoff flow and infiltration capacity, which is higher downstream than up- and midstream (Ikhsan *et al.*, 2019a). This condition affects shallow groundwater recharge at Yogyakarta-Sleman Groundwater Basin, which has become the main resource of water for residents, especially for household needs. A WRCC deficit will therefore lead to many cones of depression (Mulyadi *et al.*, 2020).

The water needs after Merapi eruption have increased due to population growth, especially at mid- and downstream of Krasak watershed. Many dryland farms have been turned into new settlements, taking up a larger area than during the post-eruption relocation as the population of Krasak watershed increased by 4.92 percent from 2008 to 2021. The regional status as a disaster-prone area has not affected people's desire to stay there because Merapi has an abundance of natural resources. These conditions have high economic value for tourism, agriculture, and animal husbandry (Priyanti and Ilham, 2011; Widodo *et al.*, 2014; Napsiah *et al.*, 2016). Global climate change, which increases the temperature, also affects the potential evapotranspiration. Krasak watershed has a threat of water loss due to these changes. In 2008, the average air temperature reached 25.90°C, and eleven years later, it increases to 27.22°C. Potential

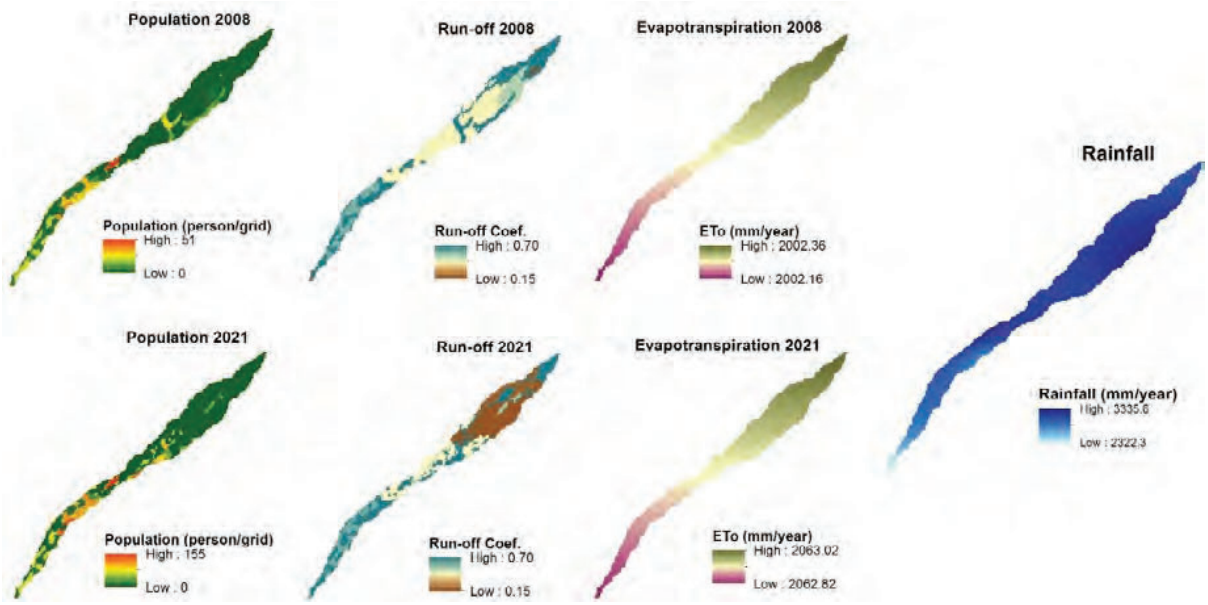

Fig. 2: Changes in WRCC parameters (rainfall is assumed to be constant according to the data span over less than 30 years)

evapotranspiration also increases significantly from 5.49 mm/day, to 5.65 mm/day for each unit area. Population growth, ecosystem changes, and increasing evapotranspiration are the main factors reducing WRCC in Krasak watershed (Fig. 2).

The population over the 13 years increases by only 1316 people, which is relatively small when compared with Indonesian average annual population growth ranging from 1.00 percent to 2.00 percent (Oey-Gardiner and Gardiner, 2013). If each resident needs 80 litres or 0.08 m^3 water per day, according to the criteria of the IMPWPH (2018) for rural areas, then each individual needs 29.20 m^3 water per year in total. It will continue to increase along with the rural-to-urban transformation of the landscape in Krasak watershed. The WRCC analysis ignored local discharges from springs due to endogenous and exogenous energy activities in the folds, faults, and weathering of rocks. There was a grid expansion of the WRCC deficit 10 years after the eruption, especially in the groundwater discharge zone close to Krasak River estuary where the confluence zone with the Progo River is located (Fig. 3). The community's water needs increased by 4.91 percent, from 781.601 m^3 (2008) to 819,973 m^3 (2021). Non-spatial WRCC calculations do not use grid units. However, Krasak watershed still has an overall surplus of more than 21 million m^3 per year. The WRCC surplus is more spread out in the recharge and transition zones, which are rarely inhabited by residents. However, between the years before Merapi's eruption in 2010, there is a significant decrease in WRCC at the transition (midstream) and discharge (downstream) of Krasak watershed. The statistical test showed this significant difference with p-value of 0.047 and 95% confidence level. Individual consumption (population growth) and ecosystem succession illustrate that WRCC is very dynamic. Therefore, these results accept the hypothesis that WRCC has a strong interaction with Merapi's eruption. Although in the initial period after the eruption, it brought losses to the landscape and communities affected by volcanic materials, a few years later, this phenomenon gave a blessing because it could rejuvenate the landscape and fertilize the soil that increasing the environmental carrying capacity (Fiantis et al., 2019), including the WRCC.

A largest surplus was found in the upstream, which has been overgrown by vegetation, while the middle has started to experience pressure on water availability. The WRCC surplus of more than 5,000 m^3 per grid was decreased. Even in 2021, it has spread to the upper reaches near Merapi's peak. The WRCC

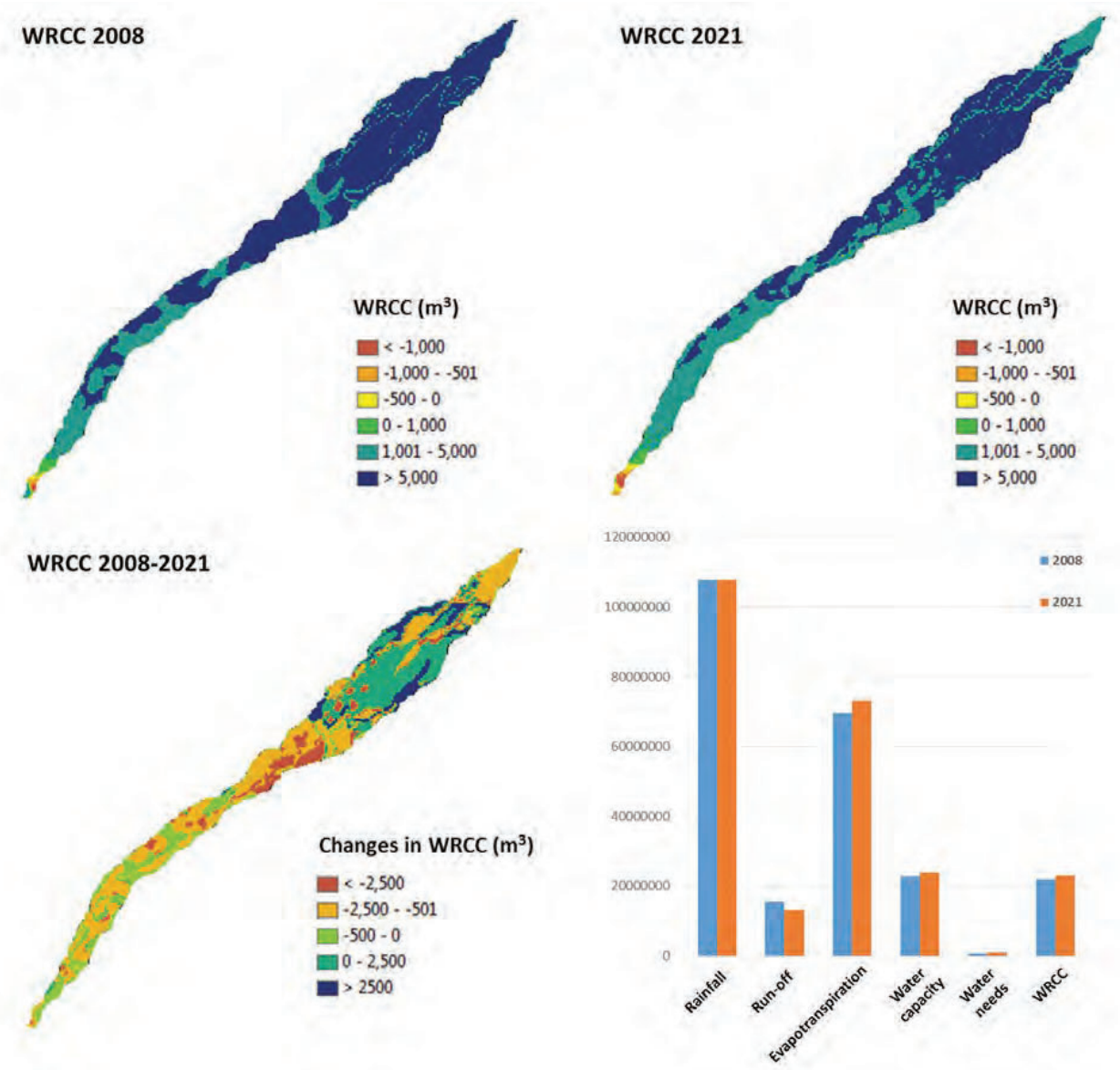

Fig. 3: WRCC Changes in Krasak Watershed (There are significant changes in surplus and deficit areas based on T-Test with p-value 0.047 and 95% confidence level).

at the peak experienced a decline of 331.50 m^3 per year for each grid cell. This phenomenon occurred on the west side of Krasak watershed, specifically in the Bebeng River segment. In this segment, there are many sand mining activities and the prices of these commodities are very high, in a linear relationship with the qualities (Sulaiman, 2008; Miller, 2021). Bebeng River segment serves 480 m^3 of volcanic sand per day, this certainly increased due to demand-driven during the rapid development on Java Island (Pangestu and Darmono, 2014). Different conditions are found on the eastern side (Krasak River segment), which is relatively greener because it is less exploited by traditional sand mining by the local community and receives less lahar flows (Lavigne, 2000). In Krasak River segment, which is steeper with many springs exposed to the ground, the topography is considered as limiting factor preventing similar exploitation. The spatial-gridded

model also shows that the east side has a very high annual WRCC (more than 5,000 m^3 per grid), it looked constant tendency to increase in intervals 0–2,500 m^3 per grid. The directional change of dominant eruptive material slide on the west side (Bebeng River segment), makes WRCC in the Krasak River segment relatively more preserved with clear water. Merapi eruption has changed the environmental carrying capacity both directly and indirectly. From this study, conservation and rehabilitation efforts are needed to maintain the watershed ecosystem thus the carrying capacity is not exceeded due to population pressure, land management, and natural resources exploitation, even though some areas of Krasak watershed belong to Mount Merapi National Park (Hartono, 2006; Thorburn, 2012).

CONCLUSION

WRCC in Krasak watershed was changed both before and after Mount Merapi eruption. Grid-based WRCC analysis shows a decline, especially in the midstream and downstream areas. WRCC at the peak occurred a decline of 331.50 m^3 per year for each grid cell. An increase in WRCC occurred only in some locations that experienced ecosystem succession after the 2010 eruption, although areas near the peak experienced a decrease due to sand mining. WRCC changes in Krasak watershed occurred significantly based on the results of T-Test (p-value 0.047 and 95% confidence level). Population growth and the economic attractiveness of pyroclastic materials from Mount Merapi are threats that need to be anticipated by governments, communities, and other stakeholders, as some locations have experienced a decline in WRCC. From this study, Merapi eruptions can increase WRCC through ecosystem succession, but also indirectly encourage various anthropogenic activities which potentially reduce WRCC in the transition and recharge zones. Without proper monitoring and management in the volcano ecosystems, it is not impossible that WRCC dynamics will decline due to unsustainable landscape. Mount Merapi has two cycles of eruption, small and large, efforts to be aware of large eruptions are very meaningful to know changes in the landscape that have impacts on land use, livelihoods, and population distribution as parameters that affect WRCC. This study has limitations in evapotranspiration measurement which is only based on numerical calculations (potential evapotranspiration), not using actual evapotranspiration. The WRCC model has the potential for further development, particularly it is able to include other parameters such as shallow groundwater, microclimate, river systems, and shallow groundwater resources.

AUTHOR CONTRIBUTIONS

M. Dede made the project plan, collected the data, processed and interpreted the data, performed WRCC model, prepared the manuscript text, and manuscript edition. S.B. Wibowo collected the data and prepared the manuscript text. Y. Prasetyo prepared the manuscript text. I.W. Nurani commented on the data. P.B. Setyowati performed the literature review. S. Sunardi made the work plan, collected the data, prepared the manuscript text, and manuscript edition.

ACKNOWLEDGEMENT

This study was funded by Hibah Riset Universitas Padjadjaran (HRU) in 2021 with contract number [1959/UN6.3.1/PT.00/21], under program of PPKI Research Collaboration of Indonesian Ministry of Education, Culture and Higher Education. The authors also thank to Millary Agung Widiawaty (Research Center for Nuclear Energy System-National Nuclear Energy Agency of Indonesia 'BATAN') for the valuable discussion in developing this model.

CONFLICT OF INTEREST

The authors declare no potential conflict of interest regarding the publication of this work. In addition, the ethical issues including plagiarism, informed consent, misconduct, data fabrication and, or falsification, double publication and, or submission, and redundancy have been completely witnessed by the authors.

OPEN ACCESS

PUBLISHER'S NOTE

GJESM Publisher remains neutral with regard to jurisdictional claims in published maps and institutional afflictions.

ABBREVIATIONS

%	Percentage
∑ ASi	Total area of land use type i
A	Catchment (area)
C	Runoff coefficient
E	Evapotranspiration
Eq	Equation
Eqs	Equations
Fig	Figure
IMPWPH	Indonesian Ministry of Public Works and Public Housing
km	Kilometer
km^2	Square kilometer
KRB	*Kawasan rawan bencana Merapi* (Merapi's disaster prone area)
m	Meter
m^3	Cubic meter
NW	Water needs per capita
P	Precipitation
p	Annual average daytime percentage
Pop	Population
Pop_i	Population in polygon i
R	Runoff capacity
S	Surface reservoir
Si	Area of polygon i
T	Annual average temperature
W	Weight for land use types
WA	Water availability
Wi	Weight of land use type i
WRCC	Water resources carrying capacity
Wy	Annual water needs per capita

REFERENCES

Anna, A.N.; Priyono, K.D.; Suharjo, S.; Priyana, Y., (2016). Using water balance to analyze water availability for communities (A case study in some areas of Bengawan Solo Watershed). Forum Geogr., 30(2): 166–175 (**10 pages**).

Asdak, C., (2020). Hidrologi dan pengelolaan daerah aliran sungai. Gadjah Mada University Press, Yogyakarta, Indonesia.

Bangyou, Y.; Jiusheng, X.; Huiru, T.; Shaoping, D.; Yinning, T., (2011). Analysis on water environment capacity of the Poyang Lake. Procedia Environ. Sci., 10: 2754–2759 (**6 pages**).

Bielecka, E., (2005). A dasymetric population density map of Poland. Proc. 22nd Int. Cartogr. Conf., 48: 9–15 (**7 pages**).

Brontowiyono, W.; Lupiyanto, R.; Malik, A.H., (2009). Improving carrying capacity by developing rainwater harvesting: A case of Oyo watershed, Gunungkidul, Indonesia. J. Sains Teknol. Lingkung., 1(1): 86–98 (**15 pages**).

Carr, B.B.; Clarke, A.B.; Vitturi, M.D.M., (2020). Volcanic conduit controls on effusive-explosive transitions and the 2010 eruption of Merapi Volcano (Indonesia). J. Volcanol. Geotherm. Res., 392: 106767 (**12 pages**).

Cheng, K.; Fu, Q.; Meng, J.; Li, T.X.; Pei, W., (2018). Analysis of the spatial variation and identification of factors affecting the water resources carrying capacity based on the cloud model. Water Resour. Manage., 32(8): 2767–2781 (**15 pages**).

Dede, M.; Widiawaty, M.A., (2020). Utilization EOS Platform as cloud-based GIS to analyze vegetation greenness in Cirebon Regency, Indonesia. J. Inf. Technol. Util., 3(1): 1–4 (**4 pages**).

Fiantis, D.; Ginting, F.I.; Nelson, M.; Minasny, B., (2019). Volcanic ash, Insecurity for the people but securing fertile soil for the future. Sustain., 11 (11): 3072 (**19 pages**).

Gob, F.; Gautier, E.; Virmoux, C.; Grancher, D.; Tamisier, V.; Primanda, K.W.; Wibowo, S.B.; Sarrazin, C.; De Bélizal, E.; Ville, A.; Lavigne, A., (2016). River responses to the 2010 major eruption of the Merapi volcano, Central Java, Indonesia. Geomorphol., 273: 244–257 (**14 pages**).

Gotardo, J.T.; Rodrigues, L.N.; Gomes, B.M., (2016).

Comparison of methods for estimating reference evapotranspiration: An approach to the management of water resources within an experimental basin in the Brazilian Cerrado. Rev. Bras. Eng. Agric., 36: 1016–1026 (**11 pages**).

Hapsari, R.I.; Sugna, B.A. I.; Novianto, D.; Asmara, R.A.; Oishi, S., (2020). Naïve Bayes classifier for debris flow disaster mitigation in Mount Merapi volcanic rivers, Indonesia, using X-band polarimetric radar. Int. J. Disaster Risk Sci., 11(6): 776–789 (**14 pages**).

Hartono, M. D., (2006). Is national park for conservation? Case study in Merapi volcano, Indonesia. Paper at 11th Biennial Conference of International Association for the Study of Common Property, Bali, Indonesia, 19–23 June 2006.

Hastoyuando, E.; Brontowiyono, W.; Hasanah, N.A.I., (2020). Environmental carrying capacity analysis based on water resources (Case study of East Surabaya area). Civ. Environ. Eng. Rep., 16(2): 229–237 (**9 pages**).

Ikhsan, J.; Hendrawan, D.; Harsanto, P., (2019a). Study on infiltration capacity at disaster-prone areas in Krasak's watershed of Mount Merapi, Indonesia. AIP Conf. Proc., 2114: 050012 (**8 pages**).

Ikhsan, J.; Hilmi, I.; Harsanto, P.; Nursetiawan, N., (2019b). The study of infrastructures and riparian area at Krasak Watershed, Indonesia. J. Tek. Sipil Perenc., 21(2): 100–109 (**10 pages).**

IMPWPH, (2018). Modul proyeksi kebutuhan air dan identifikasi pola fluktuasi pemakaian air. Perencanaan jaringan pipa transmisi dan distribusi air minum. Indonesian Ministry of Public Works and Public Housing. BPSDM Kementerian PUPR RI, Jakarta, Indonesia.

Khomarudin, M.R.; Strunz, G.; Post, J.; Zobeder, K.;Ludwig, R., (2010). Derivation of population distribution by combining census and landuse data: As an input for tsunami risk and vulnerability assessment. Int. J. Remote Sens. Earth Sci., 6(1): 46–56 (**11 pages**).

Kodoatie, R. J.; Sjarief, R., (2010). Tata ruang air. Penerbit Andi, Yogyakarta. Indonesia.

Kusumawardani, R.; Kurniadhi, R.; Mukhlisin, M.; Legono, D., (2017). Rainfall threshold for triggering debris flow on Merapi volcano area, Yogyakarta, Indonesia. AIP Conference Proceeding. 1818: 020027 (**9 pages**).

Lavigne, F.; Thouret, J.C.; Voight, B.; Suwa, H.; Sumaryono, A., (2000). Lahars at Merapi volcano, Central Java: An overview. J. Volcanol. Geotherm. Res., 100(1-4): 423–456 (**34 pages**).

Lohe, R.N.; Tyagi, B.; Singh, V.; Kumar, T.P.; Khanna, D. R.; Bhutiani, R., (2015). A comparative study for air pollution tolerance index of some terrestrial plant species. Global J. Environ. Sci. Manage., 1(4): 315–324 (**10 pages**).

Lv, A.; Han, Y.; Zhu, W.; Zhang, S.; Zhao, W., (2021). Risk assessment of water resources carrying capacity in China. JAWRA J. Am. Water Resour. Assoc., 57(4): 539–551 (**13 pages**).

Maharani, Y.N.; Lee, S.; Ki, S.J., (2016). Social vulnerability at a local level around the Merapi volcano. Int. J. Disaster Risk Reduct., 20: 63–77 (**15 pages**).

Medina, M.A.P.; Toledo-Bruno, A.G., (2016). Ecological footprint of university students: Does gender matter?. Global J. Environ. Sci. Manage., 2(4): 339–344 (**6 pages**).

Mendoza, C.J.; Peña, A.J., (2021). Reference evapotranspiration estimation by different methods for the sucroenergy sector of Colombia. Rev. Bras. Eng. Agric., 25(9): 583–590 (**8 pages**).

Mennis, J., (2009). Dasymetric mapping for estimating population in small areas. Geogr. Compass., 3(2): 727–745 (**14 pages**).

Miller, M.A., (2021). A transboundary political ecology of volcanic sand mining. Ann. Am. Assoc. Geogr., 1: 1–19 (**20 pages**).

Mulyadi, A.; Dede, M.; Widiawaty, M.A., (2020). Spatial interaction of groundwater and surface topographic using geographically weighted regression in built-up area. IOP Conf. Ser.: Earth Environ. Sci, 477: 012023 (**8 pages**).

Napsiah, N.; Gunawan, B.; Abdoellah, O.S.; Sulaeman, M., (2016). Value rationality of people living on the slope of Merapi in Yogyakarta. Analisa: J. Soc. Sci. Relig., 1(1): 105–120 (**16 pages**).

Nikiel, C.A.; Eltahir, E.A., (2021). Past and future trends of Egypt's water consumption and its sources. Nat. Commun., 12(1): 1–11 (**12 pages**).

Oey-Gardiner, M.; Gardiner, P., (2013). Indonesia's demographic dividend or window of opportunity. Masy. Indones., 39(2): 481–504 (**24 pages**).

Pangestu, L.; Darmono, D., (2014). Studi kasus imbangan angkutan sedimen di Kali Krasak. Inersia: Inf. Ekspose Has. Ris. Tek. Sipil Arsit., 10(2): 122–132 (**10 pages**).

Priatna, P.; Kadarsetia, E., (2007). Characteristics of volcanic gas correlated to the eruption activity; Case study in the Merapi volcano, periods of 1990-1994. Indones. J. Geosci., 2(4): 235–246 (**21 pages**).

Priyanti, A.; Ilham, N., (2011). The economic impact of Merapi volcano eruption in livestock farming systems. Wartazoa: Indones. Bull. Anim. Vet. Sci., 21(4): 153–160 (**8 pages**).

Raju, P.L.N., (2004). Spatial data analysis. Satellite remote sensing and GIS applications in agricultural meteorology: Proceedings of a training workshop. World Meteorological Organisation, Geneva, Switzerland.

Siljander, M., (2010). Geospatial environmental data modelling applications using remote sensing, GIS and spatial statistics. PhD's Thesis, Faculty of Science, University of Helsinki.

Sukatja, C.B.; Alfianto, A., (2017). Revitalisasi sabodam sebagai pengendali aliran lahar (studi kasus di daerah Gunungapi Merapi). J. Tek. Hidraul., 8(1): 29–42 (**14 pages**).

Sulaiman, M., (2008). Study on porosity of sediment mixtures and a bed-porosity variation model. PhD's Thesis, Disaster Prevention Research Institute, Kyoto University.

Sunardi, S.; Ariyani, M.; Withaningsih, S.; Darma, A.P.; Wikarta, K.; Parikesit, P.; Kamarudin, M.K.A.; Abdoellah, O. S., (2021). Peri-urbanization and sustainability of a groundwater resource. Environ. Dev. Sustainability. 23(6): 8394–8404 (**11 pages**).

Sutomo, S., (2013). Ecological succession on volcanic ecosystem of Mount Merapi Indonesia and its implication for restoration. Seameo Biotrop, Bogor, Indonesia.

Tarigan, I., (2018). Analisis koefisien aliran permukaan (c) akibat perubahan tata guna lahan pada daerah aliran sungai (DAS) Ular. Bachelor's Thesis, Faculty of Engineering, Universitas Sumatera Utara.

Tariq, A.; Athar, M.; Ara, J.; Sultana, V.; Ehteshamul-Haque, S.; Ahmad, M., (2015). Biochemical evaluation of antioxidant activity in extracts and polysaccharide fractions of seaweeds. Global J. Environ. Sci. Manage., 1(1): 47-62 **(6 pages).**

Thorburn, C., (2012). Farmer field schools for integrated watershed management. Dev. Pract., 22(1): 3–17 (**15 pages**).

Umami, N.; Suhartanto, B.; Suwignyo, B.; Suseno, N.; Fenila, S.A.; Fajarwati, R., (2015). Productivity of forages in grassland Merapi post-eruption area, Sleman, Yogyakarta, Indonesia. Anim. Prod., 17(2): 97–106 (**10 pages**).

Umaya, R.; Soekmadi, R.; Sunito, S., (2020). Direct economic benefits and human dependence toward Gunung Merapi National Park, Indonesia. Biodiversitas: J. Biol. Divers., 21(3): 982–993 (**12 pages**).

Utami, I.; Putra, R.A.P.; Wibowo, M.S.; Yusuf, F.I.; Husna, F.; Eko, A.; Susanto, D., (2021a). Tree stratification based on eruption damage level in Mount Merapi National Park Yogyakarta Indonesia. Media Konservasi, 26(1): 71–81 (**11 pages**).

Utami, I.; Yusuf, F.I.; Husna, F., (2021b). Tree vegetation analysis after 10 years of Mount Merapi eruption. Proc. Int. Conf. Sci. Eng., 4: 33–40 (**8 pages**).

Utami, S.N.H.; Purwanto, B.H.; Marwasta, D., (2018). Land management for agriculture after the 2010 Merapi eruption. Planta Tropika: J. Agrosains, 6(1): 32–38 (**7 pages**).

Verstappen, H.T., (2010). Indonesian landforms and plate tectonics. Indones. J. Geosci., 5(3): 197–207 (**11 pages**).

Ville, A.; Lavigne, F.; Virmoux, C.; Brunstein, D.; de Bélizal, É.; Wibowo, S.B.; Hadmoko, D.S., (2015). Evolution géomorphologique de la vallée de la Gendol à la suite de l'éruption d'octobre 2010 du volcan Merapi (Java, Indonésie). Geomorphol. Relief Process. Environ., 21(3): 235–250 (**16 pages**).

Wang, F.; Xu, W.L.; Xing, K.C.; Tang, J.; Wang, Z.W.; Sun, C.Y.; Wu, W., (2019). Temporal changes in the subduction of the Paleo-Pacific plate beneath Eurasia during the late Mesozoic: Geochronological and geochemical evidence from Cretaceous volcanic rocks in eastern NE China. Lithos, 326: 415–434 (**20 pages**).

Widodo, B.; Lupyanto, R.; Sulistiono, B.; Harjito, D.A.; Hamidin, J.; Hapsari, E.; Yasin, M.; Ellinda, C., (2015). Analysis of environmental carrying capacity for the development of sustainable settlement in Yogyakarta urban area. Procedia Environ. Sci., 28: 519–527 (**9 pages**).

Widodo, S.; Sriwidodo, S.; Irham, I.; Handoyomulyo, J., (2014). Dampak erupsi Gunung Merapi terhadap Kawasan Taman Nasional Gunung Merapi (TNGM) di DIY dan Jawa Tengah. SEPA: J. Sos. Ekon. Pertan. Agribisnis, 11(1): 130–141 (**12 pages**).

Wu, X.; Griessbach, S.; Hoffmann, L., (2018). Long-range transport of volcanic aerosol from the 2010 Merapi tropical eruption to Antarctica. Atmos. Chem. Phys., 18(21): 15859–15877 (**19 pages**).

Widiawaty, M.A., (2019). Mari mengenal sains informasi geografis. Aria Mandiri Group, Bandung, Indonesia.

Widiawaty, M.A.; Nandi, N.; Murtianto, H., (2020). Physical and social factors of shoreline change in Gebang, Cirebon Regency 1915–2019. J. Appl. Geospat. Inf., 4(1): 327–344 (**8 pages**).

Yang, S.; Yang, T., (2021). Exploration of the dynamic water resource carrying capacity of the Keriya River Basin on the southern margin of the Taklimakan Desert, China. Reg. Sustain., 2(1): 73–82 (**10 pages**).

Yang, X.; Han, W.; Mao, C., (2019). A comprehensive analysis on water resources carrying capacity in Tongliao based on ecological footprint method. IOP Conf. Ser.: Earth Environ. Sci, 237(5): 052017 (**10 pages**).

Yudistira, D.; Fadilah, R.N.; Setiawan, A.B., (2020). The impact of Merapi mountain eruption to the society. Effic. Indones. J. Dev. Econ., 3 (1): 719–725 (**7 pages**).

AUTHOR (S) BIOSKETCHES

Dede, M., M.Sc., Researcher, Center for Environment and Sustainability Science, Universitas Padjadjaran, Bandung City, Indonesia.
- Email: *m.dede.geo@gmail.com*
- ORCID: 0000-0003-4884-394X
- Web of Science ResearcherID: ABD-8995-2020
- Scopus Author ID: 57218441188
- Homepage: https://www.unpad.ac.id/2021/02/mohammad-dede-wisudawan-terbaik-magister-unpad-hobi-menulis-dan-meneliti/

Wibowo, S.B., Ph.D., Assistant Professor, Faculty of Geography, Universitas Gadjah Mada, Yogyakarta, Indonesia.
- Email: *sandy_budi_wibowo@ugm.ac.id*
- ORCID: 0000-0002-0896-3413
- Web of Science ResearcherID: NA
- Scopus Author ID: 37006340500
- Homepage: https://acadstaff.ugm.ac.id/Sandy

Prasetyo, Y., Ph.D., Assistant Professor, Department of Geodetic Engineering, Faculty of Engineering, Universitas Diponegoro, Semarang City, Indonesia
- Email: *yudo.prasetyo@ft.undip.ac.id*
- ORCID: 0000-0002-4777-8923
- Web of Science ResearcherID: AAD-5058-2019
- Scopus Author ID: 56236910500
- Homepage: https://geodesi.ft.undip.ac.id/yudo-prasetyo-st-mt/

Nurani, I.W., M.Sc., Assistant Professor, Faculty of Geography, Universitas Gadjah Mada, Yogyakarta, Indonesia; Doctoral Student, Université Paris 1 Panthéon-Sorbonne, Paris, France
- Email: *idea.nurani@ugm.ac.id*
- ORCID: 0000-0001-7523-1784
- Web of Science ResearcherID: NA
- Scopus Author ID: 57213686341
- Homepage: https://pw.geo.ugm.ac.id/2018/05/18/idea-wening-nurani-s-si-m-sc-m-il/

Setyowati, P.B., M.Sc., Assistant Professor, Faculty of Agriculture, Universitas Brawijaya, Malang, Indonesia
- Email: *putri_budi@ub.ac.id*
- ORCID: 0000-0002-0716-1793
- Web of Science ResearcherID: NA
- Scopus Author ID: 57222356792
- Homepage: https://sosek.ub.ac.id/profil/sumber-daya-manusia/dosen/putri-budi-setyowati-sp-m-sc/

Sunardi, S., Ph.D, Professor, Environmental Sciences Program, Postgraduate School, Universitas Padjadjaran, Bandung City, Indonesia
- Email: *sunardi@unpad.ac.id*
- ORCID: 0000-0001-9515-4608
- Web of Science ResearcherID: NA
- Scopus Author ID: 57223032389
- Homepage: https://pasca.unpad.ac.id/tentang-pascasarjana/struktur-organisasi/

HOW TO CITE THIS ARTICLE

Dede M.; Wibowo, S.B.; Prasetyo, Y.; Nurani, I.W.; Setyowati, P.B.; Sunardi, S., (2022). Water resources carrying capacity before and after volcanic eruption. Global J. Environ. Sci.Manage., 8(4): 473-484.

DOI: 10.22034/gjesm.2022.04.02

url: https://www.gjesm.net/article_249013.html

Global J. Environ. Sci. Manage. 8(4): 485-502, Autumn 2022, Serial #32

Global Journal of Environmental Science and Management
(GJESM)

Homepage: https://www.gjesm.net/

ORIGINAL RESEARCH ARTICLE

Inkjet printing of metal oxide coatings for enhanced photovoltaic soiling environmental applications

E. Fares[1,2], B. Aïssa[3], R.J. Isaifan[1,*]

[1] Division of Sustainable Development, College of Science and Engineering, Hamad Bin Khalifa University, Qatar Foundation, P.O. Box 5825, Doha, Qatar

[2] Department of Mechanical and Industrial Engineering, College of Engineering, Qatar University, P.O. Box 2713, Doha, Qatar

[3] Qatar Environment and Energy Research Institute, Hamad Bin Khalifa University, Qatar Foundation, P.O. Box 5825, Doha, Qatar

ARTICLE INFO

Article History:
Received 23 November 2021
Revised 01 February 2022
Accepted 5 March 2022

Keywords:
Anti-soiling
Inkjet printing
Metal oxides
Nanoparticles
Photovoltaic (PV)
Solar panels
Thin films

DOI: 10.22034/gjesm.2022.04.03

ABSTRACT

BACKGROUND AND OBJECTIVES: Global energy needs have gradually shifted toward photovoltaic solar energy, especially in the Gulf region because of the high solar-irradiance potential. However, one of the main challenges for this technology in the region is soiling, which has been reported to degrade the power output of photovoltaic modules significantly. Anti-soiling coatings are promising technologies to minimize the effect of dust on photovoltaic solar panels. Accordingly, this study aimed to synthesize aluminum, zinc, titanium, and tin oxides using mixed-based and nanoparticle-based precursors through inkjet printing techniques and investigate their potential in anti-soiling applications for PV panels.

METHODS: Four metal oxides, namely, aluminum, zinc, titanium, and tin oxides, were synthesized and deposited using the inkjet printing technique for anti-soiling application. Ultraviolet-visible spectroscopy, field emission scanning electron microscope, X-ray diffraction, X-ray photoelectron spectroscopy, and contact angle measurements were performed to characterize these thin films.

FINDINGS: The optical transmittance of the substrate using the nanoparticle ink revealed better optical properties than that using the mixed-based ink. Compared with nanoparticle samples, a homogeneous crack and a defect-free layer were observed with dense nanoparticles in all mixed inks (except for aluminum oxide ink). The contact angles indicated that the synthesized films were super-hydrophilic/hydrophilic coatings. The results of the outdoor testing revealed that up to 60% less dust was deposited on the best-performing film (aluminum oxide mixed-based ink) compared with bare glass.

CONCLUSION: The outdoor experiment revealed that mixed-based thin films were better in reducing dust deposition than nanoparticle-based thin films and bare glass. This enhancement might be due to the decreased antireflection property along with a morphological contribution related to the presence of nanoparticle voids, which reduce the spectra scattering and minimize its deterioration, thus demonstrating better anti-soiling properties. The results of the outdoor test revealed that aluminum, zinc, and titanium oxides are promising materials for anti-soiling coating applications for both ink types. However, tin oxide coatings are not recommended for anti-soiling applications, as they showed the highest dust deposition rate near the bare glass performance.

NUMBER OF REFERENCES	NUMBER OF FIGURES	NUMBER OF TABLES
54	10	0

*Corresponding Author:
Email: *risaifan@hbku.edu.qa*
Phone: +974 554 7449
ORCID: 0000-0002-9590-4939

Note: Discussion period for this manuscript open until January 1, 2023 on GJESM website at the "Show Article".

INTRODUCTION

Soiling is one of the main issues inherent to photovoltaic (PV) deployment, especially in the arid region, accounting for 70 percent (%) of PV-power losses (Micheli *et al.,* 2017). Anti-soiling coating (ASC) is one of the promising mitigation techniques for dust accumulation on PV panels (Pescheux *et al.,* 2020; Lee *et al.,* 2022; Thongsuwan *et al.,* 2022), as it efficiently reduced the operational and maintenance costs and the associated cleaning water consumption, especially in the desert environment (Alnaser *et al.,* 2018; Eihorn *et al.,* 2019). The ASC concept mainly relies on hydrophobic (contact angle (CA)>90°) or hydrophilic (CA<90°) properties, which can be achieved by a surface chemistry treatment, a surface morphology modification, and/or a combination of both (Bukhari *et al.,* 2019). Few studies have addressed both parameters; however, many researchers demonstrated the utilization of silicon and titanium dioxides (SiO_2 and TiO_2) for ASC applications (Jesus *et al.,* 2018). Jesus *et al.,* (2018) used titanium and silicon dioxides (TiO_2/SiO_2), pure TiO_2, and SiO_2 thin films and experimentally tested them for 4–5 months in Italy, Spain, and Brazil. They found that the light transmittance (T%) loss of the uncoated glass was 16%, whereas the coated ones reduced the T% loss by 50%, specifically in the TiO_2/SiO_2 sample. They emphasized the importance of ASCs for dry regions. Sueto *et al.,* (2013) found that coating a photocatalytic surface layer with a modified tungsten trioxide (WO_3) and partially hydrolyzed tetraethyl orthosilicate potentially reduced the dust adhesion from 0.25 electronvolt (eV) to 0.10 eV. Moreover, accumulated sand masses were reduced from >0.01 g to 0.005 g. Furthermore, Ota *et al.,* (2016) found that silica-based coating increased the transmittance and energy output of PV panels by >3%. Bahattab *et al.,* (2016) also observed an approximately 7% increase in the transmittance when low-iron soda-lime float glass was coated with SiO_2 nanoparticles (NP). Pendse *et al.,* (2018) found that the CA was more than 130° when depositing magnesium fluoride (MgF_2) NP on glass; accordingly, light transmittance increased by 7%–9%. On the contrary, Said *et al.,* (2015) tested the difference between textured antireflective coated and uncoated PV panels. They found that the clean PV module power output increased by an average of 4%–8% when coated panels were used because of the decreased reflection losses, whereas dust fouling was mitigated by 5% with the use of textured antireflective coatings. Li *et al.,* (2013) prepared a hydrophobic antireflective SiO_2-based coating for PV panels and found that the performance was enhanced by approximately 6.6% with a maximum transmittance of 98.3%; thus, it could also be used for self-cleaning application. Likewise, Arabatzis *et al.,* (2018) reported an increase of 5%–6% in the power gain for TiO_2/SiO_2-coated PV panels compared with the uncoated ones because of the increased light transmittance in the visible region and enhanced self-cleaning. Oh *et al.,* (2016) used SiO_2 NP-based ASC. In their study, energy soiling losses reduced up to 3.85%, and the module's power improved by approximately 2.56% because of the antireflection function. Hossain *et al.,* (2021), tested silica thin films and found that PV efficiency was improved up to 27%. Similarly, Piliougine *et al.,* (2013) found a 0.8% difference in daily energy soiling losses between coated (with metal oxide NP and a hybrid polymer binder) and uncoated PV panels. All these previous studies have utilized dip-coating, spin-coating, and vapor-deposition techniques. Essentially, none of the aforementioned studies have utilized inkjet printing. However, limitations such as coating degradation, light transmittance loss, and instability for such coatings have been reported (Eihorn *et al.,* 2019; Pescheux *et al.,* 2020). For example, Pescheux *et al.,* (2020) revealed that they have subjected their coatings to accelerated aging tests to verify their durability to real outdoor exposures. However, the coatings recorded small losses of optical performances despite the aggressiveness of the tests. Nowadays, metal oxide materials are heavily used in solar cells as transparent electrodes, light absorbers, transport layers, and other functionalities such as ASC and antireflective surfaces (Perez-Tomas *et al.,* 2018). Their widespread use was attributed to their availability in nature, nontoxicity (Nunes *et al.,* 2019), low cost (Isaifan *et al.,* 2017), and fabrication processes (Perez-Tomas *et al.,* 2018). Further, they proved to be suitable for outdoor applications because of their insolubility and chemical and thermal stability (Isaifan *et al.,* 2017; Perez-Tomas *et al.,* 2018; Nunes *et al.,* 2019). Perez-Tomas *et al.,* (2018) provided evidence that mesoporous zirconia, for instance, has high stability, can be fully printed, and eliminates the use of precious metals, which are replaced by low cost carbon-based materials. Other

important properties of metal oxide materials are their large bandgap and low reflective index, which help in harvesting more photons (Perez-Tomas *et al.,* 2018; Nunes *et al.,* 2019). Based on the above reasons, metal oxides improve the device's characteristics and increase its reliability (Perez-Tomas *et al.,* 2018). Therefore, the present study focused on metal oxides for the preparation of ASC layers. TiO_2, aluminum oxide (Al_2O_3), tin oxide (SnO_2), and zinc oxides (ZnO) were used as candidates for such purposes. Inkjet printing is a valuable technique in nanotechnology, especially for metal oxide thin film fabrication (Liu *et al.,* 2015). Metal oxide precursors could be prepared using the colloidal suspension of metal oxide NP, metal salt solution, and colloidal NPs based on sol–gel chemistry. Furthermore, Liu *et al.,* (2015) recommended using colloidal NP based on sol–gel chemistry and/or metal salt solutions, as NP tended to agglomerate in the colloidal suspension of metal oxide NP. Inkjet printing has several advantages. To name a few, it has a direct patterning (Wang *et al.,* 2014), programmed printing with precise droplet volume (Liu *et al.,* 2015), low operating cost, fast production rate, and lower environmental effect than other techniques, especially vacuum-based ones (Wang *et al.,* 2014). Moreover, it is implemented in ambient temperature (Wang *et al.,* 2014) and provides quick mass production, as Liu *et al.,* (2015) stated. Metal oxide materials synthesized using inkjet printing have been widely used for different applications, such as solar cells, electronic devices, and sensors. More than 200 scientific publications have been published on this subject area during the last decade (Liu *et al.,* 2015); however, inkjet printing techniques have not been utilized yet in ASC applications. Since the size of dust particles in Qatar ranges from 0.6 micrometers (µm) to 50 µm (Javed *et al.,* 2017; Ilse *et al.,* 2018), coatings and texturing should be in nanoscale range to decrease the adhesion forces by minimizing the contact area between the dust particles and the surface (Polizos *et al.,* 2018b), and to avoid the accumulation of dust particles in between the surface voids and textures. Likewise, surface texturing size should be smaller than the solar radiation wavelength to minimize photon scattering (Polizos *et al.,* 2018b). Finally, material preparation (i.e., precursor concentration) depends highly on the employed technique. For example, to get an acceptable super hydrophobic coating, the concentration in a spray technique should be lower than the concentration if a spin-coating is used (Polizos *et al.,* 2018a) because the higher concentration of the binder masks or overcoats the silica NP and interferes with their functionality. The present study aimed to synthesize metal oxide coatings of TiO_2, Al_2O_3, SnO_2, and ZnO using mixed-based (NP and metal oxide salts) and NP-based precursors via inkjet printing techniques and investigate their potential in ASC applications for PV panels. To the best of the authors' knowledge, no study in the literature has addressed the preparation and comparison of the four metal oxide-based coatings for ASC applications prepared with the aid of inkjet material printing. Inkjet printing is easy to use and can be implemented at ambient temperature. It has several advantages over other common techniques for film fabrication, such as material efficiency and less wastage due to programmed printing with precise droplet volume, low operating cost, fast production rate, and lower environmental effect. This study was conducted in Qatar during 2021 and 2022.

MATERIALS AND METHODS

Substrate cleaning

The soda-lime glass samples (Sigma–Aldrich, MA, USA) of size 1" × 1" were used as the substrate material for the coatings. The glass substrates were cleaned to improve the ink's wettability. Substrate cleaning was performed following the procedure reported by Buffiere *et al.,* (2020).

Ink preparation

Metal nitrate hydrate based on zinc and aluminum nitrates (i.e., $Zn(NO_3)_2{\cdot}6H_2O$ and $Al(NO_3)_3 \cdot 9H_2O$), tin chloride hydrate ($SnCl_2 \cdot 2H_2O$), nanopowder (ZnO, Al_2O_3, TiO_2 nanopowder), and SnO_2 NP ink of 7–20 nanometer (nm) in size were purchased from Sigma–Aldrich. In this study, two metal oxide precursors, i.e., pure NP-based ink and mixed-based ink (salt and NP), were synthesized and deposited on the glass surface by the inkjet printing technique following the same procedure reported by Buffiere *et al.,* (2020). NP-based ink was prepared by dispersing the nanopowder with a size of 27–43 for Al_2O_3 and <100 nm for ZnO and TiO_2 in isopropanol (IPA) with a volume ratio of 25:75 (powder: IPA). Ethylene glycol (EG) was then added with a ratio of 25:75

(precursor:EG) to adjust the precursor viscosity (Rieu *et al.,* 2016), except for SnO_2 NP-based ink, a ready-made (as purchased) ink, where no further modifications have been made. EG was added to maintain the viscosity and the surface tension within an acceptable range to the inkjet printer as described previously (Cummins *et al.,* 2012). According to Liu *et al.,* (2015), the recommended viscosity for an inkjet printer was between 1 and 20 millipascal second (mPa.s) and the surface tension was between 25 and 50 millinewton per meter (mN/m) (Cummins *et al.,* 2012). Furthermore, Quan *et al.,* (2017) used a mixture of salt-based ink solutions and NP. Salt was used to lower the surface energy, and the NP was used to increase the surface roughness, which enhances the anti-soiling properties. To this end, the mixed-based precursors using both NP- and salt-based inks were prepared with equal volume for each NP and salt (1:1). The NP-based ink was prepared following the above-mentioned procedure, whereas the salt-based ink was synthesized following the protocol adopted in this paper (Rieu *et al.,* 2016). However, TiO_2 salt-based ink was prepared using a diluted solution of titanium diisopropoxide bis(acetylacetonate) (TAA) in IPA with a volume ratio of 1:20 of TAA:IPA, and a homogeneous layer was observed (Buffiere *et al.,* 2020). Fig. 1a and b show the different inks used in the present study, their synthesis process, and thin film formation mechanism.

Before printing, the ink viscosity was measured to ensure that it fits within the acceptable range (Liu *et al.,* 2015). The viscosity at 26.5 degrees Celsius (°C) for SnO_2 ink was 8.84 mPa.s, and those for Al_2O_3 and ZnO inks were 12.8 mPa.s and 11.7 mPa.s, respectively. The viscosity of TiO_2 ink was 2.3–2.6 mPa.s at 20°C. The viscosity of all inks was within the recommended range of drop-on-demand ink properties, which should be between 1 and 20 mPa.s (Liu *et al.,* 2015). After testing the ink's properties, it was loaded in the cartridge and then clipped inside the Inkjet Dimatix Materials Printer (DMP). A cartridge of 1–10 picoliter (pL) nozzle with 16 total nozzles was used. A computer connected to the printer controlled the coordinates, path, time, and number of deposition cycles.

Coating approach

In this study, Fujifilm Dimatix Materials Printer (DMP-2850) was used to deposit the metal oxide precursors. To optimize the droplet dispatching out of the cartridge, the voltage for all precursors was kept between 8 Volts (V) minimum (for the one pL nozzle cartridge) to 17 V maximum (for the 10 pL nozzle cartridge). The droplet interspacing was 30 µm, and the plate and cartridge temperature was 45°C. The 1-pL cartridge nozzle was used for all precursors, except for Al_2O_3, where 10 pL was used, as a more homogeneous layer was observed. Ten layers were deposited. After each layer, the sample was dried in the furnace at approximately 200°C for 10 minutes (min) in the air. The effects of different surface textures were investigated using different metal precursors to determine the optimal anti-soiling texture to be deposited on the glass substrate. Thus, different ink types were used in which a pure NP and a combination of metal oxide salts and NP were utilized to prepare the precursors, as shown in Fig. 1a.

Thermal annealing

To ensure that the metal oxide thin film has been formed, it was heated up to 450°C for 30 min (thermal annealing) as per the procedure performed by Buffiere *et al.,* (2020). Thermal annealing was performed at 450°C for 30 min at a heating rate of 30°C–45°C/min.

Analysis techniques

To characterize the ink properties, viscosity was measured using a Discovery Hybrid rheometer. Approximately 5 milliliters (mL) of the ink was dispensed on a standard Peltier plate, and shear was applied using 60 millimeters (mm), 1° cone geometry. The thin films were characterized concerning the optical, structural, chemical, and anti-soiling properties. Field emission scanning electron microscopy (SEM) was used to characterize the top-view morphology and topography of the coated surfaces with 5 kilovolts (kV) using a JEOL 7610F SEM system. Optical performance was assessed using an ultraviolet-visible (UV-VIS) 5000 spectrophotometer measuring direct transmittance and reflectance in the wavelength range from 248 to 1000 nm (Karabay *et al.,* 2012). The water CA was measured by an optical CA system (DSA25 Drop Shape Analyzer) with a droplet volume of 2 microliters (µL) to test the surface hydrophobicity/hydrophilicity. The water droplet was held for approximately 40 seconds (s) before photos were captured. Surface chemistry was

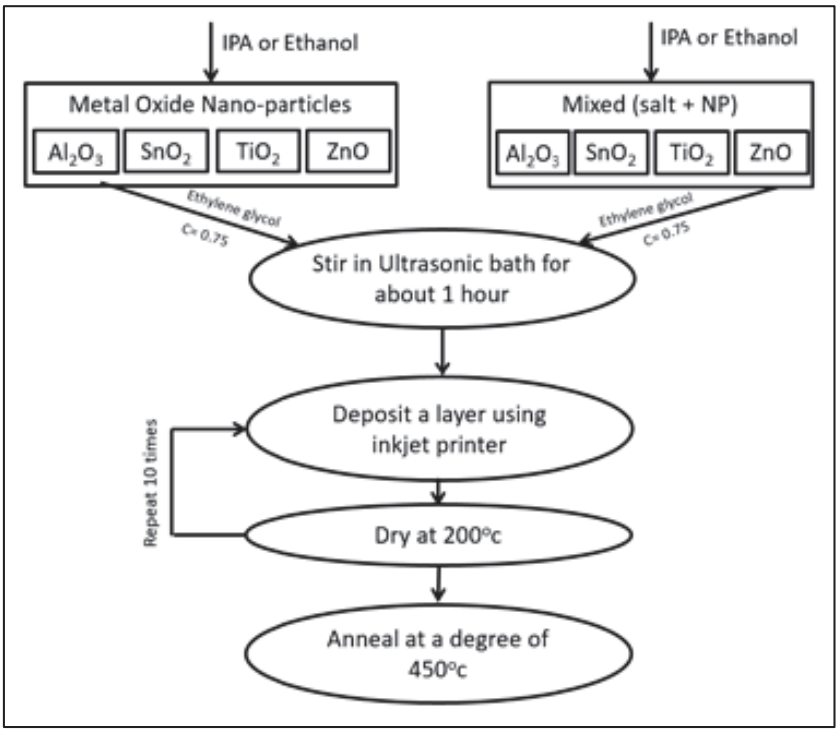

(a)

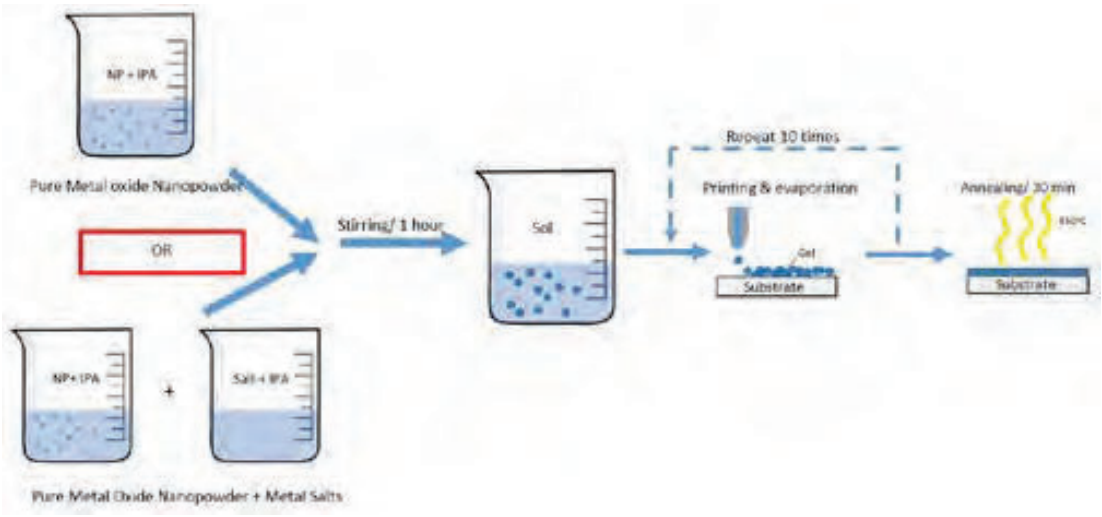

(b)

Fig. 1: Research methodology (a) Chart flow of the formation mechanism of a metal oxide thin film and (b) synthesis process based on sol–gel chemistry.

monitored using an X-ray photoelectron spectrometer (XPS; Thermo Scientific ESCALab 250Xi). X-ray powder diffraction (XRD) was performed to evaluate the crystallinity of the layer using grazing incidence XRD geometry (Rigaku SmartLab XRD), with an incidence angle of 0.2°. The X-ray generator was set at 40 kV and 30 milliamperes (mA). The measurements were performed at (2θ). The outdoor experiment was

implemented by exposing the samples to real-world environmental conditions for accurate simulation of the anti-soiling properties. The samples were located in one of the outdoor sites of the Mechanical and Industrial Engineering Department in Qatar University. They were placed at a tilt angle of 0° (facing the sky). The required climate and weather information was extracted from two weather websites: Weather Underground and Civil Aviation Authority in Qatar. During the experiment, dust removal was carefully avoided, except for natural causes, such as wind and rain. The mass of all samples was measured and recorded by a balance scale with an accuracy of 0.0001 gram (g) before the outdoor experiment. The experiment started on March 1, 2021, and lasted for 22 days. The mass of the samples was then measured regularly (every 3 days). The difference between the initial mass (before exposure) and the sample mass at each reading was recorded. Similar to the work by Isaifan *et al.,* (2017), the dust deposition rate of each sample was calculated by dividing the difference in weight by the surface area of the glass (Eq. 1).

$$Deposition\ rate = \frac{\text{Substrate mass after exposure - Substrate mass before exposure}}{\text{Substrate's surface area}} \quad (1)$$

RESULTS AND DISCUSSIONS

Optical properties

The optical transmittance (T%) and absorbance (A%) spectra in the 248–1000 nm region are shown in Fig. 2a and b for different NP and mixed thin films, respectively. In all thin film types, the performance of Al_2O_3 thin film was superior in terms of the average transmittance and reflection, followed by ZnO, TiO_2, and finally SnO_2. An average transmittance gain of 0.10% and a reflection reduction of approximately 0.08% were observed with Al_2O_3 NP thin film over the bare glass. This result agrees with those of similar studies, i.e., the transmittance of the Al_2O_3-coated substrate has increased (Kareem *et al.,* 2011). The improved performance was attributed to the reduction in reflection compared with the bare glass (Kareem *et al.,* 2011). Moreover, the NP-coated materials have better transmittance and lower reflection than the mixed thin films by approximately 0.89% and 1.21%, respectively. This might be due to nano-voids and surface roughness, which enhance the transmittance and reduce the reflection (Kauppinen *et al.,* 2017). A study reported that nanoscale texturing smaller than the solar radiation wavelength minimizes photon scattering (Polizos *et al.,* 2018b). Hence, both mixed and pure NP-coated materials have lower absorbance values than bare glass. Furthermore, the average transmittance of NP and mixed thin films was higher than 90% in the visible region, except for SnO_2 where it was higher than 85%. These results were in conformance with several studies that have reported the same observations using similar metal oxide materials (Yamaguchi *et al.,* 2005; Kareem *et al.,* 2011). Interestingly, the transmittance of TiO_2 mixed thin film in the visible region was approximately 87%, which was lower than the transmittance observed for TiO_2 of NP thin film (Arabatzis *et al.,* 2016). The absorbance A% was deduced using Eq. 2.

$$A\% = 100 - (T\% + R\%) \quad (2)$$

Structural properties

The XRD spectra of the metal oxide films were obtained after the annealing process to determine the phase and crystallographic structure (Fig. 3). The XRD data revealed that the films deposited by both precursor types (i.e., pure NP ink and mixed ink) were not crystallized, as the diffraction peaks were weak and broad. This is in agreement with previous results on the characterization of metal oxide materials (Legrand-Buscema *et al.,* 2002; Sobczyk-Guzenda *et al.,* 2013), where the phase was amorphous for films under heat treatments performed in 450°C–500°C (Legrand-Buscema *et al.,* 2002). Thus, the coated thin films were amorphous, except for the SnO_2 films. The results of the analysis of these spectra indicated that the coatings prepared from both precursor solutions correspond to the compound SnO_2 with peaks of 26°, 33°, and 52° belonging to (110), (101), and (211) planes, respectively (Aziz *et al.,* 2013). These peaks confirmed that the films were polycrystalline. The influence of the precursor type on the crystallographic orientation of the SnO_2 films was also investigated. Accordingly, the XRD patterns showed improved peak intensities of the mixed precursors compared with those of the pure NP ones. More specifically, the peak corresponding to the (110) plane indicated a preferential growth, as a higher intensity was observed over this plane. Therefore, the crystallographic characteristics

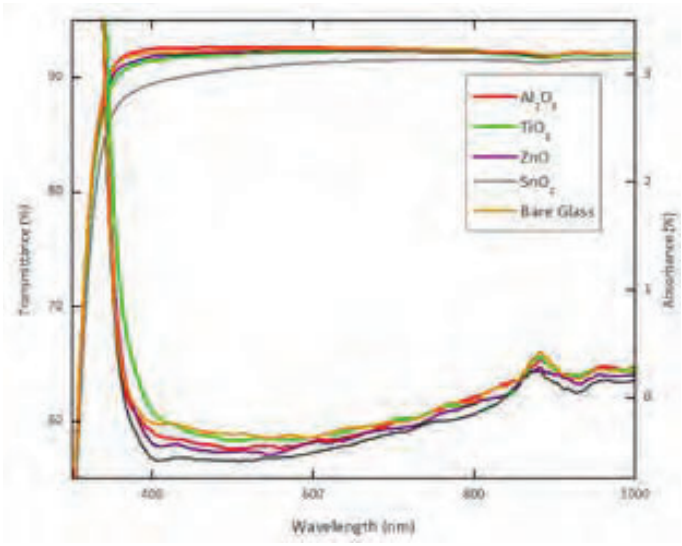

(a)

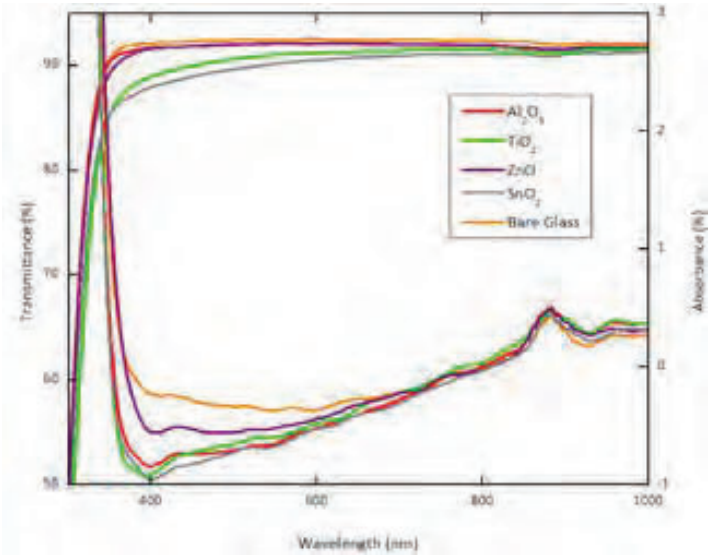

(b)

Fig. 2: Transmittance (T%) and absorbance (A%) of (a) NP films and (b) mixed films.

changed based on the precursor type, in which mixed precursors showed better crystallinity. However, the very broad peak observed around 2θ=25° in the XRD pattern of Al_2O_3 originated from the glass substrate (Huang *et al.,* 2006).

Furthermore, SEM results revealed that the coatings prepared using pure NP precursor exhibited relatively smoother and finer nano- and microstructure features in all the metal oxide samples (Fig. 4 to 7 a-c). They were uniformly distributed across the substrate area compared with the coatings prepared using mixed precursors (Fig. 4 to 7 d-f). Furthermore, the NP were more visible in the mixed precursor samples than in the pure NP precursor

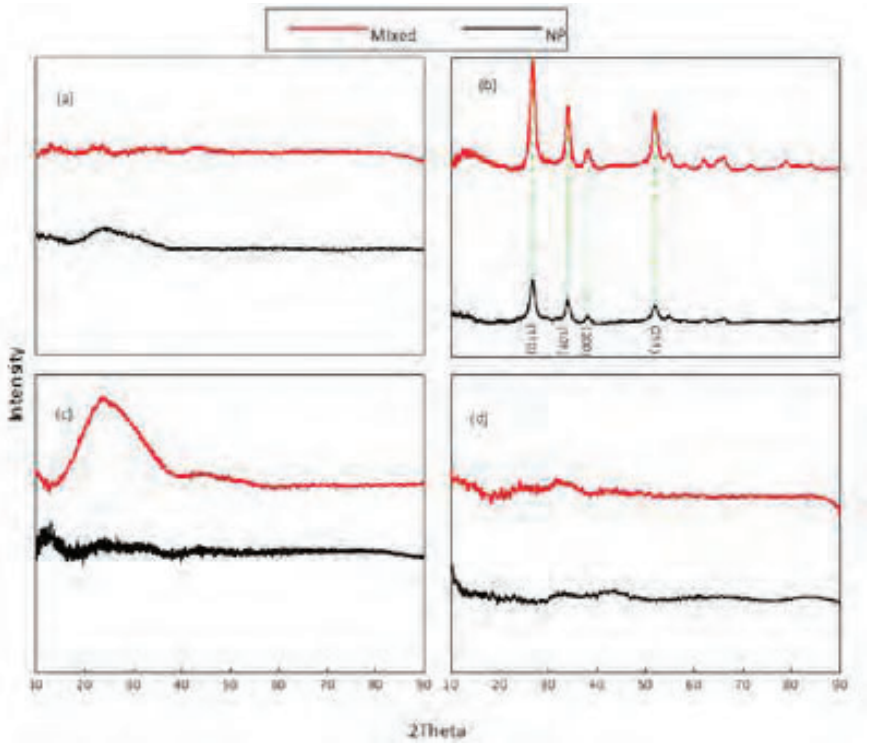

Fig. 3: XRD results for mixed and NP-based inks: (a) ZnO, (b) SnO_2, (c) Al_2O_3, and (d) TiO_2.

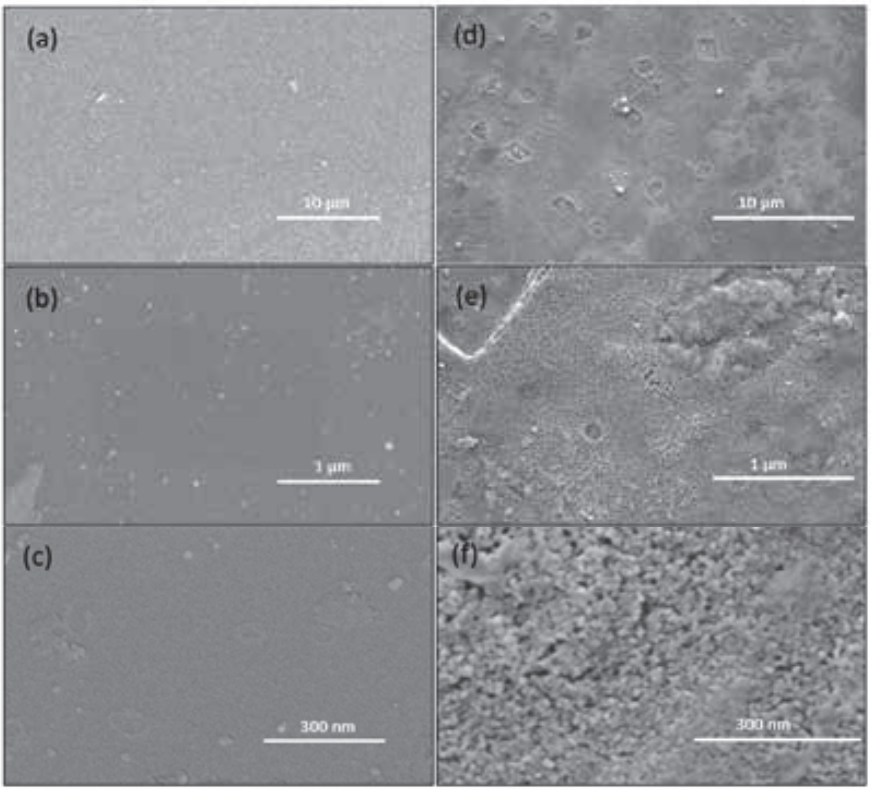

Fig. 4: SEM images for ZnO for NP-based ink (a–c), and mixed precursors NP (d–f).

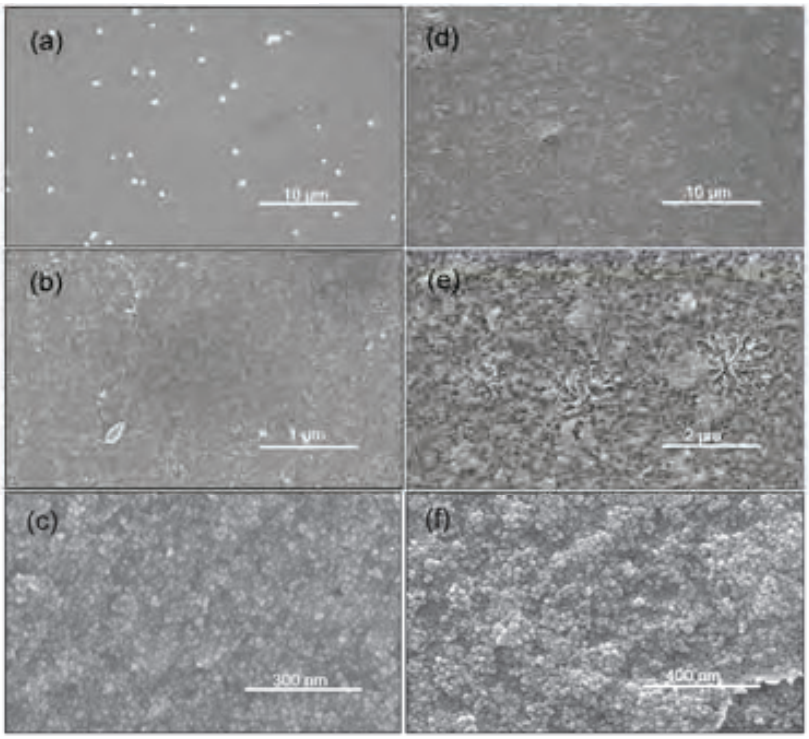

Fig. 5: SEM images for SnO_2 for NP-based ink (a–c), and mixed precursors NP (d–f).

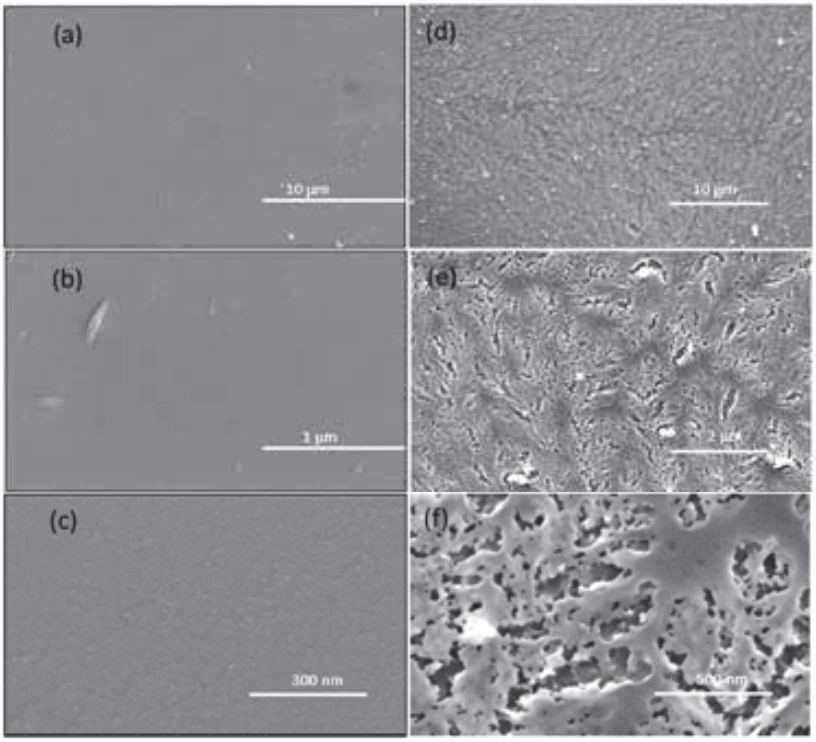

Fig. 6: SEM images for Al_2O_3 for NP-based ink (a–c), and mixed precursors NP (d–f).

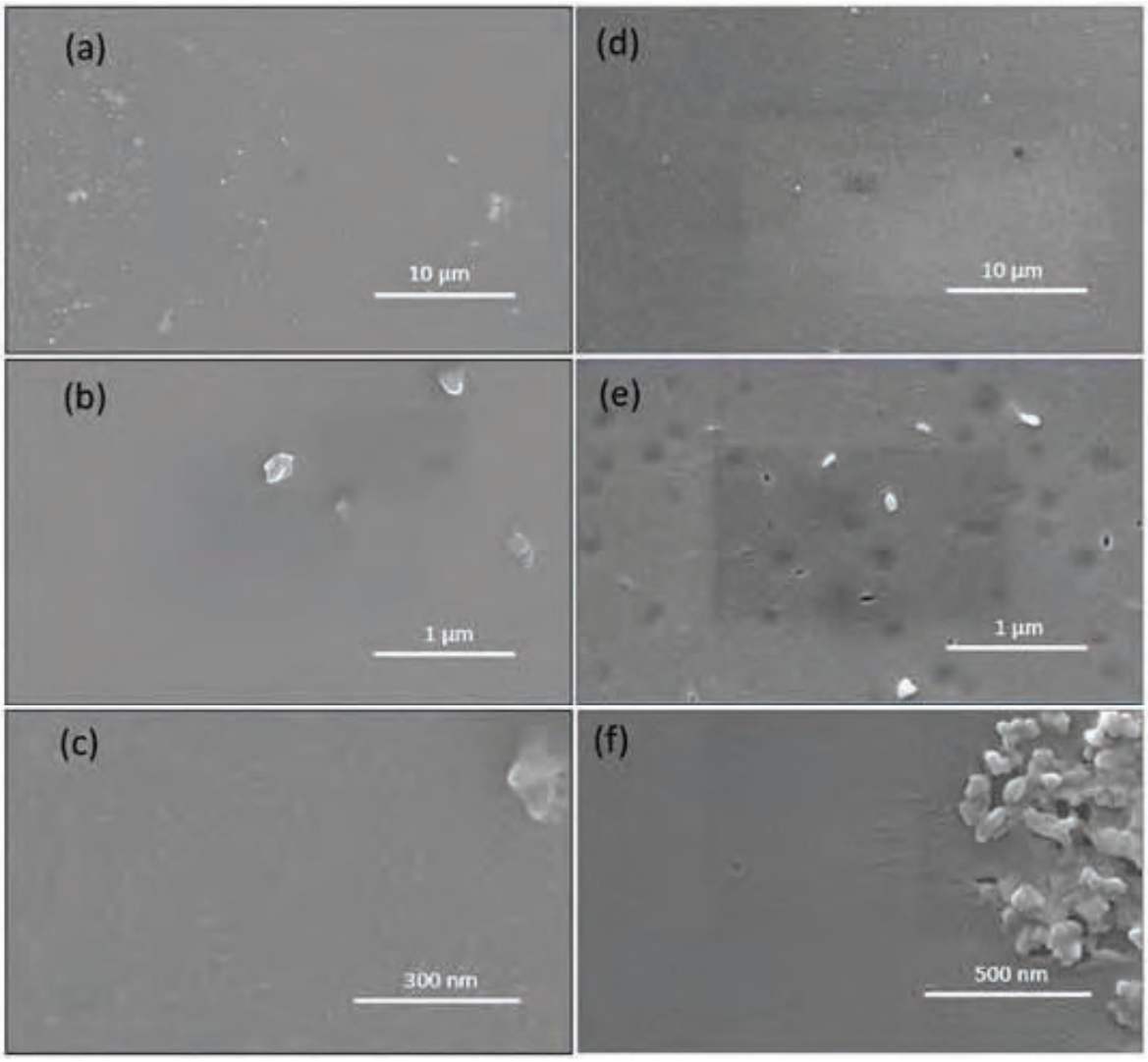

Fig. 7: SEM images for TiO_2 for NP-based ink (a–c), and mixed precursors NP (d–f).

samples (Fig. 4 to 7 c and f). Particle density and surface roughness were significant in such samples. In general, the NP sizes were uniform and spherical in ZnO and SnO_2 mixed precursors. They were dense, uniformly distributed, and well-connected over the surface. Similar to the results of Firooz *et al.,* (2008) and Lu *et al.,* (2010), a spherical morphology with porous, regular, foam-like structure particles was observed in both precursors. The synthesis procedure used in preparing SnO_2 mixed ink was similar to that used by Firooz *et al.,* (2008) to produce SnO_2 NP. They used $SnCl_2{\cdot}2H_2O$ as a precursor, whereas $SnCl_2{\cdot}2H_2O$ and SnO_2 NP were used in the present work. In both cases, SnO_2 NP were formed. In the case of ZnO, the NP were similar to the one produced by Lu *et al.,* (2010). They used zinc acetate as a primary precursor and deposited it using spin-coating techniques. According to Firooz *et al.,* (2008), the material's morphology was affected by the type of precursor and surfactant used to prepare the precursor. Parallelogram features were found in the SEM figure of the ZnO mixed thin film (Fig. 4 (d) and (e)) and a flower-like shape in the SnO_2 mixed thin film (Fig. 5e). On the contrary, the Al_2O_3 mixed thin film showed a leaf-like structure, and the TiO_2 mixed thin film exhibited an agglomeration of particles in some areas rather than a homogeneous

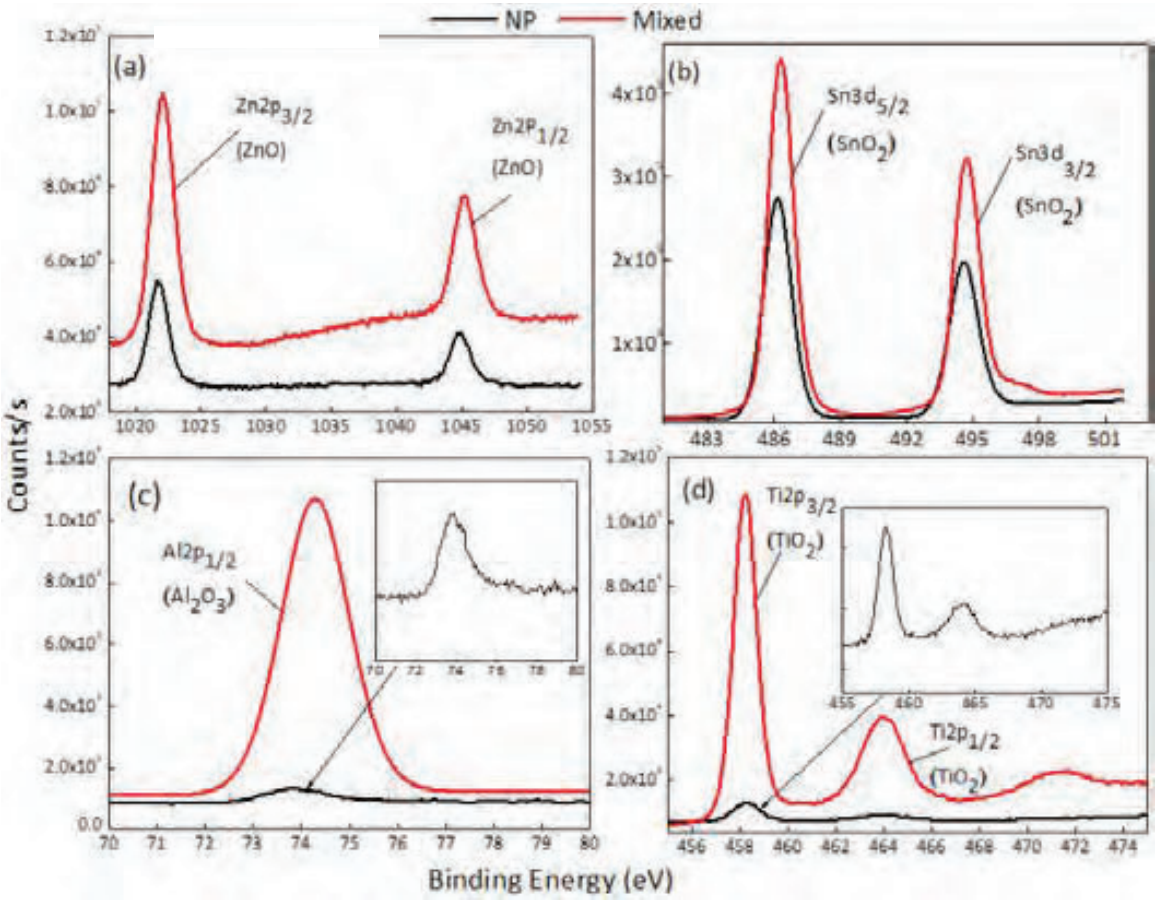

Fig. 8: XPS results of NP, salt, and mixed-based inks: (a) ZnO, (b) SnO_2, (c) Al_2O_3, and (d) TiO_2.

coverage to the substrate (see Fig. 6e and Fig. 7f). In TiO_2 mixed thin films, the granular structure can be seen in some surface areas. This may negatively affect mechanical stability, as these agglomerations adhere to the surface by the weak Van der Waals forces (Shang *et al.,* 2016). The stability over time of these coatings should be further investigated. In the case of TiO_2, the coatings exhibit a similar structure as that observed by Legrand-Buscema *et al.,* (2002), in which the samples were annealed at 400°C. The grain size was claimed to be smaller, and the porosity was lower with a low annealing temperature (<500°C). These results are in good agreement with those reported by Saini *et al.,* (2007).

Chemical properties

Fig. 8 shows the XPS results with the Zn2p spectra representing the binding energies of $Zn2p_{1/2}$ and $Zn2p_{3/2}$ for Zn^{2+}-related peaks located at 1044.7 and 1021.5 eV, respectively (Chiu *et al.,* 2015). Similarly, the Al_2O_3 sample demonstrated that the Al2p spectra were decomposed into two peaks at a binding energy of 74.5 eV for the $Al2p_{1/2}$, corresponding to the peak Al–O (Bouabibsa *et al.,* 2018). For TiO_2, the Ti2p had two spin-orbital splittings of $Ti2p_{3/2}$ at 458.5 eV and $Ti2p_{1/2}$ at 464.3 eV. These positions indicated a Ti^{4+} valence state of TiO_2 (Potlog *et al.,* 2014). However, the Sn3d core-level spectrum showed spin-orbital splittings of $Sn3d_{5/2}$ and $Sn3d_{3/2}$. The binding energy position of the $Sn3d_{5/2}$ component was located at 486.0eV, while the binding energy position of the $Sn3d_{3/2}$ component was located at 495.0 eV, corresponding to a SnO_2 state (Xia *et al.,* 2014). No clear signal from the metallic Sn at 485.0eV can be observed. The corresponding O1s spectrum in all samples was also given. The fitting indicated a metal–O component at 530 eV and other carbon-related contamination at higher binding energies (Lortie *et al.,* 2015).

Anti-soiling properties

Contact angle measurements

The CA measurement was higher in NP coatings than in the mixed ones, and this was found in all the tested samples, except for ZnO, where the CA was approximately 33° in NP coatings. The smallest CA among all samples was 8.5° in Al_2O_3 mixed coating, while the highest was 47.8° in TiO_2 mixed coating. Similar results were obtained by a previous work on TiO_2 nanofilms developed for anti-soiling application, which reported a CA of approximately 41° (Buffiere *et al.,* 2020). Therefore, all coated layers tended to be hydrophilic/super-hydrophilic. SnO_2 showed the lowest CA in general. Paul *et al.,* (2014) reported a CA of 11.8°, which was close to the values obtained in the present study, whereas the CA of TiO_2 was slightly higher, with a value of 37.4 ° (Talinungsang *et al.,* 2017). The presence of fine NP in both thin film types of SnO_2 samples increased the surface roughness, leading to a relatively low CA and thus enhanced wettability and hydrophilicity properties. They have a super-hydrophilic nature with a CA close to 0°. In this study, the CA of ZnO was lower than that reported by Jongnavakit *et al.,* (2012), considering the same annealing temperature. Jongnavakit *et al.,* (2012) reported that the lowest CA was 58° for the

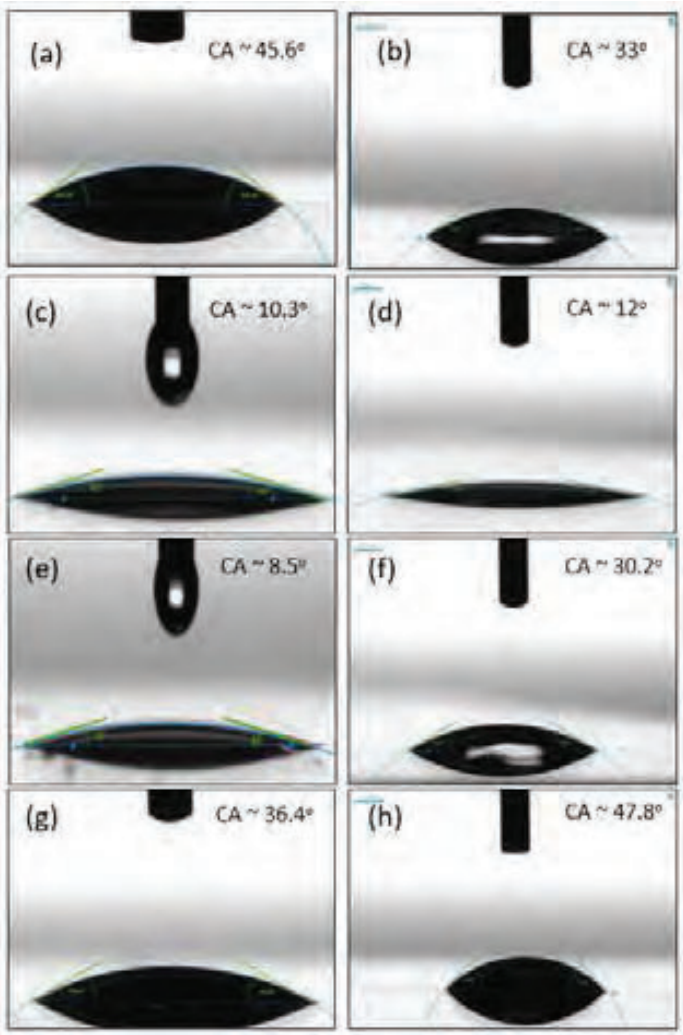

Fig. 9: Contact angle measurements to assess the hydrophilicity of (a, b) ZnO-coated samples based on mixed ink and NP ink; (c, d) SnO_2-coated samples based on mixed ink and NP ink; (e, f) Al_2O_3-coated samples based on mixed ink and NP ink; (g, h) TiO_2-coated samples based on mixed ink and NP ink.

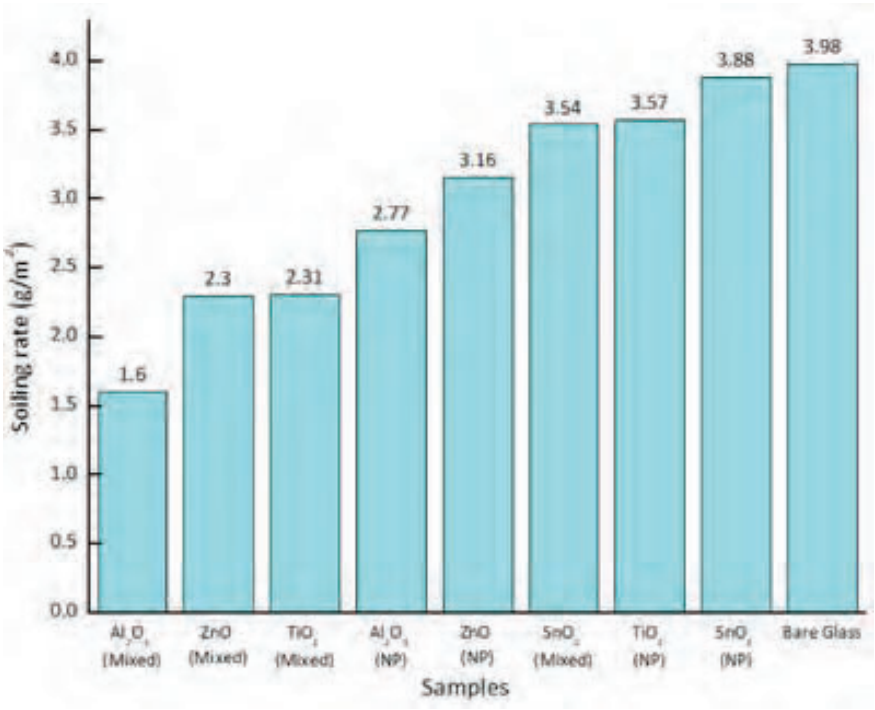

Fig. 10: Dust deposition rate for 22 days on uncoated versus coated samples.

sample prepared by dip-coating with a withdrawal speed of 3 centimeters per minute (cm/min) (Na *et al.,* 2019), whereas Lin *et al.,* (2009) reported a CA of approximately 60°. However, the CA was comparable with that reported by Lu *et al.,* (2010), when exposed to UV light for 10 min. According to Wang *et al.,* (2004), the CA of Al_2O_3 was 5°, which was in agreement with the CA of 8.5° of the mixed-based thin film in the present study. On the contrary, the CA of the NP-based thin film was similar to the results obtained by Na *et al.,* (2019) where the Al_2O_3 films were printed using a screen mask. However, Cho *et al.,* (2018) deposited Al_2O_3 NP by spray techniques. Their CA was 62°, which was significantly higher than the CA value of the NP-based thin film measured in the present study. Accordingly, the surface's hydrophilicity might be enhanced using different precursors (Fig. 9) and is dependent on the deposition techniques, as the morphology and roughness of the coated layer were affected and, accordingly, the CA values were affected. Finally, the hydrophilic property is critical in reducing the frequency of mechanical cleaning, especially in arid regions, as it reduces and releases the burden on water use, which is a scarce resource in such regions (Isaifan *et al.,* 2018).

Outdoor experiment

To accurately assess the process of dust accumulation on surfaces over time and decouple the influence of other factors such as the tilt angle, samples were placed horizontally, and the dust deposition rate is plotted in Fig. 10. Weather conditions were reported during the study period. The temperature ranged from 14°C to 40°C, the humidity was 49% on average, and the wind speed was 3.88 meters per second (m/s) on average. According to Gholami *et al.,* (2017), the results might not be applicable for the same location in other weather conditions; however, they gave a deep insight into the soiling–substrate relation. For all films, dust accumulation on the surface increased with exposure time. However, as shown in Fig. 10, which shows the dust deposition rate per surface area, a significant decrease was found in the dust deposition rate (between 2.51% and 59.80% reductions) on all coated samples compared with the bare glass substrate. All mixed thin films, except for SnO_2, showed the minimum dust deposition rates. Al_2O_3 mixed-based ink sample showed the lowest value, while the SnO_2 NP-based ink sample showed the highest one. Therefore, the mixed-based inks, especially Al_2O_3, ZnO, and TiO_2,

are promising materials for ASC applications. This is because the salt-based ink lowers the surface energy (i.e., enhances hydrophilicity), whereas the NP-based ink boosts the surface roughness, which enhances the anti-soiling properties (Quan *et al.,* 2017). Furthermore, nano-voids and surface roughness enhance the transmittance and reduce the reflection (Kauppinen *et al.,* 2017). NP-based ink comes as another alternative in which Al_2O_3, ZnO, and TiO_2 have proven to be efficient ASCs. Furthermore, for both ink types (NP and mixed-based inks), Al_2O_3 coating showed the best anti-soiling performance, whereas SnO_2 demonstrated the lowest one.

CONCLUSIONS

Soiling is one of the main issues inherent to PV applications for energy generation, especially in desert regions where the weather is characterized by high levels of particulate matter and dust formation. Although several cleaning methods have been suggested, the ASC is one of the promising mitigation techniques for dust accumulation. It reduces the operational and maintenance costs and associated cleaning water consumption. This study investigated the deposition of metal oxide thin films prepared by inkjet printing. To the best of the authors' knowledge, this is the first study to report on using films developed through inkjet printing for anti-soiling applications. The fabricated films were extensively characterized and have different textures and morphologies. Two metal oxide precursors were tested, namely, the NP ink and the mixed-based ink. The coated thin films degraded the substrate's transmittance for nearly all precursors; however, a better optical performance was observed with the NP-based coatings. This enhanced performance might be due to a lower reflection triggered by the NP's voids, which reduce the spectra scattering and deterioration and, accordingly, boost the optical transmittance. The surface morphology and profile of the coated layers were also evaluated. NPs were much more visible in mixed-based coatings than in NP-based ones. The CA values ranged from super-hydrophilic to hydrophilic (minimum of 8.5° and maximum of 47.8°). To validate the results of the outdoor tests, anti-soiling properties were further tested by exposing the samples in one of the open-air sites of Qatar University. The outdoor experiment revealed that mixed-based thin films were better in reducing dust deposition than NP-based thin films and bare glass. More specifically, approximately 60% less dust was deposited on the best-performing film (Al_2O_3 mixed-based ink) compared with bare glass. Furthermore, Al_2O_3, ZnO, and TiO_2 are promising materials for ASC applications for both ink types. Further studies on the efficiency, mechanical stability, and coating properties of anti-soiling films should be performed, especially in the outdoor environment. Moreover, measuring the effect of radiation and power output with and without coatings is recommended for practical applications and commercialization purposes.

AUTHOR CONTRIBUTIONS

E. Fares performed the experimental work, conducted the literature review, and prepared the manuscript.

B. Aissa analyzed and interpreted the film characterization data. R.J. Isaifan analyzed and interpreted the application and outdoor experimental results data, and finalized the article.

ACKNOWLEDGMENT

The authors acknowledge the support provided by Hamad Bin Khalifa University, Qatar Foundation, and Qatar University.

CONFLICT OF INTEREST

The authors declare no potential conflict of interest regarding the publication of this work. In addition, the ethical issues including plagiarism, informed consent, misconduct, data fabrication and, or falsification, double publication and, or submission, and redundancy have been completely witnessed by the authors.

OPEN ACCESS

PUBLISHER'S NOTE

GJESM Publisher remains neutral with regard to jurisdictional claims in published maps and institutional affiliations.

ABBREVIATIONS

%	Percent
A (%)	absorbance (%)
$Al(NO_3)_3\ 9H_2O$	aluminum nitrate hydrate
Al_2O_3	aluminum oxide
ASC	anti-soiling coating
°C	degree Celsius
CA	contact angle
cm/min	centimeters per minute
DMP	Dimatix Materials Printer
EG	ethylene glycol
eV	electronvolt
g	Gram
GI-XRD	grazing incidence X-ray diffraction
IPA	isopropanol
kV	kilovolts
mA	milliamperes
MgF_2	magnesium fluoride
Min	minutes
µL	microliters
mL	milliliters
µm	micrometer
mm	millimeters
mN/m	millinewton per meter
mPa.s	millipascal second
m/s	meters per second
nm	nanometer
NP	nanoparticles
pL	picoliter
PV	photovoltaic
SEM	scanning electron microscopy
SiO_2	silicon dioxide
SnO_2	tin dioxide
$SnCl_2{\cdot}2H_2O$	tin chloride hydrate
R (%)	reflection (%)
T (%)	transmittance (%)
TAA	titanium diisopropoxide bis(acetylacetonate)
TiO_2	titanium dioxide
TiO_2/SiO_2	titanium and silicon dioxides
UV	ultraviolet
UV-Vis	ultraviolet-visible
V	volt
WO_3	tungsten trioxide
XPS	X-ray photoelectron spectrometer
XRD	X-ray powder diffraction
$Zn(NO_3)_2{\cdot}6H_2O$	zinc nitrates
ZnO	zinc oxide

REFERENCES

Alnaser, N.W.; Al Othman, M.J.; Dakhel, A.A.; Batarseh, I.; Lee, J.K.; Najmaii, S.; Alothman A.; Al Shawaikh H.; Alnaser W.E., (2018). Comparison between the performance of man-made and naturally cleaned PV panels in a middle of a desert. Renew. Sustain. Energy Rev., 82: 1048–1055 **(8 Pages).**

Arabatzis, I.; Todorova, N.; Fasaki, I.; Tsesmeli, C.; Peppas, A.; Li, W.X.; Zhao, Z., (2018). Photocatalytic, self-cleaning, anti-reflective coating for photovoltaic panels: Characterization and monitoring in real conditions. Sol. Energy., 159: 251–259 **(9 Pages).**

Aziz, M.; Saber Abbas, S.; Wan Baharom, W.R., (2013). Size-controlled synthesis of SnO_2 nanoparticles by sol-gel method. Mater. Lett., 91: 31–34 **(4 Pages).**

Bahattab, M.A.; Alhomoudi, I. A.; Alhussaini, M.I.; Mirza, M.; Hegmann, J.; Glaubitt, W.; Löbmann, P., (2016). Anti-soiling surfaces for PV applications prepared by sol-gel processing: Comparison of laboratory testing and outdoor exposure. Sol. Energy Mater. Sol. Cells. 157: 422–428 **(7 Pages).**

Bouabibsa, I.; Lamri, S.; Sanchette, F., (2018). Structure, mechanical and tribological properties of Me-doped diamond-like carbon (DLC) (Me = Al, Ti, or Nb) hydrogenated amorphous carbon coatings. Coatings. 8 (10): **(15 Pages).**

Buffiere, M.; Ali, K.; Fares, E.; Samara, A.; Shetty, A.R.; Al Hassan, O.; Belaidi, A., (2020). Inkjet-printed compact TiO2 electron transport layer for perovskite solar cells. Energy Technol., 8 (10): 2000330 (7 **Pages).**

Bukhari, S.F.; Lisco, F.; Moghim, T.B.; Taylor, A.; Walls, J.M., (2019). Development of a hydrophobic, anti-soiling coating for PV module cover glass. In 2019 IEEE 46th Photovoltaic Specialists Conference (PVSC). 15-21 June. Chicago, USA, 2849-2853 **(5 Pages).**

Chiu, F.C.; Chiang, W.P., (2015). Trap exploration in amorphous boron-doped ZnO films. Materials. 8(9): 5795–5805 **(11 Pages)**.

Cho, M.Y.; Park, S.J.; Kim, S.M.; Lee, D.W.; Kim, H.K.; Koo, S.M.; Moon, K.S; Oh J.M., (2018). Hydrophobicity and transparency of Al2O3-based poly-tetra-fluoro-ethylene composite thin films using aerosol deposition. Ceram. Int., 44 (14): 16548–16555 **(8 Pages).**

Cummins, G.; Desmulliez, M.P.Y., (2012). Inkjet printing of conductive materials: A review. Circuit World, 38 (4): 193–213 **(21 Pages)**.

Eihorn, A.; Micheli, L.; Miller, D.C.; Simpson, L.J.; Moutinho, H.R.; To, B.; Lanaghan, C.L.; Muller, M.T.; Toth, S.; John, J.J.; Warade, S.; Kottantharayil, A.; Engtrakul, C., (2019). Evaluation of soiling and potential mitigation approaches on photovoltaic glass. IEEE J. Photovoltaics, 9 (1): 233–239 **(7 Pages).**

Firooz, A.A.; Mahjoub, A.R.; Khodadadi, A. A., (2008). Preparation of SnO2 nanoparticles and nanorods by using a hydrothermal method at low temperature. Mater. Lett., 62 (12–13): 1789–1792 **(4 Pages)**.

Gholami, A.; Alemrajabi, A.A.; Saboonchi, A., (2017). Experimental study of self-cleaning property of titanium dioxide and nanospray coatings in solar applications. Sol. Energy., 157: 559–565 **(7 Pages).**

Huang, Y.; Lin, J.; Du, H.; Gao, L.; Yan, H., (2006). Preparation and photoluminescence properties of ZnO/amorphous-BaTiO3 thin-films by sol–gel process. Mater. Lett., 60 (29):3818-3821 **(4 Pages).**

Ilse, K.K.; Figgis, B.W.; Werner, M.; Naumann, V.; Hagendorf, C.; Pöllmann, H.; Bagdahn, J., (2018). Comprehensive analysis of soiling and cementation processes on PV modules in Qatar. Sol. Energy Mater. Sol. Cells, 186 (2018): 309–323 **(15 Pages).**

Isaifan, R.J.; Johnson, D.; Mansour, S.; Samara, A.; Suwaileh, W.; Kakosimos, K., (2018). Theoretical and experimental characterization of efficient anti-dust coatings under desert conditions. J. Thin Film. Res., 2 (1): 25–29 **(5 Pages).**

Isaifan, R.J.; Samara, A.; Suwaileh, W.; Johnson, D.; Yiming, W.; Abdallah, A.A.; Aïssa, B., (2017). Improved self-cleaning properties of an efficient and easy to scale up Tio2 thin films prepared by adsorptive self-assembly. Sci. Rep., 7 (1): 1-9 **(9 Pages).**

Hossain, M.I.; Aïssa, B.; Samara, A.; Mansour, S.A.; Broussillou, C.A.; Bermudez Benito, V., (2021). Hydrophilic antireflection and antidust silica coatings. ACS Omega., 6(8): 5276-5286 **(11 Pages).**

Javed, W.; Wubulikasimu, Y.; Figgis, B.; Guo, B., (2017). Characterization of dust accumulated on photovoltaic panels in Doha, Qatar. Sol. Energy., 142: 123–135 **(13 Pages).**

Jesus, M.A.M. L. de; Timò, G.; Agustín-Sáenz, C.; Braceras, I.; Cornelli, M.; Ferreira, A.de M., (2018). Anti-soiling coatings for solar cell cover glass: Climate and surface properties influence. Sol. Energy Mater. Sol. Cells, 185 (2018): 517–523 **(7 Pages).**

Jongnavakit, P.; Amornpitoksuk, P.; Suwanboon, S.; Ratana, T., (2012). Surface and photocatalytic properties of ZnO thin film prepared by sol-gel method. Thin Solid Films, 520 (17): 5561–5567 **(7 Pages).**

Karabay, I.; Aydin Yüksel, S.; Ongül, F.; Öztürk, S.; Asli, M., (2012). Structural and optical characterization of TiO2 thin films prepared by sol-gel process. In Acta Phys. Pol., 121: 265-267 **(3 Pages).**

Kareem, K.S.A.; Rao, K.N.; Phani, A.R.; Rani, R.U.; Sharma, A.K., (2011). Optical and structural properties of nanostructured oxide thin films by sol-gel technique. In The American Institute of Physics Conference Proceedings. 23-25 May. Kerala, India, 1391: 600–602 **(3 Pages).**

Kauppinen, C.; Isakov, K.; Sopanen, M., (2017). Grass-like alumina with low refractive index for scalable, broadband, omnidirectional anti-reflection coatings on glass using atomic layer deposition. ACS Appl. Mater. Interfaces, 9 (17): 15038–15043 **(6 Pages).**

Lee, H.; Yi, A.; Choi, J.; Ko, D.-H.; Kim, H., (2022). Texturing of polydimethylsiloxane surface for anti-reflective films with super-hydrophobicity in solar cell application. Appl. Surf. Sci., 584: 152625 **(8 pages).**

Legrand-Buscema, C.; Malibert, C.; Bach, S., (2002). Elaboration and characterization of thin films of TiO2 prepared by sol-gel process. Thin Solid Films, 418 (2): 79–84 **(6 Pages).**

Li, X.; He, J.; Liu, W., (2013). Broadband anti-reflective and water-repellent coatings on glass substrates for self-cleaning photovoltaic cells. Mater. Res. Bull., 48 (7): 2522–2528 **(7 Pages).**

Lin, L.Y.; Kim, D.E., (2009). Effect of annealing temperature on the tribological behavior of ZnO films prepared by sol-gel method. Thin Solid Films, 517 (5): 1690–1700 **(11 Pages).**

Liu, X.; Tarn, T.J.; Huang, F.; Fan, J., (2015). Recent advances in inkjet printing synthesis of functional metal oxides. Particuology, 19 (2015): 1–13 **(14 Pages).**

Lortie, M.; Isaifan, R.J.; Liu, Y.; Mommers, S., (2015). Synthesis of CuNi/C and CuNi/-Al2O3 catalysts for the reverse water gas shift reaction. Int. J. Chem. Eng., 2015: 750689 **(9 pages).**

Lu, J.; Huang, K.; Chen, X.; Zhu, J.; Meng, F.; Song, X.; Sun, Z., (2010). Reversible wettability of nanostructured ZnO thin films by sol-gel method. Appl. Surf. Sci., 256 (14): 4720–4723 **(4 Pages).**

Micheli, L.; Muller, M., (2017). Seasonal trends of soiling on PV

systems. 2017 IEEE 44th Photovoltaic Conference (PVSC). 25-30 June. Washington, USA, 2301-2306 **(8 Pages).**

Na, M.J.; Yang, H.; Jung, H.J.; Park, S.D., (2019). Robust hydrophobic surface driven by Al2O3/glass composite coatings. Surf. Coatings Technol., 372(2019): 134–139 **(6 Pages).**

Nunes, D.; Pimentel, A.; Santos, L.; Barquinha, P.; Pereira, L.; Fortunato, E.; Martins, R., (2019). Oxide materials for energy applications. Met. Oxide Nanostructures. **(36 Pages).**

Oh, W.; Kang, B.; Choi, S.; Bae, S.; Jeong, S.; Kim, S.M.; Lee, H.S.; Kim, D.; Hwang, H.; Chan, Sung. I., (2016). Evaluation of anti-soiling and anti-reflection coating for photovoltaic modules. J. Nanosci. Nanotechnol., 16 (10): 10689–10692 **(4 Pages).**

Ota, Y.; Ahmad, N.; Nishioka, K., (2016). A 3.2% output increase in an existing photovoltaic system using an anti-reflection and anti-soiling silica-based coat. Sol. Energy., 136: 547–552 **(6 Pages).**

Paul S.; Hossain M.F.; Islam M.H.; Raihan M.A.; Chakladar S., (2014). Optical properties of ZnO thin films prepared by automatic sol-gel method. In 2013 IEEE International conference on Electrical Information and Communication Technology (EICT). 13-15 February. Khulna, Bangladesh, 1-4 **(6 Pages).**

Pendse, S.; Chandra, S.R., K.; Narendra, C.; Murugan, K.; Sakthivel, S., (2018). Dual-functional broadband anti-reflective and hydrophobic films for solar and optical applications. Sol. Energy., 163 (2018): 425–433 **(9 Pages).**

Perez-Tomas, A.; Mingorance, A.; Tanenbaum, D.; Lira-Cantú, M., (2018). Metal oxides in photovoltaics: All-oxide, ferroic, and perovskite solar cells. Metal oxides, the future of semiconductor oxides in Next-generation solar cells. 267–356. Elsevier **(90 Pages).**

Pescheux, A.C.; Raccurt, O.; Bourdon, D.; Le Baron, E., (2020). Accelerated aging tests and characterizations of innovated anti-soiling coatings for solar receiver glasses. Mater. Chem. Phys., 256: 123646 **(8 Pages).**

Piliougine, M.; Cañete, C.; Moreno, R.; Carretero, J.; Hirose, J.; Ogawa, S.; Sidrach-de-Cardona, M., (2013). Comparative analysis of energy produced by photovoltaic modules with anti-soiling coated surface in arid climates. Appl. Energy, 112(C): 626–634 **(9 Pages).**

Polizos, G.; Jang, G.G.; Smith, D.B.; List, F.A.; Lassiter, M.G.; Park, J.; Datskos, P.G., (2018a). Transparent superhydrophobic surfaces using a spray coating process. Sol. Energy Mater. Sol. Cells, 176: 405–410 **(6 Pages).**

Polizos, G.; Sharma, J.K.; Smith, D.B.; Tuncer, E.; Park, J.; Voylov, D.; Sokolov, A.P.; Meyer III, H.M.; Aman, M., (2018b). Anti-soiling and highly transparent coatings with multi-scale features. Sol. Energy Mater. Sol. Cells, 188 (2018): 255–262 **(8 Pages).**

Potlog, T.; Dumitriu, P.; Dobromir, M.; Luca, D., (2014). XRD and XPS analysis of TiO2 thin films annealed in different environments. J. Mater. Sci. Eng. B, 4 (6): **(8 Pages).**

Quan, Y.Y.; Zhang, L.Z., (2017). Experimental investigation of the anti-dust effect of transparent hydrophobic coatings applied for solar cell covering glass. Sol. Energy Mater. Sol. Cells, 160: 382–389 **(8 Pages).**

Rieu, M.; Camara, M.; Tournier, G.; Viricelle, J.-P.; Pijolat, C.; de Rooij, N.F.; Briand, D., (2016). Fully inkjet printed SnO2 gas sensor on plastic substrate. Sensors Actuators B Chem., 236: 1091–1097 **(7 Pages).**

Said, S.A.; Al-Aqeeli, N.; Walwil, H.M., (2015). The potential of using textured and anti-reflective coated glasses in minimizing dust fouling. Sol. Energy, 113: 295–302 **(8 Pages).**

Saini, K.K.; Sharma, S.D.; Chanderkant; Kar, M.; Singh, D.; Sharma, C.P., (2007). Structural and optical properties of TiO2 thin films derived by sol-gel dip coating process. J. Non. Cryst. Solids. 353 (24–25): 2469–2473 **(5 Pages).**

Shang, Q.; Zhou, Y., (2016). Fabrication of transparent superhydrophobic porous silica coating for self-cleaning and anti-fogging. Ceram. Int., 42 (7): 8706–8712 **(7 Pages).**

Sobczyk-Guzenda, A.; Pietrzyk, B.; Szymanowski, H.; Gazicki-Lipman, M.; Jakubowski, W., (2013). Photocatalytic activity of thin TiO2 films deposited using sol-gel and plasma enhanced chemical vapor deposition methods. Ceram. Int., 39 (3): 2787–2794 **(8 Pages).**

Sueto, T.; Ota, Y.; Nishioka, K., (2013). Suppression of dust adhesion on a concentrator photovoltaic module using an anti-soiling photocatalytic coating. Sol. Energy., 97: 414–417 **(4 Pages).**

Talinungsang, N.P.; Purkayastha, D.D., (2017). SnO2/TiO2 bilayer thin films exhibiting superhydrophilic properties. In The American Institute of Physics Conference Proceedings. 26-30 December. Odisha, India, 1832: 080035 **(4 Pages).**

Thongsuwan, W.; Sroila, W.; Kumpika, T.; Kantarak, E.; Singjai, P. (2022) et al. Antireflective, photocatalytic, and superhydrophilic coating prepared by facile sparking process for photovoltaic panels. Sci. Rep., 12: 1675 **(15 pages).**

Wang, J.; Yang, S.; Chen, M.; Xue, Q., (2004). Preparation and characterization of arachidic acid self-assembled monolayers on glass substrate coated with sol-gel Al2O3 thin film. Surf. Coatings Technol., 176 (2): 229–235 **(7 Pages).**

Wang, Y.; Li, B.; Liu, T.; Xu, C.; Ge, Z., (2014). Controllable fabrication of superhydrophobic TiO2 coating with improved transparency and thermostability. Colloids Surf., A 441: 298–305 **(8 Pages).**

Xia, W.; Wang, H.; Zeng, X.; Han, J.; Zhu, J.; Zhou, M.; Wu, S., (2014). High-efficiency photocatalytic activity of type II SnO/Sn3O4 heterostructures via interfacial charge transfer. Cryst. Eng. Comm., 16 (30): 6841–6847 **(7 Pages).**

Yamaguchi, N.; Tadanaga, K.; Matsuda, A.; Minami, T.; Tatsumisago, M., (2005). Anti-reflective coatings of flower-like alumina on various glass substrates by the sol-gel process with the hot water treatment. J. Sol-Gel Sci. Technol., 33 (1): 117–120 **(4 Pages).**

AUTHOR (S) BIOSKETCHES

Fares, E., Ph.D. Candidate, College of Science and Engineering, Hamad Bin Khalifa University Qatar Foundation, Doha, Qatar.

- Email: *efares@hbku.edu.qa*
- Web of Science Researcher ID: NA
- Scopus Author ID: NA
- ORCID: 0000-0001-5989-2590
- Homepage: http://www.qu.edu.qa/engineering/Academic-Departments/Department-of-Mechanical-and-Industrial-Engineering/Faculty-and-Staff

Aissa, B. Ph.D., Associate Professor, Qatar Environment and Energy Research Institute, Hamad Bin Khalifa University, Qatar Foundation, Doha, Qatar

- Email: *baissa@hbku.edu.qa*
- Web of Science Researcher ID: I-4522-2014
- Scopus Author ID: NA
- ORCID: 0000-0002-4768-9891
- Homepage: https://www.hbku.edu.qa/en/staff/brahim-aissa

Isaifan, R., Ph.D., Joint Faculty, College of Science and Engineering, Hamad Bin Khalifa University, Qatar Foundation, Doha, Qatar.

- Email: *risaifan@hbku.edu.qa*
- Web of Science Researcher ID: AAL-9634-2020
- Scopus Author ID: 54897983000
- ORCID: 0000-0002-9590-4939
- Homepage: https://www.hbku.edu.qa/ar/staff/rima-jamal-isaifan

HOW TO CITE THIS ARTICLE

Fares, E.; Aïssa, B.; Isaifan,R.J. (2022). Inkjet printing of metal oxide coatings for enhanced photovoltaic soiling environmental applications. Global J. Environ. Sci.Manage., 8(4): 485-502.

DOI: 10.22034/gjesm.2022.04.03

url: https://www.gjesm.net/article_250777.html

Global J. Environ. Sci. Manage. 8(4): 503-518, Autumn 2022, Serial #32

Global Journal of Environmental Science and Management
(GJESM)

Homepage: https://www.gjesm.net/

ORIGINAL RESEARCH PAPER

Characteristics and circulation of archipelagic waters with the three-dimensional hydrodynamic model approach

Suhaemi[1,2], D.G. Bengen[2], C.P.H. Simanjuntak[3], A.F. Koropitan[2]

[1] *Department of Marine Sciences, Faculty of Fisheries and Marine Science, University of Papua, Manokwari 98314, Indonesia*

[2] *Department of Marine Sciences and Technology, Faculty of Fisheries and Marine Science, IPB University, Bogor 16680, Indonesia*

[3] *Department of Aquatic Resources Management, Faculty of Fisheries and Marine Science, IPB University, Bogor 16680, Indonesia*

ARTICLE INFO

Article History:
Received 01 October 2021
Revised 11 January 2022
Accepted 17 February 2022

Keywords:
Barotropic tides
Misool Islands
Three-dimensional
Tidal current
Water mass

DOI: 10.22034/gjesm.2022.04.04

ABSTRACT

BACKGROUND AND OBJECTIVES: The Misool Islands are lined up regularly from west to east, the southern part of Raja Ampat Archipelago, Papua - Indonesia. The geomorphology is distinctive, and the coral reef substrate causes turbulence. Misool waters are located in the Papuan bird's head seascape, passed by Pacific water masses. The assessment status of Misool waters as a conservation area does not include hydrodynamic aspects in the decision processes. The present study is fundamental for determining and changing essential areas for conservation. The main objective of this study is to the pattern of hydrodynamic processes and investigate the features of the water mass in the Misool waters.

METHODS: An acoustic doppler current profiler was deployed to measure currents every 15 minutes for ten water column layers. Investigation of waters characteristics was using Conductivity-Temperature-Depth equipment. A three-dimensional computational model was performed using MIKE3.

FINDINGS: The water mass around the Misool Islands are more influenced by the local oceanographic processes than the water masses from the Pacific Ocean. The study site is characterized by the mixed tide, prevalence to semi-diurnal based on observational tidal data. Wind and baroclinic properties generate non-significant currents, resulting in low horizontal and vertical stratification. Intensification of tidal currents occurs along the shallow part in northeastern and part of the channel between Misool Islands and the mainland of Papua.

CONCLUSION: The interaction of barotropic tides, geomorphology, and coral reef triggers the unstratified water mass. Strong currents and turbulence on the northeast side produce homogeneous waters. The water mass in Misool waters is originated from the local dynamic.

NUMBER OF REFERENCES	NUMBER OF FIGURES	NUMBER OF TABLES
37	10	1

*Corresponding Author:
Email: *s.manaf@unipa.ac.id*
Phone: 0813 4487 9586
ORCID: 0000-0003-4585-2277

Note: Discussion period for this manuscript open until January 1, 2023 on GJESM website at the "Show Article".

INTRODUCTION

The study of hydrodynamics, especially in coastal areas, is an important thing that needs to be done. Hydrodynamics is one of the water control systems that have implications for the distribution of marine life: transport of fish eggs and larvae (George *et al*., 2013). It makes the hydrodynamics of the waters play a role in the sustainability of aquatic biodiversity. Monsoonal wind and density are driving forces for the hydrodynamics in the coastal area. In particular, coastal areas, tidal currents regulate material transport and biological processes and control the intensification of materials in the waters (Koropitan *et al*., 2006). The current patterns greatly determine water quality, oxygen distribution, temperature, salinity, nutrient supply, primary productivity (Porter *et al.*, 2018). Tides and currents are significant for coastal development planning, management, conservation, fishing, and coastal mitigation. Understanding the hydrodynamic aspects of the waters requires a long and expensive field study and an applicable completion method. The best solution that can be done is through a three-dimensional modeling approach as a prototype of the natural and factual conditions. This approach has been carried out in several other areas, including Mayalibit Bay, Raja Ampat-Indonesia (Budiman *et al*., 2014), Tomori Bay, North Morowali-Indonesia (Sabhan *et al*., 2021), the Malacca Strait-Indonesia (Haditiar *et al*., 2020), the West Coast of Badung Regency, Bali-Indonesia (Adhibusana *et al*., 2016), Benoa Bay-Indonesia (Hendrawan *et al*., 2005), and Ambon Bay (Noya *et al*., 2016; Noya *et al*., 2021). The modeling approach can be used in various water conditions, including archipelagic waters. One of the archipelagic areas with high urgency to study its hydrodynamics in Misool Islands. Misool Islands are the largest marine protected area with the highest biodiversity, located in the Raja Ampat Islands, Indonesia. Misool Islands are characterized by zonal-lined coral reef substrates and varying bathymetry (1 to 500 m). The combination of the original characteristics of the islands and the tidal dynamics produces variations in circulation (Zhang *et al*., 2018). These interactions generate internal waves and stimulate mixing (Sabhan *et al*., 2019). The shape of the waters of Misool Islands is semi-enclosed and resembles a channel, affecting tidal wave propagation (Ferrarin *et al*., 2018) and sensitivity to bathymetry (Pringle *et al*., 2018). Several studies that have been conducted on Misool Islands are still limited to the fisheries aspect, namely capture fisheries management (Sala, 2018), the ecological status of fish in Misool marine conservation (Sala *et al*., 2020), observations of the Misool marine lake ecosystem (Purba, 2020; Sawairnathan and Halimoon, 2017), monitoring grouper spawning areas. Studies that underlie these aspects, including hydrodynamics, have never been carried out. Position of the Misool waters in the Papuan bird's head seascape network is passed by the Pacific water masses to the Indian Ocean. What is the influence of the Pacific water masses in the Misool Islands? The geographical position of the Misool waters, complex geomorphology, and coral reef substrates create a unique circulation pattern, and this statement needs to be proven. What is the impact of complex geomorphology and coral reef substrate on flow patterns in the waters of the Misool Islands, West Papua? The present study aims to examine the hydrodynamics processes of the Misool Islands. The objectives of this study are to investigate the characteristics of waters masses and to analyze the impact of complex geomorphology and coral reef substrate on flow patterns in Misool waters. This study has been carried out in Misool waters during 11 - 14 May 2019 for water mass measurement and during 9 - 21 January 2020 for ocean current measurement.

MATERIALS AND METHODS

Area study

Misool Islands are located in the Raja Ampat Archipelago, West Papua Province, Indonesia. The islands have an area of 2,034 square kilometers with the highest elevation of 535 m above sea level. This island is located on the bird's head of West Papua and is directly adjacent to the Seram Sea on the south and west sides and the Halmahera Sea on the west. The waters of Misool Islands have shallow bathymetry on the east and south sides, while the west and southwest sides are deep. The water depth ranges from 1 to 500 m. Misool Islands are one of the world's coral triangles with high biodiversity and are the largest conservation area in Raja Ampat (346,189 ha). Besides coral reefs, Misool Islands' biodiversity includes turtles, manta rays, saltwater crocodiles, seagrass beds, and mangroves. Misool Islands waters are also one of the transmigration routes of whales and octopuses.

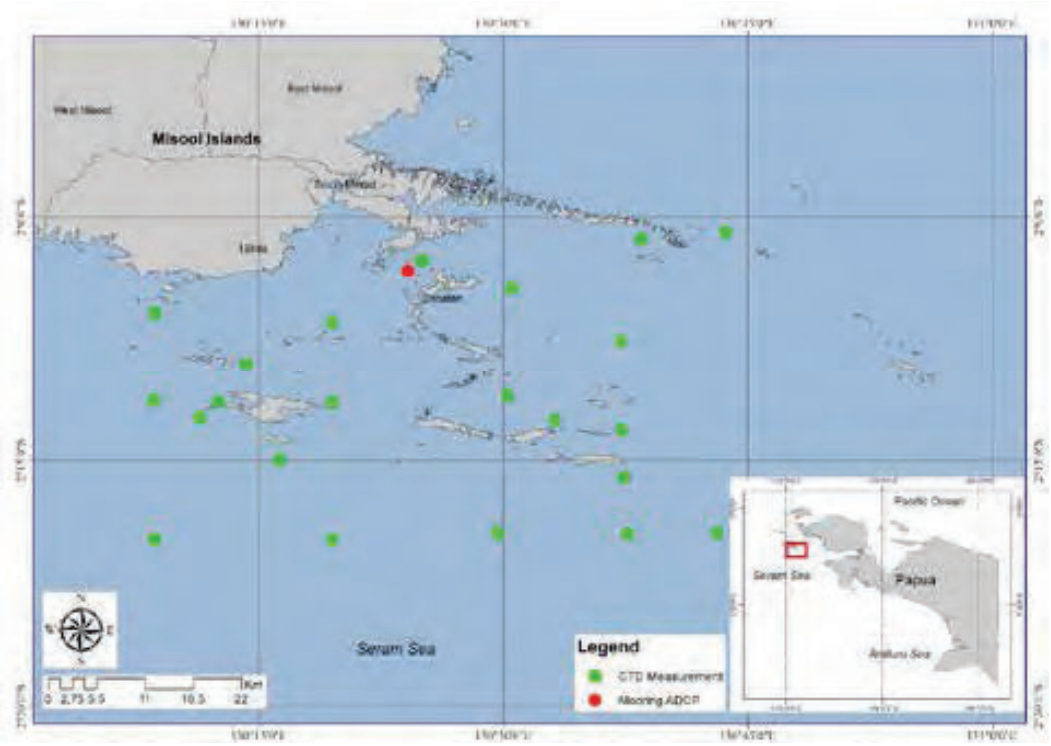

Fig. 1: Geographic location of the study area and station sampling in Misool, West Papua, Indonesia

Field sampling

Tidal forces and geomorphology were controlling current patterns in the Misool waters. Identification of the Misool waters characteristics (depth, temperature, conductivity, density) vertically and horizontally was carried out using Conductivity-Temperature-Depth (CTD) equipment at 22 stations during 11 - 14 May 2019 (Fig. 1). The CTD was deployed slowly at each station until closed to the bottom water (monitored directly via the control unit on the boat). The bathymetry (interval 10 m - 100 m) around Misool Islands was recorded using Single-Beam Echosounder G-2108. The echosounder was installed on the boat and recorded on a pre-set path. The pre-set path is perpendicular to the shoreline and concentrated on coastal areas and small islands. To avoid bias, the boat speed is adjusted around 2.5 m/s - 3.0 m/s (Koropitan *et al.,* 2021). The current was observed 13 days (9 - 21 January 2020) by employing the Acoustic Doppler Current Profiler (ADCP) SonTek Argonaut-XR (accuracy 0.5 cm/s). The ADCP was deployed at 27 m depth, equipped with buoys and anchors, and recorded every 15 minutes in 10 water column layers.

Hydrodynamic modeling

The ecological processes of Misool waters were approached using the three-dimensional (3D) numerical model by using MIKE3. Numerical solutions are based on the Navier-Stokes equation, the Boussinesq approximation, and hydrostatic pressure. The turbulent waters conditions were determined using the eddy viscosity concept. Turbulence parameters using the standard k-ε (Canuto *et al.,* 2001) and vertical eddy viscosity using the concept of Smagorinsky (1963).

The continuity is used as Eq. 1.

$$\frac{\partial u}{\partial x}+\frac{\partial v}{\partial y}+\frac{\partial w}{\partial z}=S \quad (1)$$

The horizontal momentum for the x-component is used as Eq. 2.

$$\frac{\partial u}{\partial t}+\frac{\partial u^2}{\partial x}+\frac{\partial vu}{\partial y}+\frac{\partial wu}{\partial z}=fv-g\frac{\partial \eta}{\partial x}-\frac{1}{\rho_0}\frac{\partial P_a}{\partial x}-\frac{g}{\rho_0}\int_z^{\eta}\frac{\partial \rho}{\partial x}dz-\frac{1}{\rho_0 h}\left(\frac{\partial S_{xx}}{\partial x}+\frac{\partial S_{xy}}{\partial y}\right)+F_u+\frac{\partial}{\partial z}\left(v_t\frac{\partial u}{\partial z}\right)+u_s S \quad (2)$$

The horizontal momentum for the y-component is used as Eq. 3.

$$\frac{\partial v}{\partial t}+\frac{\partial v^2}{\partial y}+\frac{\partial uv}{\partial x}+\frac{\partial wv}{\partial z}=fu-g\frac{\partial \eta}{\partial y}-\frac{1}{\rho_0}\frac{\partial P_a}{\partial y}-\frac{g}{\rho_0}\int_z^{\eta}\frac{\partial \rho}{\partial y}dz-\frac{1}{\rho_0 h}\left(\frac{\partial S_{yx}}{\partial x}+\frac{\partial S_{yy}}{\partial y}\right)+F_v+\frac{\partial}{\partial z}\left(v_t\frac{\partial v}{\partial z}\right)+v_s S \quad (3)$$

Model set-up, initial conditions, and boundary conditions

The Misool waters system is designed in a flexible mesh based on sigma coordinates (10 layers). The model domain is set to 7000 Km^2, 100 Km in zonal direction, and 70 Km in the meridional direction. The flexible mesh is also made in detail in the east-south Misool (conservation area). It also accommodates the simulation's tides, wind, salinity, and temperature. The time step was 30 seconds, 3D turbulent variables used k-epsilon, and vertical viscosity factors followed the Smagorisky formula based on an earlier study (Pradhan *et al.,* 2020). Based on the pre-test, it was found that the best viscosity and vertical diffusivity coefficient in Missol waters are $1.8x10^{-6}$ m^2/s, higher than the previous study, which only 10^{-7} m^2/s (Seiler *et al.,* 2020). The roughness sensitivity (Manning number) and horizontal turbulent viscosity are 0.02 - 0.05 and 1 m^2/s - 10 m^2/s. At the initial condition (t = 0), the waters conditions were assumed constant in all computational domains, and without vertical and horizontal disturbances (u = v = η = 0). Temperature and salinity are initialized vertically at the open boundary (Sorourian *et al.,* 2020). At the open boundary, the current is generated from the tide, temperature (29°C), salinity (33 PSU), and wind. The Misool sea level elevation data originated from the tide model in the toolbox of the Danish Hydraulic Institute (DHI). The temperature and salinity are derived from CTD measurements. The wind obtained from the European center for medium-range weather forecasts (ECMWF) reanalysis (0.125° by 0.125° resolution) in two years (2019 - 2020).

RESULTS AND DISCUSSION

The current profile of Misool waters

The ADCP data showed that the current is varied among layers. The strongest current (maximum 0.86 m/s, an average of 0.26 m/s) was recorded near-surface layers. The weakest (maximum 0.36 m/s, an average of 0.10 m/s) was near the bottom. This study found that the currents vector is not in line with depth (Fig. 2). This weakening is due to the non-linear impact of weakening winds on depth and increasing base resistance (Lee dan Beardsley, 1999). Misool waters with coral reef substrate have a high bottom resistance and reduce the current velocity. Layer 1 to 4 the current variation is homogeneous, a maximum of 0.36 m/s - 0.39 m/s, a minimum 0.001 m/s - 0.003 m/s and an average 0.01 m/s - 0.14 m/s. Layer 5 and layer 6 maximum current is 0.44 m/s and 0.59 m/s, an average 0.17 and 0.20 m/s and a minimum 0.004 m/s. Layer 7 to 10 maximum current 0.73 m/s, 0.83 m/s, 0.86 m/s, and minimum 0.006 m/s. Hadikusumah (2010) finds a similar pattern. The Misool waters current varied 0.002 m/s - 0.74 m/s. The current direction shows an alternating regularity pattern, describing Misool waters as the dominant tidal current. The main current direction to the northeast and southwest align with the tidal propagation. The current vector in layers 1 to 3 is dominant to the southwest (200° - 250°), with 22.68% - 24.37% frequency. Layers 4 to 9 are dominant to the northeast (20° - 70°) with a frequency of 32.05% - 35.24%, and layer ten dominant current 34.11% moving to the southwest (200° - 250°). The dominant current towards the northeast and southwest ensures that the dominant force of the Misool waters is tidal. At high tide, the current enters the Misool waters to the northeast and at low tide to the southwest. The waters of Misool are open on the west and south sides, bordering the Seram Sea. The Mainland of Papua connects the east side, contributing to the arrangement of the alternating flow pattern. The current circulation formed is the resultant of all the constituents of the current force. The separation of the tidal currents and residual currents indicates that the tidal currents are dominant. The maximum current was 0.64 m/s, the maximum residual current was 0.22 m/s. The non-linear effect is seen in the residual current with an irregular direction. Tidal currents create a regular pattern; at high tide, it moves to the northeast and at low tide to the southwest. Tidal currents to the northeast (20° - 70°) with a frequency of 42.70%, a maximum speed of 0.32 m/s, and an average of 0.15 m/s. The southwestward current (200° - 250°) has a frequency of 21.35%, a maximum of 0.31 m/s, and an average of 0.14 m/s. The percentage of tidal currents during the flood was more dominant

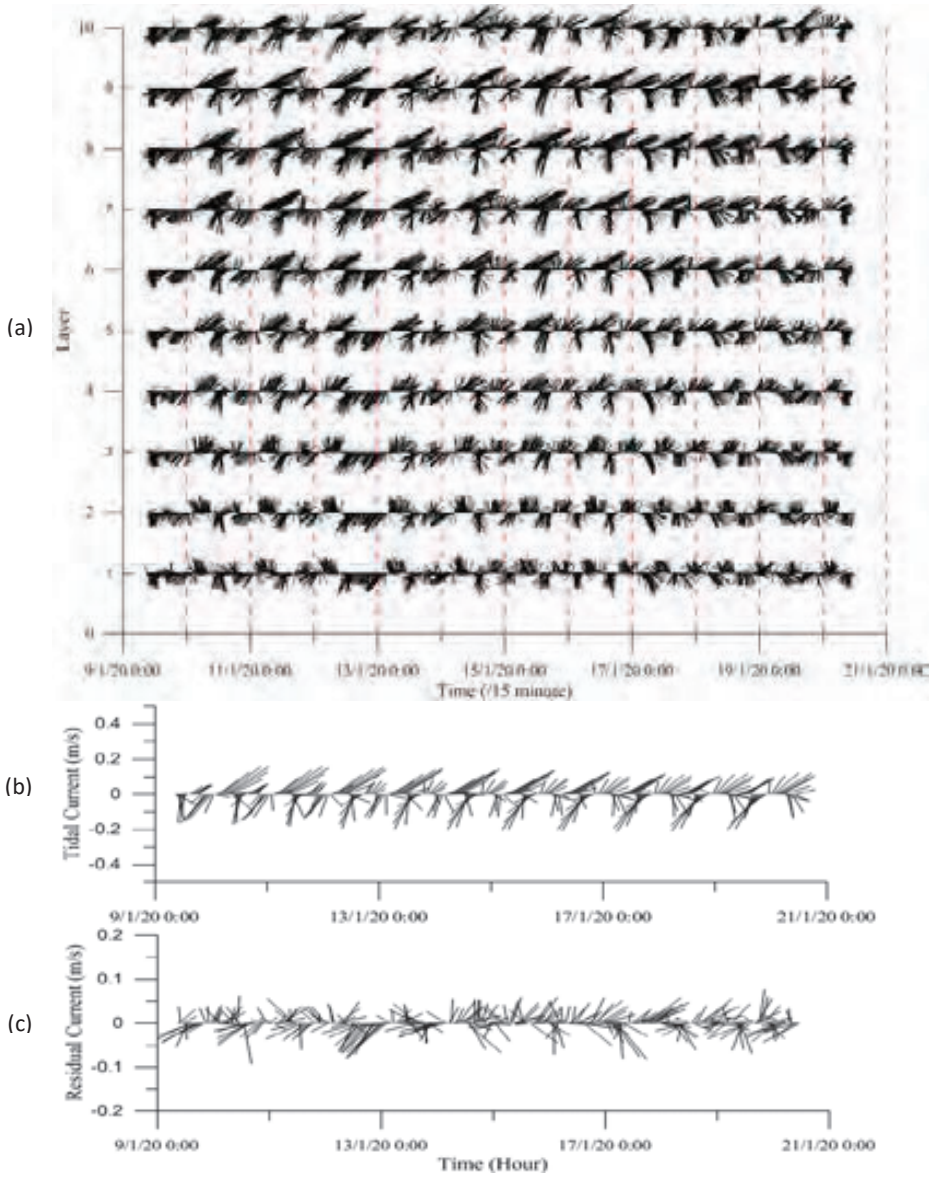

Fig. 2: Water current profile at ten layers (a); the separation of the tidal current (b) and residual current (c) components averaged to depth.

than low tide. Misool Islands are characterized by the mixed tide: semi-diurnal tides with two high tides and one low tide. The residual current flow is random, to the northeast, southwest, northwest, north, and southeast, with frequencies of 26.22%, 20.97%, 11.61%, 10.49%, and other 9.74% spread out in various directions with a small percentage. Unidirectional with the westerly monsoon that blows over the Misool waters in January, the dominant residual current spreads to the northeast. There is a positive relationship between the westerly monsoon and residual current, the westerly monsoon from the southwest, and the dominant residual current to the northeast. The progressive vector of the residual current to the northeast has a maximum speed of 0.18 m/s, with an average of 0.08 m/s. The residual current to the southwest has a maximum speed of 0.22 m/s and an average of 0.11 m/s. The velocity of the residual current that moves to the southwest is greater than the northeast direction.

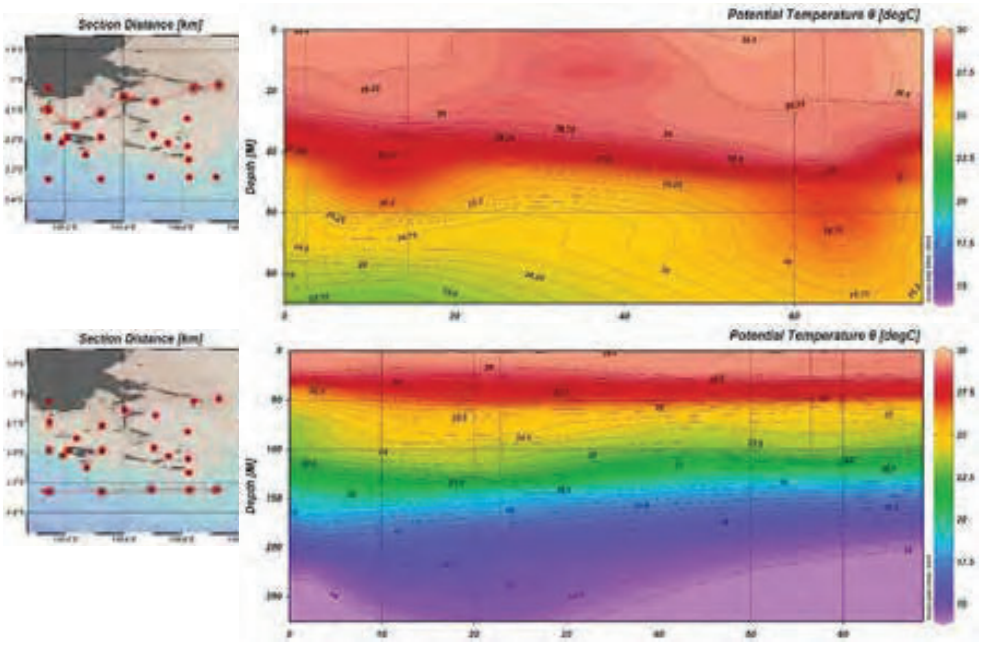

Fig. 3: The observation of spatial vertical temperature of Misool waters

Temperature and salinity of Misool waters

The characteristics of the Misool waters (temperature, salinity, density) are based on CTD recording data. This study found that the vertical water's temperature ranged from 28.9°C to 29.7°C, with an average of 29.5°C (Fig. 3). This temperature is characteristic of warm tropical waters. These findings were confirmed by a previous study that found the tropical waters have a surface temperature greater than 28°C and a range of 28°C - 30°C, and temperature variations increase towards the ocean (Ilahude and Gordon, 1996). Fig. 3 shows the vertical temperature profile from 0 to 350 m (CTD depth limit). The southern CTD station in Misool waters found that the vertical temperature varied between 14°C - 29.7°C, indicating mixed and thermocline layers in the water column. The other areas (east, northeast, and southeast) show the homogenous layers in the water column (Fig. 3). The homogenous layer is due to the shallow waters in those areas, combined with the strong current, which is the main energy for the mixing force. The maximum mixed layer depth (MLD) on Misool water was 100 m and characterized by homogeneous temperature (25.5°C - 29.5°C). The MLD shows different depths at several observation stations but has a similar pattern. The local thermocline layer in tropical waters is characterized by extreme temperature changes (over to 20°C) (Hutabarat *et al.,* 2018) and changes in the density of 0.15 kg/m^3 for each added 10 m depth (Thomson and Emery, 2014). This study found a declining temperature of 20.0°C - 21.5°C at a depth of 100 m, the thickness of the thermocline layer reaches 100 m, and the boundary between the lower thermocline and the inner layer is at a depth of > 250 m. The vertical salinity distribution for each station is invariant between stations and in line with the depth increase (Fig. 4). Depth 0 m - 100 m salinity is homogeneous, increasing at deeper depths. A depth of 100 m - 200 m indicates a halocline layer with significant salinity changes and a salinity core found at a depth of 150 m (34.25 PSU). The salinity profile is homogeneous on the northeast of the Misool waters, ranging from 32.45 PSU to 33.45 PSU. The surface salinity showed homogeneity in the range of 32.50 PSU. The vertical profile has an increasing salinity variation with depth 32.00 PSU - 34.25 PSU. The horizontal profile of salinity has a similar pattern to the temperature. The maximum salinity of 32.50 PSU was found at the Parongket Island station. The minimum salinity was found in the coastal area near the mainland of Papua. Low salinity is found at the mainland boundary due to freshwater intrusion from the Misool Islands and the west side of the river

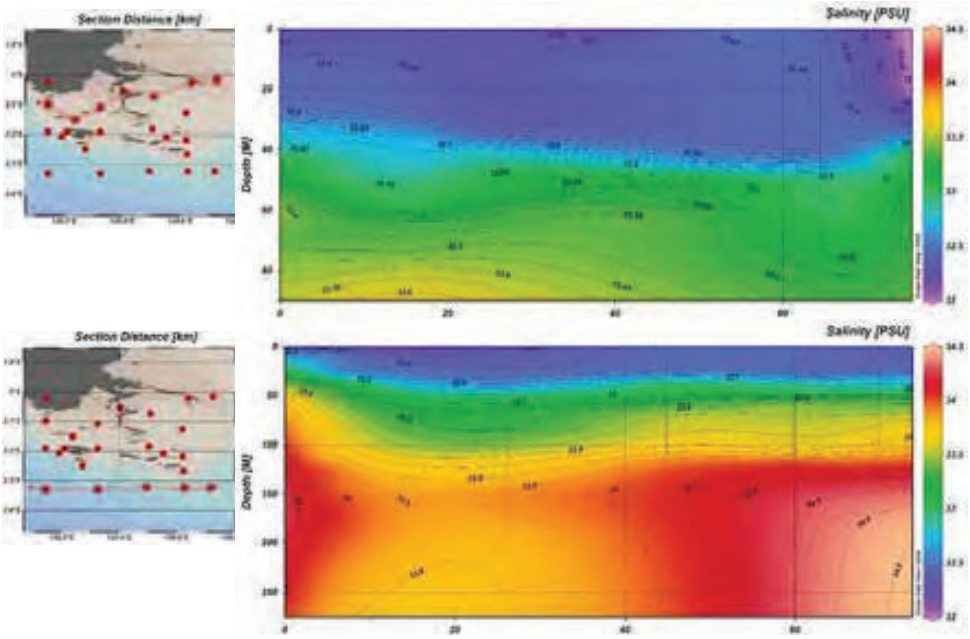

Fig. 4: The observation of spatial vertical salinity of Misool waters

discharge from the Kaimana and Bintuni Islands. Fig. 4 shows the vertical salinity distribution in the 0 m - 50 m layer of 32.15 PSU - 32.50 PSU. The salinity increases of 33.10 PSU - 33.90 PSU at a depth of 50 m - 100 m, and the maximum salinity is found at a depth of 150 m, which is 34.25 PSU. The salinity dropped to 33.85 PSU again at a depth of 200 m to the CTD depth limit. This pattern only occurs on the west and southwest sides. The east, northeast, and southeast are homogeneous vertically. In the southwest and south, at a depth of 150 m, the observation station between latitude -2.3° and longitude 130.2° - 130.4° forms a high salinity front. It is possibly due to the high salinity spooky seawater mass in the south and southwest touching with the origin water mass of Misool. As a reference, it is known that the waters off the coast of the Seram Sea have a salinity > 34.5 PSU, which is advanced than the salinity of the Misool waters < 33.5 PSU.

Characteristics of the Misool water mass

The Misool water mass description is illustrated in the T_{pot}-S diagram (Fig 5). This diagram found that the salinity increases (maximum of 34.25 PSU) from the surface to 200 m depth and then decreases at a depth of more than 200 m. It is shown by the sigma-t value, which drops at a depth of more than 250 m. At a depth of 150 m - 200 m, salinity is stable at 33.75 PSU -34.00 PSU and a sigma-t value of 24.5 kg/m^3. There is no similarity between the Misool water mass and the North and South Pacific water mass based on the T_{pot}-S diagram. It indicates that the water mass in our study area originates from Misool waters. The Misool waters are in a Papuan bird's head seascape network, where Pacific water masses cross the seas as Indonesian Throughflow (ITF). Halmahera eddy deflects Pacific water masses that flow through the eastern route. The rest is pushed through the Maluku Sea and the Seram Sea, entering the Banda Sea and exiting Indonesian waters through the Flores Sea and the Timor Sea. The water mass of the ITF is a mass of deep water that flows at a depth of more than 100 m, while the waters of the southeast Misool are shallow. This finding aligns with Radjawane and Hadipoetranto (2014), which stated that the ITF originating from the North Pacific and South Pacific via the eastern route does not flow directly to the Misool Islands waters. Hadikusumah (2010) explained that the Misool waters in the mixed layer to a depth of < 100 m found a temperature range between 29.26°C - 27.00°C and salinity between 33.90 PSU - 34.21 PSU. These conditions exhibit characteristics analogous to those obtained in this study. The characteristics of the waters (Fig. 5) show that the mixed layer is found

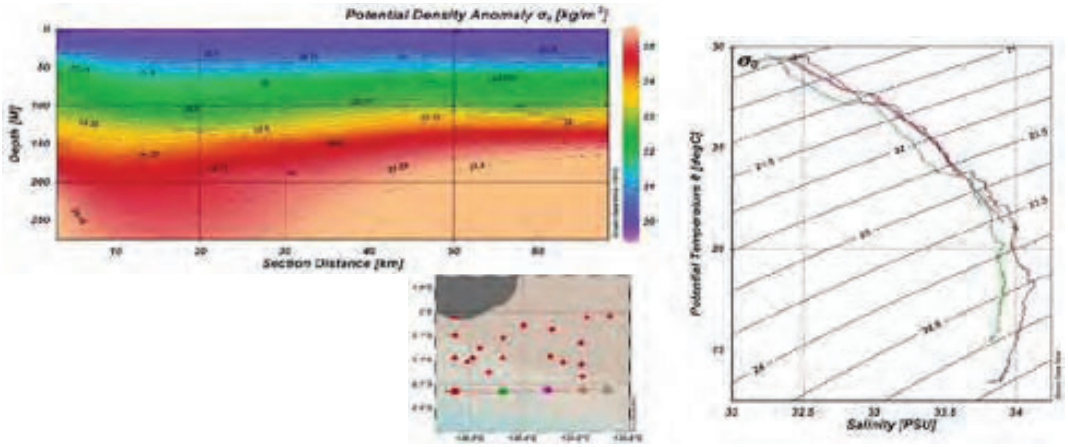

Fig. 5: The observation of vertical density potential and T_{pot}-S diagram of Misool waters

Table 1: Comparison of tidal current (ellipse constituents) between model results and observation

Layer	Tidal constituents	Delta major ellipse (cm/s)	Delta minor ellipse (cm/s)	Delta inclination (degree from the east)	Delta phase (˚GMT)
1_bottom	K1	8.22	1.58	0.71	128.83
4_column	K1	3.03	0.25	25.34	150.17
7_column	K1	1.24	0.88	22.30	145.16
10_surface	K1	6.79	0.94	3.78	145.94
1_bottom	M2	2.65	1.58	26.83	12.68
4_column	M2	1.24	3.79	7.02	15.14
7_column	M2	2.28	2.08	13.54	0.28
10_surface	M2	4.32	3.43	11.96	23.13
1_bottom	O1	2.74	3.39	36.09	77.60
4_column	O1	0.86	0.62	5.77	79.62
7_column	O1	1.99	0.94	3.59	81.30
10_surface	O1	1.52	0.77	8.19	76.09
1_bottom	S2	0.32	0.92	7.35	4.54
4_column	S2	0.82	0.19	8.88	4.68
7_column	S2	0.21	0.03	19.41	16.99
10_surface	S2	3.94	0.69	24.86	8.68

at a depth of 50 m with a temperature of 27.5°C - 29.0°C and salinity of 32.5 PSU - 32.8 PSU; at a depth of 50 m - 100 m, the temperature decreases to 24.5°C - 25.5°C and salinity of 33.5 PSU - 33.6 PSU. It is found that significant temperature changes of 22°C - 17.5°C at a depth of 125 m - 225 m. T_{pot}-S diagram shows red and green lines, indicating different salinity characteristics, with the green line reaching a maximum salinity of 33.8 PSU found at a depth of 150 m - 200 m.

Hydrodynamic modeling of Misool waters

Model verification

The model results and field observations were

verified to be very good and coherent, showing the same regularity pattern. Table 1 shows the deviation of the four major constituents in the four water layers. The difference in values for the major ellipse is 0.21 cm/s - 8 cm/s and the minor ellipse is 0.03 cm/s - 3.79 cm/s. The model results and observations also show a small phase difference value. The smallest difference in the main tidal ellipses of the main luni-solar diurnal (K1), main lunar semi-diurnal (M2), main lunar diurnal (O1) and main solar semi-diurnal (S2) is 1.2 cm/s, 1.2 cm/s, 0.86 cm/s and 0.21 cm/s. The difference in the maximum inclination value of 36.09^{o} is much lower than required (45^{o}) (Koropitan *et al.,* 2021). The model applied to the Misool waters gives excellent results in describing the natural characteristics.

Fig. 6 shows the tidal current ellipse of the diurnal constituents (K1, O1) and the semi-diurnal constituents (S2, M2). An acceptable current ellipse will show a pattern of model results in line with the observations. The elliptical vertical tidal current structure has a low amplitude to depth for K1, O1, M2, and S2 constituents. The elliptical vertical tidal current structure has a low amplitude to depth for K1, O1, M2, and S2 constituents. The ellipses of major and minor axes, the direction of rotation, and constituent phases K1 and M2 rotate to the right. On the layer near the bottom, the rotation changes to the left. It is could be due to stratification (Izquierdo dan Mikolajewicz, 2019). In all water column layers, the elliptical rotation of constituents O1 and S2 is consistent to the right. Based on the geomorphology, the tidal elliptical constituents K1, O1, S2, and M2 are oriented parallel to the central axis on Misool Islands. Tidal currents move gradually from south to southwest. The maximum tidal current K1 was recorded near the surface. The principal axis velocity (30 cm/s) is obtained near the surface and decreases as depth increases. The layer near the bottom has a speed of 5 cm/s. The tidal current ellipse of the constituents O1, M2, and S2 shows similar to K1 but with different values. The maximum velocities of the tidal currents O1, M2, and S2 occur in the layer near the surface at speeds of 15 cm/s, 50 cm/s, and 10 cm/s. Verification of the modeling results still shows differences in velocity, orientation, and phase for each constituent. The difference is thought to be due to the non-linear factor value, which is not absolute yet but is close to absolute. The Misool waters have non-uniform basic substrate characteristics in all model domains. The value of the necessary roughness is represented by the constant Smagorinsky value and causes errors in the modeling computation. These

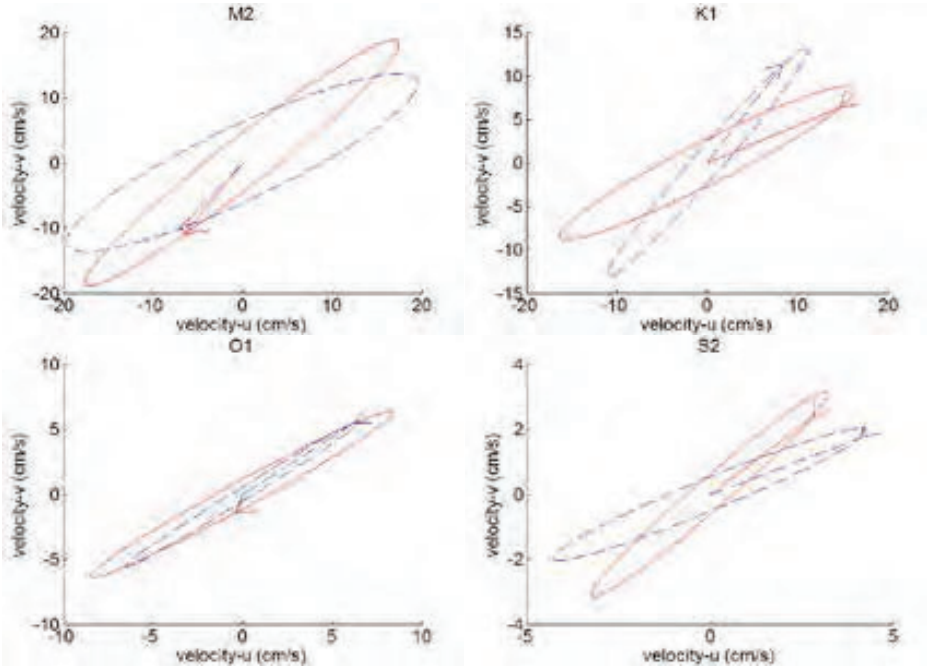

Fig. 6: Comparison between field observations (red) and model (blue) results for M2, O1, K1, S2 tidal currents

errors can be minimized by using a high-resolution domain grid and nesting in a single execution.

Simulation of tidal current patterns

Tidal forces dominate the main generator of the Misool water circulation. The main tidal constituents of Misool waters are M2, S2, K1, and O1. The ellipse of the Misool waters spatially shows variations in the range of 1.5 to 65 cm/s. Strong currents are noticed between the mainland and surrounding the islands in the strait system, and slow currents near the shore. Misool waters are the waters around the islands with a flow pattern following the topographic contours. The inflow and outflow follow flood and ebb conditions. The amplitude and propagation of tides vary. Significant velocities are seen at the land boundary inlet and narrow passages. This condition is in line with what was found by Sorourian *et al.* (2020); Sabhan *et al*. (2021). Misool with archipelagic characteristics, random bathymetry, and coral reef substrates influence tidal dynamics. Tides and their propagation are controlled by geomorphology and irregular coastlines (Ivanov *et al.,* 2020). These conditions stimulated the mixing of the water column. The interaction of barotropic tides with geomorphology triggers well mixed. This pattern can be seen on the southwestern and northeastern sides. Homogeneous waters with strong currents occur on the shallow northeast side. On the southwest side, stratification is visible. Tidal and topography interactions modulate diurnal and semi-diurnal tidal ellipses (Quaresma dan Pichon, 2013). Topographic interactions affect the tidal amplitude and induce strong currents. The coral bathymetry provides greater basic friction (Colberg *et al.,* 2020), the decay of energy by friction results in an amplitude decay (Cook *et al.,* 2019). Topographic characteristics make the tidal propagation pattern at flood and ebb. Complex topography in Misool Islands produces the tidal propagation pattern during flood and ebb tides. The mainland of Papua deflects the tidal propagation on the east and northeast sides; in the west, the tidal propagation is held back by Halmahera Island. Strong currents in the Halmahera Strait and the Maluku Islands in the south a role in pushing the water mass to the southeast, leaving the Misool waters. The magnitude of the tidal constituent varies in its propagation, and this is due to water geometry

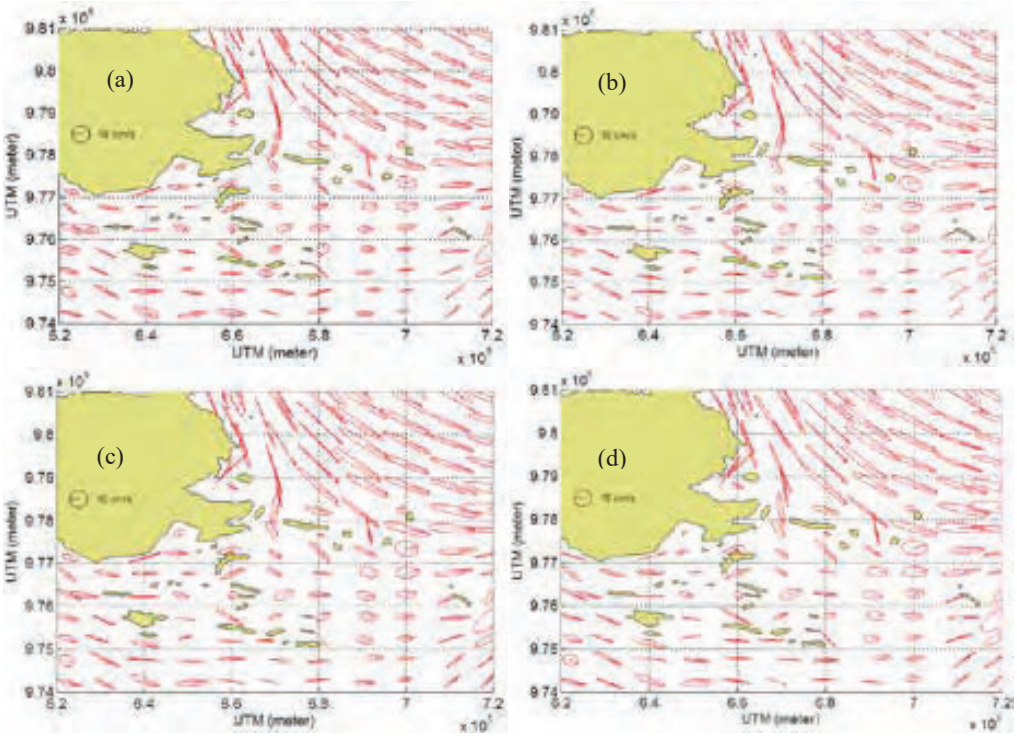

Fig. 7: The calculated K1 tidal current in layer-1 near the bottom (a), layer-4 of water column (b), layer-7 of water column (c), and layer-10 at the surface water (d)

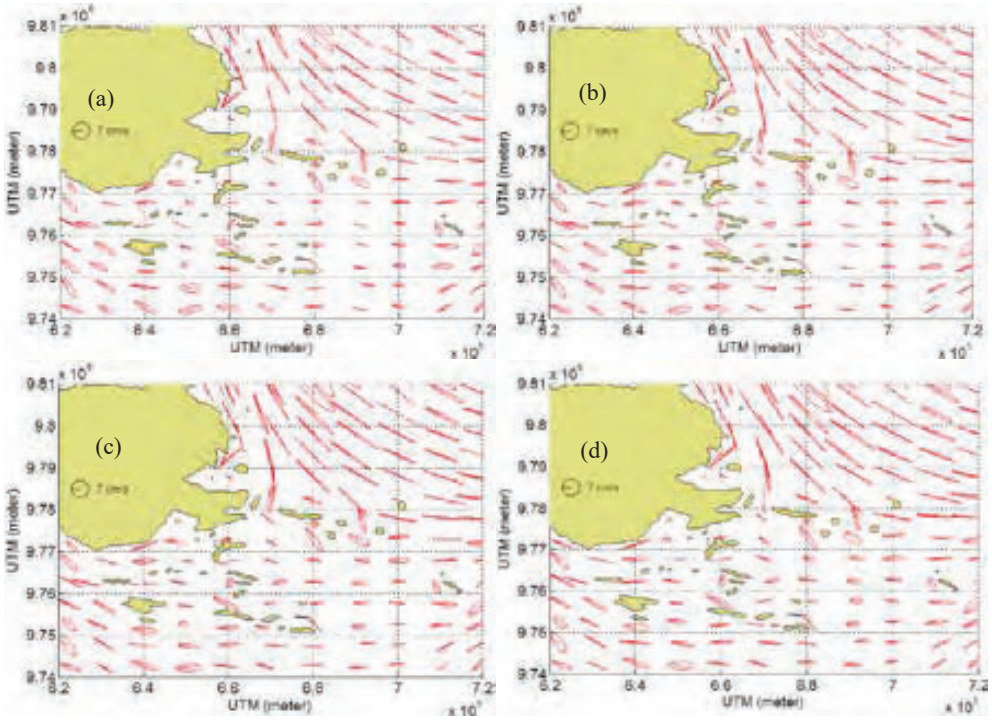

Fig. 8: The calculated O1 tidal current in layer-1 near the bottom (a), layer-4 of water column (b), layer-7 of water column (c), and layer-10 at the surface water (d)

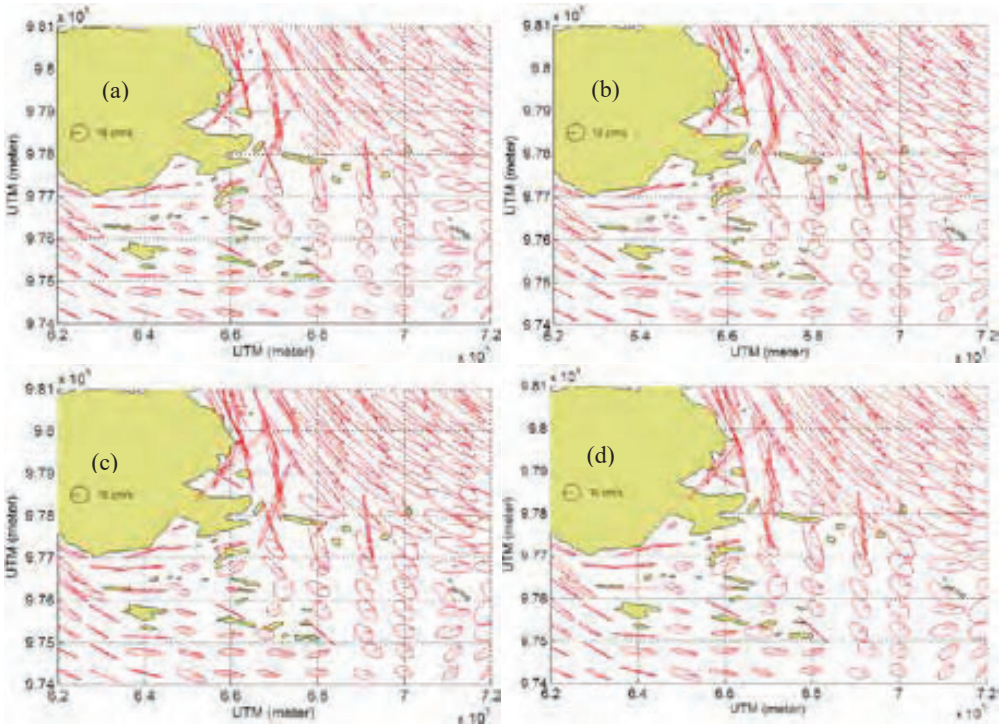

Fig. 9: The calculated M2 tidal current in layer-1 near the bottom (a), layer-4 of water column (b), layer-7 of water column, and layer-10 at the surface water (d)

factors (Rijn, 2011). Tidal deformation of the waters is increased by lateral constriction (Pradhan *et al.*, 2020). The isoline amplitude follows the depth contour. The signal of the semi-diurnal constituent is more robust in the ocean than in the coastal area. The tidal propagation of M2 and S2 constituents, from southeast to northwest, has a phase difference of 40°. Tidal current velocity for all diurnal constituents (K1, O1) and semi-diurnal constituents (M2, S2) is strong along the shallow part in northeastern, and also part of channel between Misool Islands and the mainland. The current velocity constituent of K1 has a maximum of 50 cm/s, and an average of 20 cm/s. Vertically the velocity shows variation. The maximum velocity occured in the layer near the surface reaches 50 cm/s, an average of 20 cm/s, and in the layer near the bottom, the top speed is 40 cm/s, an average of 17 cm/s (Fig. 7). The O1 tidal currents show a similar pattern to K1 tidal currents. Large velocity occurs at the strait and the continental shelf boundary with reduced velocity near the bottom (Fig. 8). The O1 constituent has a maximum velocity of 28 cm/s with an average of 11 cm/s in the near-surface layer. The near-bottom layer has a maximum of 20 cm/s with an average of 9 cm/s. Figs. 9 and 10 show that the semi-diurnal tidal currents have a similar pattern with the diurnal tidal currents with different velocities. The M2 surface tidal currents have a maximum of 65 cm/s and an average of 29 cm/s. The S2 surface tidal currents have a maximum of 20 cm/s and an average of 10 cm/s. The tidal currents in Misool waters show a strong influence by the semi-diurnal tide, particularly M2. The tidal currents vary in vertical profile with maximum velocity in the layer near-surface and decrease near the bottom layer. Strong velocities are also formed along the boundary area for all tidal constituents. In the case of Misool waters, the vertical stratification is less, resulting in a small effect on inducing currents due to stratification.

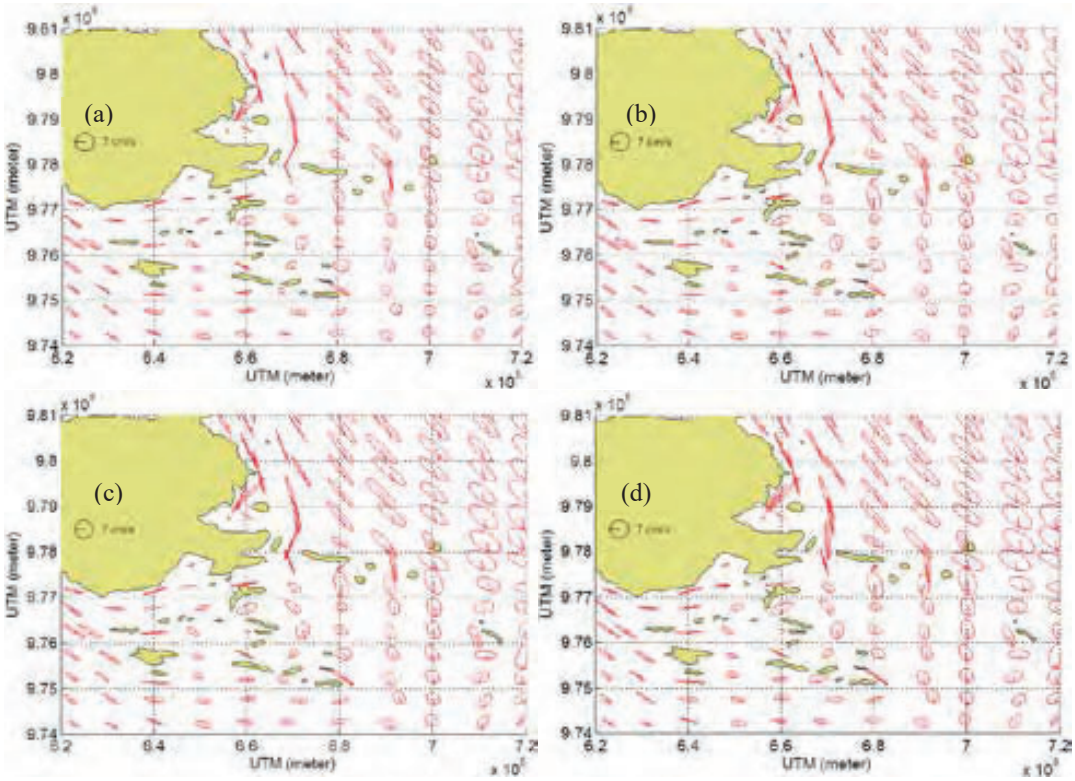

Fig. 10: The calculated S2 tidal current in layer-1 near bottom (a), layer-4 of water column (b), layer-7 of water column (c), and layer-10 at the surface water (d)

CONCLUSION

This study successfully investigates the characteristic water mass and hydrodynamic processes of Misool waters. The depiction of the water mass characteristics of Misool waters, as the Tpot-S diagram, does not show similarities to the water masses of the north and south Pacific water masses. It is characterized as origin water masses from the Misool waters. The water column is stable until the CTD depth limit; the surface layer to a depth of 200 m increases with a maximum salinity of 34.25 PSU, salinity decreases at a depth of 200 m to the CTD depth limit. The Misool waters are in a Papuan bird's head seascape network, and the Pacific water mass passes these waters as the ITF. Still, the Pacific water mass has no impact on the Misool water masses. The Halmahera eddy deflects the Pacific water masses that pass through the eastern route, and the rest is pushed through the Maluku and Seram Seas. The water masses from the Pacific Ocean flow mainly at a depth of more than 100 m, while the southeast Misool waters are shallow. Based on modeling and observations data, it was found that the tides are the main force that generates water circulation on the study site. These characters are represented from ADCP recording (maximum tidal current 65 cm/s, and maximum residual current 25 cm/s). The modeling showed that 50% of the tidal current formation components are semi-diurnal (M2) components, followed by K1, O1, and S2 components. The currents generation by wind and baroclinic properties showed the non-significant value and produced small horizontally and vertically stratification. It indicates that it has minimal effect in inducing current circulation. The tidal component amplitudes are rectified at the continental margin for all diurnal (K1, O1) and semi-diurnal (M2, S2) components. The tidal component vertically varies with the strongest magnitude in the near-surface layer. The Misool Islands are characterized by mixed tidal, prevalence to semi-diurnal. It is confirmed by the maximum speed of each component, which is 67 cm/s, 50 cm/s, 28 cm/s, and 20 cm/s for M2, K1, O1, and S2. Based on echosounder data, the bathymetry of Misool waters is varied between 1 m to 500 m depth. It also noted that the seabed forms an extreme slope around the coral reef islands (100 m - 200 m from the coastline). The island's geomorphology and coral reef substrates impact the rectification of tidal currents. Shallow bathymetry is on the eastern and northeastern sides of the islands. It creates the decay of tidal energy at high tide that propagates to the east and northeast. Tidal energy is strengthened during propagation towards the west, southwest, and southeast. According to pre-test, the 3D modeling domain for coral reef substrates obtained the best origin constant values, the coefficient of viscosity, and vertical diffusivity of $1.8x10^{-6}$ m^2/s. The hydrodynamic model was first applied to Misool waters. The present study is limited to tidal current modeling, and temperature and salinity to describe the Misool waters origin characteristics. This study needs to be re-examined for a more extended period and detailed modeling with monsoonal wind and baroclinic effects. The status of Misool waters as a conservation area does not include hydrodynamic aspects in the decision substance. This study is fundamental as a guide for determining and changing essential areas for conservation, defining the boundaries of fishing areas in the Spawning aggregation site (SPAGs) and the distribution area of fish larvae. The future research plan is modeling the distribution of multi-species coral reef fish. Hydrodynamics and water quality a role in controlling the success of fertilization, the food web of fish larvae, and the life cycle of fish larvae. Eggs and larvae are planktonic in the water column, and current patterns determine their distribution. Fish resources are sustainable, If currents spread them into good quality waters, and if not, fish deaths occur prematurely.

AUTHORS CONTRIBUTIONS

Suhaemi performed the conception and design, ran the model, conducted field sampling, analyzed and interpreted the data, and drafted the original manuscript. D.G. Bengen performed the conception and design, critical revision of the manuscript, and supervision. C.P.H. Simanjuntak performed a critical revision of the manuscript and supervision. A.F. Koropitan performed the conception and design, running the model, critical revision of the manuscript, and supervision.

ACKNOWLEDGEMENT

This study was partially funded by the United States Agency for International Development - USAID Cooperative Agreement [No. AID AID-497-A-16-00004] Sustainable Higher Education

Reseach Alliance (SHERA) Subaward No. Institute of International Education (IIE) Project [No. IIE0000078] to IPB University.

CONFLICT OF INTEREST

The authors declare no potential conflict of interest regarding the publication of this work. In addition, the ethical issues including plagiarism, informed consent, misconduct, data fabrication and, or falsification, double publication and, or submission, and redundancy have been completely witnessed by the authors.

OPEN ACCESS

PUBLISHER'S NOTE

ABBREVIATIONS

ADCP	Acoustic doppler current profiler, current recorder
CTD	Conductivity temperature-depth
cm/s	Centimeters per second
DHI	Danish hydraulic institute
dz	Differential to depth
d	depth
ECMWF	European center for medium-range weather forecasts
Eq	Equation
f	Coriolis force
F_u, F_v	Gradient friction horizontal component in x- and y-axis
Fig	Figure
g	Gravitational acceleration
GMT	Greenwich mean time
h	Total depth
Ha	Hectares
IIE	Institute of International Education
ITF	Indonesian throughflow
kg/m^3	Kilogram per cubic meter
Km	Kilometers
K1	Constituents main luni-solar diurnal
Km^2	Square kilometers
K	Turbulence energy kinetic per unit mass
m/s	Meters per second
m	Meter
m^2/s	Square meters per second
M2	Constituents main lunar semi-diurnal
MLD	Mixed layer depth
O1	Constituents main lunar diurnal
Pa	Pascal, atmospheric pressure
PSU	Practical salinity units
S2	Constituents main solar semi-diurnal
S	Source
SPAGs	Spawning aggregation site
Sxx, Sxy, Syx, Syy	Tensor stress radiation component in x- and y-axis
t	Time
T_{pot}-*S*	Potential temperature-salinity
USAID	The united states agency for international development
u, v, w	Velocity component in x-, y-, and z-axis
u_s, v_s	Sources of velocity component in x- and y-axis
vt	Eddy viscosity, turbulence vertical
x, y, z	Axes in coordinate system
<	Less than
>	Greater than

∂	Differntial
$\partial u/\partial t$	Acceleration
$\partial u/\partial x$	Differential velocity in x-direction
$\partial v/\partial y$	Differential velocity in y-direction
$\partial w/\partial z$	Differential velocity in z-direction
η	Surface elevation
%	Percent
‘	Minute
“	Second
°	Degree
°C	Degree celcius
°S	Degree south
°N	Degree north
°E	Degree east
ρ	Density
ρo	Density standard
ε	Kinetic energy dissipation per unit mass
3D	Three dimensional

REFERENCES

Adibhusana, M.N.; Hendrawan, I.G; and Karang, I.W.G.A., (2016). Model hidrodinamika pasang surut di perairan pesisir barat kabupaten Badung, Bali. J. Mar. Aquat. Sci., 2(2): 54-59 (**6 pages**).

Budiman, A.S.; Koropitan, A.F.; Wayan, N.I., (2014). Pemodelan hidrodinamika arus pasang surut Teluk Mayalibit kabupaten Raja Ampat provinsi papua barat. Depik. 3(2): 146-156 (**11 pages**).

Canuto, V.M.; Howard, A.; Cheng, Y.; Dubovikov, M.S., (2001). Ocean turbulence. Part I: One-point closure model-momentum and vertical heat diffusivities. J. Phys. Oceanogr., 31(6): 1413–1426 (**14 pages**).

Colberg, F.; Brassington, G.B.; Sandery, P.; Sakov, P.; Aijaz, S., (2020). High and medium resolution ocean models for the Great Barrier Reef. Ocean Model., 145: 101507 (**25 pages**).

Cook, S.E.; Lippmann, T.C.; Irish, J.D., (2019). Modeling non-linear tidal evolution in an energetic estuary. Ocean Model., 136: 13–27 (**15 pages**).

Ferrarin, C.; Bellafiore, D.; Sannino, G.; Bajo, M.; Umgiesser, G., (2018). Tidal dynamics in the inter-connected Mediterranean, Marmara, Black and Azov seas. Prog. Oceanogr., 161: 102–115 (**14 pages**).

George, G.; Desai, D.V.; Gaonkar, C.A.; Aboobacker, V.M.; Vethamony, P.; Anil, A.C., (2013). Barnacle larval transport in the Mandovi-Zuari estuarine system, central west coast of India. J. Oceanogr., 69(4): 451–466 (**16 pages**).

Hadikusumah, (2010). Massa air subtropical Di Perairan Halmahera. J. Ilm. Tek. Kel. Trop., 2(2): 92–108 (**17 pages**).

Haditiar, Y.; Putri, M.R.; Ismail, N.; Muchlisin, Z.A.; Ikhwan, M.; Rizal, S., (2020). Numerical study of tides in the Malacca Strait with a 3-D model. Heliyon. 6(9): e04828 (**16 pages**).

Hutabarat, M.F.; Purba, N.P.; Astuty, S.; Syamsuddin, M.L.; Kuswardani, A.R.T.D., (2018). Variabilitas lapisan termoklin terhadap kenaikan mixed layer depth (MLD) di Selat Makassar. J. Perikan. Kelaut. 9(1): 9–21 (**13 pages**).

Hendrawan, G.; Nuarsa, I. W.; Sandi, W.; Koropitan, A. F.; Sugimori, Y., (2005). Numerical Calculation for the Residual Tidal Current in Benoa Bay-Bali Island. Int. J. Remote Sens. Earth Sci., 2, 86-93 (**8 pages**).

Ilahude, A.G.; Gordon, A.L., (1996). Thermocline stratification within the Indonesian seas. J. Geophys. Res., 101(C5): 12401–12409 (**9 pages**).

Ivanov, E.; Capet, A.; Barth, A.; Delhez, E.J.M.; Soetaert, K.; Grégoire, M., (2020). Hydrodynamic variability in the southern bight of the North Sea in response to typical atmospheric and tidal regimes. Benefit of using a high resolution model. Ocean Model., 154: 101682 (**15 pages**).

Izquierdo, A.; Mikolajewicz, U., (2019). The role of tides in the spreading of Mediterranean outflow waters along the southwestern Iberian margin. Ocean Model., 133: 27–43 (**17 pages**).

Koropitan, A.F.; Hadi, S.; Radjawane, I., (2006). Three-Dimensional Simulation of Tidal Current in Lampung Bay: Diagnostic Numerical Experiments. Int. J. Remote Sens. Earth Sci., 3: 41-50 (**10 pages**).

Koropitan, A.F.; Barus, T.A.; Cordova, M.R., (2021). Coastal Water Properties and Hydrodynamic Processes in the Malacca Strait: Case Study Northeastern Coast of Sumatra, Indonesia. J. Ecol. Eng., 22(11): 16–29 (**14 pages**).

Lee Sang-Ho.; Beardsley, (1999). Influence of stratification on residual tidal current in the Yellow Sea. J. Geophys. Res., 104(7): 15,679-15,701 **(23 pages).**

Noya, Y. A.; Purba, M.; Koropitan, A. F.; Prartono, T., (2016) Cohesive sediment transport modeling on inner Ambon Bay. J. Ilmu dan Teknol. Kelaut. Tropis, 8(2): 671–687 (**18 pages**).

Noya, Y. A.; Kalay, D.E.; Purba, M.; Koropitan, A. F.; Prartono, T., (2021). Modelling baroclinic circulation and particle tracking in inner Ambon Bay. IOP Conf. Series. Earth Environ. Sci., 339: 1-13 (**13 pages**).

Porter, M.; Dale, A.C.; Jones, S.; Siemering, B.; Inall, M.E., (2018). Cross-slope flow in the Atlantic Inflow Current driven by the on-shelf deflection of a slope current. Deep Sea Res. Part I., 140: 173–185 (**13 pages**).

Pradhan, U.K.; Mishra, P.; Mohanty, P.K.; Panda, U.S.; Ramanamurthy, M.V., (2020). Modeling of tidal circulation and sediment transport near tropical estuary, east coast of India. Reg. Stud. Mar. Sci., 37: 101351 (**13 pages**).

Pringle, W.J.; Wirasaet, D.; Suhardjo, A.; Meixner, J.; Westerink, J.J.; Kennedy, A.B.; Nong, S., (2018). Finite-element barotropic model for the Indian and western Pacific oceans: Tidal model-data comparisons and sensitivities. Ocean Model., 129: 13–38 (**26 pages**).

Purba, G.Y., (2020). Water temperature increasing caused mastigias Papua disappeared in marine lake lenmakana Misool Raja Ampat regency, West Papua. J. Sumb. Akua. Indopas., 4(1): 1-10 (**10 pages**).

Quaresma, L.S.; Pichon, A., (2013). Modelling the barotropic tide along the West-Iberian margin. J. Mar. Syst., 109–110: S3–S25

(**23 pages**).
Radjawane, I.M.; Hadipoetranto, P.P., (2014). Karakteristik Massa Air di Percabangan Arus Lintas Indonesia Perairan Sangihe Talaud Menggunakan Data Index Satal 2010. J. Ilm. Tek. Kelaut. Trop., 6(2): 525–536 (**12 pages**).
Rijn, L.C., (2011). Analytical and numerical analysis of tides and salinities in estuaries; Part I: Tidal wave propagation in convergent estuaries. Ocean Dyn., 61(11): 1719–1741 (**23 pages**).
Sabhan; Labania, H.M.D.; Mudin, Y.; Rahman, A., (2021). Modeling of tidal current and residual currents patterns in Tomori Bay, North Morowali regency, Central Sulawesi province. J. Phys. Conf. Ser., 1763: 012025 (**8 pages**).
Sabhan.; Koropitan, A.F.; Purba, M.; Widodo Setiyo Pranowo, W.S., (2019). 3D Simulation Model of Tidal, Internal Mixing and Turbulent Kinetic Energy of Palu Bay. Nat. Environ. Pollut. Technol., 18 (4): 1083-1094 (**12 pages**).
Sala, R., (2018). Model pengelolaan perikanan tangkap berkelanjutan pada zona pemanfaatan tradisional di perairan selatan Pulau Misool, Raja Ampat. Dissertation. IPB University.
Sala, R.; Marsaoly, D.; Dasmasela, H.Y.; Parenden, D.; Orisu, D.; Tarigan, R.B., (2020). Ecological status of target fishes inside and outside marine conservation area of Batbitim, Misool, Raja Ampat. IOP Conference Series. Earth Environ. Sci.,. 429 012054 (**9 pages**).
Sawairnathan, M.; Halimoon, N., (2017). Assessment of the local communities' knowledge on mangrove ecology. International Journal of Human Capital in Urban Management 2(2): 125-138 (**14 pages**).
Seiler, L.; Figueira, R.C.L.; Schettini, C.A.F.; Siegle, E., (2020). Three-dimensional hydrodynamic modeling of the Santos-São Vicente-Bertioga estuarine system, Brazil. Reg. Stud. Mar., Sci., 37: 101348 (**14 pages**).
Sorourian, S.; Huang, H.; Li C.; Justic, D.; Payandeh, A.R., (2020). Wave dynamics near Barataria Bay tidal inlets during spring–summertime. Ocean Model., 147: 101553 (**22 pages**).
Smagorinsky, J., (1963). General circulation experiments with the primitive equations: I. The basic experiment. Mon. Weather Rev., 91(3): 99-164 (**66 pages**).
Thomson, R. E.; Emery, W.J., (2014). Data analysis methods in physical oceanography. Newnes.
Werner, F.E.; Cowen, R.K.; Paris, C.B., (2007). Coupled biological and physical models: Present capabilities and necessary developments for future studies of population connectivity. Oceanography. 20(3): 54–69 (**16 pages**).
Zhang, F.; Sun, J.; Lin, B.; Huang, G., (2018). Seasonal hydrodynamic interactions between tidal waves and river flows in the Yangtze Estuary. J. Mar Syst., 186: 17–28 (**12 pages**).

AUTHOR (S) BIOSKETCHES

Suhaemi, Ph.D. Candidate, Assistant Professor, Department of Marine Sciences, Faculty of Fisheries and Marine Science, University of Papua, Manokwari 98314, Indonesia.
- Email: *s.manaf@unipa.ac.id*
- ORCID: **0000-0003-4585-2277**
- Web of Science ResearcherID: AAD-3228-2022
- Scopus Author ID: 57215859670
- Homepage: https://fpik.unipa.ac.id/pendidikan/jurusan-ilmu-kelautan/

Bengen, D.G., Ph.D., Professor**,** Department of Marine Sciences and Technology, Faculty of Fisheries and Marine Science, IPB University, Bogor 16680, Indonesia.
- Email: *dieter@indo.net.id*
- ORCID: **0000-0002-3880-5117**
- Web of Science ResearcherID: NA
- Scopus Author ID: 55845650900
- Homepage: http://itk.ipb.ac.id/~itkipb/prof-dr-ir-dietriech-g-bengen-dea/

Simanjuntak, C.P.H., Ph.D., Associate Professor, Department of Aquatic Resources Management, Faculty of Fisheries and Marine Science, IPB University, Bogor 16680, Indonesia.
- Email: *charles_phs@apps.ipb.ac.id*
- **ORCID: 0000-0002-7673-0435**
- Web of Science ResearcherID: AAD-3210-2022
- Scopus Author ID: 56426082600
- Homepage: http://msp.fpik.ipb.ac.id/en/charles-p-h-simanjuntak/

Koropitan, A.F., Ph.D., Associate Professor, Department of Marine Sciences and Technology, Faculty of Fisheries and Marine Science, IPB University, Bogor 16680, Indonesia.
- Email: *alan@apps.ipb.ac.id*
- ORCID: **0000-0001-5794-094X**
- Web of Science ResearcherID: ABE-7099-2021
- Scopus Author ID: 23135214600
- Homepage: https://itk.ipb.ac.id/~itkipb/dr-alan-frendy-koropitan-s-pi-m-si/

HOW TO CITE THIS ARTICLE

Suhaemi; Bengen, D.G.; Simanjuntak, C.P.H.; Koropitan, A.F. (2022). Characteristics and circulation of archipelagic waters with the three-dimensional hydrodynamic model approach. Global J. Environ. Sci. Manage., 8(4): 503-518.

DOI: 10.22034/gjesm.2022.04.04

url: https://www.gjesm.net/article_249547.html

Global J. Environ. Sci. Manage. 8(4): 519-532, Autumn 2022, Serial #32

Global Journal of Environmental Science and Management
(GJESM)

Homepage: https://www.gjesm.net/

CASE STUDY

Boron adsorption in semiarid Mediterranean soils under the influence of background electrolytes

S. Fatnassi[1,2*], M.B. Almendro Candel[3], J. Navarro Pedreño[3], I. Gómez Lucas[3], M. Hachicha[2]

[1] Department of Geology, Faculty of Sciences of Tunis, University of Tunis El Manar, 2092 El Manar, Tunis, Tunisia

[2] National Institute of Rural Engineering, Waters and Forest, Carthage University, 2080 BP 10 Ariana, Tunisia

[3] Department of Agrochemistry and Environment, Miguel Hernández University of Elche, Avd.de la Universidad SN, 03202 Elche, Alicante, Spain

ARTICLE INFO

Article History:
Received 21 October 2021
Revised 09 December 2021
Accepted 21 January 2022

Keywords:
Clay
Divalent cations
Monovalentcations
Shaking time
Soil textur
Tunisia

DOI: 10.22034/gjesm.2022.04.05

ABSTRACT

BACKGROUND AND OBJECTIVES: Boron is a micronutrient of high importance, both for plant development and normal growth. The range between boron deficiency and toxicity is very narrow, which makes boron unique among the essential micronutrients. Boron adsorption is one of the most important factors determining the release and fixation of this micronutrient, though its adsorption has not been widely studied in semiarid Tunisian soils. This study aims to improve knowledge of B adsorption process in calcareous salt-affected soils in semiarid areas.
It equally focuses on the type of cation (monovalent and divalent) in function of the soil texture and time of shaking. These three latter factors influence boron adsorption, which also influence the availability for plants.
METHODS: A study was carried out on boron adsorption at different shaking time intervals (1, 3, 6 and 9 hours) in two soils of different textures in the absence and presence of different background electrolytes solutions (0.02 N CaCl2, 0.02 N MgCl2 , 0.02 N sodium chloride and 0.02 N potassium chloride.
FINDINGS: The soil-A (clay loam) adsorbed more boron than soil-B (sandy loam). Boron adsorption was the highest in Soil-A under the presence of potassium chloride, close to the mean values given when using calcium chloride. In Soil-B, it was found with calcium chloride background electrolyte. Minor boron adsorption was observed in both soils when boric acid solution was used without background electrolytes. Adsorbed boron showed significant differences with the shaking time in all treatments used with background electrolytes solutions, except for boron solution treatment without background electrolyte in both soils. As a comparison of divalent and monovalent cations, boron adsorbed content was higher with the solution containing calcium than in sodium chloride solution, due to the fact that calcium carbonate is an important boron adsorbing surface.
CONCLUSION: This study reveals that the best conditions for maximum boron adsorption are defined by calcium chloride background electrolyte in this type of soil in a determined shaking time interval of 3 hours. This causes a low rate of boron assimilated by plants, which leads to the decrease of the crop yield and the agricultural production, and subsequently hurt the Tunisian national economy.

NUMBER OF REFERENCES	NUMBER OF FIGURES	NUMBER OF TABLES
62	4	5

*Corresponding Author:
Email: *salmapro14@gmail.com*
Phone: +216 5596 9642
ORCID: 0000-0002-2017-1056

Note: Discussion period for this manuscript open until January 1, 2023 on GJESM website at the "Show Article".

INTRODUCTION

Boron (B) is an essential oligo-element required for the growth of plants (Wimmer *et al*., 2019). The development of floral organs and the elongation of pollen tubes are hampered by a low availability of B in soils, resulting in a crop yield loss (Shorrocks, 1997). Boron is unique among the essential micronutrients because it is presented as nonionized boric acid (H_3BO_3) over the pH range suitable for the plant growth (Arora and Chahal, 2007) and B uptake is the result of the passive assimilation of undissociated boric acid (Hu and Brown, 1997). For B vegetal-soil systems, the value between insufficiency and toxicity is the narrowest among important micronutrients (Su and Suarez, 2004; Tariq and Mott, 2006; Hilal *et al*., 2011; Abu-Dabaan and Al-Najar, 2018; Brdar-Jokanović, 2020) which makes B particular among all primordial nutrients. According to Tariq and Mott (2006), Some other elements such as potassium (K), calcium (Ca), magnesium (Mg) and sodium (Na) disponibility are affected by B deficiency and toxicity apart from crop yield. Hence, B content must be monitored frequently in soil, as its management is very critical. Boron toxicity is a far more difficult issue to manage than deficiency (Reid, 2004). Brdar-Jokanović (2020) highlighted that fertilization could be a solution for B deficiency problematics, contrarily to B toxicity which could be ameliorated using effective procedures. The majority of the world's agricultural soils contain 5–30 mg/kg of total B (determined by total digestion of air-dried soil at neutral pH). Understanding the B adsorption on soil process is necessary, as plants react to the B activity in soil solution. Soluble B availability is governed by sorption-desorption processes of this micronutrient, acting as source for plant uptake in soil solution (Chen *et al.,* 2002; Bhuyar *et al.,* 2020). B added to soils is adsorbed to a variable extent and an equilibrium exists between B in the solid and liquid phases (Bhupenchandra *et al.,* 2019). In this regard, these authors indicate that the adsorption of B is one of the most essential factors identifying the release and fixation of applied B and thus deciding the efficiency of B fertilization. Boron mobility can be very restricted for plants, which can provoke deficiency (Brown and Shelp, 1997). Boron deficiency is a widespread issue in relatively humid areas, especially in sandy soils (Santos *et al.,* 2020). On the other hand, toxic levels of this element have been reported frequently in arid zones due to anthropic activity such as fertilization and irrigation (Santos *et al.,* 2020). The data on B concentrations in sediments have been widely used as paleosalinity indicators (Mattigod *et al.,* 1985; Kot, 2009). According to Schwager-Guilloux (2014), coastal soils can be rich in B since seawater is relatively well provided in this element (B content is approximately 4.7 mg/L). For this reason, B frequently exceeds the plant's requirement in arid and semiarid environments due to low drainage, and in agricultural soils close to coastal areas due to the intrusion of B-rich seawater in fresh aquifers or as a result of dispersion of seawater aerosol. Global releases of elemental B through weathering, volcanic and geothermal processes are also relevant in enriching B concentration in some areas (Landi *et al.,* 2019). Boron adsorption is impacted by soil pH, clay percentage, and organic matter (Ramos *et al.,* 2021). In fact, B has been identified as one of the elements to be

defined in irrigation water quality since the 1950s by Richards (1954) and included in the FAO guidelines (JECFA, 1974) for the use of water for crop irrigation. It has also been considered in the use of treated wastewater (TWW) both by the World Health Organization (WHO, 2006) and in Tunisian standards (Table 1) for the discharge of these waters into the aquatic environment and the sea NT 106.02 (Errais *et al.,* 2010), the agricultural use of these waters NT 106.03 (Errais *et al.,* 2010), and for drinking water NT 09.14 (Jalal and Ezzedine, 2019). Generally, B mobility varies greatly from freely mobile to very restricted one according to the soil and the plant species (Brown and Shelp, 1997; Boaretto *et al.,* 2011). Plants are very specific regarding their B tolerance wherefore irrigation water should not contain more B than required for crop development to avoid toxicity (Maas, 1986; Corwin and Yemoto, 2020). Due to their relative sensibility towards B, the irrigation water used for cereals should not contain more B than 300-400 µg/L. Citrus fruits such as lemon can show higher vulnerability (< 0.5 mg/L) towards B concentration (Nicolás *et al.,* 2016). Consequently, the management of this micronutrient in soil has become recently a worldwide agricultural issue. The most recent similar studies often investigate the B adsorption, by the same methodology. The latter consists in shaking the soil for 24 h or 20 h, with a determined volume and concentration of a background electrolyte solution, containing different concentrations of boric acid.

Table 1: Boron Thresholds values and recommendations for different water uses and countries.

Medium	Values (mg/L)	Countries	References
Groundwater	1.0	Europe	(Albrecht, 2013)
Drinking water	2.4	Tunisia	(Jalal and Ezzedine, 2019)
Drinking water	0.5	Worldwide	(Hjelm *et al.,* 2019)
TWW for irrigation	3.0	Tunisia	(Errais *et al.,* 2010)
TWW discharged to seawater	20.0	Tunisia	(Errais *et al.,* 2010)

For instance, Terraza Pira *et al*. (2018) accomplished the B adsorption isotherms using 25 mL of seven solutions of different B concentrations (0, 2, 4, 8, 16, 32, and 64 mg/L in 0.01 M CaCl), which were added independently to 5 g soil and shaken for 20 h in a reciprocal shaker. However, the current study aim does not focus on B adsorption in soil in the presence of different B concentrations, in one shaking time interval with one cation, as mentioned in the recent studies. Actually, it concentrated on B adsorption in soil in function of different parameters effect: the type of cations in soil solution (divalent or monovalent), the soil texture and the shaking time (1, 3, 6 and 9 hour). Therefore, there are hardly any works with the same research objectives. As a matter of fact, there is a lack of investigations on boron adsorption in the case of calcareous salt-affected soils in semiarid areas particularly under the combination of various background electrolytes and shaking time effect during the quantification in laboratory. Moreover, among the metal minor elements, B is the element whose mobility increases in a basic environment. This is the case of Tunisian soils rich in limestone, which is an additional argument to highlight the importance of B in semiarid Mediterranean regions. The global aim of the study is to improve knowledge of B mobility and interaction with other chemical elements in calcareous salt-affected soils in semiarid areas. The aim of the current study is to focus on the type of cation (monovalent and divalent) that can favor the B adsorption in function of the soil texture and time of shaking. This also influence the availability of B for plants. Hence, B content must be monitored frequently in soil, as its management is very critical. This study contribution consists in providing the optimal conditions in this type of soil (type of cation and exact shaking time interval) for maximum boron adsorption. This affects the B amount assimilated by plants, which influence the crop yield and the agricultural production. This study has been carried out in Tunisia, within the research laboratory Valorization of non-conventional waters in the National Research Institute of Rural Engineering, Waters and Forests (INRGREF) for the field activities and the chemical analysis in 2018, and in Spain, in 2019, within the research laboratory at the University of Miguel Hernandez of Elche for the experimental and chemical analysis.

MATERIALS AND METHODS

The literature review highlighted the importance of B sorption-desorption processes, which dominate B availability and thus provide a source for plant uptake in soil solution. Although, there are few studies on boron adsorption in the case of calcareous salt-affected soils in semiarid areas. This context led us to hypothesize that understanding B adsorption in this type of soil is necessary, under several parameters effects such as the background electrolytes type, soil texture and shaking time. Previous studies have not attempted to demonstrate the combination effect of different background electrolytes and time of shaking intervals in the same time on B adsorbed amounts, particularly in this type of soil. The study was carried out with two Fluvisols (Sarmast *et al.,* 2015), with different textures, in order to study the adsorption of B in the soil of Cebala Borj Touil perimeter (Fig. 1).

Description of the study area and context

The sites are located at the perimeter of Cebala Borj-Touil (Fig. 1), Tunisia's most important agricultural area irrigated by treated wastewater (3200 ha). It is in the suburbs of Tunis (36°50 N; 9°75 E) in northeastern Tunisia. This area has been irrigated with treated wastewater (TWW) since 1989. These wastewaters generated from urban activities are treated at the

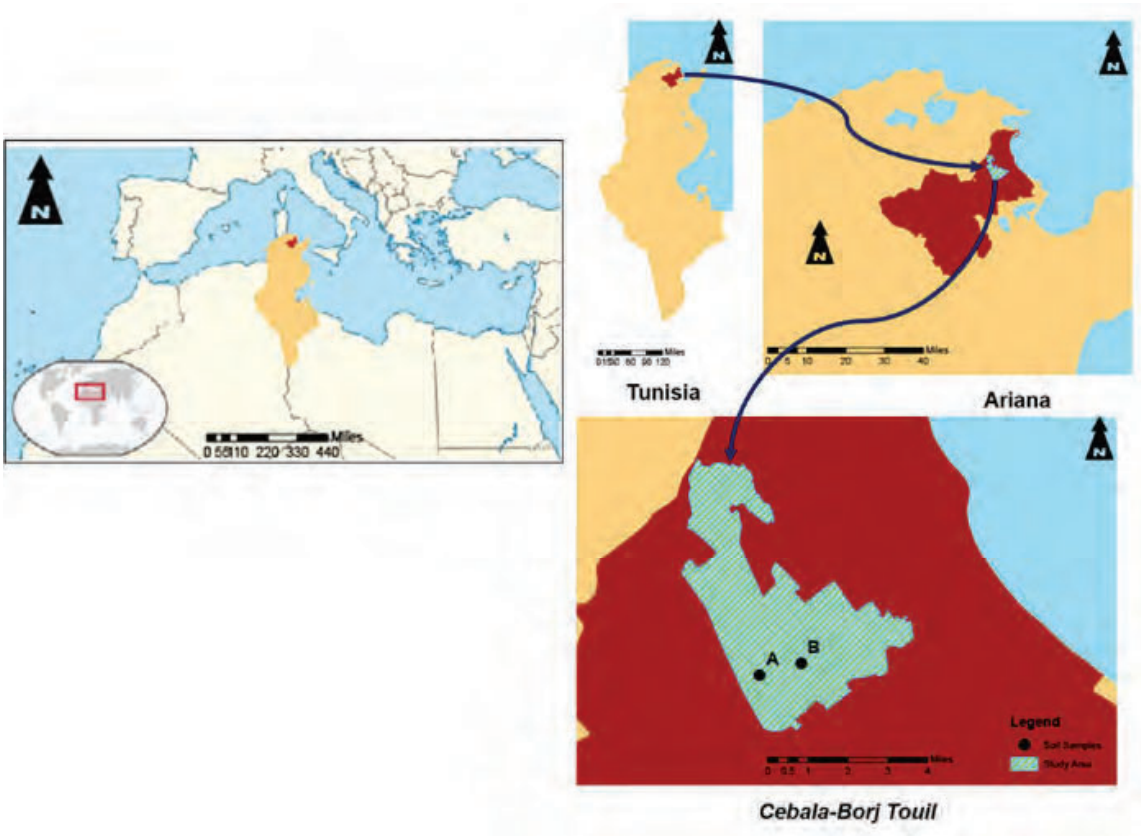

Fig. 1: Geographic location of the study area in northern Tunisia and localization of soil samples in Cebala Borj Touil perimeter

secondary level and available to agricultural and farm irrigation. The effluents were supplied by the outflow of three Great Tunis wastewater treatment plants (Choutrana, Cherguia, and north coast). The main TWW chemical characteristics are mentioned in the Table 2. The pH mean value of irrigation water varies from neutral to slightly alkaline during the summer irrigation cycle. The salinity of TWW (Ecw) is moderate with an average of 4.54 dS/m. The chemical facies is alkaline with a dominance of Na^+ cations and Cl^- anions. B concentration with a mean value 0.75 mg/L remains fairly constant over time. It is bordered on the north by the Mejerda River. The climate is semiarid, with a wet season from September to May and a dry season from June to August. The average annual rainfall is estimated at 470 mm (Dahmouni *et al.,* 2018) with an average annual evapotranspiration of 1400 mm (Khaskhoussy *et al.,* 2015). The region is characterized by a shallow saline water table ranging from 0.5 to 7.6 m. The Cebala Borj-Touil drainage system comprises of an open ditch network that covers the whole region (Dahmouni *et al.,* 2018). The land use differs depending on the season. In winter, cereals and fodders crops as wheat and alfalfa are cultivated, whereas in summer, maize and sorghum. Irrigation is mainly used during hot season for maize and sorghum.

Soil analysis

Soil samples were taken in two agricultural fields situated in the middle of the region. Both samples were air dried and sieved (2 mm) to prepare them for the analysis and laboratory experiment. The soils, Soil-A and Soil-B, selected by their difference in texture and being representative of the area, are respectively clay loam and sandy loam soils (Table 3). The soil texture was determined by using the Robinson pipette method after oxidation of the organic matter with H_2O_2 and particle dispersion with hexametaphosphate solution (NF [French norm]

Table 2: Main treated wastewater chemical characteristics

Descriptive statistics	pH	Ecw (dS/m)	Cl^- (meq/L)	HCO_3^- (meq/L)	SO_4^{2-} (meq/L)	Ca^{2+} (meq/L)	Mg^{2+} (meq/L)	K^+ (meq/L)	Na^+ (meq/L)	B (mg/kg)
Average	7.27	4.54	32.15	6.5	10.03	6.5	10	1.24	28.48	0.75
Min.	6.96	3.57	22.56	4	5.52	5	7.5	1.07	20.06	0.73
Max.	7.6	5.36	42.3	9	15.1	7.5	15	1.39	39.11	0.77

Table 3: Main soil properties

Soil	Clay (%)	Silt (%)	Sand (%)	pH	EC (dS/m)	$TCaCO_3$ (%)	OM (%)	Hot water extractable B (mg/kg)
A	36.0	42.2	21.8	8.0±0.1	3.1±0.2	35.4±7.3	1.36±0.03	1.2±0.1
B	19.0	14.8	66.2	7.9±0.1	7.6±0.6	45.7±2.2	0.75±0.06	1.4±0.1

± is followed by the standard deviation (SD).

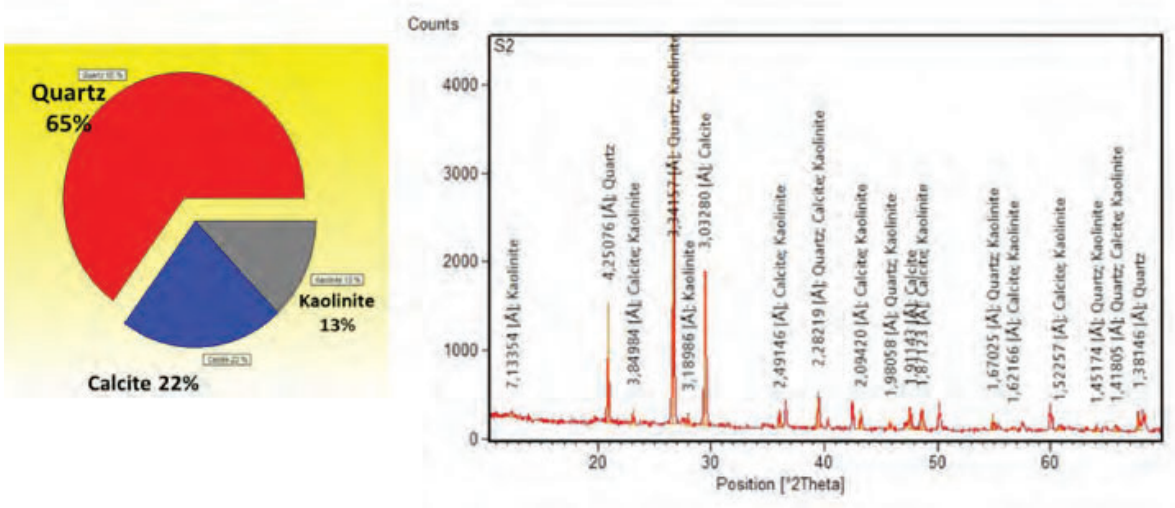

Fig. 2: X-ray diffract metric analysis of the studied soil

X31-107). The X-ray diffractometric analysis showed that the mineralogical composition of the soil is as follows: 65% of quartz, 22% of calcite and 13% of kaolinite (Fig.2). In Fig. 2, the soil X-ray diffractometric pattern presents a high signal for the diffraction lines of intensity relevant for quartz. The wide lines at 21, 27, 39 and 46° in 2θ are characteristics of quartz . Calcite was present in soil, with 23, 30, 36, 44, 47 and 61° in 2θ. In addition, Kaolinite was observed at a low intensity with other elements (quartz and calcite) in many lines (at 3, 23, 28°... in 2θ). The soil pH was measured with a pH meter in water extraction (ISO 10390). The salinity was measured determining the electrical conductivity (EC) in the soil aqueous extract (ISO 11265). The total equivalent calcium carbonate ($TCaCO_3$) was estimated by using the volumetric method and the attack of the soil sample with hydrochloric acid (NF ISO 10693) (Jerbi *et al.,* 2020). Organic matter was estimated following the loss on ignition method (Benbi, 2018). Initial available B concentration in soils was determined after hot water extraction with the Carmine method (Sah and Brown, 1997; Pena-Pereira *et al.,* 2020). The main differences observed in these soils were in texture, electrical conductivity, total equivalent calcium carbonate and organic matter. The presence of a higher percentage

Table 4: Cations and anions availability in the soils

Soil	Cl^- (meq/L)	HCO_3^- (meq/L)	SO_4^{2-} (meq/L)	Ca^{2+} (meq/L)	Mg^{2+} (meq/L)	K^+ (meq/L)	Na^+ (meq/L)
A	12.69	5.00	14.76	10.00	5.00	0.28	16.11
B	59.22	3.17	11.48	13.33	14.83	0.94	45.68

of clay fraction in Soil-A, and sand fraction in Soil-B would determine their physical characteristics. The ionic composition in the soil-B was dominated by the anion Cl^- and the cation sodium Na^+. In soil-A, it was dominated by the anion SO_4^{2-} and the cation Na^+ (Table 4).

Experimental design on B adsorption in soils

The B adsorption experimental design was based on previous studies (Tamuli *et al.,* 2017). Soil samples (8 g air-dry soil taken in each tube) with 4 replications were disposed into 50 mL polypropylene centrifuge tubes with 16 ml of solution (ratio soil-solution 1:2 w/v) containing 40 mg/L B as boric acid (H_3BO_3). They were shaken under controlled temperature conditions (20ºC) for 1, 3, 6 and 9 hours (h) by using a wrist action laboratory shaker (200 oscillations/min). The following treatments (boron solution-soil interaction) were applied: B solution without background electrolyte (TBo) or with background electrolytes: 0.02 N $CaCl_2$ (TBCa), 0.02 N $MgCl_2$ (TBMg), 0.02 N NaCl (TBNa) and 0.02 N of KCl (TBK). Although the accompanying anion was the same for all the electrolytes, chloride, there were small differences in the pH of the solutions due to the interaction between components and water (ionic strength): 6.5, 6.5, 5.7, 7.3 and 6.6 respectively. The pH of all treatments was close to 6.5 although major differences were observed in the case of TBMg (pH=5.7) and TBNa (pH=7.3). The B in the solution, after shaking time, was measured by the colorimetric method Azomethine-H (Sah and Brown, 1997; Pena-Pereira *et al.,* 2020). The spectrophotometer used was T80 (a high-performance double beam spectrophotometer). The B detection limit in the used method was 0.05 mg/L. The difference between initial concentration and the final concentration in the solution after the interaction with soil, gave the amount of B adsorbed by soil.

Statistical analysis

Descriptive statistics (mean value and standard deviation SD), Student's t- test and one- and two-ways ANOVA test were used to determine the statistical differences between samples. For the samesoil (A or B) and treatment, mean values with a letter (a, b, c), and those with different letters indicated statistical differences by using Student's t-test at $p<0.05$. For the ANOVA test comparing the effect of shaking time and the effect of background electrolyte, statistical differences are represented by using stars with the following meaning: * ($p<0.05$), ** ($p<0.01$) and *** ($p<0.001$), and no significant differences (NS).

RESULTS AND DISCUSSION

A summary of the results concerning the B adsorption in soil-A and soil-B at different time of shaking are shown in Table 5.

Soil B adsorption

Considering the divalent cations Ca and Mg, in the case of TBCa, B adsorbed in Soil-A increased from 1 h to reach a maximum after 6 h of shaking (25.4 mg B/kg soil), then decreased slightly at 9 h shaking. In Soil-B, B content adsorbed by soil increased starting from 1 h of shaking time to 3 h. It decreased after 6 h of shaking and finally increased again and reached a maximum value after 9 h of shaking (19.3 mg B/kg) but without statistical differences between 6 and 9 h of time of shaking (T test). The B adsorbed showed higher values in Soil-A than in Soil-B. In the case of TBMg, B adsorbed in Soil-A increased from 1 h to reach a maximum after 6 h of shaking (23.9 mg B/kg). In Soil-B, B content adsorbed by soil increased starting from 1 h of shaking time to 3 h, then decreased slightly and reach the maximum value at 9h (17.6 mg B/kg). Considering NaCl and KCl as background electrolytes, in both cases, the B adsorbed increased progressively in Soil-A from 1 h to 6 h of shaking, then slightly decreased at 9 h of shaking, but without statistical differences. In Soil-B, B adsorbed showed a similar behavior. As it happened in all the previous background electrolyte experiments with divalent cations, B adsorbed

Table 5: B adsorbed (mg B/kg soil), standard deviation, T test and ANOVA 1 and 2 ways in the two soils considering all the treatments (TBCa, TBMg, TBNa, TBK and TBo) and time of shaking

Treatment		TBCa		TBMg		TBNa		TBK		TBo		ANOVA 1 way (background electrolyte effect)
	Shaking time (h)	Mean	SD	Mean	SD	Mean	SD	Mean	SD	Mean	SD	
Soil A	1	23.5^{c}	0.72	21.0^{b}	0.78	23.2^{c}	0.69	26.3^{bc}	0.92	18.4^{a}	0.57	***
	3	24.0^{b}	0.35	21.9^{b}	1.03	24.2^{b}	0.25	27.8^{b}	0.36	18.5^{a}	0.67	***
	6	25.4^{a}	0.50	23.9^{a}	0.85	26.3^{a}	1.39	28.9^{a}	0.64	19.6^{a}	0.65	***
	9	24.9^{ab}	0.58	23^{ab}	1.16	23.8^{bc}	1.53	25.4^{c}	0.77	18.8^{a}	0.36	***
ANOVA 1 way (time effect)		**		**		*		***		NS		ANOVA 1 way (background electrolyte effect)
ANOVA 2 ways (time vs background electrolyte)		***		***		***		***		***		
Soil B	1	17.0^{b}	0.88	14.2^{b}	0.41	15.8^{b}	0.59	15.4^{a}	0.12	12.0^{a}	0.51	***
	3	19.1^{a}	0.93	17.1^{a}	0.95	15.8^{b}	0.59	18.6^{a}	1.21	12.2^{a}	0.86	***
	6	18.6^{a}	0.48	16.6^{a}	0.63	18.2^{a}	0.78	17.3^{ab}	0.79	12.4^{a}	0.30	***
	9	19.3^{a}	0.62	17.6^{a}	0.57	18.2^{a}	0.65	17.0^{b}	0.71	12.8^{a}	0.23	***
ANOVA 1 way (time effect)		**		***		***		**		NS		
ANOVA 2 ways (time vs background electrolyte)		***		***		***		***		***		

Different lowercase letters indicate significant differences among the different time of shaking at P<0.05 level and at the same treatment.
NS *, **, and ***indicate not significant, significant at P < 0.05, P < 0.01, and P < 0.001, respectively.

showed greater values in Soil-A than in Soil-B. Concerning boric acid solution without background electrolyte, the B adsorbed showed close values and it is independent of the time of shaking. In Soil-B, B adsorbed increased progressively from 1 h to reach the maximum at 9 h of shaking, but without significant differences. The ANOVA test confirmed that no effect associated with shaking time was noticed. However, B adsorbed showed higher values in Soil-A than in Soil-B (Table 5). Considering all the background electrolyte solutions, adsorbed B content was higher in Soil-A than in Soil-B. According to the results (Table 5) and by using ANOVA one-way test, B adsorbed showed significant differences associated to the shaking time factor in all the treatments when using background electrolytes solutions, which was opposite to the result found in TBo for both soils. In Soil-A, the highest significant difference was recorded in TBK, however in Soil-B it was associated to TBMg and TBNa. According to ANOVA two-way test, background electrolytes and shaking time gave statistical significant differences in both soils. Moreover, ANOVA one-way test indicated that the background electrolyte composition of soil solution showed higher significant difference compared to shaking time. The B adsorbed by soils showed higher values in Soil-A than in Soil-B. This behavior was the same for the divalent cations $CaCl_2$ and $MgCl_2$ as background electrolytes. Considering NaCl and KCl, as it happened in the background electrolyte experiments with divalent cations, B adsorbed showed greater values in Soil-A than in Soil-B. For boric acid solution without a background electrolyte, the B adsorbed showed close values and it was independent of the time of shaking, and the B adsorption probably reached the maximum within the first h of shaking. The ANOVA test confirmed no effect of shaking time. Fine textured soils can adsorb more B than coarse-textured soils due to the higher content of clay minerals (Al-Ameri *et al.,* 2019). Furthermore, the primary B adsorbing surfaces in soils are the surface area of soil clay minerals, calcium carbonate, aluminum and iron oxides, and organic matter (Goldberg, 1997; Al-Ameri *et al.,* 2019). In the

present study, the significant differences found by using T test ($P<0.05$) indicated that 1 h of shaking is not the sufficient time needed to reach B saturation on adsorption sites. Consequently, in both soils, 3 h appeared to be enough time in which the soil reaches maximum B adsorption. Boron adsorption showed significant differences (Table 5) considering the shaking time in all the treatments when using background electrolytes solutions. On the other hand, no significant differences were found in TBo for both soils. This result reinforces the importance of the shaking time and 3 h of shaking to reach the maximum adsorption value in the presence of background electrolyte for the determination of B adsorption in soils. However, this result is not in line with Hingston's findings (1964). He studied the effect of shaking time on B adsorption by Willalooka illite in 0.01 M $CaCl_2$. He found that adsorbed amounts of B were similar at shaking times from 30 min to 2 days. Moreover, it should be noted that even after several weeks, there was no significant difference observed. This indicates that soil is a complex system, and it is important to the texture and the presence of other ions interacting with the soil solution, among other properties commented previously. Using ANOVA two-way test, background electrolytes and shaking time gave significant differences for both soils (Soil-A and Soil-B). In addition, the background electrolyte composition of soil solution was obviously the factor of higher interest compared to shaking time, as previously indicated by ANOVA one-way test indicated. B adsorption is dependent on the soil texture (Al-Ameri *et al.,* 2019). In this case, the clay loam texture of Soil-A retained more B than the sandy loam texture of Soil-B. Actually, fine-textured soils can adsorb more B than coarse-textured soils due to their clay minerals content (high specific surface and cation exchange capacity) (Al-Ameri *et al.,* 2019). The presence of the clay minerals like montmorillonite and chlorite especially enhance B adsorption (Goldberg, 1997; Al-Ameri *et al.,* 2019). This finding was also confirmed by many other research investigations. According to Gürel *et al.* (2019) adsorbed B level heightened with an increase in clay content. Moreover, B deficiency has been commonly reported in coarse-textured acid soils of humid regions (Alam and Jahan, 2007). Although B adsorption could be associated to the presence of soil organic matter, as organic matter also contributes to B adsorption, the influence of fine texture may be the most important factor in soils with low organic matter content. Essential soil properties such as clay and organic matter content have been constantly mentioned to influence B distribution in soil (Irfan *et al.,* 2019).Organic matter content in the two soils is considered as low (Table 3). According to López *et al.* (2017), soil organic carbon levels are generally low or very low in the Mediterranean region of eastern Morocco, northern Algeria, Tunisia and western Libya. According to Sarkar *et al.* (2014), the low organic matter content in the soil resulted in an increase of B adsorption, as the sites of adsorption of oxides and hydroxides of Fe and Al on mineral surfaces are activated. Furthermore, at the same equilibrium concentration, the frequency of these processes is greater in clayey soils than in sandy loam soils (Rodrigues and Silva, 2020). This could explain the fact that soil-A adsorbs more B than soil-B.

Background electrolytes influence on B adsorption

Following the comparison of all the mean values of B adsorbed in all types of background electrolytes solutions, in both soil-A and B, minor B adsorption was found using boric acid solution without background electrolytes (Figs. 3 and 4). This proves that cations presented in background electrolyte solutions are having an important role in B adsorption. In Soil-A, the highest adsorbed B mean value was found with K, monovalent cation, although so close to the rest of the mean values excepting TBo and in Soil-B was associated to Ca, divalent cation. Focusing on $CaCl_2$ and NaCl, as a comparison of divalent and monovalent cations, the content of B adsorbed was higher with the solution containing $CaCl_2$ than in the NaCl solution, as reported earlier by Goldberg and Suárez (2011). They explained that in the Ca, the slightly greater B adsorption at high pH was caused by B adsorption onto freshly precipitated $CaCO_3$. Goldberg and Forster (1991), Goldberg (1997) and Kumar *et al.* (2018) highlighted that, in calcareous soils, calcium carbonate is an important B adsorbing surface. This confirms very well the finding of this work, as the two soils of this case study are calcareous (rich in limestone). Furthermore, ionic strength has a significant effect on B adsorption, being more important in the presence of a divalent ion such as calcium than monovalent sodium ions

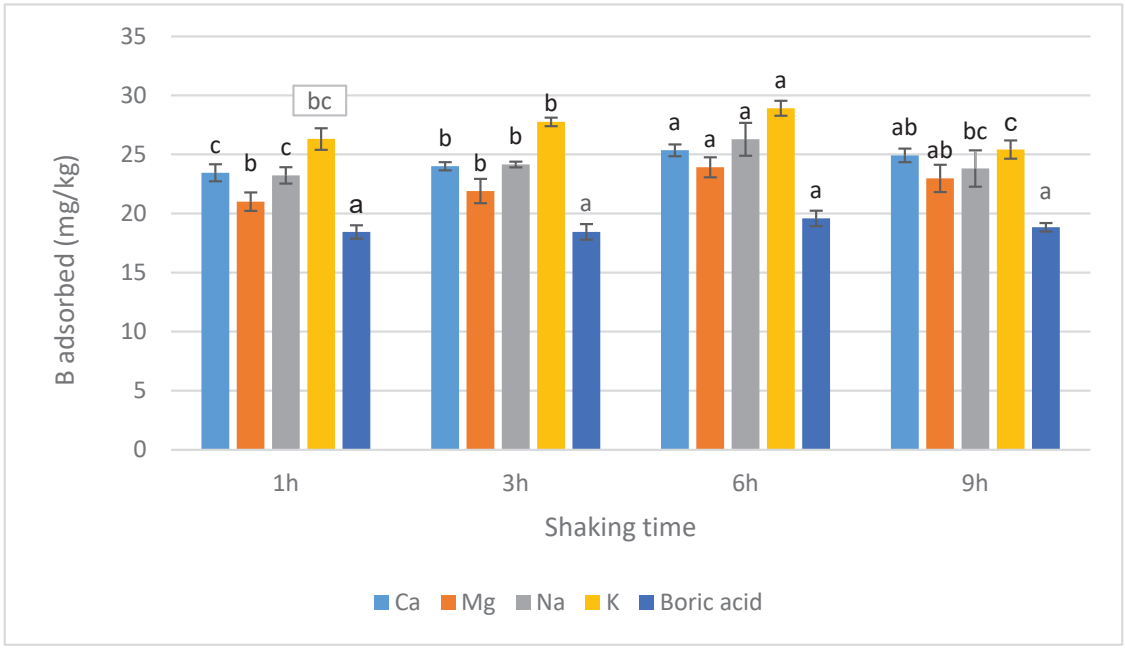

Fig.3: B adsorbed in Soil-A with different time of shaking in TBCa, TBMg, TBNa, TBK and TBo (Different letters indicate significant differences among the different time of shaking at P<0.05 level and at the same treatment)

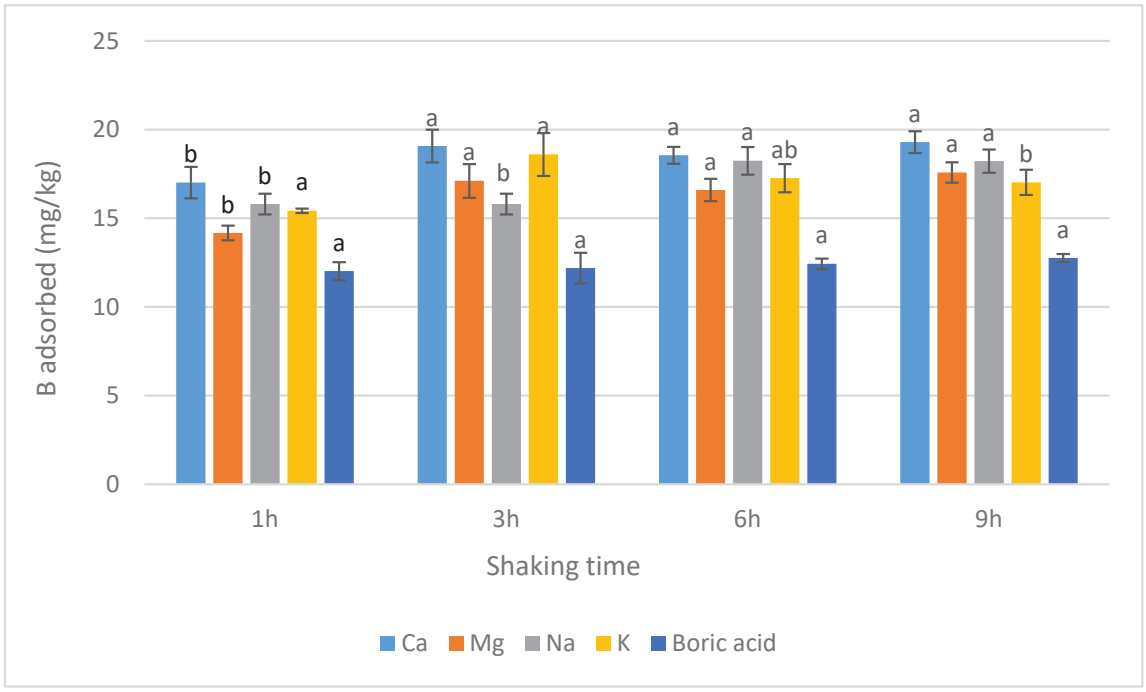

Fig.4: B adsorbed in Soil-B with different time of shaking in TBCa, TBMg, TBNa, TBK and TBo (Different letters indicate significant differences among the different time of shaking at P<0.05 level and at the same treatment)

(Rodrigues and Silva, 2020). As for clay minerals, Keren and Sparks (1994) have concluded that the negative electrical field associated with the planar surface affects the B adsorption on edge surfaces. They explained that for clay minerals, increasing ionic strength eliminates the negative electrical field of planar surface. As a result, more negative borate ions are able to approach the adsorption sites on the edge surfaces and interact with them, which contributes to greater B adsorption. Moreover, Abu-Sharar *et al.* (2014) confirmed Majidi *et al.* (2010) finding that an increasing background electrolyte concentration 0.01 M NaCl to 0.1 and 0.5 M resulted in an elevation of the maximum of B adsorption by respectively 30% and 75%. Calcium chloride at the equimolar concentration showed a more important increase in B adsorption as compared to NaCl. A divalent system will have a higher ionic strength (I) than equimolar monovalent system causing more compressed diffused double layer. These findings prove the strong effect of Ca divalent cation in B adsorption. These authors further pointed out that B was mainly adsorbed as an outer-sphere complex, favored by the presence of micro-aggregates; clay particles attached to organic molecules by polyvalent cations (Bronick and Lal, 2005). In short experiments, studying the effect of KCl on boric acid solutions, no decrease in the B concentration was found, even at higher K concentrations than in soil solution. This means that the potassium did not have a direct effect on B adsorption, but created new conditions in the soil, which favor B adsorption or provided new adsorption sites with high affinity for B (Hadas and Hagin, 1972; Tariq and Mott, 2007). This could explain somehow the results, that greater B adsorption was found in K monovalent cation in clay loam soil (Soil-A). However, no significant differences were found between K and Ca as background electrolytes. Ionic strength affects significantly B adsorption. This effect has been reported low for oxides and high for clay minerals and soils (Mattigod *et al.,* 1985; Majidi *et al.,* 2010). However, in the present study, in which Soil-B is sandy loam soil, B adsorbed highest value is associated with Ca background electrolyte solution. In clay loam soil, Soil-A (that obviously contains more clay than Soil-B), B highest adsorbed value is not associated to divalent cation as expected, but to K monovalent cation. Mattigod *et al.* (1985) and Kot (2009) developed that borate ions combine with alkali and alkaline earth cations to produce soluble complexes. Therefore, the formation of borate complexes in solution may influence the adsorption of this element on mineral surfaces. These authors highlighted the potential importance of ion-pair formation in K^+ and Ca^{2+} dominated electrolyte solutions in the context of B adsorption on kaolinite.

CONCLUSION

The Boron adsorption in soils is a significant topic in agronomy, as it can threaten plant development and crop yield. In this study, B adsorption was investigated in calcareous salt-affected soil in semiarid areas, under the effect of different background electrolytes, two soil textures and different shaking time intervals. The study findings revealed that Soil-A (clay loam) adsorbed more B than Soil-B (sandy loam), owing to soil texture and possibly organic matter content. It is of great relevance that soil texture and organic matter are key factors that can explain the boron adsorption in soils and both should be checked in cultivated soils to ensure the bioavailability of this plant nutrient. However, the analysis of boron to measure the presence and interactions with the soil matrix is a great concern. Beyond any doubt, the shaking time may have a significant impact on B adsorption in soils, as it takes 3 h of shaking to reach the maximum amount of B adsorbed. The results showed that the background electrolyte composition of soil solution is a factor of highest interest in boron adsorption mechanism. Centered in the current study, concerning Soil-A, the maximum B adsorption value was recorded with potassium chloride. As for Soil-B, it was associated with calcium chloride. Furthermore, the content of B adsorbed was higher with the solution containing calcium chloride than sodium chloride. In both soils, in general, the major B adsorption was reached by using calcium chloride as background electrolyte solution. Therefore, compared to all background electrolytes solutions, calcium chloride seemed to be the cation having the most favorable behavior for B adsorption experiments. In this sense, the presence of a predominant monovalent or divalent cation as a background electrolyte obviously determine the adsorption of B in soil and the availability of this nutrient to plants. In conclusion, the optimal

conditions for maximum boron adsorption in this type of soils are characterized by calcium chloride background electrolyte in a determined shaking time interval equal to (3h) according to the present study. Consequently the high boron adsorbed results in a low rate of boron assimilation by plants, which decrease crop yields, agricultural productivity, and equally has a negative influence on the Tunisian national economy.

AUTHOR CONTRIBUTIONS

S. Fatnassi performed the literature review, experimental design, analyzed and interpreted the data, prepared the manuscript text, and manuscript edition. J. Navarro Pedreño performed the experiment supervision in Spain, literature review, compiled and interpreted the data and contributed to the draft manuscript preparation. M.B. Almendro Candel supported the experiment in the study laboratory of Agrochemistry and Environment department in Miguel Hernández University of Elche (UMH), data preparation and review of the manuscript. I. Gómez Lucas supported the entire work in the research laboratory in UMH and afforded the necessary material and chemical products. M. Hachicha supervised and supported the study, helped in the literature review and manuscript preparation and review.

ACKNOWLEDGMENTS

This study was financially supported by the research laboratory Valorization of Non-Conventional Waters (INRGREF), two scholarships from the Faculty of Sciences of Tunis (Tunis El Manar University) and the research laboratory of Department of Agrochemistry and Environment (Miguel Hernández University of Elche).

CONFLICT OF INTEREST

The authors declare no potential conflict of interest regarding the publication of this work. In addition, the ethical issues including plagiarism, informed consent, misconduct, data fabrication and, or falsification, double publication and, or submission, and redundancy have been completely witnessed by the authors.

OPEN ACCESS

PUBLISHER'S NOTE

ABBREVIATIONS

%	Percent
Al	Aluminum
ANOVA	Analysis of variance
B	Boron
Ca	Calcium
CaCl2	Calcium chloride
Cl	Chloride
dS/m	deciSiemens per metre
EC	Electrical conductivity of the soil
Ecw	Electrical conductivity of TWW
FAO	Food and Agriculture Organization of the United Nations
Fe	Iron
H	Hour/ hours
HCO3	bicarbonate
ISO	International Organization for Standardization
JECFA	Joint FAO/WH Expert Committee on Food Additives
K	Potassium
KCl	Potassium chloride

Max.	Maximum
Min.	Minimum
mg/L	Milligrams per liter
mm	millimeter
m	meter
Mg/kg	Milligrams per kilogram
meq/L	Milliequivalents per liter
Mg	Magnesium
MgCl2	Magnesium chloride
Na	Sodium
NaCl	Sodium chloride
NF	French standard
NT	Tunisian standard
N	Normality
NS	Not significant
OM	Organic matter
pH	potential of hydrogen
SD	Standard deviation
SO4	Sulfate
TCaCO3	Total equivalent calcium carbonate
TBo	Treatment of B solution without background electrolyte
TBCa	Treatment with calcium chloride background electrolyte
TBMg	Treatment with magnesium chloride background electrolyte
TBNa	Treatment with sodium chloride background electrolyte
TBK	Treatment with potassium chloride background electrolyte
TWW	Treated wastewater
WHO	World Health Organization
w/v	Weight/volume

REFERENCES

Abu-Sharar, T.M.; Hani, N.B.; Al-Khader, S., (2014). Boron adsorption–desorption characteristics of irrigated soils in the Jordan Valley. Geoderma Reg., (2): 50-59 **(10 pages).**

Abu-Dabaan, R.; Al-Najar, H., (2018). The effect of long term irrigation by treated effluent on boron accumulation in soil and citrus plants. Asian Rev. Environ. Earth Sci., (5): 22–26 **(5 pages).**

Al-Ameri, B.H.; Al-Saedi, S.A.; Razaq, I.B., (2019). Effect of Boron supplement on yield of wheat grown in calcareous soils of different textural classes under arid conditions. J. Agric. Sci., 11(1): 112-117 **(6 pages).**

Alam, M.N.; Jahan, N., (2007). Effect of boron levels on growth and yield of cabbage in calcareous soils of Bangladesh. Res. J. Agric. Biol. Sci., 3(6): 858-865 **(8 pages).**

Albrecht, J., (2013). The Europeanization of water law by the Water Framework Directive: A second chance for water planning in Germany. Land Use Policy., 30(1): 381-391 **(11 pages).**

Arora, S.; Chahal, D.S., (2007). Comparison of kinetic models for boron adsorption in alluvium-derived soils of Punjab, India. Commun. Soil Sci. Plant Anal., 38(3-4): 523-532 **(10 pages).**

Benbi, D.K., (2018). Evaluation of a rapid microwave digestion method for determination of total organic carbon in soil. Commun. Soil Sci. Plant Anal., 49(17): 2103-2112 **(10 pages).**

Bhupenchandra, I.; Basumatary, A.; Singh, L.K.; Khwairakpam, R., (2019). Assessment of the complex relationship of boron fractions with available soil nutrient status as influenced by boron fertilization in cauliflower. Int. J. Chem. Stud., 7(3): 4253-4256 (**3 pages**).

Bhuyar, P; Rahim, M.H.; Sundararaju, S.; Maniam, G.P.; Govindan, N., (2020). Antioxidant and antibacterial activity of red seaweed; Kappaphycus alvarezii against pathogenic bacteria. Global J. Environ. Sci. Manage., 6(1): 47-58 **(12 pages).**

Boaretto, R.M.; Quaggio, J.A.; Mattos, Jr.D.; Muraoka, T.; Boaretto, A.E., (2011). Boron uptake and distribution in field grown citrus trees. J. Plant Nutr., 34(6): 839-849 (**11 pages**).

Brdar-Jokanović, M., (2020). Boron toxicity and deficiency in agricultural plants. Int. J. Mol. Sci., 21(4): 1424 (**21 pages**).

Bronick, C.J.; Lal, R., (2005). Soil structure and management: a review. Geoderma., 124(1-2): 3-22 **(20 pages).**

Brown, P. H.; Shelp, B.J., (1997). Boron mobility in plants. Plant Soil., 193(1): 85-101 (**17 pages**).

Chen, X.; Schauder, S.; Potier, N.; Van Dorsselaer, A.;Pelczer, I.; Bassler, B.L.; Hughson, F.M., (2002). Structural identification of a bacterial quorum-sensing signal containing boron. Nature., 415(6871): 545-549 **(5 pages).**

Corwin, D.L.; Yemoto, K., (2020). Salinity: Electrical conductivity and total dissolved solids. Soil Sci. Soc. Am. J., 84(5): 1442-1461 **(20 pages).**

Dahmouni, M.; Hoermann, G.; Jouzdan, O.; Hachicha, M., (2018). Export of salt and heavy metals in an area irrigated with treated wastewater: a case study from Cebala Borj-Touil (Tunisia). Desalination Water Treat., 102: 61-70 **(10 pages).**

Errais, E.; Duplay, J.; Darragi, F., (2010). Textile dye removal by natural clay–case study of Fouchana Tunisian clay. Environ. Technol., 31(4): 373-380 **(8 pages).**

Goldberg, S., (1997). Reactions of boron with soils. Plant Soil. 193(1): 35-48 **(14 pages).**

Goldberg, S.; Forster, H.S. (1991). Boron sorption on calcareous soils and reference calcites. Soil Sci., 152(4): 304-310 **(7 pages).**

Goldberg, S.; Suarez, D.L., (2011). Influence of soil solution cation composition on boron adsorption by soils. Soil sci., 176(2): 80-83 **(4 pages).**

Gürel, S.; Başar, H.; Keskin, E.; Dirim, M.S., (2019). The determination of soil boron fractions, their relationships to

soil properties and the availability to olive (Olea europea L.) trees. Commun. Soil Sci. Plant Anal., 50(8): 1044-1062 **(19 pages).**

Hadas, A.; Hagin, J., (1972). Boron adsorption by soils as influenced by potassium. Soil Sci., 113(3): 189-193 **(5 pages).**

Hilal, N.; Kim, G.J.; Somerfield, C., (2011). Boron removal from saline water: a comprehensive review. Desalination., 273(1): 23-35 **(13 pages).**

Hingston, F.J., (1964). Reactions between boron and clays. Soil Res., 2(1): 83-95 **(13 pages).**

Hjelm, C.; Harari, F.; Vahter, M., (2019). Pre-and postnatal environmental boron exposure and infant growth: Results from a mother-child cohort in northern Argentina. Environ., 171: 60-68 **(9 pages).**

Hu, H.; Brown, P.H., (1997). Absorption of boron by plant roots. Plant Soil. 193(1): 49-58 **(10 pages).**

Irfan, M.; Abbas, M.; Shah, J.A.; Depar, N.; SİAL, N.A., (2019). Interactive effect of phosphorus and boron on plant growth, nutrient accumulation and grain yield of wheat grown on calcareous soil. Eurasian J. Soil Sci., 8(1): 17-26 **(10 pages).**

Jalal, D.; Ezzedine, T., (2019). Toward a smart real time monitoring system for drinking water based on machine learning. International Conference on Software, Telecommunications and Computer Networks (SoftCOM). IEEE., 1-5 **(5 pages).**

JECFA, (1974). Seventeenth Report of the Joint FAO/WHO Expert Committee on Food Additives.

Jerbi, M.; Labidi, S.; Lounès-Hadj Sahraoui, A.; Chaar, H.; Ben Jeddi, F., (2020). Higher temperatures and lower annual rainfall do not restrict, directly or indirectly, the mycorrhizal colonization of barley (Hordeumvulgare L.) under rainfed conditions. PloS one, 15(11): **(20 pages).**

Keren, R.; Sparks, D.L., (1994). Effect of pH and ionic strength on boron adsorption by pyrophyllite. Soil Sci. Soc. Am. J., 58(4): 1095-1100 **(6 pages).**

Khaskhoussy, K.;Kahlaoui, B.; Nefzi, B.M.; Jozdan, O.; Dakheel, A.;Hachicha, M., (2015). Effect of treated wastewater irrigation on heavy metals distribution in a Tunisian soil. Eng. Technol. Appl. Sci. Res., 5(3): 805-810 **(6 pages).**

Kot, F.S., (2009). Boron sources, speciation and its potential impact on health. Rev. Environ. Sci. Biotechnol., 8(1): 3-28 **(26 pages).**

Kumar, S.; Kumar, D.; Sekhon, K.S.; Choudhary, O.P., (2018). Influence of levels and methods of boron application on the yield and uptake of boron by cotton in a calcareous soil of Punjab. Commun. Soil Sci. Plant Anal., 49(4): 499-514 **(16 pages).**

Landi, M.; Margaritopoulou, T.; Papadakis, I.E.; Araniti, F., (2019). Boron toxicity in higher plants: an update. Planta. 250(4): 1011-1032 **(22 pages).**

López, P. ; Sutanudjaja, E.H.; Schellekens, J.; Sterk, G.; Bierkens, M.F., (2017). Calibration of a large-scale hydrological model using satellite-based soil moisture and evapotranspiration products. Hydrol Earth Syst Sci., 21(6: 3125-3144 **(20 pages).**

Maas, E.V., (1986). Salt tolerance of plants. J. Appl. Agric. Res., 1(1): 12-25 **(14 pages).**

Majidi, A.; Rahnemaie, R.; Hassani, A. ; Malakouti, M.J., (2010). Adsorption and desorption processes of boron in calcareous soils. Chemosphere. 80(7): 733-739 **(7 pages).**

Mattigod, S.V.; Frampton, J.A.; Lim, C.H., (1985). Effect of ion-pair formation on boron adsorption by kaolinite. Clays Clay Miner., 33(5): 433-437 **(5 pages).**

Nicolás, E.; Alarcón, J.J.; Mounzer, O.; Pedrero, F.; Nortes, P.A.; Alcobendas, R.; Romero-Trigueros, C.; Bayona, J.M.; Maestre-Valero, J.F., (2016). Long-term physiological and agronomic responses of mandarin trees to irrigation with saline reclaimed. Agric. Water Manage., 166: 1-8 **(8 pages).**

Pena-Pereira, F.; Velazquez, A.; Lavilla, I.; Bendicho, C., (2020). A paper-based colorimetric assay with non-instrumental detection for determination of boron in water samples. Talanta., 208: 120365 **(9 pages).**

Ramos, Q.; Armienta, M.A.; Aguayo, A.; Cruz, O., (2021). Evaluation of the interactions of arsenic (As), boron (B), and lead (Pb) from geothermal production wells with agricultural soils. Ecotoxicol. Environ. Saf., 211: 111843.

Reid, R. J.; Hayes, J.E.; Post, A.;Stangoulis, J.C.R.; Graham, R.D., (2004). A critical analysis of the causes of boron toxicity in plants. Plant Cell Environ., 27(11): 1405-1414 **(10 pages).**

Richards, L.A., (1954). Diagnosis and improvement of saline and alkali soils. 78 (2): 154.

Rodrigues, L.U.; Silva, R.R.D., (2020). Boron availability in building up fertility in Cerrado Soil of Tocantins. Commun. Soil Sci. Plant Anal., 51(5): 595-603 **(9 pages).**

Sah, R.N.; Brown, P.H., (1997). Boron determination—a review of analytical methods. Microchem. J., 56(3): 285-304 **(20 pages).**

Santos, P.D.; Goldberg, S.; Costa, A.C.S.D., (2020). Modeling boron adsorption on five soils before and after removal of organic matter. Sci. Agric., 77.

Sarkar, D.; De, D.K.; Das, R.; Mandal, B., (2014). Removal of organic matter and oxides of iron and manganese from soil influences boron adsorption in soil. Geoderma. 214: 213-216 **(4 pages).**

Sarmast, M.; Farpoor, M.H.; Boroujeni, I.E., (2016). Comparing Soil Taxonomy (2014) and updated WRB (2015) for describing calcareous and gypsiferous soils, Central Iran. Catena. 145: 83-91 **(9 pages).**

Schwager-Guilloux, J., (2014). Les toitures végétalisées, puits et sources d'éléments en traces métalliques (Doctoral dissertation, Université de Lorraine).

Shorrocks, V.M., (1997). The occurrence and correction of boron deficiency. Plant Soil. 193(1): 121-148 **(28 pages).**

Su, C.; Suarez, D.L., (2004). Boron release from weathering of illites, serpentine, shales, and illitic/palygorskitic soils. Soil Sci. Soc. Am. J., 68(1): 96-105 **(10 pages).**

Tamuli, B.; Bhattacharyya, D.; Borua, N.G.;Basumatary, A.; Das, K.N.;Kurmi, K., (2017). Kinetics of boron adsorption in soils of Assam state, India. Asian J. Chem., 29(2): 313-316 **(4 pages).**

Tariq, M.; Mott, C.J.B., (2006). Effect of applied boron on the accumulation of cations and their ratios to boron in radish (Raphanussativus L.). Soil Environ., 25(1): 40-47 **(8 pages).**

Tariq, M.; Mott, C.J.B., (2007). The significance of boron in plant nutrition and environment-a review. J. Agron., 6(1): 647-650 **(4 pages).**

Terraza Pira, M. F.; Sumner, M.E., Cabrera, M. L.; Thompson, A., (2018). Boron Adsorption and Desorption on Volcanic Ash–Derived Soils. Soil Sci. Soc. Am. J., 82(1): 66-75 **(10 pages).**

Wimmer, M.A.; Abreu, I.; Bell, R.W.; Bienert, M.D.; Brown, P.H.; Dell, B., Fujiwara, T.; Goldbach, H.E.; Lehto, T.; Mock, H.P.;

Wirén, N.V.;Bassil, E.; Bienert, G.P., (2019) Boron: An essential element for vascular plants. A comment on Lewis; Boron: the essential element for vascular plants that never was'. New Phytol., 226(5): 1232-1237 **(6 pages).**

WHO, (2006). WHO guidelines for the safe use of wasterwater excreta and greywater., World Health Organization.

AUTHOR (S) BIOSKETCHES

Fatnassi, S., M.Sc., [1]Department of Geology, Faculty of Sciences of Tunis, University of Tunis El Manar, 2092 El Manar, Tunis, Tunisia. [2]National Institute of Rural Engineering, Waters and Forest, Carthage University, 2080 BP 10 Ariana, Tunisia.
- Email: *salmapro14@gmail.com*
- ORCID: 0000-0002-2017-1056
- Web of Science ResearcherID: NA
- Scopus Author ID: NA
- Homepage: NA

AlmendroCandel, M.B., Ph.D., Associate Professor, Department of Agrochemistry and Environment, Miguel Hernández University of Elche, Avd.de la Universidad SN, 03202 Elche, Alicante, Spain.
- Email: *mb.almendro@goumh.umh.es*
- ORCID: 0000-0003-3704-8078
- Web of Science ResearcherID: K-8319-2014
- ScopusAuthor ID:9332378700
- Homepage: www.umh.es/contenido/Estudios/:persona_35434/datos_en.html

Navarro Pedreño, J., Ph.D., Professor, Department of Agrochemistry and Environment, Miguel Hernández University of Elche, Avd.de la Universidad SN, 03202 Elche, Alicante, Spain.
- Email:*jonavar@umh.es*
- ORCID: 0000-0002-4765-2191
- Web of Science ResearcherID:A-7830-2010
- Scopus Author ID:6602116441
- Homepage: https://www.umh.es/contenido/Estudios/:persona_5343/datos_en.html

Gómez Lucas, I., Ph.D., Professor, Department of Agrochemistry and Environment, Miguel Hernández University of Elche, Avd.de la Universidad SN, 03202 Elche, Alicante, Spain.
- Email: *ignacio.gomez@umh.es*
- ORCID: 0000-0002-0931-9654
- Web of Science ResearcherID: H-8531-2015
- Scopus Author ID: 16315845200
- Homepage: https://www.umh.es/contenido/Universidad/:persona_117889/datos_en.html

Hachicha, M.,Ph.D., Professor, National Institute of Rural Engineering, Waters and Forest, Carthage University, 2080 BP 10 Ariana, Tunisia.
- Email: *hachicha.mohamed@iresa.agrinet.tn*
- ORCID: 000-002-5125-8541
- Web of Science ResearcherID: NA
- Scopus Author ID: NA
- Homepage: http://www.lrvenc.agrinet.tn/cv/Medhcicha.html

HOW TO CITE THIS ARTICLE

Fatnassi, S.; Almendro Candel, M.B.; Navarro Pedreño, J.; Gómez Lucas, I.; Hachicha, M., (2022). Boron adsorption in semiarid Mediterranean soils under the influence of background electrolytes. Global J. Environ. Sci.Manage., 8(4): 519-532.

DOI: 10.22034/gjesm.2022.04.05

url: https://www.gjesm.net/article_249150.html

Global J. Environ. Sci. Manage. 8(4): 533-544, Autumn 2022, Serial #32

Global Journal of Environmental Science and Management
(GJESM)

Homepage: https://www.gjesm.net/

ORIGINAL RESEARCH ARTICLE

Panel data regression approach on Inclusive green growth

E. Juniardi, S. Amar, H. Aimon

Faculty of Economy, Padang State University, Hamka Street, Padang 25171, Indonesia

ARTICLE INFO

Article History:
Received 26 August 2021
Revised 06 January 2022
Accepted 09 February 2022

Keywords:
Inclusive green growth
Inclusive human development
Industrialization
Panel data regression

DOI: 10.22034/gjesm.2022.04.06

ABSTRACT

BACKGROUND AND OBJECTIVES: This study is investigated on endogenous variables inclusive of green growth by developing the concept of inclusive green growth in Indonesia. The objective of the current study was to describe the conditions of inclusive green development in each province in Indonesia, which is due to the unavailability of data describing the conditions of inclusive green development.
METHODS: This study used time series data from 2011-2019, and cross section data of 34 provinces, which were analyzed using panel data regression research methods. The novelty of this study is the use of environmental quality variables to replace environmental degradation in calculating the composite variable of inclusive green growth. The determinants of inclusive green growth used in this study were inclusive human development, regional independence, infrastructure, crime, industrialization and natural disasters.
FINDINGS: The important study findings were inclusive human development, regional financial performance, infrastructure and natural disasters have a significant positive effect on inclusive green growth in Indonesia. On the other hand, industrialization had a significant negative effect on inclusive green growth in Indonesia, while crime did not have a significant effect on inclusive green growth in Indonesia. Simultaneously, inclusive human development, regional independence, infrastructure, crime, industrialization and natural disasters had a significant impact on inclusive green growth in Indonesia.
CONCLUSION: The second hypothesis in this study proved to be accepted. Meanwhile, the first hypothesis is not entirely accepted. Therefore, it is highly recommended for the provincial government in Indonesia to intervene on the variables of inclusive human development, regional financial performance, infrastructure, industrialization and natural disasters to increase inclusive green growth. Meanwhile, for future researchers, it is recommended to find other variables that contribute in achieving inclusive green growth.

NUMBER OF REFERENCES	NUMBER OF FIGURES	NUMBER OF TABLES
41	3	3

*Corresponding Author:
Email: *egiardi87@gmail.com*
ORCID: 0000-0001-7755-9142

Note: Discussion period for this manuscript open until January 1, 2023 on GJESM website at the "Show Article".

INTRODUCTION

The World Bank defines inclusive green growth as "sustainable economic development" (Albagory, 2016; Jha *et al.,* 2018; Sun *et al.,* 2020). Inclusive green growth is a function of economic (i.e. economic growth), social (i.e. poverty, inequality, employment) and environmental (i.e. emissions and environmental pollution) (Sun, *et al.,* 2020). Luukanen *et al.* (2019) explained that inclusive green growth (IGG) is an organic combination of two development concepts, namely green growth (GG) and inclusive growth (IG). Meanwhile, in this study, inclusive green growth is a composite of economic growth, poverty, income inequality, unemployment and environmental quality consisted of water quality, air quality and forest cover. Shcherbak *et al*., (2020) explained that forestry and household income should be a concern in increasing the economic growth of a region. In the perspective of inclusive growth, it is built through three pillars, namely economic growth and development, income distribution and poverty reduction, and expansion of access and opportunities, while from an environmental perspective, it is built from three aspects, namely air quality, water quality and the resulting area of forest cover. Therefore, inclusive green growth referred to in this study is inclusive growth that takes into account the ecological balance seen from the quality of the environment itself. Thus, the IGG is a function of inclusive growth (which refers to economic growth, income distribution and poverty reduction and expansion of access to and job opportunities) and green growth (which refers to environmental quality). Indonesia as a developing country has also adopted the concept of sustainable growth to ensure an increase in economic output and preserve the environment. However, currently, the calculation of inclusive green growth in Indonesia is still very minimal, so data describing the IGG phenomenon is still difficult to obtain. For this reason, the phenomenon that describes the IGG is a composite calculated from the inclusive growth index published by Central bureau of statistic (CBS) of Indonesia, national development planning agency (NDPA) of Indonesia and the environmental quality index published by the ministry of environment and forestry (MEF) of Indonesia. The result from range of 2011-2018 is shown in Fig. 1.

Based on Fig. 1, it can be seen that in aggregate, the IGG phenomenon that occurs is getting more satisfactory (good) every year in the 2011-2018 period, although from 2011 to 2013 and 2015 to 2016 there was a slight fluctuation of 0.01. Furthermore, the satisfying IGG certainly provided an illustration of the increase in economic output to meet human needs that has occurred along with improvements in environmental quality such as water quality, air quality and forest conditions in the satisfactory category, thus, in aggregate, the IGG was in the satisfactory category. However, when comparing the IGG rate with the conventional economic growth (CEG) rate, in aggregate, the IGG rate was smaller than CEG rate. This indicates that Indonesia's economic growth is still focused on increasing the production output of each sector, thus ignoring environmental issues such as water quality, air quality and forest sustainability, while also not focusing on poverty, income inequality and employment expansion. For more details, it can be seen in Fig. 2.

Based on Fig. 2, it can be seen that during the comparison period, although in 2014 the IGG rate

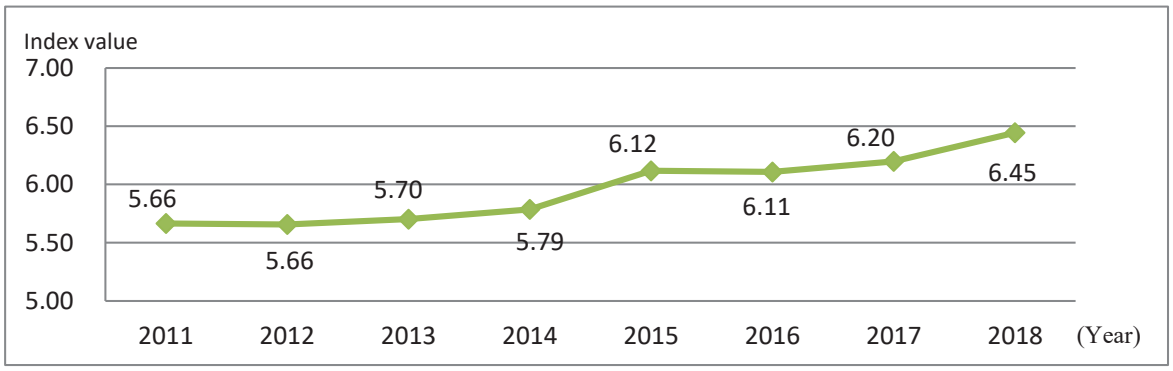

Fig. 1: Indonesia's inclusive green growth (in the index) (CBS, 2020; NDPA, 2020; MEF, 2020)

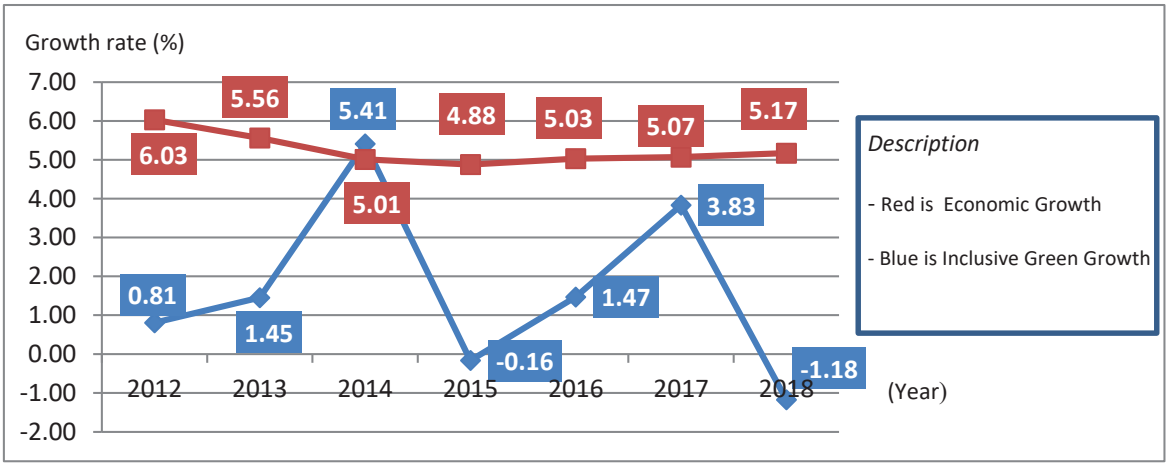

Fig. 2: Comparison of inclusive green growth with conventional economic growth in Indonesia (in percent) (CBS, 2020; NDPA, 2020; MEF, 2020)

increased significantly during that period and was higher than CEG, this occurred when CEG experienced a growth of minus 0.55%. In general, this growth pattern is repeated every year during the observation period, i.e. if the CEG decreased, the IGG tent to increase. The phenomenon in Fig. 2 certainly reflects that the economic growth occurred in Indonesia has not been in accordance with the goals of sustainable development, environmentally friendly development. In addition, the phenomenon of IGG raises a question whether the development carried out has reached IGG in each province in Indonesia. Therefore, it is important to calculate the IGG in each province, considering that the IGG in each province is an integral part of the IGG in Indonesia. To achieve sustainable development in Indonesia as stated in the sustainable development goals (SDGs), every country must focus on inclusive green growth. Thus, Based on the phenomena described, it is necessary to analyze inclusive green growth in Indonesia. The IGG condition is derived from the derivative of the concept of inclusive green growth conducted by Luukkanen *et al.* (2019) and concept change studied by Sun *et al.* (2020) towards inclusive green growth (IGG). Sun *et al.* (2020) stated that IGG is a function of economic growth, social, emission and environmental pollution, while in this study IGG is expressed as a function of inclusive growth variables (which consist of economic growth and social growth as measured by poverty reduction, unemployment rate reduction and income distribution), and environmental quality variables (consisting of air quality, water quality and forest cover area). The use of these two variables is because the relationship between economic growth, social growth and environmental quality is linear. The reason for substituting the emission and environmental pollution variables in the research of Sun *et al.* (2020) with environmental quality variables is because the environmental quality variable describes a wider impact of pollution than emissions. The environmental quality is the impact of environmental pollution consisting of water quality as a result of water pollution, air quality as a result of air pollution and forest cover area as a result of forest damage. The aims of the current study is to describe the conditions of inclusive green development in each province in Indonesia, which is due to the unavailability of data describing the conditions of inclusive green development. The study is also expected to tackle the lack of the previous research. This study has been carried out in Padang, Indonesia, in 2020 and 2021.

MATERIALS AND METHODS

Research method

The method used in this research was descriptive quantitative. Descriptive method was used to determine the value of variable independently, either one or more variables, without making comparisons or connecting one variable to another.

Types of data, data collection techniques and research variables

This study used secondary data. The objects

of research were 34 provinces in Indonesia. The observation year ranged from 2011-2019. The data collection technique used in this research was documentation, by collecting reports, documents, or records issued by relevant agencies such as publications from the Indonesian Central Bureau of Statistics, Ministry of Environment and Forestry, National Development Planning Agency Republic of Indonesia, National Disaster Management Agency, Indonesian Police.The determinants of inclusive green growth used in this study were inclusive human development, regional independence, infrastructure, crime, industrialization and natural disasters.

Variable operational definition

Inclusive green growth (Y)

IGG is economic growth that is in line with reducing poverty, unemployment and inequality as well as improving the quality of the environment. IGG is a composite of the Inclusive Growth Index (IGI) and the Environmental Quality Index (EQI) divided by two. IGG parameters in this study can be seen from 3 categories as follows, a value of $0 \leq IGG < 40$ means "not satisfactory", a value of $40 \leq IGG < 80$ means "satisfactory", and a value of $80 \leq IGG \leq 100$ means "very satisfactory".

Inclusive human development (IHD) (X1)

IHD is human development aligned with gender equality. This IHD is expressed by the Gender Development Index (GDI). The GDI in this study was obtained from the GDI published by Indonesian Central Bureau of Statistics. IHD parameter can be explained by the value of IHD. If the IHD value almost reached 100, the IHD is getting better.

Regional financial performance (RFP) (X2)

RFP is the average of the components of budget solvency (BS), financial independence (FI) and service solvency (SS). BS is total regional income divided by total expenditure, FI is total local revenue divided by total expenditure, SS is total expenditure divided by population. RFP parameter can be explained by the value of RFP. If the RFP value almost reached 100, the RFP is getting better.

Infrastructure (X3)

Infrastructure is the average component of economic infrastructure with social infrastructure. The components of economic infrastructure consist of proxies of the economic situation of the community in the use of infrastructure, especially in public utilities such as the percentage of households that have a source of lighting from electricity, the percentage of households that have access to proper sanitation, the percentage of households with a source of proper drinking water. Meanwhile, the components of social infrastructure consist of the number of primary schools and the number of health facilities at the public health centre. Infrastructure parameter can be explained by the value of infrastructure. If the infrastructure value almost reached 100, the infrastructure development is getting more quality.

Crime (X4)

Crime is a form of government response to security in the community, so the government must resolve every reported case or what is known as crime clearance. Thus, crime clearance is the number of resolved cases divided by the number of reported cases. Crime parameter can be explained by the value of crime. If the crime value almost reached 100, government's response to crime in Indonesia is getting better.

Industrialization (X5)

Industrialization is gross regional domestic product (GRDP) in the industrial sector. Data obtained from the Indonesian central bureau of statistics. The higher industrialization value means the high industrial growth in Indonesia.

Natural disaster (X6)

Natural disasters are the number of natural disasters occur every month. The higher percentage value of natural disasters showed the more frequent of the occurrence of natural disasters in Indonesia.

Model specification

The relationships between these variables are summarized in Fig. 3.

Based on Fig. 3, the mathematical equation for the simultaneous equation using the econometric approach for the inclusive green growth equation can be written using Eq. 1.

$$Y_{1it} = \beta_0 + \beta_1 X_{1it} + \beta_2 X_{2it} + \beta_3 X_{3it} + \beta_4 X_{4it} + \beta_5 X_{5it} + \beta_6 X_{6it} + \mu_{it} \quad (1)$$

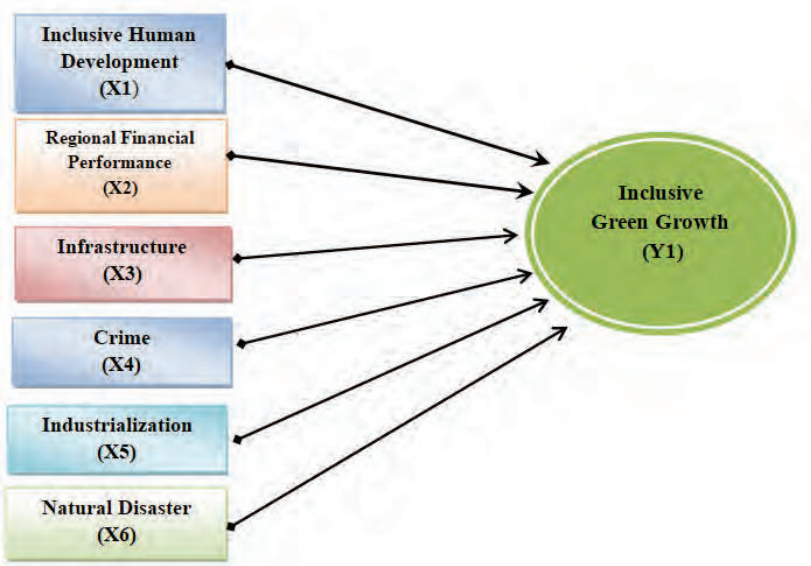

Fig. 3: The conceptual framework of study

Data analysis technique

Panel Data Regression

In this study, panel data regression was used because the purpose of this study was to analyze what factors influence inclusive green growth between provinces (cross section) and across time (time series). Ghozali (2013) explained that there are several methods commonly used to estimate regression models with panel data, including:

a. Common effect model (CEM)
b. Fixed effect model (FEM)
c. Random effect model (REM)

Classical assumption test

In this research, the classical assumption test used normality test, multicollinearity test, and heteroscedasticity test to see the correlation between independent variables. Normality test used Jarque-Bera (JB).The regression equation model is said to be good if the data is normally distributed or close to normal, the calculated JB probability value is greater than 0.05. A good regression model should not have a correlation between independent variables (Ghozali, 2013) where the correlation coefficient (R2) is < 0.80. Heteroscedasticity test used the Glejser method, a good regression model is homoscedasticity or there is no heteroscedasticity where the probability value is > 0.05 (Ghozali, 2013).

Statistical test

In this research, statistical test using t- test to find out whether the exogenous variable (X) has a significant effect on the endogenous variable (Y) partially, where the probability value of the exogenous variable is small than α= 0.05 (tcount ttable or – tcount <- ttable) on endogenous variables, then H0 is rejected and Ha is accepted, indicated that there is a significant effect between exogenous variables on endogenous variables. On the other hand, if the probability value of the exogenous variable is greater than α= 0.05 (tcount < ttable or – tcount - ttable) on the endogenous variable, then H0 is accepted and Ha is rejected, indicated that there is no significant effect between the exogenous variables on the endogenous variables. Furthermore, using the f- test to find out whether the exogenous variables silmutaneously (X1, X2,….Xn) have a significant effect on the endogenous variable (Y), where the probability value of Fcount < 0.05, the null hypothesis (Ho) is rejected and the alternative hypothesis (Ha) is accepted, indicated that the exogenous variables silmutaneously have a significant effect on the endogenous variables. This study also used t test (partial) called as probability test. If the probability value of the exogenous variable is smaller than α = 0.05 to the endogenous variable, then H0 is rejected and Ha is accepted, indicated that there is a significant effect between the exogenous variables on the endogenous variable partially.

Research hypothesis

1. Partially, inclusive human development, regional financial performance, infrastructure, crime, industrialization and natural disasters towards inclusive green development in Indonesia.

Ho : $\alpha_1 = \alpha_2 = \alpha_3 = \alpha_4 = \alpha_5 = \alpha_6 = \alpha_7 = 0$

Ha : $\alpha_1 \neq \alpha_2 \neq \alpha_3 \neq \alpha_4 \neq \alpha_5 \neq \alpha_6 \neq \alpha_7 \neq 0$

2. Silmutaneously, inclusive human development, regional financial performance, infrastructure, crime, industrialization and natural disasters towards inclusive green development in Indonesia.

Ho : $\lambda_1 = \lambda_2 = \lambda_3 = \lambda_4 = \lambda_5 = \lambda_6 = \lambda_7 = 0$

Ha : $\lambda_1 \neq \lambda_2 \neq \lambda_3 \neq \lambda_4 \neq \lambda_5 \neq \lambda_6 \neq \lambda_7 \neq 0$

RESULTS AND DISCUSSIONS

Classical assumption test results

The results of the normality test on the inclusive green growth equation model indicated by the JB Probability Value of 0.056786 or the value is greater than 0.05, thus the residuals are normally distributed in the equation or the classical assumption of normality is achieved. The results of the multicollinearity test in the inclusive green growth equation model show that all correlation values between independent variables are less than 0.8, thus both models of this equation do not contain multicollinearity problems. The results of the estimation of heteroscedasticity through the Glejser Test on the inclusive green growth equation showed that the Probability values of X1, X2, X3, X4, X5 and X6 are greater than 0.05. Thus, it can be concluded that the equation model does not contain heteroscedasticity problems

Panel data regression results

Chow test

From the results of the Chow test in Table 1, it can be seen that the probability value of the cross section f is 0.0000 or less than 0.05. Therefore, the best model in this study is the fixed effect. To determine which model is selected for the fixed effect or random effect, the Hausman test is conducted.

Hausman test

From the results of the Hausman test in Table 2, it can be seen that the probability value of a random cross-section is 0.0000 or less than 0.05. Therefore, the best model in this study is the fixed effect. Thus, according to Ghozali (2013), it is no longer necessary to perform the Lagrange multiplier test.

Results of fixed effect

The results of panel data analysis are shown in Table 3.

From the results of the analysis, the inclusive green growth equation model is obtained using Eq. 2.

$$Y1 = 69.63627 + 0.391629\,X1 + 0.029884\,X2 + 0.053866\,X3 - 0.014244\,X4 - 0.020618\,X5 - 0.145195\,X6 \quad (2)$$

Based on the results of the analysis of the inclusive green growth equation, it can be seen that if the inclusive human development, social inclusion, regional financial performance, infrastructure, crime,

Table 1: Results of chow test

Redundant fixed effects tests			
Equation: Untitled			
Test cross-section fixed effects			
Effects Test	Statistic	d.f.	Prob.
Cross-section F	19.403104	(32,248)	0.0000
Cross-section Chi-square	359.840174	32	0.0000

Table 2: Results of hausman test

Correlated random effects - Hausman test			
Equation: Untitled			
Test cross-section random effects			
Test Summary	Chi-Sq. Statistic	Chi-Sq. d.f.	Prob.
Cross-section random	74.760331	6	0.0000

Table 3: Results of analysis of inclusive green growth variables (Y)

Variable	Coefficient	SE[1]	t-Statistics	Prob.[2]
C	69.63627	5.799432	12.00743	0.0000
Inclusive Human Development (X1)	0.391629	0.065486	5.980310	0.0000
Regional Financial Performance (X2)	0.029884	0.013076	2.285404	0.0230
Infrastructure (X3)	0.053866	0.012542	4.294886	0.0000
Crime (X4)	-0.014244	0.008744	-1.629002	0.1046
Industrialization (X5)	-0.020618	0.002664	-7.740095	0.0000
Natural Disaster (X6)	-0.145195	0.033424	-4.344078	0.0000
Effects specification				
Cross-section fixed (dummy variables)				
R-squared	0.851776	Mean dependent var[3]		35.85704
Adjusted R-squared	0.829064	SD dependent var		5.049856
SE of regression	2.087832	Akaike info criterion		4.435853
Sum squared resid	1081.042	Schwarz criterion		4.933134
Likelihood logs	-597.5449	Hannan-Quinn Criterion		4.635156
F-statistics	37.50376	Durbin-Watson statistics		1.786219
Prob(F-statistic)	0.000000			

[1-] Standard Error
[2-] Probabitity
[3-] Variable

industrialization and natural disasters were fixed (constant), then the value of the inclusive green growth index was 69,63627 . The R-squared value of the IGG equation was 0.851776. This showed that the contribution of exogenous variables (Inclusive Human Development, Regional Financial Performance, Infrastructure, Crime, Industrialization and Natural Disasters) to endogenous variables (IGG) was 85.18% while 14.82% was influenced by other variables not included in this IGG equation model.

Statistical t test results

The probability value of each variable can be seen in Table 3. The results of Table 3 showed that the Inclusive Human Development variable had a significant effect on the Inclusive Green Growth variable. This is indicated by the probability value of Inclusive Human Development was 0.0000or less than 0.05. Therefore, Inclusive Human Development partially had a significant effect on Inclusive Green Growth in Indonesia. On the other hand, the Regional Financial Performance variable had a positive and significant effect on the Inclusive Green Growth variable. This is because the probability value of Regional Financial Performance was 0.0230 or less than 0.05. Therefore, Regional Financial Performance partially had a significant effect on Inclusive Green Growth in Indonesia. Furthermore, the Infrastructure variable had a significant effect on the Inclusive Green Growth variable. This is because the probability value of the Infrastructure was 0.0000 or less than 0.05. Therefore, infrastructure partially had a significant effect on Inclusive Green Growth in Indonesia. In addition, the crime variable did not have a significant effect on the inclusive green growth variable. This is because the crime probability value was 0.1046 or greater than 0.05. Therefore, partially, crime had a significant effect on inclusive green growth in Indonesia. Furthermore, the Industrialization variable had a significant effect on the Inclusive Green Growth variable. This is because the probability value of Industrialization was 0.0000 or less than 0.05. Therefore, partially Industrialization had a significant effect on Inclusive Green Growth in Indonesia. Then, the Natural Disaster variable also had a significant effect on the Inclusive Green Growth variable. This is because the probability value of Natural Disaster was 0.0000 or less than 0.05. Therefore, partially, Natural Disasters had a significant effect on Inclusive Green Growth in Indonesia.

F test results

The results of the analysis on the inclusive green development equation explain the probability value

of F statistic was 0.000000. By using level 95 percent confidence or = 0.05, then value probability in equation inclusive green development with F statistic 0.000000 was less than 0.05. Therefore, in the inclusive green development equation, Ho is rejected and Ha is accepted. Thus, the variables of X1, X2, X3, X4, X5 and X6 silmutaneously had a positive and significant effect on the Inclusive Green Growth variable (Y). Partially, inclusive human development had a positive and significant impact on inclusive green growth in Indonesia. If inclusive human development (in this study using gender development data) is improved, it will encourage an increase in inclusive green growth. On the other hand, if inclusive human development decreases or does not increase, then inclusive green growth also decreases or does not increase. The decline in inclusive human development will make it difficult for all levels of society to enjoy equitable growth that is environmentally friendly or inclusive green growth (Koziuk *et al*., 2019). The above conditions are in accordance with the endogenous growth theory pioneered by Romer, (1986) and Lucas, (1988), which in its development state that human resources are the main key to increasing economic productivity through learning-by-doing behavior that can provide an introduction to new things in the economy as a driver in increasing economic productivity, as well as new discoveries that continue to be made will be the main source for increasing economic productivity (Arsyad, 2006). In general, it is stated that human development has a positive effect on economic growth, inclusive growth and environmental sustainability so that Human development is important to encourage future economic growth that continues to grow and leads to inclusiveness or equity and is environmentally friendly (Li *et al.*, 2021; Aimon *et al*., 2020; Tran *et al.*, 2019). In addition, the regional financial performance generated by local governments partially also has a positive and significant influence on inclusive green growth in Indonesia. If the regional financial performance, such as, fiscal decentralization ratio, regional financial independence ratio, government expenditure or expenditure, which are produced by local governments in Indonesia are effective, then inclusive green growth can be achieved. On the other hand, if the regional financial performance produced by the regional government is not effective in supporting development, then inclusive green growth is difficult to realize. This finding is also in line with previous findings which stated that good financial management can affect regional progress both economically, effectively and efficiently, thereby encouraging economic growth, equitable economic growth, access to employment and reducing poverty so that it has an impact on the community to control the use of natural resources available in the environment (Faridi *et al*., 2019; Kolawole, 2016; Oyinlola 2013). Infrastructure provides a large multiplier effect in creating jobs and creating sustainable growth so that it can create inclusive green growth and have a partially positive and significant impact on inclusive green growth in Indonesia. The absence of infrastructure will certainly slow down the realization of inclusive green growth. This phenomenon is in accordance with Harrod-Domar's Theory of Economic Growth, which stated that to grow the economy, new investments are needed in addition to the capital stock. The relationship between infrastructure and economic growth shows positive and significant results (Kodongo *et al*., 2016; Daido *et al.*, 2013; Sahoo *et al.,* 2012). However, in other forming variables, infrastructure has a significant negative relationship with poverty (Asian Development Bank, 2012). In terms of infrastructure development, care is needed so that it does not have a negative impact on this growth because infrastructure is less useful for the community while the level of costs incurred for development is very high (Shi *et al*., 2017). Partially, crime does not have a significant effect on inclusive green growth in Indonesia. This means that if the crime rate increases or decreases in Indonesia, then it does not have a significant impact on increasing inclusive green growth in Indonesia. This phenomenon is relevant to previous researches which stated that if the government has a high concern for reducing crime rates, other government programs can be implemented, so that people can ignore crime to continue their activities (Kumar *et al.,* 2020; Siwach, 2018; Iyer *et al.*, 2015). This finding is not relevant to previous research which stated that crime is a major impediment to economic growth and development and crime rates substantially increase income inequality (Anser *et al*., 2020; Hipp *et al.*, 2019; Athukorala *et al.*, 2015). However, further analysis is needed for the findings. Lorenc *et al.* (2012) who found crime and fear had a large impact on well-being, but the relationship was often highly indirect, but was mediated by environmental factors. On the other hand, reduced industrial activity is followed

by reduced exploitation of natural resources so as to preserve the environment. However, inclusive green growth which is a composite of inclusive growth and green growth is negatively affected by industrial growth. This phenomenon clarifies the hypothesis *Environmental Kuznets Curve (EKC)* which illustrates the contribution of economic growth to higher emissions but at the time of further economic growth can reduce environmental degradation due to technological advances and the shift of the industrial sector to the service sector (Usenata, 2018). Thus, an increase in the role of the industrial sector in the economy of a country will lead to an increase in pollution in that country, thereby reducing the quality of the environment. This result contradicts the previous finding which stated that an increase in industrial output will increase economic growth, which means that industrialization is positively and significantly related to economic growth (Ndiaya *et al.*, 2018). In addition, research on industrial growth is also relevant to previous research that industrial growth has a negative effect on green growth (Appiah *et al.*, 2019; Bhuyar *et al.*, 2020; Cherniwchan, 2012). Natural disasters that often occur in Indonesia partially have a negative and significant impact on inclusive green growth in Indonesia. If the incidence of natural disasters decreases, it will have an impact on increasing inclusive green growth. On the other hand, if the incidence of natural disasters increases, it will also be followed by a decrease in inclusive green growth.Thus, an increase in the incidence of natural disasters will increase environmental degradation and have an impact on environmental damage that provides resources for production activities so that it can inhibit the rate of output growth, thereby causing an increase in unemployment, an increase in poverty and income inequality. This finding is relevant to the findings in previous studies which stated that is natural disasters that occur have a negative and significant relationship to the variables forming green inclusive growth (Goebel *et al.*, 2015; Felbermayr *et al*., 2014; Rodriguez-Oreggia *et al.*, 2013). The most consistent response of economic growth to disasters has been a decline in local productivity and labor demand (Boustan *et al*., 2020), natural disasters widen income inequality in the short term for 5 years, but this effect disappears in the long term for 10 years (Yamamura, 2015).

CONCLUSION

The second hypothesis in this study proved to be accepted. Thus inclusive human development, regional financial performance, infrastructure, crime, industrialization and natural disasters had a significant effect on inclusive green growth in Indonesia. Meanwhile, the first hypothesis is not entirely accepted, thus, partially, inclusive human development, regional financial performance, infrastructure and natural disasters had a positive and significant impact on inclusive green growth in Indonesia. On the other hand, industrialization had a significant negative effect on inclusive green growth in Indonesia. Then, partially, crime did not have a significant effect on the inclusive green growth variable in Indonesia. To realize inclusive green growth in Indonesia, it is recommended to stakeholders, especially the government or policy makers to be able to continue to increase the distribution of human development for men and women, increase social inclusion by providing access to women to participate in various fields of life, especially in the political and economic fields. Furthermore, the government needs to improve regional financial performance by increasing income in order to be able to finance equitable and environmentally friendly growth programs, addition or improvement of economic infrastructure such as additional provision of proper environmental sanitation, clean drinking water and electricity installations for people who have not been able to receive it. Providing technology that supports environmentally friendly industries to support green industry programs as well as social infrastructure such as increasing the capacity of schools towards technology-friendly schools, increasing the capacity of health centers and adding additional health centers in areas not yet reached by health facilities. Furthermore, the government must strive to encourage the growth of environmentally friendly industries and can also create jobs to reduce the rate of growth of poverty and income inequality. Then the government must be able to mitigate natural disasters to avoid environmental damage and losses as a result of these natural disasters. The author understands that there are many other variables that also have a contribution to increase inclusive green growth, not only limited to exogenous variables in this study. Therefore, future researchers can observe these

other variables, thereby enriching the references for variables that encourage inclusive green growth in their research areas.

AUTHOR CONTRIBUTIONS

E. Juniardi conducted the literature review, research design, developed the model, collected and analyzed the data, and prepared the manuscript text. S. Amar reviewed the manuscript and guided the study. H. Aimon reviewed the manuscript.

ACKNOWLEDGEMENT

Authors would like to thank Padang State University as facilitator to carry out this study.

CONFLICT OF INTEREST

The authors declare no potential conflict of interest regarding the publication of this work. In addition, the ethical issues including plagiarism, informed consent, misconduct, data fabrication and, or falsification, double publication and, or submission, and redundancy have been completely witnessed by the authors.

ABBREVIATIONS

%	Percent
α	Alpha
β	Beta
λ	Lambda
μ	Micro
=	Equal sign
≠	Not equal sign
+	Plus sign
-	Minus sign
≥	Inequality (greater than or equal to)
≤	Inequality (less than or equal to)
>	Strict inequality (greater than)
<	Strict inequality (less than)
BS	Budget solvency
CBS	Central bureau of statistic
CEG	Conventional economic growth
CEM	Common effect model
Chi-sq.	Chi square
D.f.	Degree of freedom
Eq.	Equation
EQI	Environmental quality index
et al.	Et alia
FEM	Fixed effect model
FI	Financial independence
Fig.	Figure
GDI	Gender development index
GG	Green growth
GRDP	Gross regional domestic product
Ha	Alternative hypothesis
Ho	Null hypothesis
i.e.	Id est
IG	Inclusive growth
IGG	Inclusive green growth
IGI	Inclusive growth index
IHD	Inclusive human development
JB	Jarque-Bera
MEF	Ministry of environment and forestry

NDPA	National development planning agency
Prob	Probability
R2	Correlation coefficient
REM	Random effect model
RFP	Regional financial performance
R-Square	Determination coefficient
SD	Standar deviation
SDGs	Sustainable development goals
SE	Standard error
SS	Service solvency
T-statistics	Hypothesis test statistic
Var	Variable
X1	Inclusive human development
X2	Regional financial performance
X3	Infrastructure
X4	Crime
X5	Industrialization
X6	Natural disaster
Y	Inclusive green growth

REFERENCES

Aimon, H.; Kurniadi, A.P.; Satrio, M.K., (2020). Analysis of inclusive growth in poverty, unemployment and income inequality in West Sumatra Province: Panel error correction model approach. Benefita J., 5(1): 19-38 **(20 pages)**.

Albagory, S., (2016). Inclusive green growth in Africa: Ethiopia Case Study. 74364. MPRA Paper No. 74364.

Anser, M.K.; Yousaf, Z.; Nassani, A.A.; Alotaibi, S.M.; Kabbani, A.; Zaman, K., (2020). Dynamic linkages between poverty, inequality, crime, and social expenditures in a panel of 16 countries: two-step GMM estimates. J. Econ. Struct., 9 (43): 1-25 **(25 pages)**.

Appiah, K.; Du, J.; Yeboah, M.; Appiah, R., (2019). Causal relationship between industrialization, energy intensity, economic growth and carbon dioxide emissions: Recent evidence from Uganda. Int. J. Energy Econ. Policy, 9(2): 237–245 **(9 pages).**

Arsyad, L., (2010). Economic development 5th edition. Yogyakarta. UPP STIM YKPN.

Asian Development Bank, (2012). Infrastructure for supporting inclusive growth and poverty reduction in Asia. Manila, Philippines. Asia Development Bank.

Athukorala, P.; Sen, K., (2015). Industrialisation, Emplloyment and Poverty. Working Paper. 15: 1-20 **(20 pages).**

Boustan, L.P.; Kahn, M.E.; Rhode, P.W.; Yanguas, M.L., (2020). The effect of natural disasters on economic activity in US counties: A century of data. J. Urban Econ., 118 (102357): 1-61 **(61 pages)**.

Bhuyar, P; Rahim, M.H.; Sundararaju, S.; Maniam, G.P.; Govindan, N., (2020). Antioxidant and antibacterial activity of red seaweed; Kappaphycus alvarezii against pathogenic bacteria. Global J. Environ. Sci. Manage., 6(1): 47-58 **(12 pages).**

CBS, (2020). Statistical yearbook of Indonesia 2020. Jakarta. Central bureau of statistic.

Cherniwchan, J., (2012). Economic growth, industrialization, and the environment. Resour. Energy Econ., 34(4): 442–467 **(26 pages).**

Daido, K.; Tabata, K., (2013). Public infrastructure, production organization, and economic development. J. Macroecon., 38(PB): 330–346 **(17 pages).**

Faridi, M.Z.; Mehmood, K.A.; Azam, A.; Taqi, M., (2019). Fiscal decentralization and economic growth in South Asian Countries. Pak. J. Commer. Soc. Sci., 13(2): 529–546 **(18 pages).**

Felbermayr, G.; Gröschl, J., (2014). Naturally negative: The growth effects of natural disasters. J. Dev. Econ., 111: 92-106 **(15 pages).**

Ghozali, I., (2013). Aplikasi Analisis Multivariate dengan Program IBM SPSS 21 Update PLS Regresi. Semarang. Badan Penerbit Universitas Diponegoro.

Goebel, J.; Krekel, C.; Tiefenbach, T.; Ziebarth, N.R., (2015). How natural disasters can affect environmental concerns, risk aversion, and even politics: evidence from Fukushima and three European countries. J. Popul. Econ., 28(4): 1137–1180 **(44 pages).**

Hipp, J. R.; Kim, Y-A.; Kane, K., (2019). The effect of the physical environment on crime rates: capturing housing age and housing type at varying spatial scales. Crime Delinq., 65(11): 1570–1595 **(26 pages).**

Iyer, L.; Mani, A.; Mishra, P.; Topalova, P., (2012). The power of political voice : women's political representation and crime in India. Am. Econ. J. Appl. Econ., 4(4): 165–193 **(29 pages).**

Jha, S.; Sandhu, S. C.; Wachirapunyanont, R., (2018). Inclusive green growth index: A new benchmark for quality of growth. Asian Development Bank. **(64 pages).**

Kodongo, O.; Ojah, K., (2016). Does infrastructure really explain economic growth in Sub-Saharan Africa? Rev. Dev. Finance. 6(2): 105–125 **(26 pages).**

Kolawole, B.O., (2016). Government spending and inclusive-growth relationship in Nigeria: An empirical investigation. Zagreb Int. Rev. Econ. Bus., 19(2): 33–56 **(24 pages).**

Koziuk, V.; Dluhopolskyi, O.; Hayda, Y.; Klapkiv, Y., (2019). Does educational quality drive ecological performance? Case of high and low developed countries. Globzl J. Environ. Sci. Manage., 5(Special Issue), 22–32 **(11 pages).**

Kumar, S.; Kuncharam, S.R., (2020). Determinants of women empowerment responsible for reducing crime against women in India. Violence Gender. 7(4): 182–187 **(6 pages).**

Li, X.; Xu, L., (2021). Human development associated with environmental quality in China. PLoS ONE, 16(2): 1–21 **(21 pages).**

Lorenc, T.; Clayton, S.; Neary, D.; Whitehead, M.; Petticrew, M; Thomson, H.; Cummins S.; Sowden A,; Renton, A., (2012). Crime, fear of crime, environment, and mental health and wellbeing: mapping review of theories and causal pathways. Health Place. 18(4).

Lucas, R., (1988). On the mechanics of economic development. J. Monet. Econ., 22(1): 3-42 **(40 pages).**

Luukkanen, J.; Kaivo-oja, J.; Vähäkari, N.; O'Mahony, T.; Korkeakoski, M.; Panula-Ontto, J.; Phonhalath, K.; Nanthavong, K.; Reincke, K.; Vehmas, J.; Hogarth, N., (2019). Green economic development in Lao PDR: A sustainability window analysis of green grow.

MEF, (2020). Book of Environmental quality index. Jakarta. Ministry

of Environment and Forestry, 53(9).
NDPA, (2020). Book of Technical note of inclusive economic development index. Jakarta.National Development Planning Agency.
Ndiaya, C.; Lv, K., (2018). Role of industrialization on economic growth: The experience of Senegal (1960-2017). Am. J. Ind. Bus. Manage., 08(10): 2072–2085 **(14 pages).**
Oyinlola, M.A.; Akinnibosun, O., (2013). Public expenditure and economic growth nexus: Further evidence from Nigeria. J. Econ. Int. Finance, 5(4): 146–154 **(9 pages).**
Rodriguez-Oreggia, E.; De La Fuente, A.; De La Torre, R.; Moreno, H., (2013). Natural disasters, human development and poverty at the municipal level in Mexico. J. Dev. Stud., 49(3): 442–455 **(14 pages).**
Romer, P.M., (1986). Increasing returns and long-run growth. J. Polit. Econ., 94(5): 1002-1037 **(36 pages).**
Sahoo, P.; Dash, R.K., (2012). Economic growth in South Asia: Role of infrastructure. J. Int.Trade Econ. Dev., 21(2): 217-252 **(36 pages).**
Shcherbak, V.; Ganushchak-Yefimenko, L.; Nifatova, O.; Fastovets, N.; Plysenko, H.; Lutay, L.; Tkachuk, V.; Ptashchenko, O., (2020). Use of key indicators to monitor sustainable development of rural areas. Global J. Environ. Sci. Manage., 6(2), 175–190 **(16 pages).**
Shi, Y.; Guo, S.; Sun, P., (2017). The role of infrastructure in China's regional economic growth. J. Asian Econ., 49: 26–41 **(16 pages).**
Siwach, G., (2018). Crimes against women in India: Evaluating the role of a gender representative police force. SSRN Electron. J., **(51 pages).**
Sun, Y.; Ding, W.; Yang, Z.; Yang, G. Du, J., (2020). Measuring China's regional inclusive green growth. Sci. Total Environ., 713 (136367).
Tran, N.V.; Tran, Q.V; Do, L.T.T.; Dinh, L.H.; Do, H.T.T., (2019). Trade off between environment, energy consumption and human development: Do levels of economic development matter? Energy. 173: 483–493 **(11 pages).**
Usenata, N., (2018). Environmental Kuznets curve (EKC): A Review of theoretical and empirical literature. IDEAS Working Paper Series from RePEc, 85024 **(19 pages).**
Yamamura, E., (2015). The Impact of natural disasters on income inequality: Analysis using panel data during the period 1970 to 2004. Int. Econ. J., 29(3): 359–374 **(16 pages).**

AUTHOR (S) BIOSKETCHES

Juniardi, E., Ph.D. Candidate, Faculty of Economy, Padang State University, Hamka street, Padang 25171, Indonesia.
- Email: *egiardi87@gmail.com*
- ORCID: 0000-0001-7755-9142
- Web of Science ResearcherID: NA
- Scopus Author ID: NA
- Homepage: http://fe.unp.ac.id/faculty/

Amar, S., Ph.D., Professor, Faculty of Economy, Padang State University, Hamka street, Padang 25171, Indonesia.
- Email: *syamsul_amar3@yahoo.com*
- Web of Science ResearcherID: NA
- Scopus Author ID: 57210914776
- ORCID: 0000-0002-7759-8528
- Homepage:http://fe.unp.ac.id/faculty/syamsul-amar-b

Aimon, H., Ph.D., Professor, Faculty of Economy, Padang State University, Hamka street, Padang 25171, Indonesia.
- Email: *s3dkpl@gmail.com*
- Web of Science ResearcherID: AAH-4156-2019
- Scopus Author ID:57209619142
- ORCID:0000-0002-7630-4751
- Homepage:http://fe.unp.ac.id/en/faculty/prof-dr-hasdi-aimon-msi

HOW TO CITE THIS ARTICLE

Juniardi, E.; Amar, S.; Aimon H., (2022). Panel data regression approach on Inclusive green growth. Global J. Environ. Sci.Manage., 8(4): 533-544.

DOI: 10.22034/gjesm.2022.04.06

url: https://www.gjesm.net/article_249432.html

Global J. Environ. Sci. Manage. 8(4): 545-560, Autumn 2022, Serial #32

Global Journal of Environmental Science and Management
(GJESM)

Homepage: https://www.gjesm.net/

CASE STUDY

Satellite imagery system in malaria transmission resulting from the land use/land cover change

C.M. Payus[1, 2,*]; J. Sentian[1,2]

[1] *Faculty of Science and Natural Resources, Universiti Malaysia Sabah, 88400 Kota Kinabalu, Sabah, Malaysia*

[2] *Natural Disasters Research Centre, Universiti Malaysia Sabah, 88400 Kota Kinabalu, Sabah, Malaysia*

ARTICLE INFO

Article History:
Received 23 November 2021
Revised 04 January 2022
Accepted 09 March 2022

Keywords:
Climate change
Geographic information system (GIS)
Land use and land cover change
Malaria
Remote sensing
Topography
Transmission risk

DOI: 10.22034/gjesm.2022.04.07

ABSTRACT

BACKGROUND AND OBJECTIVES: This study analyzed the changes in land use and land cover trends and their implication on malaria transmission using satellite imagery applications. Deforestation or human land use activity related to water and development has expanded the ideal habitats for malaria-carrying mosquitoes, resulting in an upsurge of malaria transmission.

The presence of these habitats and breeding increased the contact between humans and mosquitoes, thus increasing the number of malaria cases. The decrease of canopy and forest cover has increased the temperature, resulting in the shortening of aquatic stages and sporogony development of the mosquitoes. This study aims to provide an understanding of the relationship between the topography effect over the land-use factor and land cover change on malaria for more than ten years from 2005 to 2019 of transmission.

METHODS: Malaria case data obtained were analyzed for the trends, incidence rate, and spatial distribution. Remote Sensing and geographic information system were used to determine the land use and land cover change in selected districts of North Borneo in Sabah, as the study areas.

FINDINGS: The malaria incidence rate shows an increase from 2005 to 2019, with 149.64%. The transmission of the malaria vector dynamics and abundance with topography changes has changed with time, including with forest declination at 8.38%, and cropland change decreased at 16.61%. However, an expansion of 33.6% was observed for oil palm plantations. Overall, the results have shown that the range of incidence rate was found` highly viable from 0.29/1000 persons to 4.09/1000 people.

CONCLUSION: In conclusion, using geographic information system remote sensing with malaria integrated topography transmission information will be targeted by zoning most affected areas or the most productive larval habitat for remedial measures. This study can help to reduce the malaria vector population through environmental management related to the mosquito larval cycle in different land-use settings and change by minimizing the transmission by the targeted malaria control program.

NUMBER OF REFERENCES	NUMBER OF FIGURES	NUMBER OF TABLES
42	6	5

*Corresponding Author:
Email: *cpayus@gmail.com*
Phone: +6088 320 000
ORCID: 0000-0003-1947-2844

Note: Discussion period for this manuscript open until January 1, 2023 on GJESM website at the "Show Article".

INTRODUCTION

Urbanization is one of the main contributors to land-use change and contributes to an increase in the occurrence of malaria (Tatem *et al*., 2013). It builds a suitable environment for mosquito breeding, thus inducing higher malaria occurrence. The hidden place that will be removed from mosquitoes' breeding habitats (Tucker *et al*., 2017) will lead them to travel to the nearest residential area, thus increase the transmission. Apart from that, man-made activities which have converted land for agriculture, such as oil palm plantations, logging, or mining (WWF, 2020), will alter the ecological balance and suitable climatic conditions for breeding, thus transmitting malaria (Baeza *et al*., 2017). The population changes will increase malaria transmission as it increases the rate of spreading cases from one region to another due to higher contact between humans and mosquitoes (Martens and Hall, 2000). Mosquitoes' larval abundance and survival rates are affected by land-use change such as reducing the canopy of forest cover, increasing the availability of open and sunlit habitats and crop activity that will provide higher breeding ground (Yadav *et al*., 2014). The larval habitat that has altered makes the larval survivorship increased by accelerating their development rate or increasing larval pupation rate, and adult emergence rate (Brown *et al*., 2018). Deforestation and land clearance will change the climate effect by increasing the temperature that will also increase the malaria vector reproductive rate. Blood meal digestion rates have been found directly proportional to the surrounding temperature. Weather conditions during rainy weather with a lower temperature will slow the blood meal digestion compared to warmer temperatures (Mawili-Mboumba *et al*., 2013). The temperature will affect the gonotrophic cycle length with the time between a blood meal and oviposition (Bousema and Drakeley, 2011). In the adult stage, an increase in ambient temperature will accelerate the digestion of blood meals (Babaie *et al*., 2018). Increased biting frequency and faster blood meal digestion also mean increased fecundity and reproductive fitness (Lowassa *et al*., 2012). For rainfall amount, it will influence the habitat of mosquitoes breeding, and humidity will control their activities and life duration (Le *et al*., 2019). During rainy seasons, it is attributed to lower larval density due to the flush effect by washing eggs and larvae from the habitat (CDC, 2018). However, some findings show rainfall coincided with the abundance of adult mosquitoes due to a habitat rich with food resources and nutrients (Kweka *et al*. 2016; Mukhtar *et al*., 2019). Lower humidity in houses coincided with a negative survival rate of malaria mosquitoes, and they have a higher net reproductive rate with higher fecundity (Haque and Basak, 2017). The study of land use and land cover (LULC) changes is essential for effective natural resource planning, exploitation, and management (Pohl, 2014). Traditional methods for gathering demographic data, censuses, and environmental sample analysis are insufficient for multicomplex environmental studies (Rawat and Kumar, 2015). Geographic information system (GIS) is computer software capable of acquiring, analyzing, and presenting geographically related (spatial) LULC changes information (Mark and George, 2018). Geographic information systems and remote sensing have a wide range of applications in agriculture, environment, and integrated eco-environmental evaluation to assist in development-oriented management and decision-making processes (Torbick *et al*., 2016). GIS and satellite remote sensing has evolved into a viable tool for developing and interpreting global, physical processes impacting the environment (Bouzekri *et al*., 2015). When dealing with land-use changes with visualization tools and imaging using satellite, it can be more efficient if compared to the traditional/conservative application of using time series and long-term statistical analysis just for looking at the significant changes (Mark and George, 2018). Due to the involvement of multiple data sets, we used the latest technologies, remote sensing, and GIS, to quantify LULC and its impact on the emergence of malaria cases. This study is useful in assessing relative mosquito abundance by above-ground biomass from different land cover classifications such as forested land, cropland and oil palm conversions. Based on GIS analysis, a targeted malaria control strategy was suggested to achieve cost-effective measures of malaria on a sustainable basis. Sabah's forest resources have been over-exploited for the last 30 years and mostly were cleared due to oil palm plantation (Toh and Grace, 2005). Sabah recorded 45% of malaria cases reported in Malaysia from 2010 to 2014 (Ramdzan *et al*., 2020). However, the major causes of spatial differences in vector distribution and abundance in this region with

heterogeneous environments with various changes in land use and land cover have never been investigated, mainly using satellite imagery by GIS and remote sensing. Therefore, this study aimed to determine the presence and magnitude of malaria transmission related to the land use and cover change in North Borneo of Sabah, Malaysia, from 2005 to 2019.

MATERIALS AND METHODS

Description of the study area and context

The study area in this study was focused on the North Borneo of Sabah. The locations involved in this study, Ranau, Tambunan, Keningau and Tenom, were coincidentally designated as study sites. One of the reasons these highland districts were chosen for the study was the large increase in malaria cases recorded in these areas. Highland area had reported experiencing a surge in the number of malaria cases, and the spatial-temporal patterns in the different mountainous regions have yet and seldom focused in this area (WHO, 2014). The total land area of the study area is approximately 10267 kilometers square (Ranau 2978 km^2; Tambunan 1347 km^2; Keningau 3533 km^2; Tenom 2409 km^2). Fig. 1 shows the geographic location of the study area in the highland districts of Sabah, Malaysia.

Besides the climate factor, land use has many effects on disease transmission and occurrence. The Sabah's land use and land cover (LULC) map that the public can obtain is only updated to 2008 (MAMPU, 2018). Lack of up-to-date data is hard to implement better planning and management on land. In this study, an updated land use map of selected districts in Sabah was produced for a specific study period of 2005, 2010, 2015, and 2019. The LULC maps are required to provide information on which activities have been done from the past then compare them to the present and how they affected the environment. It is also helpful for assessing land cover change of origin and occupied areas in each period. The information can be used to evaluate the relationship between land use type changes and the occurrence of malaria in a specific region. The multi-temporal satellite image was acquired from Moderate Resolution Imaging Spectroradiometer (MODIS) satellite, and Geographic Information System (GIS)

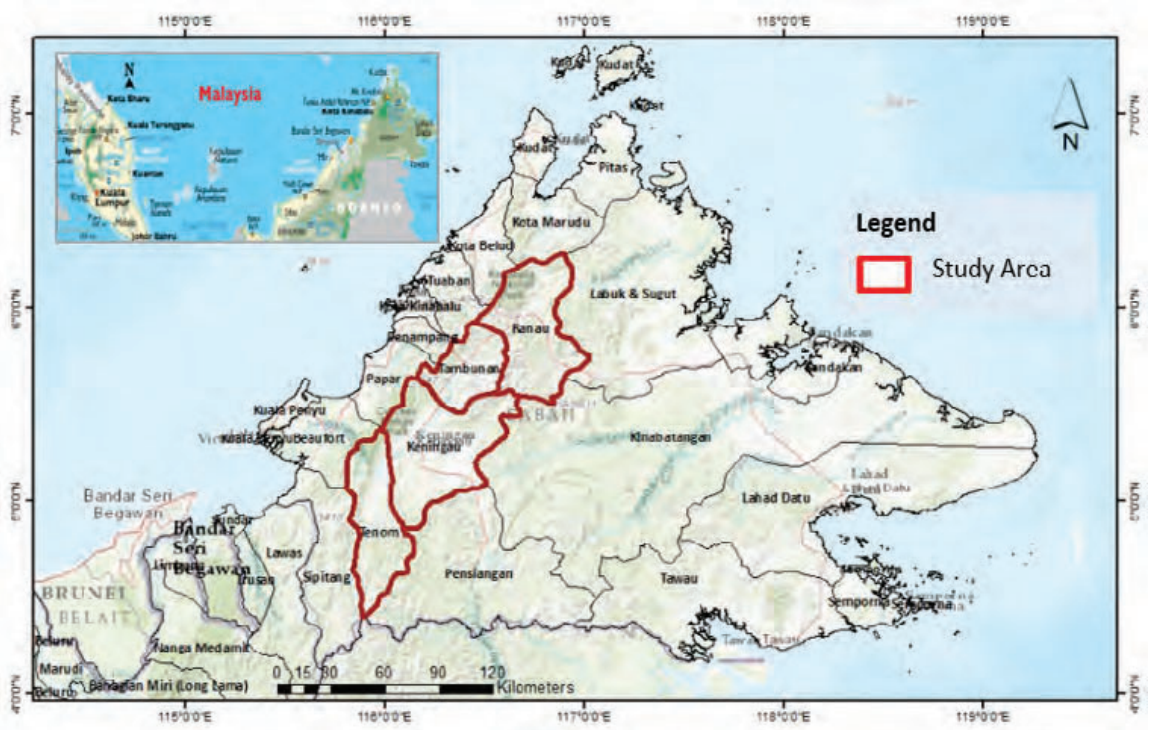

Fig. 1: Geographic location of the study area in selected districts of Sabah, Malaysia with a red line indicated the boundary of each district which the study was conducted

software was employed to generate the land cover map for highland districts of Sabah for the years 2005, 2010, 2015, and 2019 for malaria cases data in selected districts of Sabah.

Land cover change data and accuracy assessment

Multi-temporal satellite image of the study area was acquired from the United States Geological Survey (USGS) (USGS, 2020). The 14 years range time frame of the satellite image was obtained from MCD12Q1 Version 6 with 500 m spatial resolution. The year of satellite image selected is from 2005 as a starting point of widespread malaria after 2004, with a five-year interval period. The year 2019 will represent the latest changes that can be observed in the study area. Moderate Resolution Imaging Spectroradiometer (MODIS) images have a low spatial resolution (500 m), yet it has a higher observation frequency (Miuse and Kamlun, 2019). MODIS images were chosen for this study over Landsat images (higher spatial resolution) because the study area is highland, where the cloud will always be prevalent. All satellite images obtained from MCD12Q1 Version 6 were cloud-free images. Land cover is classified based on the International Geosphere-Biosphere Program (IGBP) classification scheme, consisting of 17 classes. In this study, the 17 classes from the IGBP classification scheme were simplified into 4 main classes, forests, oil palm, croplands, and urban. The accuracy assessment in the land cover classified map indicated the accuracy level of the study comparison of a classified map and ground truth data (Kamlun *et al*., 2016). Ground truthing data was chosen to conduct field inspection, and the random points were generated from ArcGIS software (ArcMap 10.8). The point's data was then transferred into KML file type to refer on Google Earth Pro in the specific study period of 2005, 2010, 2015, and 2019. The steps of this accuracy assessment involve stratified random sampling, which proceeds on the defined land cover classes. In this study, 50 random points were assigned for the forest and oil palm areas, respectively (study area main focus), and 20 random points were assigned for cropland and urban areas. The land cover change classification accuracy was evaluated by calculation on error matrix that includes user's accuracy, producer's accuracy, overall accuracy, and Kappa coefficient. Kappa coefficient is a statistical measure that can be used to validate the generated map. It is also an accuracy assessment that has been widely used by the study on remote sensing field (Phua and Tsuyuki, 2004). Kappa statistics can help determine how closely the occurrences are classified by matching the data labelled as ground truth with the random classified data by estimated accuracy. This study conducted post-classification change detection for land cover changes analysis on each class. Change detection is a process to determine the changes in the state of something by observing it from time to time (Alawamy *et al*., 2020). The advantages of applying change detection in post-classification include minimization of atmospheric or environmental differences between maps, thus more information provided from matrix table of land cover changes, and a better evaluation of the change rates (Ukor *et al*., 2016). Calculation of change for each land cover class includes the magnitude of change (the difference between years), percentage of change (magnitude of change divided by the initial year and multiplied by 100%), and the annual rate of percentage change (magnitude of change divide by the initial year times number of years of the period and multiply with 100%) (Alawamy *et al*., 2020). The changes in the land cover area of each highland district from 2005 to 2019 are shown in the land cover conversion map and tabulated in a cross table to analyse the 'from-to' of each land cover class. Thematic map involved in this study is the land cover classification, which are forest, cropland, and oil palm, to assess land cover changes by above-ground biomass, and based on malaria incidence rates category of risk, with remote sensed data and topo sheets of 1:50,000 and 1:125,000 in preparing the thematic maps. Digitized overlaid maps were subjected to computer analysis using ARC/INFO 3.1 software.

Malaria transmission cases and data analyses

The malaria cases data in Sabah were obtained from the Malaysian Ministry of Health. Malaria cases have shown increased from the year 2005 in the highland district, data from the year 2005 to 2015 was chosen to make a comparison by an interval of 5 years range (2005, 2010, and 2015), whereas 2019 was chosen as MODIS image only available latest in this year. Data analysis was conducted to show the spatial movement of malaria transmission in study areas from 2005 to 2019. The incidence rate of malaria in each selected district will be calculated

based on the population from each district according to the Malaysian Census. The annual population of the district was estimated based on the 2000 Malaysian Census, 2010 Malaysian Census and open population data from the Department of Statistics Malaysia. The annual incidence rate of malaria was calculated using the number of malaria cases per year divided by the annual population data for each district and multiplied by 1000. A map of malaria incidence rate per 1000 population annually for each district was generated using ArcMap 10.8. Data acquired from the Malaysian Ministry of Health was used to analyse the peak occurrence of malaria disease and combine it with the land cover to determine the transmission factor. The malaria incidence rate per 1000 persons and the land cover changes data were used to analyse the cumulative changes from 2005 to 2019. Only land cover of the forest, oil palm, and cropland were chosen for the analysis because urban had no significant effect or changes during the study period. Pearson's correlation and Multiple Linear Regression analyses were carried out to determine the relationship between annual land cover changes and malaria incidence rate per 1000 persons in the study area yearly from 2005 to 2019. This analysis is important to reveal the susceptibility of malaria cases towards the land cover changes (Franzese and Iuliano, 2019).

RESULTS AND DISCUSSION

Spatial distribution of malaria in highland districts

Fig. 2 shows the trend of incidence rate per 1000 persons for the four selected districts. From 2005 it was recorded at 3.26 to 6.98 incidence in 2019 with an increment of 149.64%. Overall findings show that the malaria incidence rate is highest at Ranau district at 2.67 incident rate and 40.56% compared to the other districts percentage. The second-highest recorded at 2.26 for Tenom district (17.95%), followed by Tambunan (31.78%) at 1.20 and the least Keningau district (9.71%) at 0.83 incident rate during 2005 until 2019. However, by annual rate, Tenom recorded the highest increment with 946.67%, followed by Ranau 155.46%, then Tambunan 79.31%, and Keningau 36.46% of increased for the 14-years. Apart from that, the malaria incidence rate has dropped significantly from 2009 until 2011, recorded at 6.87 (-9.42%, 2009), 5.11 (-29.64%, 2010) and 4.39 (-40.12%, 2011) from 7.84 incident rate and decreased during the year 2015 to 2016 at 4.23 (43.64%, 2015) and 2.91 (-58.96%, 2016) from 7.19 incidence rate for all of the districts. For temporal distributions, the findings show that 2017 recorded the highest malaria transmission rate at 10.33, followed by 2018 at 9.03 incident rate, and thirdly in 2008, recorded at 7.84.

The incidence rate of malaria for each district was found highly variable from the year 2005 to

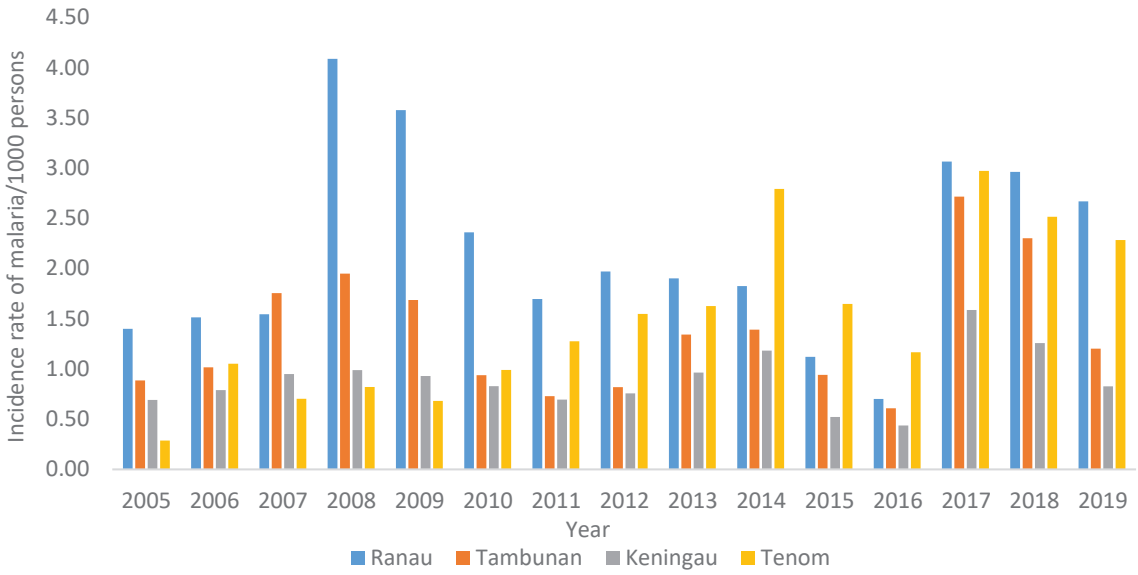

Fig. 2: Malaria incidence rate/1000 persons for study areas

2019, and the range of incidence rate was found from 0.29/1000 persons to 4.09/1000 persons. Fig. 3 shows the malaria incidence rate per 1000 persons in each highland district (Ranau, Tambunan, Keningau, Tenom) in 2005, 2010, 2015, and 2019.

The level of malaria incidence rate was classified as low (0 – 1.0), moderate (1.1 – 2.0), and high (2.1 – 3.0). In 2005, only the Ranau district showed a moderate incidence rate, whereas the other three districts were under a low incidence rate. In the year 2010, the malaria incidence rate of Ranau district increased to a high level, whereas the other three districts remained at a low-level incidence rate. In 2015, the malaria incidence rate of Tenom district increased to a moderate level together with Ranau district (decreased from a high level), and the other two districts remained a low level of malaria incidence rate. In 2019, only Keningau district remained a low malaria incidence rate where Tambunan district increased to a moderate level of incidence rate, Ranau district, and Tenom district increased to a high level of malaria incidence rate. Overall, the malaria incidence rate is decreased in 2015 as the malaria cases were reported lesser. Meanwhile, through visual observation on distribution maps, the malaria incidence rate increased from 2005 to 2010 and 2015 to 2019. Ranau district has the highest incidence rate, followed by Tenom district, Tambunan district, and Keningau district. This may be due to the expansion of oil palm plantation from forest land cover, which mainly occurs nearby Ranau district and Tenom district, as observed from the land cover map in the following subsection.

Land cover change in highland districts

The land cover changes in selected districts of Sabah (Ranau, Tambunan, Keningau, and Tenom) were compared for the years 2005, 2010, 2015, and 2019. The land cover map was generated consisting of four primary spatial information: forest, oil palm,

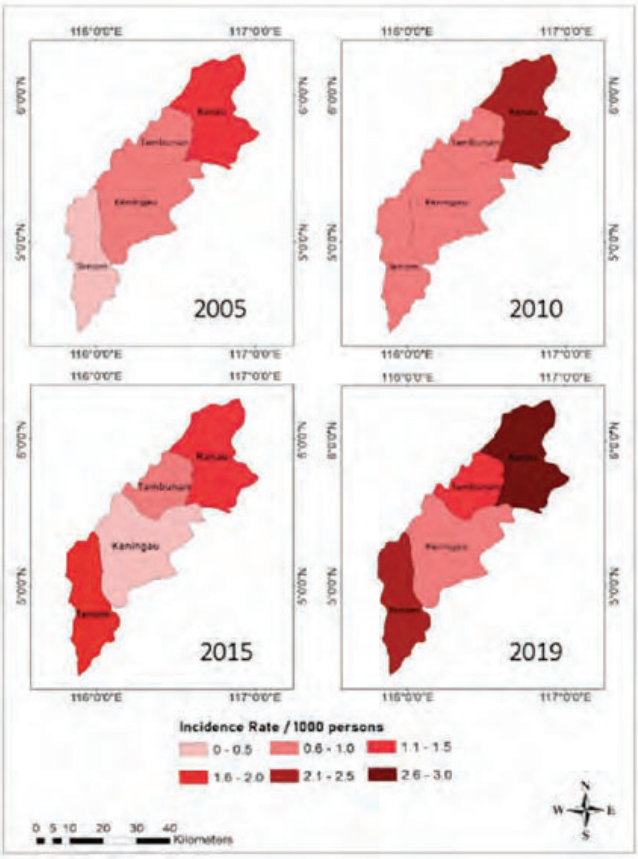

Fig. 3: Spatial distribution of malaria incidence rate per 1000 persons in each selected district of Sabah

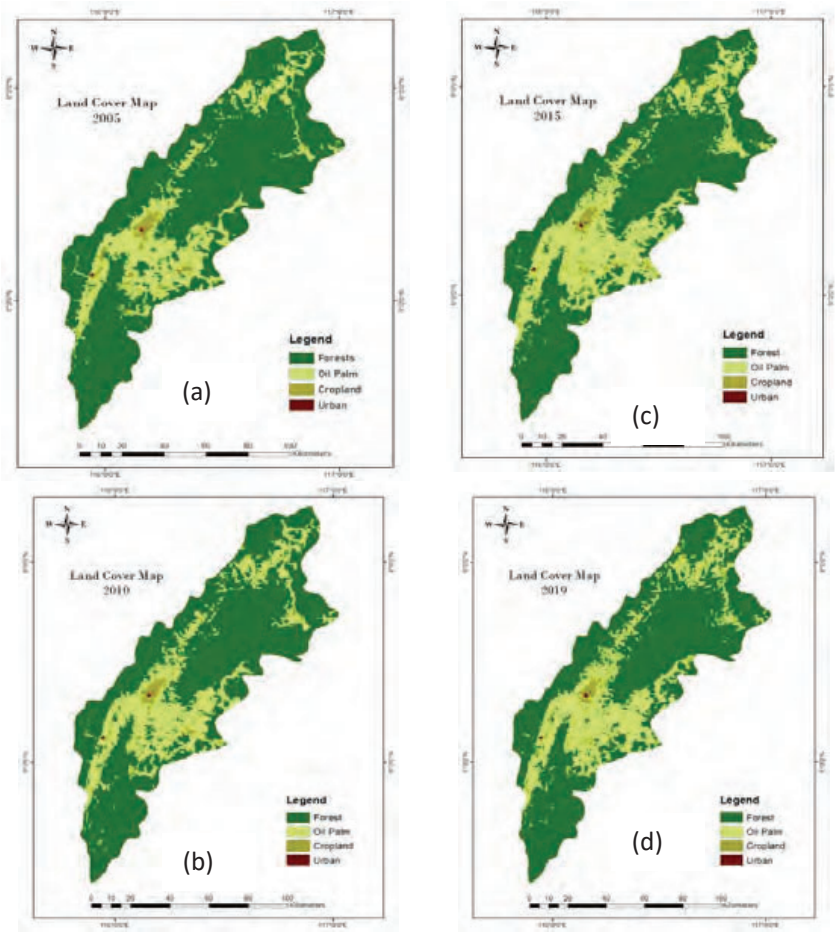

Fig. 4: Land cover map of each district for the year (a) 2005; (b) 2010; (c) 2015; and (d) 2019

cropland, and urban for this study. Fig. 4 shows the land cover classification map of highland districts in the years 2005 (a), 2010 (b), 2015 (c), and 2019 (d).

From the observation of the maps, the forest was found to predominate the land cover type followed by oil palm, cropland, and urban. A visual comparison of the land cover maps from 2005 to 2015 revealed that the forest coverage on the land cover map decreased significantly, and oil palm coverage increased significantly. However, from 2015 to 2019, forest coverage had been slightly increased. Forest class had the most extensive coverage area with 7958 km^2 (76.73%), followed by oil palm with 2134 km^2 (20.57%), cropland with 271 km^2 (2.61%), and urban with 9 km^2 (0.09%) in 2005; and 2010 with 7512 km^2 (72.13%), followed by oil palm with 2633 km^2 (25.39%), cropland with 217 km^2 (2.09%), and urban with 9 km^2 (0.09%). In the year 2015, the most extensive coverage of land cover class in the study area was also forest with 7076 km^2 (70.76%), followed by oil palm with 3035 km^2 (29.26%), cropland with 252 km^2 (2.43%), and urban with 9 km^2 (0.09%). However, the lowest coverage of forest investigated in 2015 may be related to the occurrence of an earthquake at Ranau district, Sabah. In the year 2019, forest class remained the most extensive coverage in the study area with 7291 km^2 (70.30%), followed by oil palm with 2846 km^2 (27.44%), cropland 226 km^2 (2.18%), and urban 9 km^2 (0.09%). The overall classification accuracies for the generated highland district map images are recorded at the range of 86% to 100% accuracy with kappa coefficients value of 0.78 to 0.83. Fig. 5 shows the changes for each land cover type in study areas during the study period. In the

14 years, forest coverage showed a drastic decline. Between years 2005 – 2010 and years 2010 – 2015, forest area showed extreme losses by 446 km^2 and 436 km^2, while between years 2015 – 2019 showed a moderate increase in area by 215 km^2.

This may be due to the implementation of the land usage policy by the Sabah state government on the restoration of degraded forests (Jaafar *et al.*, 2020). Between years 2005 – 2010 and years 2010 – 2015, the oil palm area showed a drastic increase by 499 km^2 and 402 km^2, whereas between the years 2015 – 2019 showed a moderate decline by 189 km^2. The decline of oil palm plantations was associated with the Crude Palm Oil prices, which were relatively low in that period (CPO, 2019). Also, the efforts of NGOs and some journalists may have impacts on the implementation of constrained plantation expansion by the government (Gaveau *et al.*, 2018). Cropland area showed slightly decreased between years 2005 – 2010 and years 2015 – 2019 by 54 km^2 and 26 km^2 respectively but increased somewhat between years 2010 – 2015 by 35 km^2. The slight increase in cropland area from 2010 to 2015 may be due to the Sabah earthquake in Ranau district, which induced barren land coverage (Miuse and Kamlun, 2019). However, the urban area does not change from 2005 to 2019. The area changes indicated that most forest reduction was related to expanding of oil palm plantations. Over time, the cover type of land was changed due to various anthropogenic activities such as plantation, agriculture, construction, and more to overcome human demands and population growth (Kweka *et al.*, 2016). A recent study by Miuse and Kamlun (2019) indicated that the land cover changes of highland districts of Sabah were related to both natural and anthropogenic factors, as the protected forest area also found drastic losses in the study period. Table 1 shows the total area changes and annual change rate from 2005 to 2019.

Overall, cropland area had found dramatically

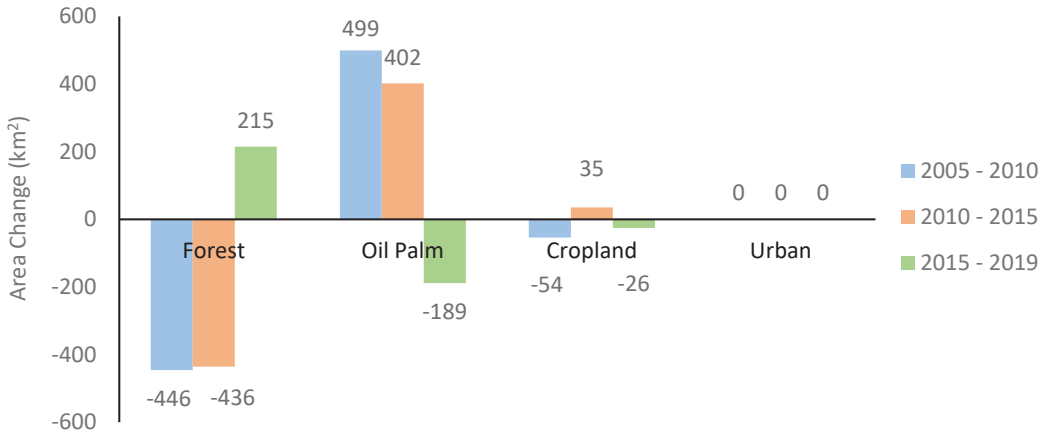

Fig. 5: Land cover change trends of study areas during the study period

Table 1: Land cover change from the year 2005 to 2019

Land Cover Classes	2005	2019	Area change		Annual change rate	
	Area (km^2)	Area (km^2)	km^2	%	km^2/year	%
Forest	7958	7291	-667	-8.38	-47.64	-0.60
Oil Palm	2134	2846	712	33.36	50.86	2.38
Cropland	271	226	-45	-16.61	-3.21	-1.19
Urban	9	9	0	0	0	0

decreased in 16.61% with 45 km^2, and the annual rate of change was -3.21 km^2/year (1.19%). Forest area also dropped in extensive coverage with 667 km^2, but lower in percentage (8.38%), and the annual rate of change was -47.64 km^2/year (0.60%). A recent study by Jaafar *et al.* (2020) indicated that a large percentage of oil palm cover was on the agricultural land compared to the forest in Sabah from 1990 to 2018. This can be explained due to the implementation of the land usage policy by the Sabah state government, which restricted the cultivation of oil palm in specific designated agricultural land. The oil palm area had drastically inclined between the years 2005 to 2019 with 712 km^2 (33.36%) in a total of study areas, and the annual rate of change was 50.86 km^2/year (2.38%). This result indicated that the oil palm plantation had expanded rapidly in highland areas of Sabah specifically between these periods. However, this study does not significantly change urban areas due to MODIS images with low spatial resolution. Table 2 shows a more detailed land cover change rate for each district from 2005 to 2019. For Ranau and Tambunan district, only forest cover decreased in the area where oil palm cover and cropland cover gained between the years 2005 to 2019. For Keningau and Tenom districts, cropland

Table 2: Land cover change for each district from the year 2005 to 2019

Land Cover Classes	2005	2019	Area change		Annual change rate	
	Area (km^2)	Area (km^2)	km^2	%	km^2/year	%
Ranau district						
Forest	2515	2353	-162	-6.44	-11.57	-0.46
Oil Palm	421	569	148	35.15	10.57	2.51
Cropland	20	34	14	70.00	1.00	5.00
Urban	1	1	0	0	0	0
Tambunan District						
Forest	1366	1295	-71	-5.20	-5.07	-0.37
Oil Palm	121	190	69	57.02	4.93	4.07
Cropland	8	10	2	25.00	0.14	1.79
Urban	0	0	0	0	0	0
Keningau District						
Forest	2143	1785	-358	-16.71	-25.57	-1.19
Oil Palm	1309	1713	404	30.86	28.86	2.20
Cropland	195	149	-46	-23.59	-3.29	-1.68
Urban	6	6	0	0	0	0
Tenom District						
Forest	1934	1858	-76	-3.93	-5.43	-0.28
Oil Palm	283	374	91	32.16	6.50	2.30
Cropland	49	35	-14	-28.57	-1.00	-2.04
Urban	2	2	0	0	0	0

cover was found mainly loss, followed by forest cover where oil palm cover gained between years 2005 to 2019. A generated land cover conversion map from the change detection analysis from 2005 to 2019 is shown in Fig. 6. The land cover classes have their gain, loss, and unchanged area between these 14 years. From the visual observation on the map, the most apparent conversion occurred was forest cover to oil palm cover (pink color), followed by cropland cover converted to oil palm cover (blue color), and oil palm converted to the forest (orange color). The conversion of mostly land-use class to oil palm was due to fulfilling the growing demand of the oil palm industry (Wicke *et al*., 2011). Besides, the Sabah state government also implemented a specific land usage policy to restore degraded forests to overcome oil palm cultivation and reduce environmental impacts (Jaafar *et al*., 2020). The total area of land cover conversion 'from-to' for each class between the years 2005 to 2019 would be determined in the cross-tabulation matrix.

Table 3 shows the cross-tabulation of land cover class 'from-to' between 2005 and 2019. The cross-tabulation of land cover conversion analysis consists of rows representing land cover in 2005 and columns representing land cover in 2019. The highlighted diagonal value in Table 3 represented each class's unchanged area from 2005 to 2019. Readings according to rows show the land cover area loss from 2005 to 2019, and the readings

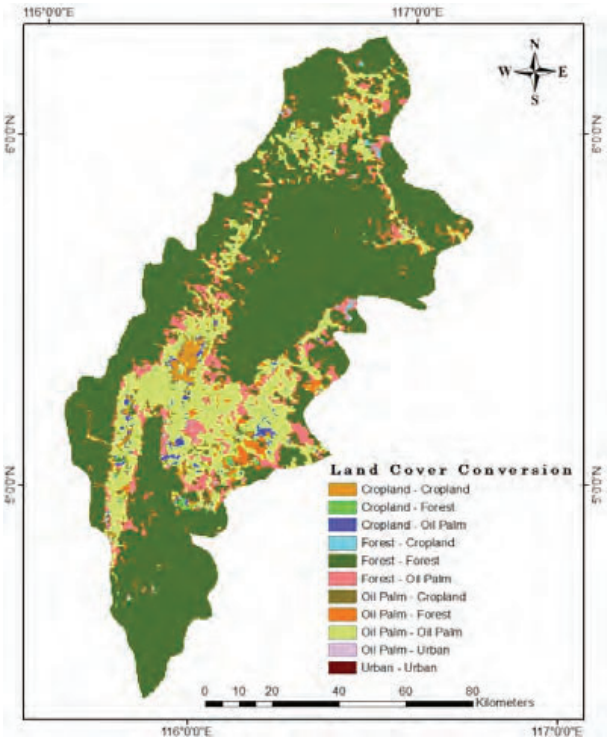

Fig. 6: Land cover conversion of study areas from the year 2005 to 2019

Table 3: Cross-tabulation of land cover change between the year 2005 to 2019

Land cover class area (km^2)		2019				
		Forest	Oil palm	Cropland	Urban	Grand total
2005	Forest	7002.60	916.59	39.07	0	7958.26
	Oil Palm	261.02	1810.65	61.61	0.64	2133.92
	Cropland	27.26	118.28	125.79	0	271.33
	Urban	0	0	0	8.80	8.80
	Grand total	7290.88	2845.52	226.46	9.44	10372.31

Table 4: Correlation of land cover changes and malaria incidence rate in selected districts of Sabah

Coefficient (r)	Forest	Oil palm	Cropland	Malaria incidence
Forest	1			
Oil Palm	-0.999	1		
Cropland	0.102	-0.146	1	
Malaria incidence	-0.135	0.144	-0.219	1

according to columns show the land cover area gain of the year 2019 from 2015. Out of the 7958.26 km^2 of forest area coverage in 2005, 7002.60 km^2 remained unchanged in 2019, while 916.59 km^2 and 39.07 km^2 were converted to oil palm and cropland, respectively. Also, some forest areas increase from oil palm (261.02 km^2) and cropland (27.26 km^2) from 2005 to 2019. Oil palm area out of 2845.52 km^2 in 2019 gained mainly from the forest as mentioned before, and cropland gained 118.18 km^2 in 2005. Oil palm area from 2005 remains unchanged to 2019 at 1810.65 km^2. Out of 271.33 km^2 of cropland area in 2005, 125.79 km^2 remained unchanged in 2019. The cropland area gained in 2019 from oil palm at 61.61 km^2. Out of the 9.44 km^2 urban class in 2019, 8.80 km^2 remained unchanged from the year 2005. Only a minimal area from the oil palm class (0.64 km^2) in 2005 was converted to urban in 2019.

Land cover change effects on malaria occurrences

Statistical analysis was performed on the cumulative annual land cover changes and annual malaria incidence rate per 1000 persons of the study area. Table 4 shows the correlation of land cover changes and malaria incidence in study areas of Sabah. Interpretation of analysis focused on each land cover type change and the malaria incidence rate. Where r = -0.135 shows a weak negative correlation for the forest, r = 0.144 shows a weak positive correlation for the oil palm, and r = -0.219 shows a weak negative correlation for the cropland.

The correlation performed between forest area changes and malaria incidence showed a weak negative result indicating there was a possibility that the more significant the forest change (forest loss) it will cause the higher malaria incidence rate. The result was consistent with previous studies in African highlands where deforestation was the main factor that promoted the vector population growth and survival rate that caused the high occurrence of malaria, mainly in the deforested area (Kweka *et al.,* 2016; Tuno *et al.,* 2005), which indicated that forest area changes might have indirect impacts on the malaria cases in highland districts of Sabah. The correlation performed between oil palm area changes and malaria incidence showed a weak positive result, indicating that there was a possibility as the more significant the oil palm change (oil palm gain), the higher the malaria incidence rate reported. From the result of land cover change presented before, most of the deforestation area in the highland of Sabah was due to conversion to oil palm plantation. A recent study by Yusof and Rusli (2018) reported that 24.2% of the land-use area of Sabah converted to oil palm plantation in the year 2000 to 2016 was due to the increase of oil palm industry demand. For the cropland area changes and malaria incidence, the correlation performed showed a weak negative result, which indicated there was a possibility that the more significant the cropland area change (cropland loss), the malaria incidence rate would be higher. An interesting study found that cropland activity was positively associated with malaria prevalence but only with a specific condition (fire-fallow cultivation), not including deforestation (Vittor *et al.,* 2009). Therefore, the changes of cropland area to oil palm area in the study areas of Sabah were probably through deforestation. Multiple linear regression analysis was used to define the association between land cover changes (forest, oil palm, and cropland) and malaria incidence in highland districts of Sabah. Table 5 shows the relationship between land cover changes and malaria incidence in the study area. The regression statistics adjusted R square showed a negative value (-0.183), which indicated insignificance on independent variables. The same goes for evaluating the ANOVA table, which showed the same results. The significance of F > 0.05 concluded that this model is not a significantly good fit. Also, since all of the p-value > 0.05, a large p-value represented

Table 5: Regression analysis of land cover changes and malaria incidence rate

Regression Statistics					
Multiple R		0.300			
R square		0.090			
Adjusted R Square		-0.183			
Standard Error		2.239			
Observations		14			
ANOVA	df	SS	MS	F	Significance F
Regression	3	4.973	1.658	0.331	0.803
Residual	10	50.120	5.012		
Total	13	55.093			
Variable	Coefficients	SE		t Stat	P-value
Intercept	4.326	2.187		1.978	0.076
Forest	0.682	1.198		0.570	0.582
Oil Palm	0.682	1.196		0.570	0.581
Cropland	0.626	1.161		0.539	0.602

insignificantly, indicating that the land cover changes have no significance associated with the malaria incidence.

Therefore, land cover changes did not significantly associate with the malaria incidence rate in selected districts of Sabah. This work's efforts to do the statistical analysis for correlation and regression can still be the framework and guidance for assessing the relationship of malaria transmission cases related to land use and cover change. Both analyses show no significance and weak relationships are believed due to the sample number of cases that are relatively low for a time series type of analysis. The study only depends on the limited data given by the Health Ministry of Malaysia, which only involved the total average by yearly cases that may affect the significant and relative comparison for the statistical analysis. Nevertheless, still with the added value of using GIS and remote sensing application onto the imaging map produced from this study, it could help to show how significant increased and decreased of the malaria cases only by viewing the maps based on the targeted area, rather than depending 100% on the statistical analysis for time series. Anyhow, this result was acceptable by referring to Singkong and Aralas (2017) study, which found that land cover changes significantly explained the malaria cases but not malaria incidences in Malaysia. Overall, land cover changes weakly correlate with the malaria incidences, as they may not be directly impacted. Many other factors, such as vector population, growth rate, survival rate, or temperature rise, show more significant direct effects toward malaria incidences that not been covered by this study; and in this research, only the land cover changes were the main drivers for promoting those factors (Kweka *et al.*, 2016). Moreover, an overview study in Africa concluded that land cover change effects on malaria transmission were regionally unique according to the vector distribution and adaptation preference. According to the vector species in this case study, a specific analysis will better understand the relationship between land cover change and malaria transmission. This research application can be a tool that is easy to interpret by visualizing the transmission cases and contributes to a more interactive and visualization instrument by GIS mapping and remote sensing simulation. Thus, it can ultimately support policymaking to target the general condition of whether the disease is hazardous or not. This research is novel based on the application of GIS as a visualization instrument to map the malaria cases associated with the land use/cover type. By this study, we also utilize fewer malaria cases data by getting the absolute mean average, which is the same thing that will be used at the end of the long-term analysis, as the components of variation (trend, seasonality and the remainder) (Archer *et al.*, 2017). It also fits to be applied for the extreme event (extreme data) when it reoccurs at

the specific period of time and the specific period of that transmission peak (Rani *et al*., 2018). The absence of data set and the problem of accessibility to this kind of database for some countries makes it even more difficult to do the long-term analyses that normally will involve lots of databases and extensive work that is complex in technicality and interpretations for the final findings. These obstacles and limitations create a research gap in environmental science and health that often will stop other researchers from continuing the long-term analysis due to the incomplete dataset for the analysis, which they forget this type of limited data set can be very important to extract the information from it. By this research, instead of using a huge number of the database for the time series and long-term analysis, the absolute average of the mean yearly from any existing data could be used, which will give the same results as the traditional method (Lang *et al*., 2019). Hence, this research was performed to maximize the usage of GIS and remote sensing mapping by filling up the gap in the efforts to simplify the methodology to be more practical and functional by targeting the specific event at the exact period of time, in order to overcome data limitations and deem to maximizing the efficiency of the malaria diseases control and management. However, in a different context, it is recommended that future research include all the other factors together in the analysis, especially for climate effect analysis integrated with the malaria transmission for a better significance of findings. In addition, number sets of data probably are required just for getting a more reliable of difference and relationship significantly for the statistical analysis. Comparison for the selected study areas located at the highlands with the lower lands for the malaria transmission cases is also important for future research to analyze the emergence of highland malaria transmission. By this, it can detect the affected by the climate-driven or non-climate factor such as the topography factor in the different altitudinal zone to minimize the transmission so that more robust and effective management can be conducted for public health.

CONCLUSION

In conclusion, the malaria incidence rate for each district was found highly viable from 2005 to 2019, ranging from 0.29/1000 persons to 4.09/1000 persons. In 2019, Ranau and Tenom districts had a high malaria incidence rate compared to previous years. Overall, the malaria incidence rate shows an increment from 2005 to 2019, increasing 149.64%. Through visual observation on distribution maps produced, the malaria incidence rate shows the increment from 2005 to 2010 and the year 2015 to 2019, and Ranau district still showing in the transmission map the highest distribution of malaria among the other districts of Sabah during the final year of 2019. This is believed due to the expansion of 33.6 % oil palm plantation with an annual rate of 2.38 %, which mainly occurs near Ranau and Tenom district as observed from the land cover map. Overall, cropland area had found dramatically decreased in 16.61% with an annual rate of change at 1.19%. Forest area also dropped in extensive coverage 8.38%, with an annual change rate of 0.60%. The correlation result showed a significant relationship but rather weak between land cover changes and malaria incidence in highland districts of Sabah. Somehow, regression results showed an insignificantly associated for independent variables (land cover changes of forest, oil palm, and cropland) towards the dependent variable (malaria incidence rate/1000 persons). In addition, the land cover change of forest to oil palm class was significant, yet there was no causality relationship with regards to the malaria incidence. More factors need to be investigated, including climatic (rainfall density, land surface temperature, or humidity) and non-climatic (vectors population or human movement) to understand malaria transmission better. Improvement of these data and analysis tools was helpful to develop the policies and implementation methods for malaria control and future vector-borne disease prevention. Nevertheless, the study can be the blueprint and guideline framework to analyse the emergence of malaria transmission so that a more pragmatic and dynamic health control program can be conducted.

AUTHOR CONTRIBUTIONS

C. Payus conceptualized the study framework and performed the experimental design, analyzed and interpreted the data, prepared the manuscript text, and manuscript edition. J. Sentian helped in

the experiments and literature review, compiled the data and manuscript preparation. A. Farrah helped with the proofread preparation and the final draft of the manuscript.

ACKNOWLEDGEMENT

This study was supported by Universiti Malaysia Sabah (UMS) with the financial number [D-72527], in collaboration with the Natural Disasters Research Centre of UMS. Great acknowledgement to all our students involved during the entire work of this project, particularly Tan Shi Min.

ABBREVIATIONS

%	Percentage
-	Negative
/	Per
°E	East of prime meridian
°N	North of equator
ANOVA	Analysis of variance
ArcGIS	Aeronautical Reconnaissance Coverage Geographic Information System
ArcMap	Aeronautical Reconnaissance Coverage Map
df	Degree of freedom
E	East
F	F-test
Fig.	Figure
GIS	Geographic Information System
IGBP	International Geosphere-Biosphere Program
Km^2	Square kilometer
KML	Keyhole markup language
LULC	Land use land cover
MCD	MODIS land cover product and modeling grid
MODIS	Moderate resolution imaging Spectroradiometer
MS	Mean square
m	Meter
N	*North*
P. knowlesi	*Plasmodium knowlesi*
P-value	Probability value
R	Regression
r	Coefficient value
Significance F	Significance value from F-distribution table
S	South
SE	Standard error
SS	Sum of square
t Stat	T-test calculation statistic value
USGS	United States Geological Survey
W	West
WHO	World Health Organization

REFERENCES

Alawamy, J.S.; Balasundram, S.K.; Hanif, A.H.M.; Sung, C.T.B., (2020). Detecting and analyzing land use and land cover changes in the region of al-jabal al-akhdar, libya using time-series landsat data from 1985 to 2017. Sustainability. 12(11): 4490 **(8 pages).**

Archer, E.R.; Landman, W.A.; Tadross, M.A.; Malherbe, J.; Weepener, H.; Maluleke, P.; Marumbwa, F.M., (2017). Understanding the evolution of the 2014–2016 summer rainfall seasons in Southern Africa: Key lessons. Clim. Risk Manage., 16: 22–28 **(7 pages).**

Babaie, J.; Barati, M.; Azizi, M.; Ephtekhari, A.; Sadat, S.J., (2018). A systematic evidence review of the effect of climate change on malaria in Iran. J. Parasit. Dis., 42(3): 331-340 **(10 pages).**

Baeza, A.; Santos-Vega, M.; Dobson, A. P.; Pascual, M., (2017). The rise and fall of malaria under land-use change in frontier regions. Nat. Ecol. Evol., 1(5): 0108 **(7 pages).**

Bousema, T.; Drakeley, C., (2011). Epidemiology and infectivity of Plasmodium falciparum and Plasmodium vivax gametocytes in relation to malaria control and elimination. Clin. Microbiol. Rev., 24(2): 377-410 **(34 pages).**

Bouzekri, S.; Lasbet, A.A.; Lachehab, A., (2015). A new spectral index for extraction of built-up area using Landsat-8 data. J. Indian Soc. Remote Sens., 43(4): 867-873 **(7 pages).**

CDC, (2018). About Malaria: Lifecycle. Centers for Disease Control and Preventions.

CPO, (2019). Average yearly price calculated from monthly prices in USD using IMF data, Federal Reserve Bank of St. Louis, citing: International Monetary Fund.

Franzese, M.; Iuliano, A., (2019). Correlation analysis. Institute for Applied Mathematics (IAC) (**128 pages**).

Gaveau, D. L.; Locatelli, B.; Salim, M. A.; Yaen, H.; Pacheco, P.; Sheil, D., (2019). Rise and fall of forest loss and industrial plantations in Borneo (2000–2017). Conserv. Lett., 12(3): e12622 (**8 pages**).

Haque, I.; Basak R., (2017). Land cover change detection using GIS and Remote Sensing techniques: A spatio-temporal study on Tanguar Haor, Sunamganj, Bangladesh. Egypt. J. Remote Sens. Space Sci., 20(2):251-263 **(13 pages).**

Jaafar, W.S.W.M.; Said, N.F.S.; Maulud, K.N.A.; Uning, R.; Latif, M.T.; Kamarulzaman, A.M.M.; Mohan, M.; Pradhan, B.; Saad, S.N.M.; Broadbent, E.N.; Cardil, A., (2020). Carbon Emissions from Oil Palm Induced Forest and Peatland Conversion in Sabah and Sarawak, Malaysia. Forests, 11(12): 1285 **(10 pages).**

Kamlun, K.U.; Arndt, R. B.; Phua, M. H., (2016). Monitoring deforestation in Malaysia between 1985 and 2013: Insight from South-Western Sabah and its protected peat swamp area. Land Use Policy. 57: 418-430 **(13 pages).**

Kweka, E.J.; Kimaro, E.E.; Munga, S., (2016). Effect of deforestation and land use changes on mosquito productivity and development in Western Kenya Highlands: implication for malaria risk. Public Health Front., 4: 238 **(9 pages).**

Lang, P.E.; Carslaw, D.C.; Moller, S.J., (2019). A trend analysis approach for air quality network data. Atmos. Environ.: X, 2: 100030 **(10 pages).**

Le, P.V.; Kumar, P.; Ruiz, M.O.; Mbogo, C.; Muturi, E.J., (2019). Predicting the direct and indirect impacts of climate change on malaria in coastal Kenya. PloS One, 14(2): e0211258 **(7 pages).**

Lowassa, A.; Mazigo, H.D.; Mahande, A.M.; Mwang'onde, B.J.; Msangi, S.; Mahande, M.J.; Kimaro, E.E.; Elisante, E.; Kweka, E.J., (2012). Social economic factors and malaria transmission in Lower Moshi, northern Tanzania. Parasites Vectors. 5(1): 1-9 **(9 pages).**

MAMPU, (2018). Senarai Peta Topografi Siri T931 - Senarai Peta Topografi Siri T931. Malaysian Administrative Modernisation and Management Planning Unit.

Mark, D.C.J.; George, R.P., (2017). Land use and land cover (LULC) change detection using multi- temporal landsat imagery: A case study in Allah Valley Landscape in Southern, Philippines. J.Biodevers. Environ. Sci., 12(2): 98-108 **(11 pages).**

Martens, P.; Hall, L., (2000). Malaria on the move: human population movement and malaria transmission. Emerg. Infect. Dis., 6(2): 103 **(6 pages).**

Mawili-Mboumba, D.P.; Akotet, M. K.B.; Kendjo, E.; Nzamba, J.; Medang, M.O.; Mbina, J.R.M.; Kombila, M., (2013). Increase in malaria prevalence and age of at risk population in different areas of Gabon. Malar. J., 12(1): 1-7 **(7 pages).**

Miuse, C.F.; Kamlun, K.U., (2019). Multi-temporal Land-Cover Classification of Kinabalu Eco-Linc Site and the Protected Park Areas. In Journal of Physics: Conference Series, 1358(1): 012034. IOP Publishing **(5 pages).**

Mukhtar, A.Y.; Munyakazi, J.B.; Ouifki, R., (2019). Assessing the role of climate factors on malaria transmission dynamics in South Sudan. Math. Biosci., 310: 13-23 **(11 pages).**

Phua, M.H.; Tsuyuki, S., (2004). Deforestation detection in Kinabalu Area, Sabah, Malaysia by using multi-sensor remote sensing approach. J. Plan., 10(1): 31-40 **(10 pages).**

Pohl, C., (2014). Mapping palm oil expansion using SAR to study the impact on the CO2 cycle. 7th IGRSM International Remote Sensing and GIS Conference and Exhibition. IOP Conf. Ser. Earth Environ. Sci., 20: 012012 **(8 pages).**

Ramdzan, A.R.; Ismail, A.; Zanib, Z.M., (2020). Prevalence of malaria and its risk factors in Sabah, Malaysia. Int. J. Infect. Dis., 91: 68-72 **(5 pages).**

Rani, N.A.; Azid, A.; Khalit, S.I.; Juahir, H.; Samsudin, M.S., (2018). Air pollution index trend analysis in Malaysia, 2010-15. Pol. J. Environ. Stud., 27(2): 801 – 807 **(7 pages).**

Rawat, J.S.; Kumar, M., (2015). Monitoring land use/cover change using remote sensing and GIS techniques: A case study of Hawalbagh block, District Almora, Uttarakhand, India. Egypt. J. Remote Sens. Space Sci., 18(1): 77-84 **(8 pages).**

Singkong, F.B.; Aralas, S.B., (2017). An Empirical Study of Malaria Incidence and Land Use Change of Palm Oil Industries in Malaysia. Malaysian Journal of Business and Economics (MJBE) **(16 pages).**

Tatem, A.J.; Gething, P.W.; Smith, D.L.; Hay, S.I., (2013). Urbanization and the global malaria recession. Malar. J., 12(1): 133 **(10 pages).**

Toh, S.M.; Grace, K.T., (2005). Case study: Sabah forest ownership. Report produced for Food and Agriculture Organization of the United Nations. Global Forestry Services Inc, Kuala Lumpur **(23 pages).**

Torbick, N.; Ledoux, L.; Salas, W.; Zhao, M., (2016). Regional mapping of plantation extent using multisensor imagery. Remote Sens., 8(3):236 **(21 pages).**

Tucker Lima, J.M.; Vittor, A.; Rifai, S.; Valle, D., (2017). Does deforestation promote or inhibit malaria transmission in the Amazon? A systematic literature review and critical appraisal of current evidence. Philos. Trans. R. Soc. Lond., B, Biol. Sci., 372(1722): 20160125 **(11 pages).**

Tuno, N.; Okeka, W.; Minakawa, N.; Takagi, M.; Yan, G., (2005).

Survivorship of Anopheles gambiae sensu stricto (Diptera: Culicidae) larvae in western Kenya highland forest. J. Med. Entomol., 42(3): 270-277 **(8 pages).**

Ukor, C.D.; Ogbole, J.; Alaga, A., (2016). Analysis of Land Use Land Cover Change in Ikeja, Lagose State. Nigeria Using Remote Sensing and Gis Techniques. Int. J. Eng. Sci. Technol., 5(10): 462-472 **(11 pages).**

USGS, (2020). MCD12Q1VOO6 MODIS/Terra Aqua Land Cover Type Yearly L3 Global 500 m SIN Grid. United States Geological Survey.

Vittor, A.Y.; Pan, W.; Gilman, R.H.; Tielsch, J.; Glass, G.; Shields, T.; Sánchez-Lozano, W.; Pinedo, V.V.; Salas-Cobos, E.; Flores, S.; Patz, J.A., (2009). Linking deforestation to malaria in the Amazon: characterization of the breeding habitat of the principal malaria vector, Anopheles darlingi. Am. J.Trop. Med., 81(1): 5 **(16 pages).**

Wicke, B.; Sikkema, R.; Dornburg, V.; Faaij, A., (2011). Exploring land use changes and the role of palm oil production in Indonesia and Malaysia. Land Use Policy, 28(1): 193-206 **(14 pages).**

WHO, (2014). International Travel and Health Publication 2014. World Health Organization, Geneva **(244 pages).**

WWF, (2020). Borneo_Forest: The Problems. World Wide Fund For Nature.

Yadav, K.; Dhiman, S.; Rabha, B.; Saikia, P.K.; Veer, V., (2014). Socio-economic determinants for malaria transmission risk in an endemic primary health centre in Assam, India. Infect. Dis. Poverty, 3(1): 1-8 **(8 pages).**

Yusof, A.A.; Rusli, N., (2018). The investigation of the Land Use Changes from Forest to Oil Palm in Sabah. Geomatics Res. Innovation Competition **(5 pages).**

AUTHOR (S) BIOSKETCHES

Payus, C.M., Ph.D., Associate Professor, Faculty of Science and Natural Resources, Universiti Malaysia Sabah, Jalan UMS, 88400, Kota Kinabalu, Sabah, Malaysia.
- Email: *melpayus@ums.edu.my*
- Web of Science Researcher ID: ADM-9304-2022
- Scopus Author ID: 56087857400
- ORCID: 0000-0003-1947-2844
- Homepage: https://www.ums.edu.my/fssa/environmentalscience/

Sentian, J., Ph.D., Associate Professor, Faculty of Science and Natural Resources, Universiti Malaysia Sabah, Jalan UMS, 88400, Kota Kinabalu, Sabah, Malaysia.
- Email: *jsentian@ums.edu.my*
- Web of Science Researcher ID: ABE-2542-2021
- Scopus Author ID: 16307875900
- ORCID: 0000-0002-7121-2372
- Homepage: https://www.ums.edu.my/fssa/environmentalscience/

HOW TO CITE THIS ARTICLE

Payus, C.M.; Sentian, J. (2022). Satellite imagery system in malaria transmission resulting from the land use/ land cover change. Global J. Environ. Sci.Manage., 8(4): 545-560.

DOI: 10.22034/gjesm.2022.04.07

url: https://www.gjesm.net/article_250969.html

Global J. Environ. Sci. Manage. 8(4): 561-574, Autumn 2022, Serial #32

Global Journal of Environmental Science and Management
(GJESM)

Homepage: https://www.gjesm.net/

CASE STUDY

Microalgae diversity in several different sub-habitats

S. Arsad[1,4,5,*], Y.W. Mulasari[1], N.Y. Sari1, E.D. Lusiana[1,4,5], Y. Risjani[1,6], M. Musa[1,4,5], M. Mahmudi[1,4], F.S. Prasetiya[2], L.A. Sari[3]

[1] *Department of Aquatic Resources Management, Faculty of Fisheries and Marine Science, Universitas Brawijaya, Jl. Veteran Malang 65145, Indonesia*

[2] *Marine Science Department, Faculty of Fisheries and Marine Sciences, Universitas Padjadjaran, Jl. Raya Bandung Sumedang KM. 21, 45363 Jatinangor, Indonesia*

[3] *Department of Aquaculture, Faculty of Fisheries and Marine Universitas Airlangga, Surabaya 60115, Indonesia*

[4] *Aquatic Resources and Ecological Research Group (AquaRES), Faculty of Fisheries and Marine Science, Universitas Brawijaya, Jl. Veteran Malang 65145, Indonesia*

[5] *Microbiol Resources and Technology (MicroBase) Group, Post-graduate program Universitas Brawijaya, Jl. Veteran Malang 65145, Indonesia*

[6] *BioEcotox Research Group, Faculty of Fisheries and Marine Science, Universitas Brawijaya, Jl. Veteran Malang 65145, Indonesia*

ARTICLE INFO

Article History:
Received 01 October 2021
Revised 11 January 2022
Accepted 21 February 2022

Keywords:
Benthic environment
epiphytic
macroalgae and microalgae
non-metric multidimensional scaling (nMDS)
planktonic

DOI: 10.22034/gjesm.2022.04.08

ABSTRACT

BACKGROUND AND OBJECTIVES: Biodiversity is the variety of life that exists on Earth, including all the organisms, species, and populations that come together in a complex manner to form communities and ecosystems. This study aimed to assess the diversity of microalgae in several different sub-habitats by identifying their types and abundance in sediments, mangroves, macroalgae, and water columns; additionally, this study analyses the environmental factors that affected the abundance of microalgae in several sub-habitats.

METHODS: This study used a quantitative descriptive method with data collection techniques, incorporating the purposive sampling method. Data were analysed using non-metric multidimensional scaling.

FINDINGS: The results showed that the composition of microalgae species found in the sub-habitats of sediments, mangroves, macroalgae, and water columns at Siwil Beach were the class of Bacillariophyceae (70%), Chlorophyceae (17%), and Cyanophyceae (13%) in all sub-habitats. In Sempu Island, microalgae were found only from Bacillariophyceae (100%) in the four sub-habitats. The highest abundance of microalgae on Siwil Beach was in the sub-habitat of mangroves, with a total of 5,423,073 cells/cm^2, while the highest abundance in Sempu Island was in the sub-habitat of macroalgae, with a value of 1,986,252 cells/cm^2. Moreover, based on non-metric multidimensional scaling analyses, there was no similarity of algae diversity between Siwil Beach and Sempu Island, with a high variation of microalgae.

CONCLUSION: The present study demonstrated that the class Bacillariophyceae dominated the communities of microalgae found both in Siwil Beach and Sempu Island. Moreover, factors that mainly affected the abundance of microalgae were environmental, which is already proven by the measurement of water quality in each sub-habitat at both locations. Siwil Beach and Sempu Island water quality was relatively still under the Indonesian national quality standard for seawater. This research is thought to be the first step in exploring the diversity of microalgae in several sub-habitats in East Java, Indonesia, and linking the type and availability of microalgae found in various sub-habitats with environmental water quality parameters and human activities around the waters. In addition, this paper provides the basic information of microalgae diversity based on sub-habitats, especially in the southern part of East Java Indonesia.

NUMBER OF REFERENCES	NUMBER OF FIGURES	NUMBER OF TABLES
48	5	1

*Corresponding Author:
Email: *sulastriarsad@ub.ac.id*
Phone: +6234 1553 512
ORCID: 0000-0002-7322-7834

Note: Discussion period for this manuscript open until January 1, 2023 on GJESM website at the "Show Article".

INTRODUCTION

Biodiversity is the variety of life that exists on earth, including all the organisms, species and populations that come together in a complex manner to form communities and ecosystems. Biodiversity describes the diversity both in number and frequency in nature. It is usually used in plants, animals, microorganisms and others that make up an ecosystem (Rawat and Agarwal, 2015). As a mega biodiversity nation, the diversity and abundance of microalgae in Indonesia are very high (Pikoli *et al.,* 2019). The characteristics of microalgae are that they are planktonic, epiphytic and benthic. Microalgae live in various sub-habitats (Hopes and Mock, 2015), such as benthic microalgae found in sedimentary habitats, epiphytic microalgae attached to substrates such as seaweed (Al-Harbi, 2017) and mangrove roots, and planktonic microalgae found in the water column. Microalgae are autotrophic organisms that use light to synthesize compounds such as carbohydrate, proteins and lipids (Musa *et al.,* 2021). Benthic microalgae, called microphytobenthos, are microscopic and capable of photosynthesis in sediments. This type of microalgae can grow at low light levels by utilizing a high concentration of nutrients in the sediment. These microalgae are widely distributed in nature, adapted to different environments and have high diversity in size, morphology, life cycle, pigment and metabolism (Baklouti *et al.,* 2018). This is in accordance with the statement of Risjani et *al.* (2021), suggesting that microalgae can live in various habitats with high levels of biodiversity. Habitats of microalgae in various areas have different environmental conditions. Environmental parameters such as physical, chemical and biological parameters significantly affect environmental conditions in microalgae habitats (Prazukin et *al.,* 2021). In every coastal ecosystem, there are biotic and abiotic components that interact. East Java has coastal areas with abundant microalgae. The study of distribution of marine microalgae has been carried out in several regions in Indonesia such as in Tanjung Benoa Bali (Suteja *et al*., 2021), West Coast South of Celebes (Tambaru *et al*., 2021), Simeulue Island (Purbani *et al*., 2021), Tambrauw sea West Papua (Purbani *et al.,* 2019), Negeri Waai Beach of Maluku Tengah Regency (Hulopi *et al.,* 2016) and East Java coast (Zakiyah et al., 2020). However, the study of microalgae in several sub-habitats in Siwil beach and Sempu Island is not done yet. The previous research on both places was focused on distribution of brown algae (Achmadi dan Arisandi, 2021) and mangrove, respectively (Suhardjono, 2013). Siwil Beach and Sempu Island are often used for touristic activities, aquaculture and domestic activities. Therefore, the availability and the abundance of microalgae are very influenced by the environmental factors (Astuti *et al.,* 2020). In addition, the analysis of the relationship between microalgae abundance and environmental factors is still limited to the influence of two variables, namely the relationship between microalgae in the water column and the environmental parameters (Golubkov *et al.,* 2019). In previous studies, there has not been an analysis of the relationship between microalgae in various sub-habitats with different locations nor has there been an analysis of the relationship between microalgae and environmental parameters. Based on this, this study will compare the relationship between microalgae, various sub-habitats in different locations and environmental factors. The aims of the current study are to assess the diversity of microalgae in several different sub-habitats, by identifying their types and abundance of microalgae in sediments, mangroves, macroalgae and water columns, and to analyse the environmental factors that affected the abundance of microalgae in these sub-habitats, to provide the database information of microalgae diversity based on sub-habitats. This study has been carried out in the South Coast of East Java of Indonesia in 2021.

MATERIALS AND METHODS

Study area

This study was conducted in the South Coast of East Java in two locations (Fig. 1a and 1b), namely Siwil Beach, Pacitan Regency (8° 15’ 53.5” S and 111° 16’ 48.8” E) and Sempu Island, Malang Regency (8° 27’ 24” - 8° 4’ 54” S and 112° 40’ 45” - 112° 42’ 45” E). The selection of locations on Siwil Beach and Sempu Island was done because these locations represented the distribution of microalgae on Java Island, especially in the southern part; besides, Siwil Beach is used for various water use activities such as tourism, aquaculture and domestic activities, whereas Sempu Island is used for tourism and domestic activities. In addition, the current strength in the waters around Sempu Island range from 0.3–0.6 m/s (Luthfi *et al.,* 2018); from the observation station with its back to the Indian Ocean, the waves in the waters around Sempu Island are low, while the current velocity in Siwil Beach, according to

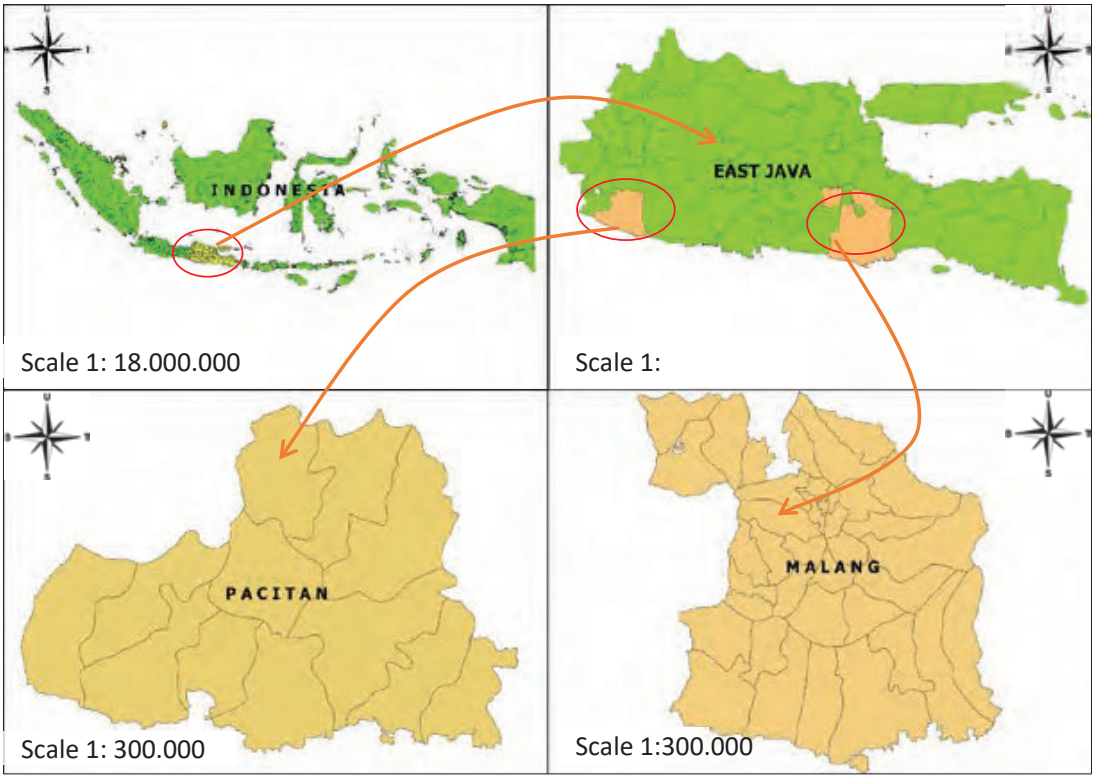

Fig. 1(a): Geographic location of the study area at the Siwil Beach and Sempu Island, in Indonesia

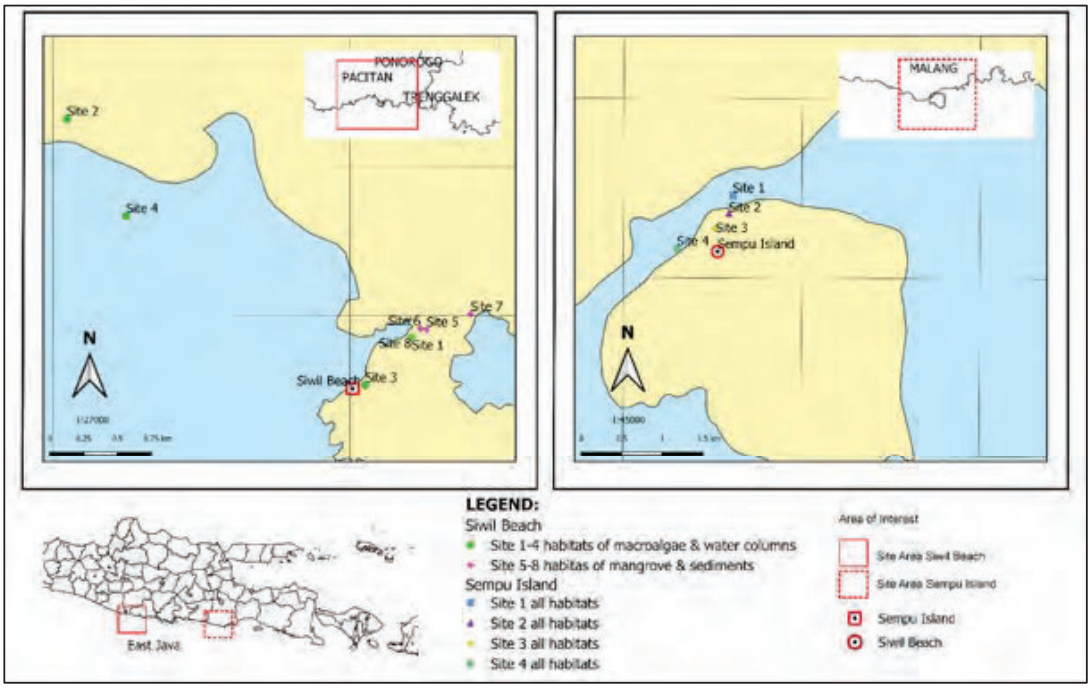

Fig. 1(b): The sampling sites details of Siwil Beach and Sempu Island, in Indonesia

Khotimah *et al*. (2018), can reach 17 m/s with a wave range of 4–5 m. Sampling on Siwil Beach was carried out at eight sites: four sites were located in the sub-habitats of mangroves and sediments and four sites in the sub-habitats of macroalgae and water columns. Meanwhile, sampling in Sempu Island was carried out at four sites, with each site containing the sub-habitats of sediments, mangrove roots, macroalgae and water columns. The determination of the sampling location was carried out to represent the population in Siwil Beach and Sempu Island. The present study was carried out in April–June 2021, during the dry season. Water quality and microalgae sampling in the water column sub-habitat was conducted at high tide. In contrast, sampling of microalgae in the sub-habitats of sediments, mangrove roots and macroalgae was carried out at low tide, as these conditions allow epiphytic microalgae to stick to the sediment surface, mangrove roots and macroalgae. As stated by Garcia *et al.* (2012), taking epiphytic microalgae at low tide can facilitate sampling because of the short immersion.

Research procedure

Sampling of microalgae

Microalgae sampling in the sub-habitats of sediments, mangrove roots and macroalgae was carried out at the lowest tide using the transect technique, by taking samples on the surface of the substrate on which a rectangular slate mold (5 x 5 cm^2) had been placed, following the protocol from Essien *et al.* (2008). On the other hand, microalgae sampling in the water column sub-habitat was carried out following Kadim and Arsad (2016). Briefly, samples were taken using a plankton net (mesh size 25 mm). The filtered sample was placed into a 30 mL sample bottle and was preserved using Lugol's 4%.

Sample Analysis of Microalgae

Identification and calculation of microalgae were carried out in the laboratory using an Olympus light microscope with a magnification of 4x10 morphologically, by using book of Prescott (1970) and the Lackey drop method modified from Clark (1981), respectively. It was then continued with the calculation of the abundance of microalgae in the water column habitat (APHA, 1989), relative abundance (Kusumaningsari *et al.,* 2015), the abundance of epiphytic and benthic microalgae (APHA, 1989), diversity and uniformity index (Shannon, 1948) and dominance index (Kadim and Arsad, 2016).

Water quality measurements

Water quality measurements were performed *in situ* that covers temperature (°C, PDO-520 DO meter), transparency (cm, Secchi disk), pH (mediatech digital pH meter 009), dissolved oxygen (DO) (mg/L, PDO-520 DO meter) and salinity (‰, refractometer). Furthermore, nitrate (mg/L, UV-VIS spectrophotometer), phosphate (mg/L, Genesys 10S UV-VIS spectrophotometer) and biological parameters including chlorophyll-a (mg/L, Genesys 10S UV-VIS spectrophotometer) were measured *ex-situ*. All the water parameters were taken once on each site during the study.

Data analysis

In this study, data were analysed using the non-metric multidimensional scaling (nMDS) method with the plot of the nMDS method referring to the Bray Curtis matrix equation, used to detect species composition (Borchhardt *et al.,* 2017). This nMDS analysis was carried out using PAST software version 403 for Windows Operating System.

RESULTS AND DISCUSSION

The composition of microalgae found

Based on the analysis of microalgae found at Siwil Beach and Sempu Island, it was found that the species and composition on Siwil Beach were in more significant number than those in Sempu Island, with a percentage ratio of species of 67% on Siwil Beach and only 33% in Sempu Island. The Bacillariophyceae, Chlorophyceae and Cyanophyceae dominated the microalgae found on Siwil Beach (Fig. 2a). In contrast, only Bacillariophyceae was detected on Sempu Island (Fig. 2b). This is due to the low nitrate and phosphate content in these waters; thus, only tolerant microalgae can live. Bacillariophyceae was the most commonly found in various waters, with high adaptability to various environmental conditions (Arsad et *al.,* 2021; Everest and Aslan, 2016). Moreover, diatoms can be found in various places where water is available; they can stick to all substrates such as gravels and plants, and can live in various places in the aquatic environment (Kwon *et al.,* 2021). The genera found in all sub-habitats at Siwil Beach and Sempu Island were genera from the class of Bacillariophyceae, namely *Amphora*, *Cyclotella*, *Diploneis*, *Grammatophora*, *Pleurosigma*, *Rhizosolenia*, *Synedra*, *Nitzschia* and

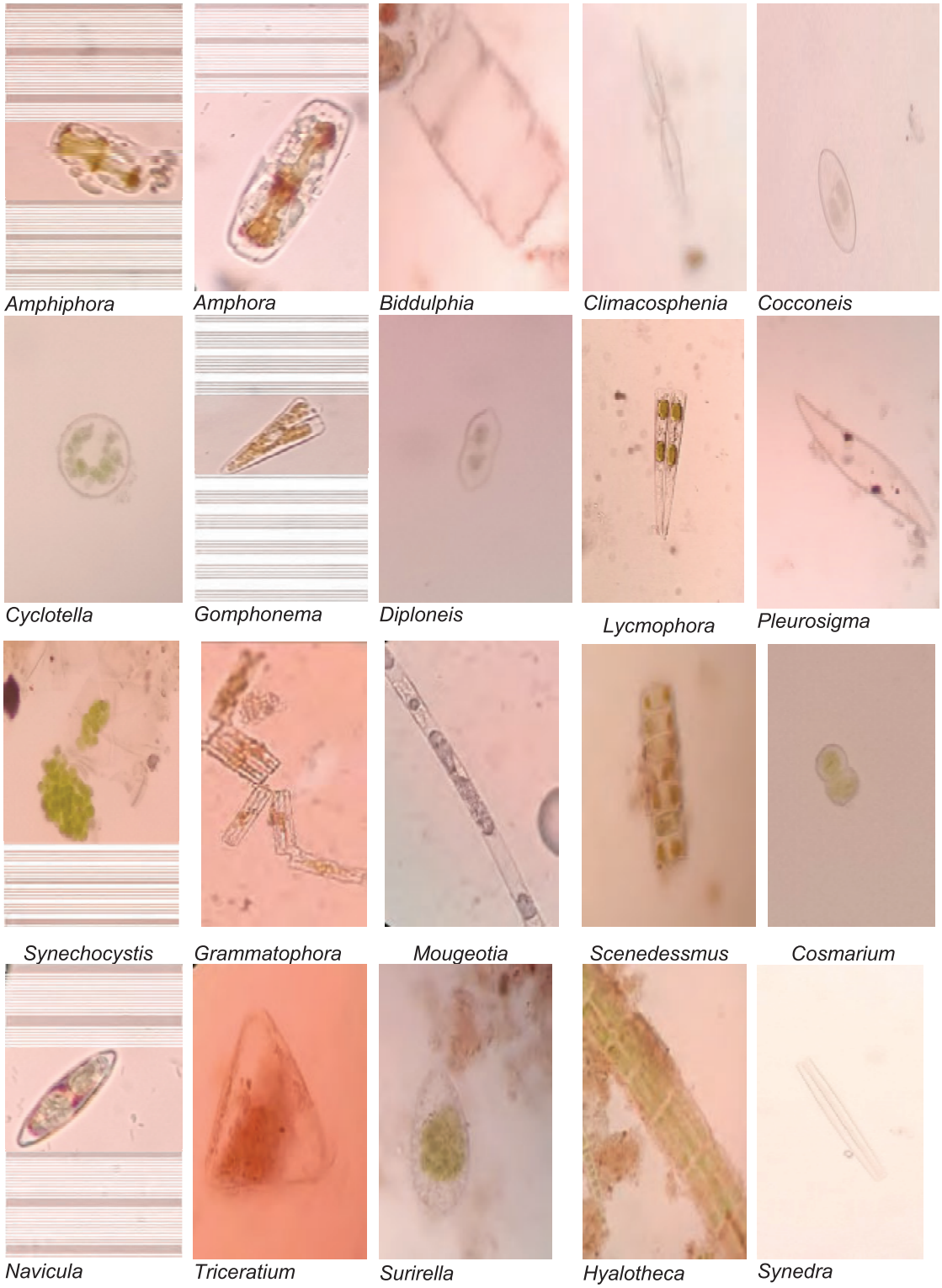

Fig. 2a: Several microalgae found in Siwil Beach (magnification 4x10)

Fig. 2b: Several microalgae found in Sempu Island (magnification 4x10)

Navicula. However, of the genera found in all sub-habitats, some genera dominated in all sub-habitats at Siwil Beach and Sempu Island, namely *Nitzschia* and *Navicula*. This is in line with what was stated by Mucko *et al.* (2021) that the genera *Nitzschia* and *Navicula* were found in various habitats; historically, they have been camouflaged within a category of small pennate diatoms with single-celled cells that can reach very high relative abundance, accounting for 60% or even 90% of the total number of the class Bacillariophyceae. The genera *Nitzschia* and *Navicula* can live in waters with both high and low salinity; therefore, the genera *Nitzschia* and *Navicula* are also found on Siwil Beach, which has high salinity (Akcalan, 2020).

Microalgae abundance

The highest abundance of microalgae was found on Siwil Beach in the sub-habitat of mangrove roots with a value of 5,423,073 cells/cm^2, whereas the lowest was detected in the sub-habitat of water columns with a value of 890,457 cells/L. Most of the microalgae associated with mangroves could be found in the mangrove roots and the surrounding water columns. The microalgae abundance in the mangrove area is influenced by the mangrove canopy cover and the level of turbidity of the waters (Essien et *al.,* 2008). On the other hand, the highest abundance found in Sempu Island was in the macroalgae sub-habitat, with a value of 1,986,252 cells/cm^2, and the lowest was found in the sub-habitat of water columns, with a value of 371,362 cells/L. Waters with a high density of macroalgae will create many substrates for the attachment of microalgae. The process of fouling in macroalgae takes a long time; thus, the epiphytic microalgae will be abundant in a stable macroalgae habitat. Macroalgae can also affect the structure, type and community of microalgae (Zadorozhna et *al.,* 2017). The category of abundance of phytoplankton in the waters is 0–2,000 cell/L (oligotrophic), 2,000–15,000 cell/L (mesotrophic) and more than 15,000 cell/L (eutrophic) (Linus *et al.,* 2016). Therefore, it can be said that Siwil Beach and Sempu Island are included in eutrophic waters with an abundance value of > 15,000 cells/L. The abundance of microalgae is presented in Fig. 3.

Relative abundance

In Siwil Beach, the highest relative abundance was detected from the genus *Nitzschia* (35.8%), *Synechocystis* (36.1%), *Navicula* (35.2%) and *Gramatophora* (23%) from the sub-habitat of sediments, mangrove roots, macroalgae and water columns, respectively. As stated by Garcia et *al.* (2012), *Nitzschia* can tolerate a less favourable environment and an environment with hyper eutrophication. Meanwhile, *Synechocystis* is often found in mangrove areas because it is an epiphytic microalga that favours habitats with high nitrogen levels (Alvarenga *et al.,* 2015). On the other hand, *Navicula* microalgae can adapt to their habitat and have a wide distribution, both vertically and horizontally in the waters (Buczko *et al.,* 2015). In contrast, *Grammatophora* sp. has colonizing cells and is a planktonic and epiphytic microalga with a cosmopolitan distribution, so it is commonly found in the sub-habitat of water columns (Klein, 2017). As for Sempu Island, the highest relative abundance was observed from the genus *Pinnularia* (53.85%) in the sub-habitats of sediments and macroalgae, while *Cyclotella* (71.43%) and *Navicula* (53.85%) were detected in mangrove roots and water column sub-habitats, respectively. *Pinnularia* can live in waters with low or high nutrients, usually found in sediments or substrates containing moss, and cluster in distribution. This is reinforced by the study from Silva *et al.* (2016), who demonstrated that *Pinnularia* can live in oligotrophic waters, has low salinity and has low pH. On the other hand, the distribution of *Cyclotella* is influenced by the mixing in the waters, and these microalgae can usually be found in shallow waters. *Cyclotella* lives in both solitary and colonies, in fresh and coastal waters (Houk *et al.,* 2015). Meanwhile, *Navicula* is a microalga of the Bacillariophyceae class that can multiply rapidly, thus increasing its abundance. According to Vijver *et al.* (2011), the number of *Navicula* will be abundant and dominate as benthic diatom microalgae, particularly in areas with temperate and tropical climates.

Biological index

The calculation of the microalgae diversity index at Siwil Beach and Sempu Island resulted in various values. According to Farhadian et *al.* (2015), this diversity index is correlated with aquatic environmental conditions, in which when the diversity index is low, some species may be dominant in these waters. Based on the diversity index calculation results in both locations, it appeared that Siwil Beach had moderate microalgae community stability, and Sempu Island had moderate community stability except in the sub-habitats of sediments and mangrove roots. The diversity index, which has a value of less than three and more than one, could be interpreted to have a moderate level of stability in the biota community. Additionally, it could show that the quality of the waters is still relatively good for the growth of aquatic biota (Winahyu *et al., 2*013). The results of the uniformity index values

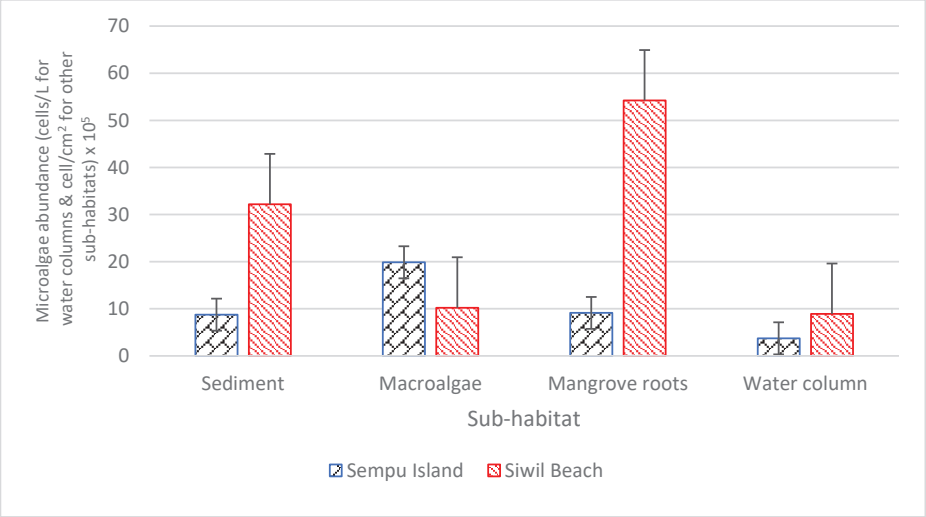

Fig. 3: Microalgae abundance at Siwil Beach and Sempu Island. Mean ± SE

found at Siwil Beach and Sempu Island showed values close to 1 and >0.5, indicating that the uniformity in these waters was in a balanced state, and there was no competition for food or living space (Fan *et al.,* 2021). In this study, Siwil Beach had a low dominance index, meaning no dominant species in the waters. A similar condition was also found in Sempu Island, with a dominance index value of <1. Hence, there was no dominance in the waters. According to Marsela *et al.* (2021), the dominance index ranges from 0 to 1, where a smaller value of the dominance index shows that no species dominates, while a higher value of the dominance index indicates the presence of a dominating species.

Water quality parameters

The water quality measurements (Table 1) in all sub-habitats revealed that the water quality at both Siwil Beach and Sempu Island were classified in good condition because it is still below the quality standard based on the Indonesian Government Regulation (Peraturan Pemerintah, 2021), and in these water conditions, microalgae can grow. This is indicated by the temperature that ranged from 20 to 30°C. Arsad *et al.* (2019) demonstrated that water temperature with more than 35°C could potentially kill microalgae. Moreover, the pH in this study ranged from 7 to 9, which is considered to be favourable (Nurhayati *et al.*, 2014). In addition, DO from the sampling sites were of >5 mg/L, which is still a good condition (Patty *et al.,* 2015). The lowest salinity level was detected around 35 ppm, whereas the normal and the highest values were 40 and 45 ppm, respectively (Altaee e*t al.,* 2018). As for nitrate and phosphate, they ranged from 0.10 to 0.50 mg/L and from 0.002 to 0.050 mg/L, respectively (Patty *et al.,* 2015). In this study, the chlorophyll-a

Table 1: Water quality measurement results

Parameter	Siwil Beach (Sub-habitats of sediments and mangroves)				
	Site 1	Site 2	Site 3	Site 4	Peraturan Pemerintah, (2021)
Temperature (°C)	29.9	30.3	30.6	31.8	28-32
Transparency (cm)	23.35	32.85	25.55	32.05	> 5 m
pH	8	8.2	8.3	8.3	7-8.5
DO (mg/L)	8.5	8.8	7.5	7.5	>5
Nitrate (mg/L)	0.268	0.27	0.346	0.189	0.06
Phosphate (mg/L)	0.04	0.023	0.026	0.027	0.015
Salinity (‰)	35	40	40	41	34
Chlorophyll-a (mg/L)	2.035	2.921	2.889	5.317	-
Parameter	Siwil Beach (Sub-habitats of water columns and macroalgae)				
	Site 1	Site 2	Site 3	Site 4	Peraturan Pemerintah, (2021)
Temperature (°C)	30.2	29.6	31.6	30	28-32
Transparency (cm)	54.3	35.6	100	100	> 5 m
pH	8.2	8.2	8.4	8.4	7-8.5
DO (mg/L)	8	8.2	5.6	6	>5
Nitrate (mg/L)	0.288	0.323	0.238	0.174	0.06
Phosphate (mg/L)	0.038	0.019	0.04	0.02	0.015
Salinity (‰)	40	43	45	42	34
Chlorophyll-a (mg/L)	4.434	5.516	1.836	1.807	-
Parameter	Sempu Island (Sub-habitats of sediments, macroalgae, mangroves, and water columns)				
	Site 1	Site 2	Site 3	Site 4	Peraturan Pemerintah, (2021)
Temperature (°C)	29.2	29.2	32.5	32.6	28-32
Transparency (cm)	100	60	45	85	> 5 m
pH	8.2	8.1	8.1	8.2	7-8.5
DO (mg/L)	10.7	6.6	6.7	6.1	>5
Nitrate (mg/L)	0.203	0.325	0.214	0.203	0.06
Phosphate (mg/L)	0.036	0.037	0.032	0.024	0.015
Salinity (‰)	45	40	40	40	34
Chlorophyll-a (mg/L)	1.807	1.807	1.574	2.431	-

also correlated with the abundance of microalgae. A study conducted by Ratomski and Paw (2021) showed that there was a correlation between microalgae and chlorophyll-a, as this parameter could be determined by the biomass of microalgae in the water column. This result is also supported by Diana *et al.* (2021), suggesting that the availability of nutrients in the water column is positively related to the abundance of phytoplankton, which eventually will affect the level of chlorophyll-a in these waters.

The similarity of microalgae in different locations and sub-habitats

The nMDS method was used to analyse the proximity of the number of microalgae found in each sub-habitat in two locations, namely Sempu Island and Siwil Beach, which were grouped by class, namely Bacillariophyceae, Chlorophyceae and Cyanophyceae, and the results of measurements of environmental parameters, namely temperature, transparency, pH, DO, nitrate, phosphate, salinity and chlorophyll-a. The result of the nMDS analysis is presented in Fig. 4. From Fig. 4, the nMDS plot shows similarities between associated microalgal on Siwil Beach for sediment, mangrove, macroalgae and water column sub-habitat (SWL SD, SWL MG, SWL MK and SWL WC, respectively). Associated microalgal in Sempu Island for sediment, mangrove, macroalgae and water column sub-habitat was indicated by SMP SD, SMP MG, SMP MK and SMP WC, respectively. It appeared that the points in each sub-habitat at Siwil Beach and Sempu Island were far from each other and did not show the closeness between the points of Siwil Beach and Sempu Island. This result indicates that there was no similarity in the composition of microalgae found between Siwil Beach and Sempu Island, with a high variation of microalgae in both locations. This is presumably due to different characteristics and environmental conditions between Siwil Beach and Sempu Island, which can be proven by the measurements of water quality both sites; for example, Siwil Beach had a higher chlorophyll-a level than Sempu Island, resulting in the high abundance of microalgae. Additionally, vegetation density and current conditions at Siwil Beach were also higher than those in Sempu Island, so they have the potential to carry more nutrients to help microalgae growth. As demonstrated by Kramer (2015), nutrient concentrations in the waters will control the growth of microalgae. In contrast, low nitrate content may cause death to the microalgae. Moreover, according to Safi (2003), currents and waves could also affect the composition of microalgae that are more varied. The non-parametric analyses produced on the environmental parameters in nMDS revealed a positive close correlation between the DO, nitrate and phosphate parameters, where graphically, these three parameters produced an angle between vector lines that were close to each other. This result can be interpreted such that if DO value is high, then the value of nitrate and phosphate in the waters is also high. This is further supported by Yolanda *et al.* (2016), who demonstrated that there was a positive relationship between DO and nitrate, where the oxygen content could help the decomposition process of organic

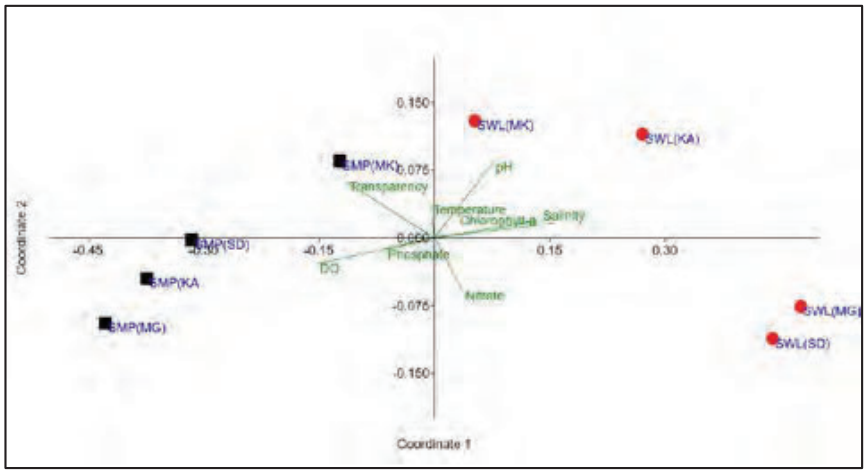

Fig. 4: nMDS analysis performance

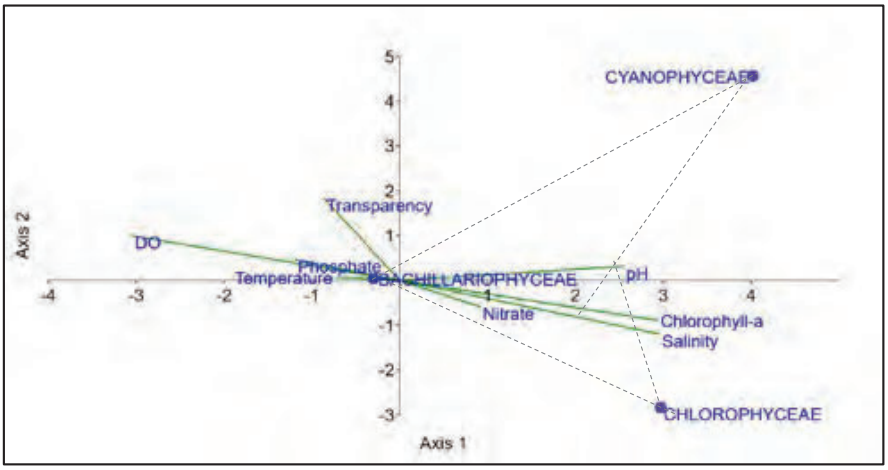

Fig. 5: CCA plot showing the relationship between the microalgal composition and environmental parameters

matter in the waters. The similar condition occurred for salinity, temperature, pH, chlorophyll-a, and transparency, where these environmental parameters formed an angle between vector lines that were close together. This means that if the salinity value is high, the pH, temperature and transparency values are also high.

Relationship of environmental parameters with microalgae distribution

In this study, the canonical correspondence analysis (CCA) was performed to determine the relationship between environmental parameters and the distribution of microalgae abundance (Fig. 5). The CCA analysis showed that the growth of Chlorophyceae and Cyanophyceae were positively correlated with the parameters of nitrate, pH, salinity and chlorophyll-a. This result is indicated by the projections of Chlorophyceae and Cyanophyceae, which were closer to the thick line on the nitrate parameter, pH, salinity and chlorophyll-a. Therefore, it can be assumed that the appearance of classes Chlorophyceae and Cyanophyceae is associated with high concentrations of nitrate, pH and salinity, and chlorophyll-a. This result is in accordance with Gardner *et al.* (2011), who demonstrated that an increase in nitrate will trigger an increase in pH as well as an increase in the photosynthesis process in Chlorophyceae and Cyanophyceae; hence, high abundance of Chlorophyceae and Cyanophyceae may increase chlorophyll-a (Kadim *et al.,* 2019). Additionally, Sari *et al.* (2019) also confirmed that nitrate plays an important role for the growth of plankton, especially in the class Cyanophyceae. The class Bacillariophyceae, on the other hand, is different from the classes Chlorophyceae and Cyanophyceae in terms of projection, where the class Bacillariophyceae was in the middle of the line. This indicates that the appearance of the class Bacillariophyceae is associated with all environmental parameters with moderate concentrations. The class Bacillariophyceae had a high abundance at Siwil Beach and Sempu Island, and this correlated with the measurement results of environmental parameters at Siwil Beach and Sempu Island, which were still classified as good waters for microalgae growth.

CONCLUSION

The present study demonstrated that the class Bacillariophyceae dominated the microalgae found in Siwil Beach and Sempu Island. At Siwil Beach, Cyanophyceae were found in sub-habitats of mangrove roots, macroalgae and the water column. Furthermore, microalgae from the class of Bacillariophyceae and Chlorophyceae were found in all sub-habitats; however, the numbers of Bacillariophyceae were greater than Chlorophyceae. Moreover, the microalgae found on Sempu Island in all sub-habitats were only from the Bacillariophyceae class, with the highest genus found in the sediment sub-habitat and the lowest genus found in the mangrove sub-habitat. Microalgae composition could be useful to determine ecosystem stability and

water quality in these waters. In addition, by knowing the distribution of microalgae in an area, it can be used as a source of germplasm. Based on the results of the nMDS analysis, there is no similarity in the composition of microalgae species on Siwil Beach and Sempu Island: both had a high variation of microalgae. Different uses also cause differences in the distribution of microalgae. Siwil Beach is used as a shrimp pond and Sempu Island is used for tourism and fishing activities such as painting boats and cleaning fishing nets. Factors that mainly affected the abundance of microalgae were the environmental factors in each sub-habitat at both locations. Siwil Beach and Sempu Island water quality was relatively still under the Indonesian national quality standard for seawater. Nevertheless, microalgae found on both sites were dominated from the class of Bacillariophyceae; thus, the water quality at Siwil Beach and Sempu Island has the potential to be poor. This research is thought to be the first step in exploring the diversity of microalgae in several sub-habitats in East Java, Indonesia, and linking the type and availability of microalgae found in various sub-habitats with environmental water quality parameters and human activities around the waters. In addition, this study provides the database information about the diversity of microalgae in Siwil Beach and Sempu Island in several sub-habitats including sediment, macroalgae, mangrove roots and water column in the southern part of East Java Indonesia. Next, phylogeny analysis needs to be carried out using molecular biology for microalgae found in several sub-habitats in Indonesia.

AUTHOR CONTRIBUTIONS

S. Arsad initiated the study design, prepared and edited the manuscript preparation, and provided the literature research. Y.W. Mulasari worked on data collection, statistical analyses, literature research and manuscript preparation. N.Y. Sari focused on data collection, statistical analyses, literature research and manuscript preparation. E.D. Lusiana prepared the statistical analyses. Y. Risjani interpretated the data. M. Musa participated on data interpretation. M. Mahmudi prepared the statistical analyses. F.S. Prasetiya performed the English grammatical correction. L.A. Sari performed the critical review of the manuscript.

ACKNOWLEDGEMENT

This study was financially supported by the Faculty of Fisheries and Marine Sciences through the Non-Tax State Revenue Fund (PNBP) Universitas Brawijaya Number: [DIPA-023.17.2.677512/2021], with the contract number: [54/UN10.F06.06/2021].

CONFLICT OF INTEREST

The authors declare no potential conflict of interest regarding the publication of this work. In addition, the ethical issues including plagiarism, informed consent, misconduct, data fabrication and, or falsification, double publication and, or submission, and redundancy have been completely witnessed by the authors.

OPEN ACCESS

PUBLISHER'S NOTE

GJESM Publisher remains neutral with regard to jurisdictional claims in published maps and institutional affiliations.

ABBREVIATIONS

%	Per cent
°C	Degree Celsius
‰	Per Mille
mm	Micro meter
CCA	Canonical correspondence analysis
cell/L	Cell per litre
cell/cm²	Cell per square centimetre
cm	Centimetre

cm^2	Square centimetre
DO	Dissolved oxygen
E	East longitude
et al.,	And others
Fig.	Figure
L	Litre
m	Meter
mg/L	Milligram per Litre
ml	Millilitre
nMDS	non-metric multidimensional scaling
PAST	Paleontological Statistics
pH	Power of hydrogen
PP	Peraturan Pemerintah (Government regulation)
ppm	Part per Million
S	South latitude
SD	Standard deviation
SE	Standard error
SMP SD	Sempu sediment
SMP MG	Sempu mangrove
SMP MK	Sempu macroalgae
SMP WC	Sempu water column
SWL SD	Siwil sediment
SWL MG	Siwil mangrove
SWL MK	Siwil macroalgae
SWL WC	Siwil water column

REFERENCES

Akcalan, A.R., (2020). Composition and Distribution of Benthic Diatoms in Different Habitats of Burdur River Basin. Turk. J. Water Sci. Manage., 4(1): 31–57 **(27 pages).**

Al Harbi, S.M., (2017). Epiphytic Microalgal Dynamics and Species Composition on Brown Seaweeds (Phaeophyceae) on the Northern Coast of Jeddah, Saudi Arabia. J. Oceanogr. Mar. Res., 5(1): 1–9 **(9 pages).**

Altaee, A.; Alanezi, A.A.; Hawari, A.H., (2018). Forward osmosis feasibility and potential future application for desalination. In Emerging Technologies for Sustainable Desalination Handbook. Book Capter 250–260 (**11 pages**).

Alvarenga, D.O.; Rigonato, J.; Branco, L.H.Z.; Fiore, M.F., (2015). Cyanobacteria in mangrove ecosystems. Biodivers. Conserv., 24: 799–817 **(19 pages).**

Anbuchezhian, R.; Karuppiah, V.; Li, Z., (2015). Prospect of marine algae for production of industrially important chemicals. In Algal Biorefinery: An Integrated Approach. Capital Publishing Company. Chapter 9: 195–217 **(23 pages).**

APHA, (1989). Standar methods for the examination of water and wastewater. American Public Control Federation. 20th edition, Washington DC. American Public Health Asosiation.

Arsad, S.; Zsalzsabil, N.A.N.; Prasetiya, F.S.; Safitri, I.; Saputra, D.K.; Musa, M., (2019). Komunitas mikroalga perifiton pada substrat berbeda dan perannya sebagai bioindikator perairan. SAINTEK PERIKANAN: Indonesian J. Fish. Sci. Technol., 15(1): 73–79 **(7 pages)**.

Arsad, S.; Putra, K.T.; Latifah, N.; Kadim, M.K.; Musa, M., (2021). Epiphytic microalgae community as aquatic bioindicator in Brantas River, east java, Indonesia. Biodiversity. 22(7): 2961–2971 **(11 pages)**.

Baklouti, L.A.; Feki, S.W.; Hamza, A.; Abdennadher, M.; Mahfoudhi, M.; Bouain, A.; Jarboui, O., (2018). Controlling factors of harmful microalgae distribution in water column, biofilm and sediment in shellfish production area (South of Sfax, Gulf of Gabes) from southern Tunisia. Cont. Shelf Res., 152: 1–30 **(30 pages)**.

Borchhardt, N.; Baum, C.; Mikhailyuk, T.; Karsten, U., (2017). Biological soil crusts of arctic svalbard-water availability as potential controlling factor for microalgal biodiversity. Front. Microbiol., 8: 1–12 **(12 pages)**.

Buczko, K.; Wojtal, A.Z.; Beszteri, B.; Magyari, E.K., (2015). Morphology and distribution of Navicula Schmassmannii and its transfer to genus Humidohila. Stud. Bot. Hung., 46(1): 25–41 **(17 pages)**.

Clark, W.J., (1981). The key organism-percent composition procedure: a microplankton enumeration technique. J. Freshwater Ecol., 1(2): 237-241 **(5 pages)**.

Diana, N.Z.L.; Sari, L.A.; Arsad, S.; Pursetyo, K.T.; Cahyoko, Y., (2021). Monitoring of phytoplankton abudance and chlorophyll-a content in the Estuary of Banjar Kemuning River, Sidoarjo Regency, East Java. J. Ecol. Eng., 22(1): 29–35 **(7 pages)**.

Essien, J.P.; Antai, S.P.; Benson, N.U., (2008). Microalgae biodiversity and biomass status in Qua Iboe Estuary mangrove swamp, Nigeria. Aquat. Ecol., 42: 71–81 **(11 pages)**.

Everest, A.; Aslan, D.C., (2016). Seasonal diatom density investigation of the Mersin Rivers. World J. Res. Rev., 2(5): 21–30 **(10 pages)**.

Fan, G.; Chen, Z.; Xia, M.; Du, B.; Bao, M.; Wu, S.; Zhan, J.; Luo, J., (2021). Optimization of remedial nano-agent and its effect on dominant algal species succession in eutrophic water body. J. Environ. Manage., 281(1): 123–234 **(112 pages)**.

Farhadian, O.; Pouladi, M.; Vazirizadeh, A.; Sedaghat, R., (2015). A study of diatoms seasonal distribution and biodiversity in Helleh River Estuary, Persian Gulf. Environ. Stud. Persian Gulf. 2(1): 32–44 **(13 pages)**.

García, V.S.; Uriza, E.A.C.; Israde, I.; Maidana, N., (2012). Epilithic diatoms (Bacillariophyceae) as indicators of water quality in the Upper Lerma River, Mexico. Hidrobiologica, 22(1): 16-27 **(12 pages)**.

Gardner, R.; Peters, P.; Peyton, B.; Cooksey, K.E., (2011). Medium pH and nitrate concentration effects on accumulation of triacylglycerol in two members of the chlorophyta. J. Appl. Phycol., 23(6): 1005–1016 **(12 pages)**.

Hopes, A.; Mock, T., (2015). Evolution of microalgae and their adaptations in different marine ecosystem. In eLS. **(9 pages)**.

Houk, V.; König, C.; Klee, R., (2015). Cyclotella hinziae sp. nov. a small Cyclotella (Bacillariophyceae) from subalpine lake Schliersee (Bavaria, Germany). J. Czech Phycol. Soc., 15(2): 235–243 **(9 pages)**.

Kadim, M.K.; Arsad, S., (2016). Distribution and abudance of microalgae based on coastal characteristic and ecology in Bone Bolango Coastal Region, Indonesia. Asian J. Microbiol., Biotechnol., Environ. Sci., 18(2): 395–401 **(7 pages)**.

Kadim, M.K.; Pasisingi, N.; Arsad, S., (2019). Horizontal distribution of chlorophyll-α in the Gorontalo Bay. Nat. Environ. Pollut. Technol., 18(4): 1381–1385 **(5 pages)**.

Klein, G., (2017). Biological synopsis of phytoplankton new to the Bay of Fundy Biological Synopsis of Phytoplankton Fisheries and Oceans Canada Science Branch Maritimes Region St . Andrews Biological Station 531 Brandy Cove Road Canadian Manuscript. Rep. Fish. Can. Manuscr. Rep. Fish. Aquat., 37(5): 1–37 **(38 pages)**.

Kusumaningsari, S.D.; Hendrarto, B.; Ruswahyuni., (2015). Kelimpahan hewan makrobentos pada dua umur tanam rhizophora sp. di Kelurahan Mangunharjo, Semarang. Diponegoro J. Maquares., 4(2): 58-64 (**6 pages**).

Kwon, D.; Park, M.; Lee, C.S.; Park, C.; Lee, S.D., (2021). New records of the diatoms (Bacillariophyceae) from the coastal lagoons in Korea. J. Mar. Sci. Eng., 9(7): 1–13 **(13 pages)**.

Marsela, K.; Hamdani, H.; Anna, Z.; Herawati, H., (2021). The relation of nitrate and phosphate to phytoplankton abundance in the upstream Citarum River, West Java, Indonesia. Asian J. Fish. Aquat. Res., 11(5): 21–31 **(11 pages)**.

Mucko, M.; Bosak, S.; Mann, D.G.; Trobajo, R.; Wetzel, C.E.; Peharec, Š.P.; Ljubešić, Z., (2021). A polyphasic approach to the study of the genus Nitzschia (Bacillariophyta): three new planktonic species from the Adriatic Sea. J. Phycol., 57: 145–159 **(15 pages)**.

Musa, M.; Arsad, S.; Sari, L.A.; Lusiana, E.D.; Kasitowati, R.D.; Yulinda, E.N.; Nadhira, T.; Cahyani, D., (2021). Does Tofu Wastewater Conversions Nutrient Increase the Content of the Chlorella pyrenoidosa? J. Ecol. Eng., 22(2): 70–76 **(7 pages)**.

Nurhayati, C.; Hamzah, B.; Pambayun, R., (2014). Pengaruh pH, konsentrasi isolat Chlorella vulgaris dan waktu pengamatan terhadap tingkat cemaran limbah cair crumb rubber. J. Dinamika Penelitian Industri, 25(2): 97-106 **(10 pages)**.

Patty, S.I.; Arfah, H.; Abdul, M.S., (2015). Zat hara (fosfat, nitrat), oksigen terlarut dan pH kaitannya dengan kesuburan di perairan Jikumerasa, Pulau Buru. J. Pesisir dan Laut Tropis, 1(1): 43–50 **(8 pages)**.

Peraturan Pemerintah, (2021). Peraturan Pemerintah Republik Indonesia (Government Regulations of Republic Indonesia: PP No. 22) No. 22 Tahun 2021 tentang penyelenggaraan perlindungan dan pengelolaan lingkungan hidup **(483 pages)**.

Pikoli, M.R.; Sari, A.F.; Solihat, N.A.; Permana, A.H., (2019). Characteristics of tropical freshwater microalgae Micractinium conductrix, Monoraphidium sp. and Choricystis parasitica, and their potency as biodiesel feedstock. Heliyon, 5(12): 1–9 **(9 pages)**.

Prazukin, A.; Shadrin, N.; Balycheva, D.; Firsov, Y.; Lee, R.; Anufriieva, E., (2021). Cladophora spp. (Chlorophyta) modulate environment and create a habitat for microalgae in hypersaline waters. Eur. J. Phycol., 1–14 **(14 pages)**.

Ratomski, P.; Hawrot P.M., (2021). Influence of nutrient-stress conditions on chlorella vulgaris biomass production and lipid content. Catalysts, 11(573): 2–13 **(12 pages)**.

Rawat, U.S.; Agarwal, N.K., (2015). Biodiversity: Concept, threats and conservation. Enviro. Conserv. J., 16(3): 19–28 **(10 pages)**.

Risjani, Y.; Witkowski, A.; Kryk, A.; Yunianta, G.E.; Krzywda, M.; Safitri, I.; Sapar, A.; Dąbek, P.; Arsad, S.; Gusev, E.; Rudiyansyah P.L.; Wróbel, R.J., (2021). Indonesian coral reef habitats reveal exceptionally high species richness and biodiversity of diatom assemblages. Estuarine, Coastal and Shelf Sci., 261.

Kramer, S., (2015). The relationship between nitrate concentration and phytoplankton blooms in harpswell sound. Bowdoin Digital Common, 23 **(3 pages)**.

Safi, K.A., (2003). Microalgal populations of three New Zealand coastal locations: Forcing functions and benthic-pelagic links. Mar. Ecol. Prog. Ser., 259: 67–78 **(12 pages).**

Sari, L.A.; Pursetyo, K.T.; Arsad, S.; Masithah, E.D.; Setiawan, E.; Affandi, M., (2019). The effect of nutrient abundance on distribution of cyanobacteria and chlorophyll-a in sedati water, Sidoarjo. Pollut. Res. Pap., 38: 38-43 **(6 pages)**.

Shannon, C.E., (1948). The Mathematical Theory of Communication. The Bell Syst. Tech. J., 27: 623-656 **(34 pages).**

Silva, D.W.J.; Ruwer, D.; Nogueira, I.; Dunck, B., (2016). The genus Pinnularia (Bacillariophyta, Pinnulariaceae) from Lago dos Tigres, Britania, Goias, Brazil. Biota Neotrop., 16(1): 1–26 **(27 pages)**.

Tang, D.Y.Y.; Khoo, K.S.; Chew, K.W.; Tao, Y.; Ho, S.H.; Show, P.L., (2020). Potential utilization of bioproducts from microalgae for the quality enhancement of natural products. Bioresour. Technol., 1–11 **(11 pages)**.

Vijver, B.V.D.; Zidarova, R.; Sterken, M.; Verleven, E.; Haan, M.D.; Vyverman, W.; Hinz, F.; Sabbe, K., (2011). Revision of the genus Navicula s. S. (Bacillariophyceae) in inland waters of the Sub-Antartic and Antartic with the dscription of five new species. Phycologia, 50(3): 281–297 **(17 pages)**.

Winahyu, D.A.; Anggraini, Y.; Rustiati, E.L.; Master, J.; Setiawan, A., (2013). Studi pendahuluan mengenai keanekaragaman mikroalga di pusat konservasi gajah, Taman Nasional Way Kambas. Prosiding Semirata FMIPA Universitas Lampung.

Yin, Z.; Zhu, L.; Li, S.; Hu, T.; Chu, R.; Mo, F.; Hu, D.; Liu, C.; Li, B., (2020). A comprehensive review on cultivation and harvesting of microalgae for biodiesel production: Environmental pollution control and future directions. Bioresour. Technol., 1–19 **(19 pages)**.

Yolanda, D.S.; Muhsoni, F.; Siswanto, A., (2016). Distribusi nitrat, oksigen terlarut, dan suhu di Perairan Socah-Kamal Kabupaten Bangkalan. J. Kelautan, 9(2): 93-98 **(6 pages)**.

Zadorozhna, H.; Semeniuk, N.; Shcherbak, V., (2017). Interaction between Phytoplankton and Epiphytic Algae in the Kaniv Water Reservoir (Ukraine). Int. Lett. Nat. Sci., 61: 56–68 **(13 pages).**

AUTHOR (S) BIOSKETCHES

Arsad, S., M.Sc., Assistant Professor, [1]Department of Aquatic Resources Management, Faculty of Fisheries and Marine Science, Universitas Brawijaya, Jl. Veteran Malang 65145, Indonesia. [2]Aquatic Resources and Ecological Research Group (AquaRES), Faculty of Fisheries and Marine Science, Universitas Brawijaya, Jl. Veteran Malang 65145, Indonesia. [3]Microbiol Resources and Technology Group, Post-graduate program Universitas Brawijaya, Jl. Veteran Malang 65145, Jawa Timur Indonesia.

- Email: *sulastriarsad@ub.ac.id*
- ORCID: 0000-0002-7322-7834
- Web of Science ResearcherID: ABG-9716-2021
- Scopus Author ID: 56239034700
- Homepage: https://fpik.ub.ac.id/en/dosen/

AUTHOR (S) BIOSKETCHES (Continued)

Mulasari, Y.W., B.Sc., Department of Aquatic Resources Management, Faculty of Fisheries and Marine Science, Universitas Brawijaya, Jl. Veteran Malang 65145, Indonesia.
- Email: *yasinta.wenda@student.ub.ac.id*
- ORCID: 0000-0001-7618-1993
- Web of Science ResearcherID: NA
- Scopus Author ID: NA
- Homepage: https://fpik.ub.ac.id/en/alumni/

Sari, N.Y., B.Sc., Department of Aquatic Resources Management, Faculty of Fisheries and Marine Science, Universitas Brawijaya, Jl. Veteran Malang 65145, Indonesia.
- Email: *nita_yuliana@student.ub.ac.id*
- ORCID: 0000-0002-8241-9096
- Web of Science ResearcherID: NA
- Scopus Author ID: NA
- Homepage: https://fpik.ub.ac.id/en/alumni/

Lusiana, E.D., M.Sc., Assistant Professor, [1]Department of Aquatic Resources Management, Faculty of Fisheries and Marine Science, Universitas Brawijaya, Jl. Veteran Malang 65145, Indonesia. [2]Aquatic Resources and Ecological Research Group (AquaRES), Faculty of Fisheries and Marine Science, Universitas Brawijaya, Jl. Veteran Malang 65145, Indonesia. [3]Microbiol Resources and Technology (MicroBase) Group, Post-graduate program Universitas Brawijaya, Jl. Veteran Malang 65145, Jawa Timur Indonesia.
- Email: *evellinlusiana@ub.ac.id*
- ORCID: 0000-0001-8672-3661
- Web of Science ResearcherID: AAB-7081-2021
- Scopus Author ID: 57199329869
- Homepage: https://fpik.ub.ac.id/en/dosen/

Risjani, Y., Ph.D., Professor, [1]Department of Aquatic Resources Management, Faculty of Fisheries and Marine Science, Universitas Brawijaya, Jl. Veteran Malang 65145, Indonesia. [2]BioECOTOX Research Group, Faculty of Fisheries and Marine Science, Universitas Brawijaya, Jl. Veteran Malang 65145, Indonesia.
- Email: *risjani@ub.ac.id*
- ORCID: 0000-0002-6191-5824
- Web of Science ResearcherID: AAP-5118-2020
- Scopus Author ID: 55210896000

Homepage: https://fpik.ub.ac.id/en/dosen/

Musa, M., Ph.D., Professor, [1]Department of Aquatic Resources Management, Faculty of Fisheries and Marine Science, Universitas Brawijaya, Jl. Veteran Malang 65145, Indonesia. [2]Aquatic Resources and Ecological Research Group (AquaRES), Faculty of Fisheries and Marine Science, Universitas Brawijaya, Jl. Veteran Malang 65145, Indonesia. [3]Microbiol Resources and Technology Group, Post-graduate program Universitas Brawijaya, Jl. Veteran Malang 65145, Jawa Timur Indonesia.
- Email: *musa_fpi@ub.ac.id*
- ORCID: 0000-0003-3352-7725
- Web of Science ResearcherID: NA
- Scopus Author ID: 53980003100
- Homepage: https://fpik.ub.ac.id/en/dosen/

Mahmudi, M., Ph.D., Associate Professor, [1]Department of Aquatic Resources Management, Faculty of Fisheries and Marine Science, Universitas Brawijaya, Jl. Veteran Malang 65145, Indonesia. [2]Aquatic Resources and Ecological Research Group, Faculty of Fisheries and Marine Science, Universitas Brawijaya, Jl. Veteran Malang 65145, Indonesia.
- Email: *mudi@ub.ac.id*
- ORCID: 0000-0001-7303-5675
- Web of Science ResearcherID: NA
- Scopus Author ID: 57191167767
- Homepage: https://fpik.ub.ac.id/en/dosen/

Prasetiya, F.S., Ph.D., Assistant Professor, Marine Science Department, Faculty of Fisheries and Marine Sciences, Universitas Padjadjaran, Jl. Raya Bandung Sumedang KM. 21, 45363 Jatinangor, Indonesia.
- Email: *fiddy.semba.prasetiya@unpad.ac.id*
- ORCID: 0000-0001-6474-2319
- Web of Science ResearcherID: ABH-1561-2021
- Scopus Author ID: 56239582500
- Homepage: https://fpik.unpad.ac.id/departemen-kelautan/

Sari, L.A., M.Sc., Assistant Professor, Department of Fish Health Management and Aquaculture, Faculty of Fisheries and Marine Universitas Airlangga, Surabaya 60115, Indonesia.
- Email: *luthfianaas@fpk.unair.ac.id*
- ORCID: 0000-0001-7387-9958
- Web of Science ResearcherID: NA
- Scopus Author ID: 57201778593
- Homepage: https://fpk.unair.ac.id/dosen-departemen-akuakultur/

HOW TO CITE THIS ARTICLE

Arsad, S.; Mulasari, Y.W.; Sari, N.Y.; Lusiana, E.D.; Risjani, Y.; Musa, M.; Mahmudi, M.; Prasetiya, F.S.; Sari, L.A. (2022). Microalgae diversity in several different sub-habitats. Global J. Environ. Sci. Manage., 8(4): 561-574.

DOI: 10.22034/gjesm.2022.04.08

url: https://www.gjesm.net/article_249637.html

Global J. Environ. Sci. Manage. 8(4): 575-588, Autumn 2022, Serial #32

Global Journal of Environmental Science and Management
(GJESM)

Homepage: https://www.gjesm.net/

CASE STUDY

Phosphorus recovery from domestic sewage sludge in the presence of waste grape pruning biochar

M. Piri, E. Sepehr

Department of Soil Science, Faculty of Agriculture, Urmia University, Iran

ARTICLE INFO

Article History:
Received 12 December 2021
Revised 02 March 2022
Accepted 02 April 2022

Keywords:
Biochar
Citric acid
Digested sewage sludge
Recycling
Slow-release fertilizer
Struvite precipitates

DOI: 10.22034/gjesm.2022.04.09

ABSTRACT

BACKGROUND AND OBJECTIVES: Phosphorus is an essential and limiting nutrient for all living organisms. Although phosphorus is a finite resource on earth, it is usually wasted today. Precipitation of struvite from waste residues is mainly carried out to recover phosphorus. This study aimed to investigate the percentage of phosphorous recovery from sewage sludge in the presence of grape-biochar via the formation of biochar/struvite precipitates.

METHODS: Different amounts of grape-biochar were applied to recover nutrients (phosphorus, nitrogen, and magnesium) from sewage sludge via the formation of struvite by digestion of sewage sludge with H_2SO_4 and the molar ratio of magnesium/ ammonium/ phosphorus in 2:1:1 at pH=8.5. Solubility and release properties of the precipitates were determined and the equations, such as first-order, parabolic diffusion, power function, and simple Elovich models, were fitted to the kinetic data.

FINDINGS: The phosphorus recovery from sewage sludge increased by application of grape biochar in the precipitation system, and the accumulation release of nutrients (phosphorus, nitrogen, and magnesium) from samples increased in the presence of grape biochar, especially in high amounts. Increasing the remove and recovery of phosphorus from sewage sludge by application of grape-biochar decreased the incidence of eutrophication, as an environmental dilemma, and provided the requirement for phosphorus-fertilizers by solid waste management. The solubility of the samples was 0.5 mole per liter hydrochloric acid > in 20 gram per liter citric acid > water. The results showed that the phosphorus- cumulative - release of composites in water good fitted the parabolic kinetic model (R^2=0.97-0.99), whereas it followed the simple Elovich model (R^2=0.86-0.92) in 0.5 mole per liter hydrochloric acid and first-order kinetics model (R^2=0.76-0.92) in 20 gram per liter critic acid.

CONCLUSION: The results indicated that the presence of grape-biochar for recovery of phosphorus from sludge as struvite had a good potential for increasing the release of nutrients for the formation of struvite, and these precipitates had a high potential to be used as a slow-release phosphorus-fertilizer.

NUMBER OF REFERENCES	NUMBER OF FIGURES	NUMBER OF TABLES
47	3	8

*Corresponding Author:
Email: *ma.piri@urmia.ac.ir*
Phone: +914 883 7751
ORCID: 0000-0003-0042-5060

Note: Discussion period for this manuscript open until January 1, 2023 on GJESM website at the "Show Article".

INTRODUCTION

Phosphorus (P) is a key element for life on the earth, facing various limitations for crop production. Being a nonrenewable P source and having different interactions with soil components have attracted the globe's attention to the management of unsustainable P fertilizer (Tosun, 2021). The world's mining of nonrenewable phosphate rock for production of P-fertilizers, such as ammonium phosphates and superphosphates, is running out (Li *et al*., 2018). Therefore, dependency on minable P-sources should be developed procedures for recovering any P-rich resources, especially from residues and secondary raw P (Yetilmezsoy *et al*., 2017). The European Union (EU) confirmed this by putting phosphate rock on its list of critical raw materials in 2014 (Muys *et al*., 2021). Sewage sludge (SS) from municipal solid waste is determined by high value of P_2O_5 (about 4-26%), and nearly 80-90% of P-sewage accumulated in SS (Semerci *et al*., 2020) is determined as a potential p-resource (Adam *et al*., 2009). Accordingly, recovery of the nutrients, especially P and N, from SS has been a noteworthy option and recently received great attention. Chemical precipitation is considered as an important process for recovering the elements (P, Mg, and N) as struvite (magnesium ammonium phosphate hexahydrate), $MgNH_4PO_4.6H_2O$ for reuse of essential ions in SS (Koga 2019; Kim *et al*., 2018). This procedure not only recovers phosphorus, decreasing the emphasis on restricted non-production phosphate rock sources, but also decreases the P content that would, in other ways, be poured into aquatic environments (Rahman *et al*., 2014). P-rich wastewater provides eutrophication and harmful algal blooms which threaten the aquatic ecosystems (Siciliano *et al*., 2016; De *et al*., 2016). Struvite is a P-mineral that can be applied as a slow-releasing agricultural fertilizer by providing Mg, P, and N for plant growth (Muys *et al*., 2021). There are possible benefits in low solubility of struvite in water compared to more soluble conventional P-fertilizers. However, struvite is a root-activated mineral because it has good solubility in acid citric that exudates from roots (Hertzberger *et al*., 2020). Slow-release properties of struvite could reduce losses of nutrients by precipitation and leaching, leading to enhanced crop response to the application of fertilizer (Hertzberger *et al*., 2020). The nutrient release from fertilizers has been specified as a worldwide challenge for the agricultural part in plant nutrition management. The formation of struvite creates in the alkaline range of pH (7<pH<11) and includes 13% P, 6% N, and 10% Mg (Egle *et al*., 2016). The recovery of P content, as struvite, can be influenced by various operating parameters, including pH, the molar ratio of Mg^{2+}: NH_4^+: PO_4^{3-}, time, reaction temperature, organic matter, the presence of other ions, the ratio of liquid/solid (L/S), *etc.* (Doyle and Parsons, 2002). Previous researches on P recovery from P-rich effluent/wastewater and SS have been presented in Table 1. Biochar is determined as an efficient substance for the recovery of surplus nutrients, containing P, from aqueous solutions (Dugdug *et al*., 2018). Biochar is a type of organic material created by the pyrolysis of agricultural wastes and other biomass at 300–1500 °C in oxygen-free conditions, and it has been reported for usage as a P sorbent (Lehmann and Joseph, 2015). Sorption of P by biochar from aqueous solutions accrues through precipitation of P with Mg (Shepherd *et al*., 2016). Increasing sorption of P by application of biochar can be due to its high surface area and AEC (anion exchange capacity) (Lehmann *et al*., 2015). Many materials were recommended for increasing the recycling efficiency for the formation of struvite, including quartz, steel mesh, pumice, and borosilicate glass (Le Corre *et al*., 2007). Consumption of the biochar with high surface area, CEC (cation exchange capacity) and porosity is eco-friendly in the crystallization of struvite to ameliorate nutrient recovery for application of fertilizer and can be used as a good strategy (Muhmood *et al*., 2019). Hu *et al*., (2019) reported the recovery rates of P, Mg, and N increased for precipitation of struvite by application of the biochar obtained from straw and wheat shells. Muhmood *et al*., (2019) showed that wheat straw biochar and rice husk biochar as seeding materials in the precipitation of the struvite from digested chicken slurry increased the formation of struvite and intensified element recovery. Enhancing the recovery of nutrients is necessary to examine many eco-friendly materials, such as biochar of grape residues (Gr) from pruning manufactured in high amounts in vineyards, in struvite precipitation process. To the best of the authors' knowledge, the use of Gr-biochar, as seeding material, in the struvite

Table 1: Summary of the recent studies about P-recovery

Relevant aspects	References
The current study was designed to use a different light spectrum to enhance carbon-based metal nanocomposites adsorbent for the augmented removal of nitrate and phosphate from aqueous solution. The revealed nanocomposites increased the removal of nitrate and phosphate ions up to 95%.	Velu *et al.,* (2020)
Acceptable phosphorus recovery (80-90%) was achievable by using seawater as the magnesium source for struvite precipitation. The increase of temperature from 20 °C to 30 °C reduced the phosphorus recovery.	Shaddel *et al.,* (2020)
This manuscript provides a comprehensive review on the recent developments related to the removal and recovery of nutrients (nitrogen and phosphorus) from aqueous waste and wastewater.	Siciliano *et al.,* (2020)
This paper reviews the recent studies on the potential of aquatic plants, such as free-floating, submerged, and emergent plants, and microalgae for the removal of P in different types of wastewater.	Rezania *et al.,* (2021)
The P extraction from P-rich sludge with oxalic acid proved to be effective for P- extraction and iron removal prior to struvite precipitation. Due to the high iron concentration in liquor, the product of direct precipitation contains a high amount of iron that limits its use as phosphate fertilizer.	Numviyimana *et al*., (2022)

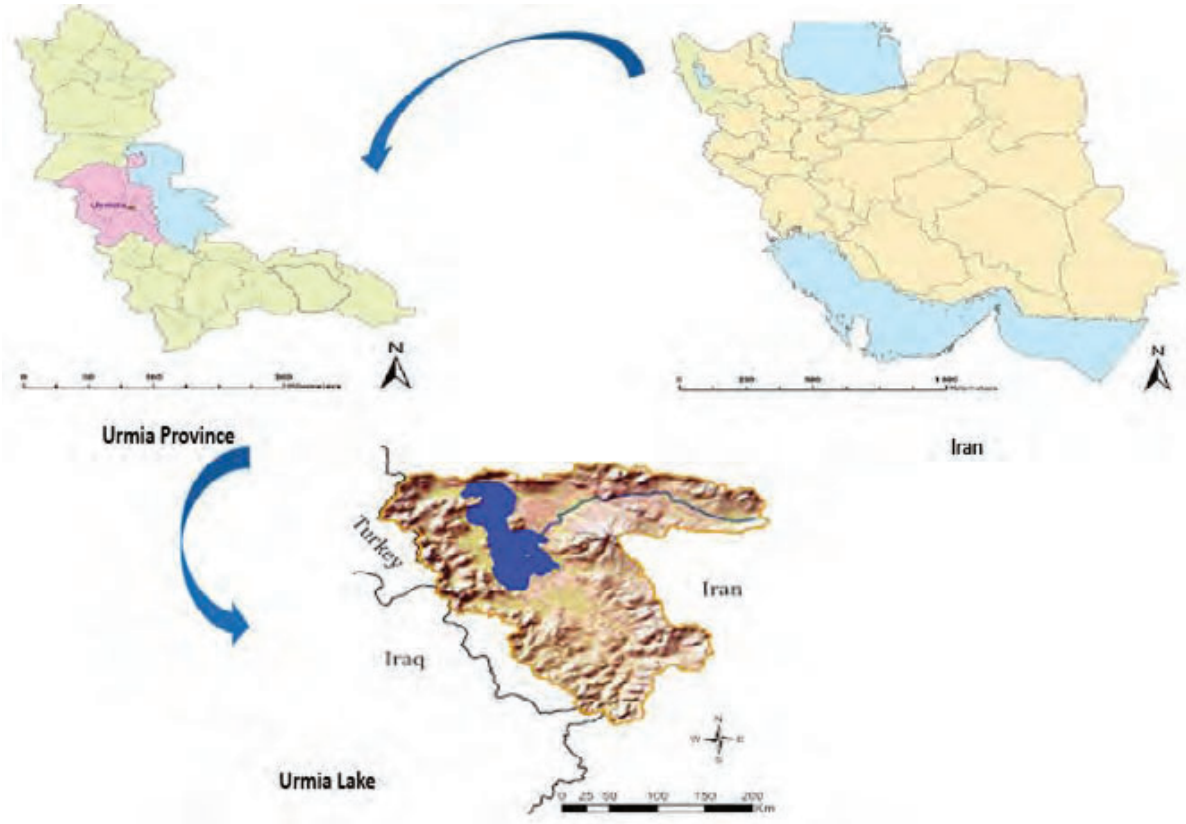

Fig. 1: Geographic location of the study area in Urmia, West Azerbaijan province, Iran

precipitation process has not been investigated yet. The objectives of this study were to: 1) reuse P as struvite and composites of struvite/biochar from sewage sludge; 2) investigate the efficacy of different values of Gr-biochar on the recovery of nutrients (P, N, and Mg); and 3) study the ability of P, Mg, and N ions to be dissolved and examine their slow-release-properties in composites of struvite/biochar. This study aimed to contribute to the environmentally friendly process of P-recovery via struvite precipitation by solid waste management. This study was carried out at the Soil Department of Urmia University, Urmia, Iran, during 2021-2022.

MATERIALS AND METHODS

Preparation of sewage sludge (SS) and biochar of grape residues (Gr-biochar)

Dewatered sewage sludge (SS) was sampled from a domestic wastewater treatment plant in Urmia (37° 35' 37.1" N 45° 07' 43.7" E), West Azerbaijan Province, Iran (Fig. 1).

The SS was air-dried and sieved to pass a 1 mm. Some physicochemical properties of SS, such as total organic carbon (TOC), electrical conductivity (EC), pH, total nitrogen (TN), ammonia nitrogen (NH_4^+-N), total phosphorus (TP), orthophosphate (PO_4^{3-}-P) and potassium content (K), were determined according to Semerci *et al.*, (2019). Total recoverable concentrations of metals (Ca, Mg, Na, Fe, Zn, Cu, Pb, and Cd) were also determined (Malwina, 2019). The grape pruning residues applied to prepare biochar were collected from vineyards in the West Azerbaijan Province, Iran. The grape cane was cut into small pieces and put into an oxygen-free cast iron bioreactor. The Gr-biochar was gathered by pyrolysis at 500 degrees Celsius (°C) at 10 degrees Celsius per minute (°C/min) heating rate for 2 hours (h). The prepared Gr-biochar was then ground and sieved (through a 0.5 mm sieve) for application as seeding materials for the production of struvite. The Gr-biochar was analyzed for some physicochemical properties.

P-extraction experiment

To extract P from SS, two steps were carried out: 1) digestion of H_2SO_4 0.2 N (98% Merck, Germany) into a solid to liquid ratio of 1:10; 2) precipitation. Prior to P-precipitation, citric acid ($C_6H_8O_7$) (50% w/v) (Sigma-Aldrich) was added, as a chelating agent, for the removal of heavy metals. Using sodium hydroxide (NaOH) 5N (>98% Sigma-Aldrich), the potential of hydrogen (pH) of the solution raised to 8.5 after adding $MgCl_2.6H_2O$ (Sigma-Aldrich) as Mg source (Meyer *et al.*, 2015). The precipitation was conducted at 2:1:1 molar ratios of Mg^{2+} /PO_4^{3-}/ NH^{4+} respectively, at room temperature and stirring speed of 150 rpm for 30 min, and finally stayed for 30 min for reacting. Then, the solution rested for 30 min to influence the precipitation of struvite (Huang *et al.*, 2015). Samples were filtered through Whatman No. 42 and allowed oven-dried at 40 °C for 48 h, weighed, and applied for analyzing the nutrient and metal contents. To obtain struvite/biochar precipitations, the Gr-biochar was used in 0, 2.33, 7, and 21 g of Gr-biochar (the ratios of the struvite mass to GR-biochar of 0%:100%, 75%:25%, 50%:50%, and 25%:75%). After shaking the solution for 30 min and leaving to rest for 24 h at room temperature (Hu *et al.*, 2019), it was washed up to pH of 7. The P-recovery was evaluated using Eq. 1.

$$\text{P-recovery\%} = \left(\frac{P_i - P_F}{P_i}\right) \times 100 \quad (1)$$

Where, P_i is the initial concentration of P mg/L; and P_F is the final concentration of P mg/L.

The composites of struvite/biochar were analyzed by XRF for the determination of chemical composition. Content of the metals was determined by inductively coupled plasma optical emission spectroscopy (Varian, Vista-Pro-ICP-OES). Surface morphology of precipitates was recognized by Scanning Electron Microscopy (SEM- XL 30-Philips).

Solubility struvite/ GR-biochar composites

The HG 2598-94 protocol was applied to determine the solubility of the precipitates (Hu *et al.*, 2019). One gram of the precipitates, 150 mL of HCl 0.50 mole per liter (mol/L) (98% Sigma-Aldrich) and 20 gram per liter (g/L) of citric acid (CA) were applied, respectively. Then, the solution was shaken in a 250-mL volumetric flask (80 min at 180 rpm), and the P contents in the samples were evaluated by an ultraviolet light (UV) spectrophotometer (Shimadzu UV3100) by monitoring the absorbance changes at 470 nanometers (nm). The Mg content was assessed by the titrimetric method using Ethylene diamine tetra acetic acid (EDTA) (99%- Sigma-Aldrich). To determine the N-concentration, the titrimetric

method was applied after distillation.

Kinetics and slow-release properties

Release properties of the samples were evaluated according to the GB 23348 2009 protocol (Hu *et al.* 2018). One gram of each precipitate was added to 20 mL of deionized water in a 50-mL volumetric flask and placed in an incubator at 25 °C. To determine the amounts of N, P, and Mg in the solutions, they were filtered in intervals of 24 h after 3, 5, 10, 14, 28, 42, 56, and 84 days. The cumulative release values (%) of N, P and Mg were determined according to Eq. 2.

$$\text{Accumulative release (\%)} = \frac{C_t \times V}{M_{total}} \times 100 \quad (2)$$

Where, c_t is the concentration of N, Mg and P (mg/kg) at different times; and M_{total} is the total nutrient amount in the sample. To evaluate the release mechanism of the elements, four kinetic equations, including the first order (Eq. 3), power function (Eq. 4), parabolic diffusion (Eq. 5), and simple Elovich models (Eq. 6), were applied to fit the results (Jalali 2006).

$$\text{First−order model: } \ln(q_0 - q_t) = a - bt \quad (3)$$

$$\text{Power function model: } lnq = lna + b\,lnt \quad (4)$$

$$\text{Parabolic diffusion model: } q = a + bt^{1/2} \quad (5)$$

$$\text{Elovich model: } q = a + lnt \quad (6)$$

Where, q is the cumulative release of the elements; t is the time of release; and a and b are the constants of the equations. b is an essential parameter in these models, which shows the release rate of the ions. The coefficients of determination (R^2) were applied to determine the best model describing the release mechanism process.

RESULTS AND DISCUSSION

Properties of SS and Gr-biochar

Some characteristics of the SS are presented in Tables 2 and 3. The total phosphorus and total nitrogen in SS were more than 1.5%. The main chemical composites of SS were SiO_2, CaO, P_2O_5, Fe_2O_3, and Al_2O_3 (Table 3). The P_2O_5 content in the SS sample had a potential of P-source and providing source conservation (Shiba and Ntuli, 2016; Adam *et al.*, 2009). The pH and EC of SS were 6.6 and 1.79, respectively.

The amount of heavy metals (Pb, Cd, Zn, Cr, Cu and Ni) in SS was lower than the standard concentration limit in sludge as using fertilizer (Xu *et al.*, 2012). The total ratio of aluminum and iron to phosphorus is a valuable index for the P-supplying power of a SS (Shiba and Ntuli, 2016). The molar ratio of the sum of the aluminum and iron to phosphorus is an okay indicator for the P-reserving power of a SS, with amounts < 1 being characteristic of a SS able to supply high amounts of soluble P (Pastene, 1981). The molar ratio of Al + Fe/P for the SS applied in this study was obtained to be more than the ratio reported based on ICP results (Table 2), indicating a meager potential for P-supply. This factor determined the limitation for direct application of the SS as a fertilizer.

The physicochemical properties of GR-biochar and other biochars are presented in Table 4. Surface area of the Gr-biochar was 277 m^2/g, and its pH was 9.6, suggesting an alkaline characteristic. Evidently, the pH of the Gr-biochar was different from the pH of the wheat shell and other biochars (Hu *et al.*, 2019; Lu *et al.* 2016; Park *et al.*, 2011).

Table 2: Chemical properties of sewage sludge

pH	$EC_{(1:5)}$	TOC (%)	TP	NH_4^+-N	TN	Mg	Na	K	Moisture
	dS/m				mg/kg				%
6.6	1.79	48	15927	904	18605	6513	2967	11207	14.03
Total concentration of metals (mg/kg)									
Pb	Cd	Fe	Zn	Al	Cr	As	Cu	Ni	Ag
57	0.32	13230	731	21063	18	1.9	179	30	2.3
Heavy metal concentration limit (EPA 503)									
750-1200	20-40	-	2500-4000	-	25	-	1000-1750	300-400	-

EC: electrical conductivity; PO_4^{3-}P: orthophosphate; TP: total phosphorus; TN: total nitrogen; TOC: total organic carbon

Table 3: Chemical composition of sewage sludge

Constituent	Sample	Adam *et al.* (2009)	Ntuli *et al.* (2013)	Shiba and Ntuli (2016)
P_2O_5	4.00	3-25	14.6	15.2
SiO_2	14.48	13-43	38.4	36.40
CaO	11.33	12-18	11.0	11.3
Fe_2O_3	1.89	3.2-22	10.3	12.2
SO_3	1.57	-	5.5	5.31
Al_2O_3	3.93	8-24	11.9	12.0
MgO	1.08	1.7-3.5	1.7	1.04
K_2O	1.35	0.95-2.7	1.7	1.79
MnO	<0.05	0.09-0.35	0.6	0.613
TiO_2	0.32	-	1.1	1.16

Table 4: Some properties of Gr-biochar

Biochar	pH	EC (dS/m)	C	N	H	CEC ($cmol_c/kg$)	Surface aria (m^2/g)	Ash (%)	References
Grape	9.6	0.2	71	0.87	2.9	34	277	11	This study
wheat shell	7.3	-	-	-	-	77.8	168.3	-	Hu *et al.*, 2019
Rice straw	10.1	-	51	1.66	1.70	43	37	-	Lu *et al.*, 2016
Green waste	7.7	-	77	0.26	2.6	250	6.87		Park *et al.*, 2011

EC: electrical conductivity; CEC: cation exchange capacity.

Table 5: Chemical analysis of composites (struvite:Gr-biochar)

Struvite (%): Biochar (%)	SiO_2	Al_2O_3	BaO	P_2O_5	Fe_2O_3	MgO	Na_2O	SO_3	K_2O	CaO	TiO_2
					(%)						
100:0	0.53	1.05	<0.05	28.19	2.77	16.51	1.45	1.38	1.59	14.77	<0.05
75:25	1.36	0.86	<0.05	25.40	0.30	11.53	0.85	2.36	0.22	14.27	<0.05
50:50	0.72	0.75	<0.05	22.63	0.16	10.23	1.06	0.78	0.34	9.32	<0.05
25:75	0.43	0.65	<0.05	13.44	0.43	7.17	1.37	1.30	0.65	4.22	<0.05

Table 6: Properties of composites (struvite: biochar)

Parameter	%struvite:%biochar				EU fertilizer limit (Muys *et al.*, 2021)
%	100:0	75:25	50:50	25:75	
P	12.67	10.36	9.38	6.27	-
N	8.40	7.46	5.60	4.60	-
Mg	9.88	7.87	6.14	4.89	-
K	1.20	0.26	0.40	0.78	-
SI	4.74	6.25	9.63	11.24	-
$pH_{(1:10)}$	7.48	8.23	8.32	8.43	-
$EC_{(1:10)}$ (dS/m)	3.15	4.15	6.39	7.46	-
Cd (mg/kg)	2.80	1.80	1.90	2.40	60
Pb (mg/kg)	7	6	16	19	120
Cu (mg/kg)	16	37	43	51	600
Zn (mg/kg)	900	1011	1132	1321	1500
AS (mg/kg)	29.30	32.10	33.90	37.14	40
Mo (mg/kg)	0.55	0.57	0.87	1.19	-
Ni (mg/kg)	13	13	14	15	

SI: salt index, EC= electrical conductivity

Table 7: Solubility of samples in water, citric acid, and HCl

Struvite (%): Biochar (%)	Solution	P (g/L)	Dissolution rate (%)	N (g/L)	Dissolution rate (%)	Mg (g/L)	Dissolution rate (%)
	water	1.35	1.06	0.046	5.50	0.0096	1.45
100:0	20 g/L citric acid	77.88	61.43	0.17	20.41	0.4464	67.71
	0.5 mol/L HCl	104.05	82.08	0.23	27.32	0.648	98.30
	water	1.16	1.12	0.047	6.31	0.0096	1.82
75:25	20 g/L citric acid	73.51	70.89	0.18	33.34	0.3793	72.20
	0.5 mol/L HCl	90.95	87.71	0.25	33.24	0.520	99.69
	water	1.09	1.16	0.048	8.56	0.0096	2.34
50:50	20 g/L citric acid	78.24	83.41	0.19	33.62	0.2976	72.20
	0.5 mol/L HCl	85.16	90.79	0.26	45.78	0.40	99.60
	water	0.83	1.33	0.50	10.78	0.0096	2.94
25:75	20 g/L citric acid	54.94	87.55	0.19	45.32	0.2544	77.90
	0.5 mol/L HCl	57.12	91.03	0.28	59.90	0.32	100

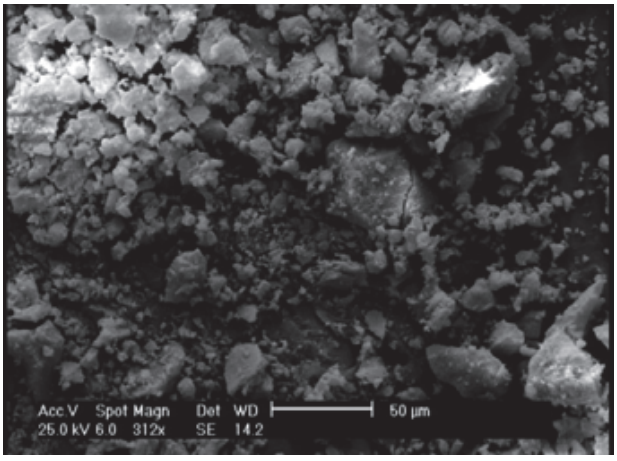

100% Struvite: 0% Biochar

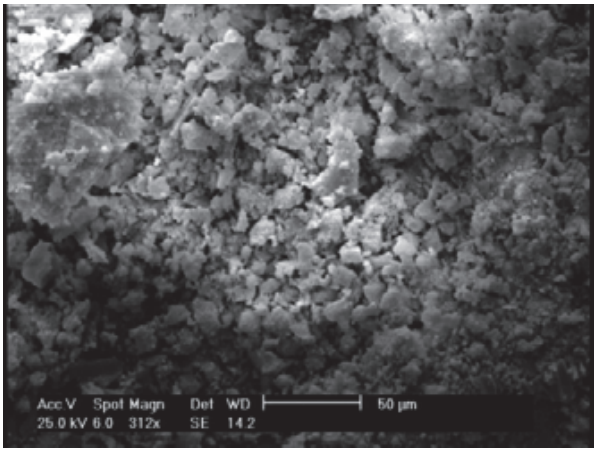

75% Struvite: 25% Biochar

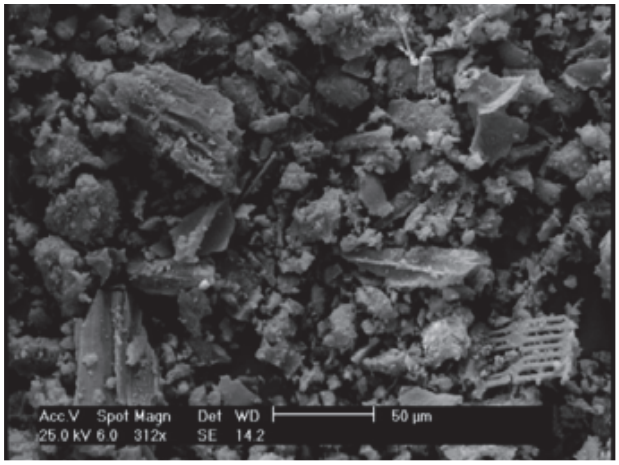

50% Struvite: 50% Biochar

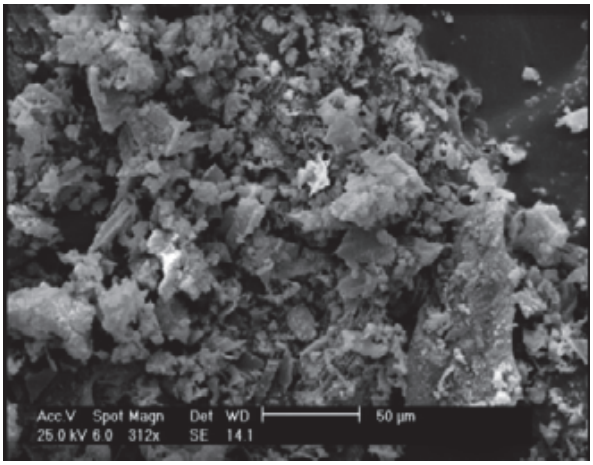

25% Struvite: 75% Biochar

Fig. 2: Scanning Electron Microscopy of samples

Fig. 3:

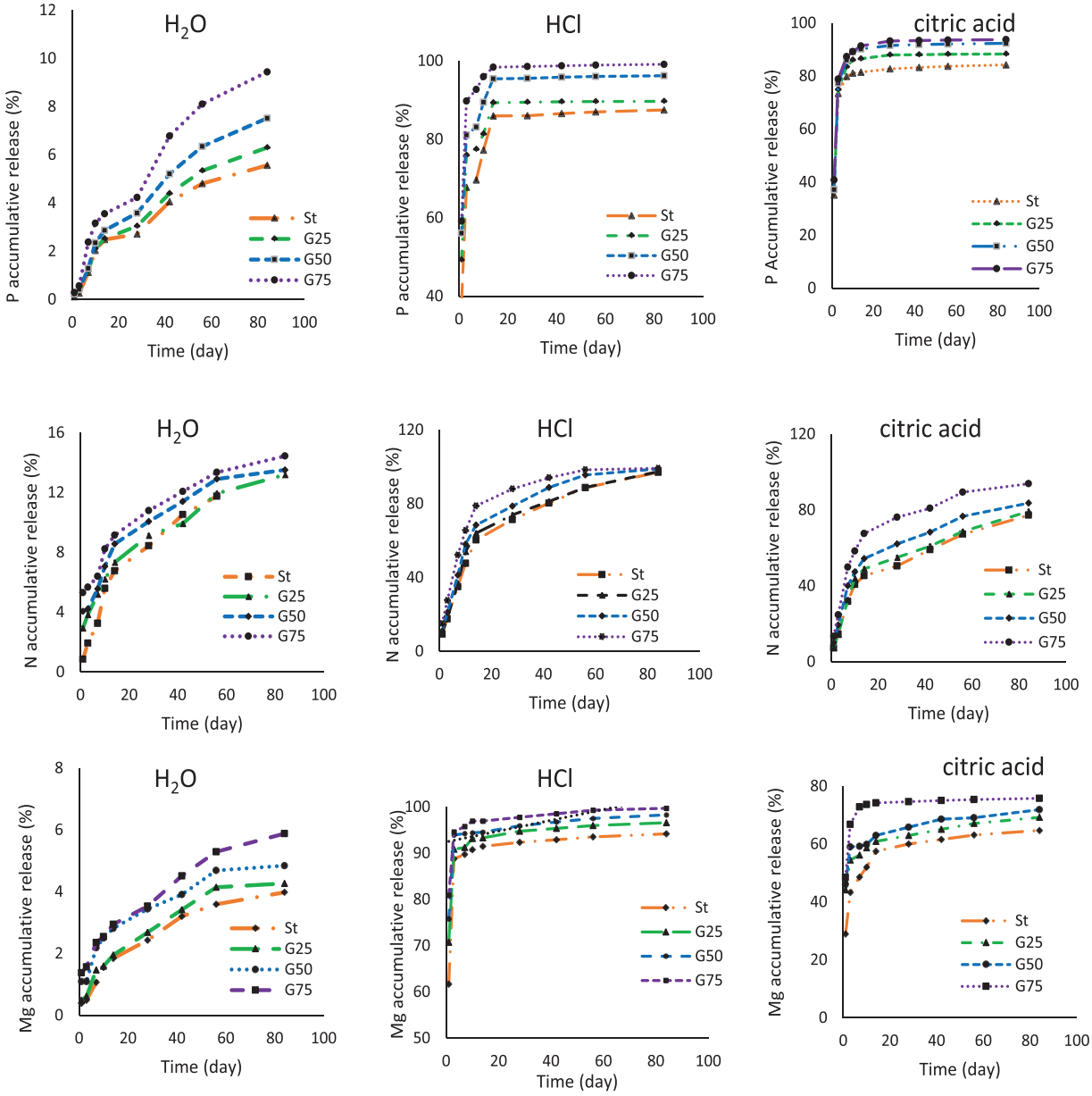

Fig. 3: Cumulative releases of P, N, and Mg from differente %Struvite:%Bbiochar (100:0 (St), 75:25 (G25), 50:50 (G50), 25:75 (G75)) in water, 20 g/L citric acid and 0.5 mol/L HCl.

P- Precipitates

The XRF results of the samples are presented in Table 5. Amount of P_2O_5 for %struvite: %Gr-biochar of 100:25, 75:25, 50:50 and 25:75 were 28, 25, 22, and 13%, respectively. This could be due to the presence of other particles such as Fe, Al and biochars (Rahman *et al.*, 2014; Shiba and Freeman, 2016). The amount of MgO in the samples decreased by increasing the amount of Gr-biochar. Shiba and Ntuli (2016) reported that the amount of P_2O_5 in the struvite from sewage sludge in different conditions was from 14.0 to 32.50%. Also, Hu *et al.*, (2019) showed that the amount of P_2O_5 in the samples was in the range of 22 and 30%. P-amount generally ranges as 11–26% in struvite by deferent precipitation methods (Johnston and Richards, 2003; Khan *et al.*, 2019).

Table 8: Parameters of kinetic models for P release from the samples in water, HCL and citric acid

Equation		Water			0.5 mol/L HCL			20 g/L citric acid	
First-order	R^2	a	b	R^2	a	b	R^2	a	b
St	0.95	1.66	0.031	0.82	2.62	0.06	0.92	1.84	0.05
G25	0.95	1.79	0.029	0.83	2.24	0.10	0.92	1.87	0.08
G50	0.96	1.99	0.029	0.84	2.30	0.07	0.92	2.063	0.06
G75	0.94	2.19	0.030	0.84	1.69	0.06	0.76	2.18	0.0
		Water			0.5 mol/L HCL			20 g/L citric acid	
Power function	R^2	a	b	R^2	a	b	R^2	a	b
St	0.94	0.94	0.63	0.89	4.33	0.05	0.87	11.46	0.02
G25	0.97	6.23	0.58	0.86	11.35	0.04	0.81	11.30	0.03
G50	0.97	6.18	0.62	0.89	11.27	0.04	0.85	11.23	0.04
G75	0.92	6.21	0.56	0.91	10.95	0.02	0.88	10.84	0.04
		Water			0.5 mol/L HCL			20 g/L citric acid	
Parabolic	R^2	a	b	R^2	a	b	R^2	a	b
St	0.98	-0.122	0.63	0.74	78.35	2.49	0.70	76.35	1.01
G25	0.98	-0.22	0.71	0.72	83.67	1.78	0.58	79.70	1.21
G50	0.99	-0.41	0.86	0.72	85.22	1.86	0.63	82.03	1.42
G75	0.97	-0.21	1.040	0.71	91.61	1.03	0.67	83.08	1.46
		Water			0.5 mol/L HCL			20 g/L citric acid	
Elovich	R^2	a	b	R^2	a	b	R^2	a	b
St	0.92	-0.20	1.14	0.89	76.41	3.12	0.88	75.40	2.14
G25	0.89	-0.26	1.27	0.86	82.29	3.65	0.82	78.17	2.70
G50	0.88	-0.44	1.53	0.89	83.60	3.89	0.87	80.39	3.11
G75	0.86	-0.23	1.85	0.92	90.60	4.19	0.88	81.55	3.15

The NPK fertilizers must have 5 to 12% of P_2O_5, and the PK fertilizers must have 18 to 20% P_2O_5 (Adam, 2009). Precipitates in this study were appropriate for creating P fertilizers from secondary raw materials and could be applied to preserve rock phosphates and contribute to source protection. However, %struvite: %biochar samples contained both valuable elements (P, Mg, N and K) and carriers of heavy metals (Table 6).

Generally, struvite ($MgNH_4PO_4.6H_2O$) has 6% N, 13% P, and 10% Mg (Rahman *et al*., 2013). The concentration of heavy metals in struvite/biochar samples was lower than the permissible limit (Table 6). As already described, the content of metals increased by increasing the amount of Gr-biochar in the samples probably due to either sorption or co-precipitation (Muhmood *et al*., 2019; Ma and Rouff, 2012; Uysal *et al*., 2014). In addition, biochar has been used to immobilize heavy metals (Lu *et al*., 2017; Wu *et al*., 2017; O'Connor *et al*., 2018) and increase nutrient availability (Li *et al*., 2019). The SEM of precipitates exhibited that the particles had a rod-like shape (Fig. 2) and this was consistent with the results detected by Rahman *et al*., (2014), Shiba and Freeman (2016), and Hu *et al*., (2019). P-recovery at pH=8.5 and in %struvite: %biochar ratios of 100:25, 75:25, 50:50 and 25:75 were 92, 92, 93 and 96%, respectively. Similarly, Kobar *et al*., (2020) reported that recovery of P and N from biogas slurry increased by 71 and 94%, respectively, with the incorporation of rice-biochar and struvite. Zheng *et al*., (2018) found that N and P recoveries from urine intensified by nearly 40–50% and 97% by combining biochar and struvite at pH=9, respectively. High surface area and high CEC of biochar may be valuable for adsorbing N and P from wastewater and reducing their losses (Kobar *et al*., 2020).

Solubility and kinetic properties of samples

The solubility of the samples in deferent amounts of the Gr-biochar was calculated by the procedure determined previously. The solubility results of the samples in water, CA, and HCl are shown in Table 7. The solubility was higher in HCl and CA than in water. The amount of P, Mg and N in the samples were in an order of 100% struvite > 75% struvite: 25% Gr-biochar > 50% struvite: 50% Gr-biochar > 25% struvite=75% Gr-biochar (Table 7). Thus, the extracted concentrations of P, Mg and N were the same, but their dissolution rate increased by increasing the Gr-

biochar, indicating that the Gr-biochar could intensify the release properties of P-precipitates. Dong *et al*., (2020) reported that the biochar-based slow-release fertilizer, which included natural materials, not only reduced N-leaching, but also supplied a high amount of N to the rice plant in later stages of the production cycle.

The accumulative P, Mg and N releases from precipitates began with a rapid reaction and followed by a slow reaction (Fig. 3). The accumulative release nutrients from samples were as follows: 25% struvite=75% Gr-biochar (G75) > 50% struvite: 50% Gr-biochar (G50) > 75% struvite: 25% Gr-biochar (G25) > 100% struvite (St) (Fig. 3). The initial fast release of ions was a characteristic of their high lability, whereas the slow fraction could be related to their low mobility (Hosseinpur, 2011). The initial rapid reaction was related to the rapid release of poorly crystalline phosphates in the precipitates, especially with a high amount of Gr-biochar, which were metastable ions and rapidly released. Gr-biochar, with a high surface area, had a high efficacy on the adsorption of ions during precipitation of samples. The P-accumulative releases in water from St, G25, G50, and G75 were 5.57, 6.30, 7.52, and 9.44%, respectively, and P-releases of them in 20 g/L CA were 84, 88, 92, and 94% respectively, and in 0.5 mol/L HCl were 87, 90, 96, and 99%, respectively, after 84 days. The Mg and N-accumulative releases from the mentioned samples followed the same trend. The accumulative release of nutrients was higher in 0.5 mol/L HCl (pH=0.3) than in water and CA (20 g/L) (pH~3). Since, struvite is a root-activated fertilizer, increasing the release of phosphorus from its compounds in the presence of Gr-biochar, especially in CA solution, can be effective in the early stages of plant growth to provide P, which requires greenhouse studies.

The P-release results from samples in water, CA (20 g/L), and HCl (0.5 mol/L) solutions were fitted to the first-order, power function, parabolic diffusion, and simple Elovich models presented in Table 8. The parabolic model with a high R^2 (R^2= 0.97-0.98) represents the P-cumulative release from samples in water (Table 8). The parabolic kinetic model indicated that the release of P from these precipitates in water was controlled by the diffusion process (Hosseinpur, 2011). Also, the P-releases in the samples well fitted to the Elovich model in HCl solution and the first-order model in CA solution well described them. This was consistent with results reported by other researchers (Hu *et al*., 2019; Jalali, 2006). The b parameter showed the slope and it could be applied as an index for the release of P from the samples. Based on the Elovich equation, the release rates of P from the samples were as follows: HCl> CA> water. The parameters of this model increased by increasing the amount of the Gr-biochar (G75> G50> G25> St), implying that high amount of Gr-biochar could intensify P-release from precipitates. Wang *et al*., (2010) reported that the Elovich equation could explain a lot of reaction mechanisms including not only the diffusion of P-released at the surface or interface, but also the activation energy and deactivation of the surface. Kong *et al*., (2020) reported that the first-order, and the Elovich models could well fit the kinetic data in P-release from a fish feed.

CONCLUSION

In this study, the values of heavy metals in sewage sludge were lower than the standard limits in sludge using fertilizer, while the molar ratio of Al + Fe/P of SS was more than the standard limits indicating its low potential to be directly used as P-fertilizer. Increasing Gr-biochar for the removal of P from SS increased the P-recovery. Moreover, the value of heavy metals in precipitates increased in the presence of Gr-biochar, but their values were lower than the permissible limit. The nutrient's accumulative releases from the samples were as follows: G75 > G50> G25 > St. The accumulative release of P, Mg and N from the samples began with a rapid reaction and followed by a slow reaction. The highest solubility of the samples was observed in HCl and then in CA, and water. The parabolic model good described the P-cumulative release from composites in water. It followed the Elovich model in 0.5 mol/L HCl solutions and the first-order equation in 20 g/L CA. The amount of P_2O_5 in the precipitates was higher than 12%, indicating that these precipitates could be applied as P-fertilizer. This study showed the efficiency of P-recovery from SS in the presence of the Gr-biochar by struvite precipitation and then provided a sustainable matter for agriculture. The precipitation method applied in this study could help in solving the difficulties of disposing SS. Before planning for

P-recovery by biochar/struvite composites, further different options of P- recovery should be analyzed for their cost and environmental efficiency. The accumulation of heavy metals in Gr-biochar/struvite precipitates from SS should be further explored in greater detail in future research for P-recovery from wastewater with a high amount of heavy metal. Furthermore, field experimentation would be needed to determine the effectiveness of these P-precipitates fertilizers for many types of soils and cropping systems in future studies.

AUTHOR CONTRIBUTIONS

M. Piri performed the literature review, analyzed and interpreted the data, prepared the manuscript text, and manuscript edition. E. Sepehr performed the literature review, data analysis and manuscript preparation as well as provided critical revision of the manuscript.

ACKNOWLEDGEMENTS

The authors would like to thank the "Iran national Science foundation Science deputy of presidency" for its financial support [Project code number: 99016005], and the Urmia university, Iran, for carrying out the project by using laboratory equipment's.

CONFLICT OF INTEREST

The authors declare no potential conflict of interest regarding the publication of this work. In addition, the ethical issues including plagiarism, informed consent, misconduct, data fabrication and, or falsification, double publication and, or submission, and redundancy have been completely witnessed by the authors

OPEN ACCESS

PUBLISHER'S NOTE

GJESM Publisher remains neutral with regard to jurisdictional claims in published maps and institutional affiliations.

ABBREVIATIONS

Ag	Silver
As	Arsenic
Al_2O_3	Aluminum oxide
Ca	Calcium
Cu	Copper
Cr	chromium
C	Carbon
CEC	Cation exchange capacity
Cd	Cadmium
ºC	Degree Celsius
CaO	Calcium oxide
Cº/min	degree Celsius per minute
Eq.	Equation
EC	electrical conductivity
EDTA	Ethylene diamine tetra acetic acid
CA	citric acid
Fe	Iron
Fig.	Figure
Fe_2O_3	Iron (III) oxide
g/L	gram per liter
Gr-biochar	biochar of grape residues
HCl	Hydrochloric acid
H	Hydrogen
h	Hour
H_2SO_4	Sulfuric acid
K_2O	Potassium oxide
K	Potassium
mg/L	milligrams per liter

Mg	Magnesium
mm	millimeter
mg/kg	milligram per kilogram
mol/L	mole per liter
MnO	Manganese (II) oxide
MgO	Magnesium oxide
nm	nanometer
N	Nitrogen
Na	Sodium
Ni	Nickel
NH_4^+	Ammonium
N	Normality
NaOH	Sodium hydroxide
Pb	Lead
P	Phosphorus
pH	Potential of hydrogen
P_2O_5	Phosphorus pentoxide
R^2	R-squred
SS	*Sewage sludge*
SiO_2	Silicon dioxide
SO_4	sulfate
SI	salt index
TOC	total organic carbon
TN	total nitrogen
TP	total phosphorus
TiO_2	Titanium dioxide
UV	ultraviolet light
Zn	Zinc

REFERENCES

Adam, C.; Peplinski, B.; Michaelis, M.; Kley, G.; Simon, F.G., (2009). Thermochemical treatment of sewage sludge ashes for phosphorus recovery. Waste, Manage., 29(3): 1122–1128 **(7 pages)**.

De, S.; Maiti, S.K.; Hazra, T.; Debsarkar, A.; Dutta, A., (2016). Leachate characterization and identification of dominant pollutants using leachate pollution index for an uncontrolled landfill site. Global J. Environ. Sci. Manage., 2(2): 177-186 **(10 pages)**.

Dong, D.; Wang, C.; Zwieten, L.V.; Wang, H.; Jiang, P.; Zhou, M.; Wu, W., (2020). An effective biochar-based slow-release fertilizer for reducing nitrogen loss in paddy fields. J. Soils Sediments., 20: 3027–3040 **(14 pages)**.

Dugdug, A.A.; Chang, S.X.; Ok, Y.S.; Rajapaksha, A.U.; Anyia, A., (2018). Phosphorus sorption capacity of biochars varies with biochar type and salinity level. Environ. Sci. Pollut. Res Int., 25(26): 25799-25812 (**14 pages**).

Doyle, J.D.; Parsons, S.A., (2002). Struvite formation, control and recovery. Water Res., 36: 3925–3940 **(16 pages)**.

Egle, L.; Rechberger, H.; Krampe, J.; Zessner, M., (2016). Phosphorus recovery from municipal wastewater: an integrated comparative technological, environmental and economic assessment of P recovery technologies. Sci. Total Environ., 571: 522–542 (**21 pages**).

Jalali, M., (2006) Kinetics of non-exchangeable potassium release and availability in some calcareous soils of western Iran. Geoderma., 135: 63–71 (**9 pages**).

Johnston, A.E.; Richards, I.R., (2003) Effectiveness of different precipitated phosphates as phosphorus sources for plants. Soil Use Manag., 19: 45–49 (**5 pages**).

Hertzberger A.J.; Cusick R.D.; Margenot A.J., (2020). A review and meta-analysis of the agricultural potential of struvite as a phosphorus fertilizer. Soil Sci. Soc. Am. J., 84: 653–671 (**19 pages**).

Hosseinpur, A.R.; Sadate, F.; Alikhani, H. A., (2011). Impact of Poultry Manure Application on Phosphorus Desorption in Some Calcareous. Commun. Soil Sci. Plant Anal., 42: 208–219 (**12 pages**).

Huang, H.; Huang, L.; Zhang, Q.; Jiang, Y.; Ding, L., (2015). Chlorination decomposition of struvite and recycling of its product for the removal of ammonium-nitrogen from landfill leachate. Chemosphere, 136: 289–296 (**8 pages**).

Hu, P.; Zhang, Y.; Liu, L.; Wang, X.; Luan, X.; Ma, X.; Chu, P.K.; Zhou, J.; Zhao, P., (2019). Biochar/struvite composite as a novel potential material for slow release of N and P. Environ. Sci. Pollut. Res., 26(17): 17152-17162 (**11 pages**).

Khan, A.; Jilani, G.; Zhang, D.; Akbar, S.; Malik, M.K.; Rukh, S., (2019). *Acidithiobacillus thiooxidans* IW16 and Sulfur Synergistically with Struvite Aggrandize the Phosphorus Bioavailability to Wheat in Alkaline Soil. Soil Sci. Plant Nutr., 20: 95–104 (**10 pages**).

Kim, J.H.; An, B.M.; Lim, D.H.; Park, J.Y., (2018). Electricity production and phosphorus recovery as struvite from synthetic wastewater using magnesium-air fuel cell electrocoagulation. Water Res., 132: 200–210 (**11 pages**).

Kong, W.; Huang, S.; Shi, F.; Yang, Z.; Feng, Y.; Khatoon, Z.; Zhou, J.; Xiao, Y., (2020). Study on release kinetics of nitrogen and phosphorus from fish feed. Aquac. Res., 3216–3229 (**14 pages**).

Kubar, A.A.; Huang, Q.; Sajjad, M.; Yang, C.; Lian, F.; Wang, J.; Kubar, K.A., (2021). The Recovery of Phosphate and Ammonium from Biogas Slurry as Value-Added Fertilizer by Biochar and Struvite Co-Precipitation. Sustainability, 13: 2-17 **(16 pages)**.

Le Corre, K.S.; Valsami-Jones, E.; Hobbs, P.; Jefferson, B.; Parsons, S.A., (2007). Struvite crystallization and recovery using a stainless steel structure as a seed material. Water Res., 41: 2449–2456 (**8 pages**).

Lehmann, J.; Kuzyakov, Y.; Pan, G.; Ok, Y. S., (2015). Biochars and the plant-soil interface. Plant Soil. 395(1-2): 1–5 (**5 pages**).

Lehmann, J.; Joseph, S., (2015). Biochar for Environmental Management: Science, Technology and Implementation. Second ed. Routledge, New York, USA.

Li, B.; Irina, B.; Wei, Y.; Hai, M.H.; Tajammal, M.; Guang, Q.W.; Brent, R. Y., (2018) Phosphorous recovery through struvite crystallization: challenges for future design. Sci. Total. Environ., 648: 1244–1256 (**13 pages**).

Li, Z.; Song, Z.; Singh, B. P.; Wang, H., (2019). The impact of crop residue biochars on silicon and nutrient cycles in croplands. Sci. Total Environ., 659: 673–680 (**8 pages**).

Lu, K.; Yang, X.; Gielen, G.; Bolan, N.; Ok, Y.S.; Niazi, N.K.; Xu, S.; Yuan, G.; Chen, X.; Zhang, X.; *et al*., (2016). Effect of bamboo and rice straw biochars on the mobility and redistribution of heavy metals (Cd, Cu, Pb and Zn) in contaminated soil. J. Environ. Manage., 186: 285–292 (**8 pages**).

Malwina, T., (2019). Assessment of Heavy Metal Pollution and Potential Ecological Risk in Sewage Sludge from Municipal Wastewater Treatment Plant Located in the Most Industrialized Region in Poland—Case Study. Int. J. Environ. Res. Public Health. 16: 2-16 (**14 pages**).

Ma, N.; Rouff, A.A., (2012). Influence of pH and oxidation state on the interaction of arsenic with struvite during mineral formation. Environ. Sci. Technol., 46: 8791–8798 (**8 pages**).

Meyer, C.; Preyl, V.; Steinmetz, H.; Maier, W.; Mohn, R. E.; Schönberger, H.; Piersson, T., (2018). The Stuttgart Process. In: Schaum, Chr. (editor) Phosphorus: Polluter and Resource of the Future: Removal and Recovery from Wastewater, IWA Publishing, ISBN13: 9781780408354, eISBN: 9781780408361.

Muys, M.; Phukan, R.; Brader, G.; Samad, A.; Moretti, M.; Haiden, B.; Pluchon, S.; Roest, K.; Vlaeminck, S. E.; Spiller, M., (2021). A systematic comparison of commercially produced struvite: Quantities, qualities and soil-maize phosphorus availability. Sci. Total Environ., 756: 143726.

Muhmood, A.; Lu, J.; Kadam, R.; Dong, R.; Guo, J.; Wu, S., (2019) Biochar seeding promotes struvite formation, but accelerates heavy metal accumulation. Sci. Total Environ., 652: 623–632 (**10 pages**).

Numviyimana, C.; Warchoł, J.; Khalaf, N.; Leahy, J.; Chojnacka, K., (2022). Phosphorus recovery as struvite from hydrothermal carbonization liquor of chemically produced dairy sludge by extraction and precipitation. J. Environ. Chem. Eng., 10: 1-12 **(12 pages)**.

O'Connor, D.; Peng, T.; Zhang, J.; Tsang, D.C.W.; Alessi, D.S.; Shen, Z.; Bolan, N.S.; Hou, D., (2018). Biochar application for the remediation of heavy metal polluted land: a review of in situ field trials. Sci. Total Environ., 619-620: 815–826 (**12 pages**).

Park, J.H.; Choppala, G.K.; Bolan, N.S.; Chung, J.W.; Chuasavathi, T., (2011). Biochar reduces the bioavailability and phytotoxicity of heavy metals. Plant Soil. 348: 439–451 (**13 pages**).

Pastene, A.J., (1981). Factors affecting the crop availability of phosphorus in sewage sludge amended soils. M.S. thesis. University. of Wisconsin, Madison.

Rahman, Md. M.; Salleh, M.A.M.; Rashid, U.; Ahsan, A.; Hossain, M.M.; Ra, C.S., (2013). Production of slow release crystal fertilizer from wastewaters through struvite crystallization – A review. Arab. J. Chem., 7: 139–155 (**17 pages**).

Rezania, S.; Kamyab, H.; Rupani, P.F.; Park, J.; Nawrot, N.; Wojciechowska, E.; Yadav, K.K.; Ghahroud, M.L.; Mohammadi , A.A.; Sathiabama, T.; Chelliapan, S.; Cabral-Pinto, M., (2021). Recent advances on the removal of phosphorus in aquatic plant-based systems. Environ. Technol. Innov., 24: 1-25 **(25 pages).**

Semerci, N.; Ahadi, S.; Coşgun, S., (2020). Comparison of dried sludge and sludge ash for phosphorus recovery with acidic and alkaline leaching. Water Environ J., 35: 359-370 (**17 pages**).

Shaddel, S.; Grini, T.; Ucar, S.; Azrague, K.; Andreassen, J.; Østerhus, S.W., (2020). Struvite crystallization by using raw seawater: Improving economic and environmental footprint while maintaining phosphorus recovery and product quality. Water Res., 173: 1-12 **(12 pages)**.

Shiba, N.C.; Ntuli, F., (2016). Extraction and precipitation of phosphorus from sewage sludge. Waste Management. Waste Manage., 60: 191–200 (**10 pages**).

Siciliano, A.; Limonti, C.; Curcio, G.M.; Molinari, M., (2020). Advances in struvite precipitation technologies for nutrients removal and recovery from aqueous waste and wastewater. Sustainability. 12: 2-36 **(35 pages).**

Siciliano, A.; Stillitano, M.A.; Limonti, C.; Marchio, F., (2016). Ammonium Removal from Landfill Leachate by Means of Multiple Recycling of Struvite Residues Obtained through Acid Decomposition. Appl. Sci., 6: 375.

Shepherd, J.G.; Sohi, S.P.; Heal, K.V., (2016). Optimising the recovery and re-use of phosphorus from wastewater effluent for sustainable fertilizer development. Water Res., 94: 155–165.

Tosun, G.U.; Sakhno, Y.; Jaisi, D.P., (2021). Synthesis of Hydroxyapatite Nanoparticles from Phosphorus Recovered from Animal Wastes. ACS Sustain. Chem. Eng., 9: 15117–15126 (**10 pages**).

Uysal, A.; Tuncer, D.; Kır, E.; Sardohan Köseoğlu, T., (2016). Phosphorus recovery from hydrolysed sewage sludge liquid containing metals using Donnan dialysis. In: 6th International Conference on Environmental Pollution and Remediation (ICEPR'16), Proceedings of the 2nd World Congress on New Technologies (NewTech'16) Budapest, Hungary, August 18–19, 2016, ICEPR 125 1-7, ISBN: 978-1-927877-26-5. Bitton G. 1999. Wastewater Microbiology. 2nd Edition. Wiley-Liss (**8 pages**).

Velu, M.; Balasubramanian, B.; Palanivel, V.; Kamyab, H.; Ravi, A.V.; Chelliapan, S.; Chew Lee, C.T.; Palaniyappan, J., (2020). Fabrication of nanocomposites mediated from aluminum nanoparticles/Moringa oleifera gum activated carbon for effective photocatalytic removal of nitrate and phosphate in aqueous solution. J. Clean. Prod., 281: 1-16 **(16 pages).**

Wang, J.Q.; Shen, Y. H.; Ma, Y.P., (2010). Release kinetics of rock phosphorus in the Chaohu Lake area. Acta Sci. Circumstantiae., 30(5): 979–984 (**6 pages**).

Wu, W.D.; Li. J.H.; Lan, T.; Muller, K.; Niazi, N.K.; Chen, X.; Xu, S.; Zheng, L.R.; Chu, Y.C.; Li, J.W.; Yuan, G.D.; Wang, H.L., (2017). Unraveling sorption of lead in aqueous solutions by chemically modified biochar derived from coconut fiber: a microscopic and spectroscopic investigation. Sci. Total Environ., 576: 766–774 (**9 pages**).

Xu, H.; He, P.; Gu, W.; Wang, G.; Shao, L., (2012). Recovery of phosphorus as struvite from sewage sludge ash. Res. J. Environ. Sci., 24(8): 1533–1538 (**6 pages**).

Yetilmezsoy, K.; Sertyesilisik, B.; Kocak, E.; Sapci-Zengin, Z., (2009). Ameliorative effect of different doses of MgNH4PO4·6H2O precipitate recovered from the effluent of UASB treating poultry manure wastewater: growth of Lolium perenne. J. Food. Agric. Environ., 7: 823–831 (**9 pages**).

Zheng, M.; Xie, T.; Li, J.; Xu, K.; Wang, C., (2018). Biochar as a carrier of struvite precipitation for nitrogen and phosphorus recovery from urine. J. Environ. Eng., 144: 1-7 **(7 pages).**

AUTHOR (S) BIOSKETCHES

Piri, M., Ph.D., Post-Doctoral research fellow, Department of Soil Science, Faculty of Agriculture, Urmia University, Iran.
- Email: *ma.piri@urmia.ac.ir*
- ORCID: 0000-0003-0042-5060
- Web of Science Researcher ID: AEA-5696-2022
- Scopus Author ID: 57205460316
- Homepage: https://en.urmia.ac.ir/Agriculture-Faculty/agriculture_Soil%20Science_department

Sepehr, E., Ph.D., Professor, Department of Soil Science, Faculty of Agriculture, Urmia University, Iran.
- Email: *e.sepehr@urmia.ac.ir*
- ORCID: 0000-0001-5843-0669
- Web of Science Researcher ID: AFI-2691-2022
- Scopus Author ID: 36896944500
- Homepage: https://en.urmia.ac.ir/content/agricultureagrologysection4esepehr

HOW TO CITE THIS ARTICLE

Piri, M.; Sepehr, E., (2022). Phosphorus recovery from domestic sewage sludge in the presence of waste grape pruning biochar. Global J. Environ. Sci.Manage., 8(4): 575-588.

DOI: 10.22034/gjesm.2022.04.09

url: https://www.gjesm.net/article_251285.html

Global J. Environ. Sci. Manage. 8(4): 589-606, Autumn 2022, Serial #32

Global Journal of Environmental Science and Management
(GJESM)

Homepage: https://www.gjesm.net/

REVIEW PAPERPAPER

A bibliometric analysis of the effects of electronic waste on the environment

M. Maphosa[1,*], V. Maphosa[2]

1 School of Information Technology, Varsity College, Independent Institute of Education, Sandton, South Africa

[2] Information Communication and Technology Services Department, Lupane State University, Bulawayo, Zimbabwe

ARTICLE INFO

Article History:
Received 06 December 2021
Revised 13 February 2022
Accepted 16 Match 2022

Keywords:
Electrical and electronic equipment
Electronic waste
Environment
Health
Recycle
Waste management

DOI: 10.22034/gjesm.2022.04.10

ABSTRACT

The outcome of improper electronic waste management is an environmental and epidemiological catastrophe; therefore, its management has become crucial given the increase in e-waste generation. Global e-waste output eclipsed 52 million metric tonnes in 2020, growing at 3% per annum. The United Nations Sustainable Development Goal number 12 highlights that only 20% of the generated e-waste was properly recycled, with the remainder indiscriminately disposed of. There has been considerable growth in publications on e-waste and the environment over the past few decades. This study provides an overview of the research landscape on the impact of e-waste on the environment using bibliometric analysis. VOSviewer software is used to visualise the current trends and the recent hotspots. It is observed that the research hotspots in the field are: soil, health, environmental impact, recovery, electronic equipment, and waste electrical and electronic equipment. By tracing the evolutionary research pathway, it is clear that the research hotspots have shifted focus to e-waste generation, laser-induced breakdown spectroscopy, and circular economy. A total of 141 articles on e-waste and the environment published between 2003 and 2021 were selected for the study. The publication and citation analysis showed a steady increase in publications and citations. China dominates with a third of articles published by authors, followed by India and the United States. Developing countries contributed about 17% of total publications. The articles retrieved were cited 5290 times and had an h-index of 39. Finally, using network analysis techniques, four key themes are identified. The first theme relates to the strategies employed in recovering minerals from e-waste. The second theme focuses on the concentration levels of the heavy minerals found in e-waste. The third theme visualises the impact of e-waste on health, and finally, the fourth theme highlights the effects of e-waste on the environment. The study adds valuable insights to the body of literature in hazardous and toxic substances management. No studies were found chronicling the environmental effects of e-waste using bibliometric analysis. In light of the Sustainable Development Goals, further research needs to be undertaken, and these findings serve as a baseline for policymakers and scholars as more management strategies and policies are enacted.

NUMBER OF REFERENCES	NUMBER OF FIGURES	NUMBER OF TABLES
102	4	4

*Corresponding Author:
Email: *mfowabo@gmail.com/mmfowabo@varsitycollege.co.za*
Phone: +27117846939
ORCID: 0000-0003-3702-6821

Note: Discussion period for this manuscript open until January 1, 2023 on GJESM website at the “Show Article”.

INTRODUCTION

The fourth industrial revolution (4IR), urbanisation, and advances in information technology have radically transformed humanity in the past few decades. Information and communication technologies (ICTs) have permeated every aspect of human life, promoting and maintaining a higher standard of living, and have become the foundation for health, education, transport, security, and energy operations. Although this development has been transformational, irresponsible management of technological resources has raised environmental quandaries. Balancing technological advancements and environmental sustainability remains a challenge for current and future generations (Maphosa, 2021). The United Nation's Sustainable Development Goals (SDGs) foster sustainable economic, social and environmental development across the globe. The SDGs provide a framework for solving problems affecting humanity and the environment (Akon-Yamga, 2021). Rapid industrialisation and product innovations, population boom, shorter product lifespans and consumer demand and cheaper ICT products contribute to the growth of the electrical and electronic equipment (EEE) product market (Lin *et al.*, 2022). However, most of these developments do not promote environmental sustainability by lowering environmental degradation and reducing global warming (Sztumski, 2014). Computing activities contribute to global warming through carbon emissions released during the manufacture, use and recycling of the resultant e-waste through the release of harmful chemicals into the environment (Perkins *et al.*, 2014).

State of the art of e-waste management

The past decades have witnessed increased adoption of EEE; once this equipment is obsolete or unusable, it constitutes electronic waste (e-waste). E-waste is the fastest-growing solid waste stream at about 5% per annum (Amankwah-Amoah, 2016). Globally, e-waste output will rise to over 52.2 million metric tonnes in 2020, causing an environmental crisis (Baldé *et al.*, 2017). Only 17.4% of e-waste was collected and recycled, with 82.6% of the e-waste illegally exported to developing countries (Forti *et al.*, 2020). Developing countries have become an accessible channel for e-waste dumping. High unemployment rates have created employment opportunities where pervasive and informal processing is prominent in recovering rare earth minerals, but this is done at the expense of the environment and public health (Sthiannopkao and Wong, 2013). Although Africa is the largest recipient of e-waste, the International Telecommunications Union reports that only 0.1% of e-waste is formally recycled in Africa and has targeted a global collection and recycling rate of 30% by 2023 (Forti *et al.*, 2020). In most informal recycling areas, children are at risk due to exposure to Pb and PAHs, resulting in inflamed vascular endothelial (Zheng *et al.*, 2019).

Barriers to e-waste management

The manufacture of EEE is complex, with over 1000 substances used, including precious minerals such as platinum, palladium, gold, and copper, together with toxic elements such as lead, mercury, cadmium, arsenic, and many others (Maphosa and Maphosa, 2020). Deubzer *et al.* (2019) contended that it was challenging to manage e-waste. Some components had over 69 chemical elements composed of valuable and hazardous elements, which require complex processes and recycling technologies to recover the precious minerals. Over 50 tons of mercury were contained in e-waste produced in 2019, with brominated flame retardants accounting for 71-kilo tons, detrimental to the environment and human health if improperly handled (Sabra *et al.*, 2017). Developing countries lack the finances and infrastructure to set up formal e-waste processing. Informal management is unlicensed and unregulated, where individuals use primitive and rudimentary techniques such as burning, leaching, and heating, which negatively affect the environment and public health (Pathak *et al.*, 2019). Aimin *et al.* (2011) reported that pregnant women and children dwelling around e-waste dumpsites suffered perturbations of the fetus and neurodevelopment challenges. The precious materials found in e-waste are ten times purer than minerals found in mines, therefore, putting pressure on the environment through informal recycling (Vi and Matthew, 2014). Ardolino *et al.* (2021) report adverse environmental and public health outcomes in most developing countries, where e-waste is exported and improperly treated and managed.

E-waste recycling methods

Methods used to recycle and recover rare metals from e-waste should protect the environment and human health. E-waste recycling is highly informal in developing countries (Maphosa and Maphosa, 2020), with scholars estimating that 90% of recycling activities use rudimentary methods such as stones, hammers, and chisels to separate components (Pathak *et al.*, 2019). Cyanide has been used to extract gold from e-waste for centuries. Its use has been prohibited in many countries due to poisoning and contamination of the environment resulting in human and animal fatalities (Ghasem and Khoramnejadian, 2015). Material smelting has been used to recycle printed circuit boards, and the method has been condemned for being primitive and polluting the environment (Ye *et al.*, 2021). Hydrometallurgical techniques are used in recycling using leaching, purification, and electrowinning. This process uses many leaching reagents and is only applied to a few minerals, while the leachates contain heavy metals which are detrimental to the environment and human health (Wang and Xu, 2014). Recycling enterprises in developed countries have perfected e-waste recycling technologies using mechanical crushing, magnetic separation, and eddy current separation and have reached high levels of efficiency (Abdul *et al.*, 2014).

Movement of e-waste into developing countries

The United Nations (UN) SDG 12 specifically addresses e-waste management and highlights that only 22.9% of global e-waste is recycled, while the rest is improperly disposed of, affecting the environment (UN, 2021). Once labelled the dark continent, Africa has witnessed unprecedented growth in its cyberspace, leading to increased socio-economic development and sustained economic growth. Cheaper telecommunications equipment, computers, and mobile phones are being assembled and refurbished for low-income countries to bridge the digital divide and promote inclusive development (Chitotombe, 2013). Over 80% of the e-waste produced by developed countries is illegally exported to Africa, where primitive techniques are used to recover precious materials, thus harming the environment and public health (Grant *et al*., 2013). The demand for cheaper second-hand EEE is high in developing countries, and many communities survive by scavenging the resultant e-waste (Omobowale, 2013). Thus, most e-waste flows to the global south are illegal and disguised as genuine efforts to bridge the digital divide (Lambrechts, 2016). In a Kenyan study earlier, Mureithi and Waema (2008) reported that about 75% of second-hand EEE was exported illegally in the pretence that it was usable and repairable; beneficiaries such as schools reported that over 60% of the donated EEE was unusable and beyond repair. To manage e-waste without harming the environment and human health is costly. Therefore, in most developing countries, e-waste is indiscriminately disposed of, thereby posing a hazard to the environment.

E-waste management policies

Most of the global e-waste is produced by developed countries, which often view developing countries as an outlet for cheaper disposal due to the unavailability of environmental policies. Globally, 71% of the countries have crafted national e-waste policies for collection and management, although the majority still experience inefficient management due to lack of investment and partnerships, lack of compliance, and no harmonisation across countries (Lundgren, 2012). In 2019, only 13 African countries had an e-waste policy, legislation, or regulation (Avis, 2021). Thus, over 80% of the African countries do not have formal e-waste collection and recycling systems, and e-waste is mixed with municipal waste and dumped in landfills where informal workers salvage valuable materials through burning (Ongondo *et al.*, 2011). Lack of e-waste policies, laws, and legislation in most developing countries results in low awareness among those in the value chain from manufacturers to recyclers (Nwagwu and Okuneye, 2016). This remains the greatest threat to managing e-waste (Mutsau *et al.*, 2015).

Aim of the study

The study is motivated by Kiddee *et al.* (2013), who highlighted that the scientific community was concerned with the unsafe handling of e-waste in developing countries, threatening the environment. There is evidence of growth in studies focusing on e-waste, focussing on different aspects of e-waste. As early as 2014, Premalatha *et al.* (2014) opined that the e-waste problem was increasing at a much faster rate than the proposed solutions to contain

it. A study by Hossain *et al.* (2015) showed that global e-waste management practices could prolong SDG achievement. Zeng and Li (2016) proposed a recyclability map that can serve as a guideline for establishing a feasible funding system for e-waste management. E-waste is a growing global concern, and a significant amount of e-waste is being added to the global waste inventory every year (Kumar *et al.*, 2017). Ikhlayel (2018) suggested implementing an integrated e-waste management system to prevent improper e-waste management in developing countries. Li and Xu (2019) compared supercritical fluid technology with traditional methods such as hydrometallurgy and pyrometallurgy. They found that supercritical fluid technology could recover valuable materials and remove hazardous components without secondary pollution. An aspect of e-waste management that has received attention is legislation. Patil and Ramakrishna (2020) compared different e-waste legislation enacted and proposed a generic e-waste management model for countries worldwide. The lack of proper technologies makes it difficult for many developing countries to formalise e-waste recycling (Rautela *et al.,* 2021). A few bibliometric studies on e-waste have been conducted. A study by Andrade *et al.* (2019) sought to assess recent research trends using the keyword e-waste from studies published between 1998 and 2018. Another study by Zhang *et al*. (2019) depicted the trends and features of WEEE-related studies. Gao et al. (2019) explored e-waste's status quo, hot topics, and future prospects. A study by Singh *et al*. (2021) provided an overview of e-waste and the circular economy using articles published between 2008 and 2020. The last study explored focus areas on e-waste and ascertained Brazil's ranking globally (de Albuquerque *et al.*, 2021). This study aims to use bibliometric indicators to review global research on e-waste and its effects on the environment in the past decade, compare publication trends over the years, and highlight the contributions of developing countries on e-waste research. This study is different from the studies discussed above in that it provides a bibliometric and visualisation of research on e-waste and its environmental impact in the past decade. The study explores the publication distribution by geography, journals, and citation trends. The study also assessed the frequency of keywords and H-index analysis and used bibliometric mapping tools to demonstrate developments in e-waste research covering environmental issues. No bibliometric studies published using the Web of Science database focusing on e-waste and the environment were found. This study aims to analyse and assess global research on e-waste and the environment, realising that issues to do with environmental sustainability are very urgent and topical. This study, therefore, provides a baseline for policymakers and researchers to plan and research on e-waste and climate change. This study was carried out between December 2021 and February 2022.

METHODS OF STUDY

The Web of Science database is one of the largest databases generally used for bibliometric analysis. One database is preferred when conducting bibliometric studies, as mapping indicators across several databases may be challenging (Sweileh, 2021). Accurate analysis of bibliometric studies is guaranteed by developing a comprehensive search query. The search query was identified and developed after conducting a literature review and identifying gaps in research covering e-waste and the environment. In December 2021 – January 2022, the Web of Science database was searched in the four indexes - Science Citation Index Expanded, Social Sciences Citation Index, Arts and Humanities Citation Index, and the Emerging Sources Citation Index. Multiple searches with multiple keywords search strings were used with the Boolean operators "AND" and "OR" to obtain relevant documents. The first search string retrieved articles related to climate, the environment, and sustainability. The search string TI = ("climate" OR "climate change" OR "environment" OR "sustainability" yielded 667 616 articles. The second search string TI = ("e-waste" OR "electronic waste" OR "electrical and electronic equipment" OR "EEE" yielded 2336 articles. The two search queries Were then combined to obtain articles appearing in both queries, and there were 166 articles. Articles published in 2022 were excluded, resulting in an exclusion of two publications leaving 164 articles. Filtered the papers by document types led to the exclusion of editorial materials, meeting abstracts, book reviews, corrections, letters, and news items, leaving 141 articles. The bibliometric analysis uses statistics and procedures to visually express general

and dynamic patterns found in scientific publications (Ho, 2007). The Web of Science's database functionality to analyse search results were used to analyse results. The bibliometric data for analysis in text and excel file formats were exported. The text and excel data were imported to VOSViewer (van Eck and Waltman, 2010) to create the keyword occurrence network and density visualisation maps (Schulz and Schumann, 2006).

Publications and Citation Trends

Fig. 1 plots the publications and citation trends. The first article on e-waste and environment-related research was published in 2003. Between 2003 and 2013, less than ten were published per year. More authors started to research this field, leading to a steady increase in publications. The years 2016 to 2021 recorded more than ten publications except for 2019. In terms of citations, there were low citations between 2003 and 2009, with less than 100 citations per year. 2011 to 2020 saw citations in the hundreds between 113 in 2011 and 811 in 2020. The year 2021 saw more than 1000 citations. The last three years saw astronomical growth in citations, with 2019 having 790, 2020 having 811 and 2021 having 1049.

Table 1 shows the top 15 cited research articles in the field of e-waste and the environment. As shown, the study "E-waste: An assessment of global production and environmental impacts" published in 2009 is the most cited with 937 citations. This is followed by the article "Potential environmental and human health impacts of rechargeable lithium batteries in electronic waste" published in 2013 with 214 citations and the article "Electrical and electronic waste: a global environmental problem" published in 2007 with 174 citations. Thus, the top 15 cited articles have been cited more than 100 times.

Distribution of articles by journal

The 141 articles analysed were published in 76 journals. Of these, 53 (69.7%) journals had a single publication each, 13 had two. The top ten journals published just over 40 (43.9%), as shown in Table 2. The journal with the most significant number of publications is the "Journal of Cleaner Production", with 11 publications. This is followed by "Science of

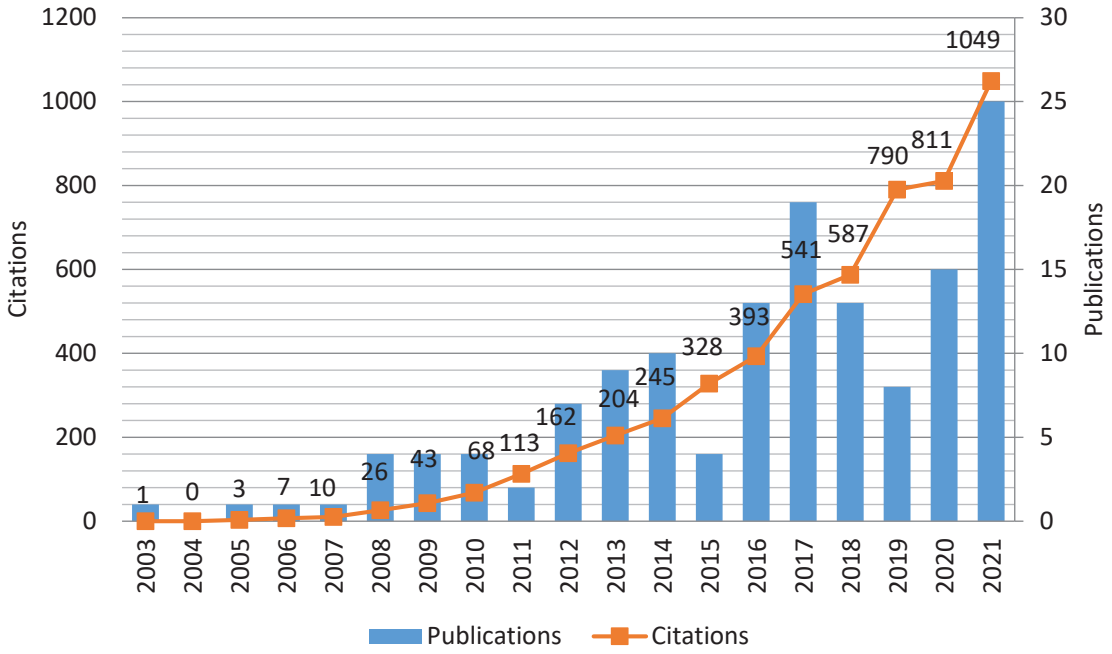

Fig. 1: Publication and citation index

Table 1: Top 15 cited articles

No.	Article	Year	Count	Reference
1	E-waste: An assessment of global production and environmental impacts	2009	937	(Robinson, 2009)
2	Potential environmental and human health impacts of rechargeable lithium batteries in electronic waste	2013	214	(Kang *et al.*, 2013)
3	Electrical and electronic waste: a global environmental problem	2007	174	(Babu *et al.*, 2007)
4	Does WEEE recycling make sense from an environmental perspective? The environmental impacts of the Swiss take-back and recycling systems for waste electrical and electronic equipment (WEEE)	2005	170	(Hischier *et al.*, 2005)
5	Willingness to engage in a pro-environmental behavior: an analysis of e-waste recycling based on a national survey of U.S. households	2012	168	(Saphores *et al.*, 2012)
6	Environmental pollution of electronic waste recycling in India: a critical review	2016	151	(Awasthi *et al.*, 2016)
7	Sustainability in electrical and electronic equipment closed-loop supply chains: a system dynamics approach	2008	147	(Georgiadis and Besiou, 2008)
8	Environmental impact and human exposure to PCBs in Guiyu, an electronic waste recycling site in China	2009	136	(Xing *et al.*, 2009)
9	Environmental impacts of the Swiss collection and recovery systems for waste electrical and electronic equipment (WEEE): a follow-up	2011	134	(Wäger *et al.*, 2011)
10	Toward sustainability for recovery of critical metals from electronic waste: the hydrochemistry processes	2017	132	(Sun *et al.*, 2017)
11	Environmental effects of heavy metals derived from the e-waste recycling activities in China: a systematic review	2014	128	(Song and Li, 2014)
12	Electronic waste - an emerging threat to the environment of urban India	2014	118	(Needhidasan *et al.*, 2014)
13	Flame retardant emission from e-waste recycling operation in northern Vietnam: environmental occurrence of emerging organophosphorus esters used as alternatives for PBDEs	2015	115	(Matsukami *et al.*, 2015)
14	E-waste recycling induced polybrominated diphenyl ethers, polychlorinated biphenyls, polychlorinated dibenzo-p-dioxins and dibenzo-furans pollution in the ambient environment	2007	108	(Liu *et al.*, 2008)
15	An analysis of some environmental consequences of European electrical and electronic waste regulation	2008	102	(Barba-Gutiérrez *et al.*, 2008)

Table 2: Top 10 journals

No.	Journal	Count	Percentage
1	Journal of Cleaner Production	11	7.8
2	Science of the Total Environment	10	7.1
3	Resources Conservation and Recycling	8	5.7
4	Environmental Science and Pollution Research	7	5
5	Waste Management	7	5
6	Environmental Science Technology	6	4.3
7	Environment International	4	2.8
8	Chemosphere	3	2.1
9	Environmental Pollution	3	2.1
10	International Journal of Environmental Research and Public Health	3	2.1

the Total Environment" with ten articles and then the "Resources Conservation and Recycling" with eight publications.

Geographical distribution of articles

Researchers from 48 countries authored the 141 articles analysed. Table 3 shows publications by country. As shown, China dominates with a third of articles published by authors in the country, followed by India with 19 articles (13.5%) and then the United States with 18 articles (12.8%). Developing countries contributed about 17% of total publications. Ghana and Pakistan are leading developing countries, contributing 3.5% of the research, while Nigeria, Bangladesh, Algeria contributed 1.7% each. Morocco, Benin, Iran and South Africa contributed 0.7% each.

Table 3: Geographical distribution of articles

No	Country	Count	Percentage
1	China	47	33.3
2	India	19	13.5
3	USA	18	12.8
4	Brazil	7	5.0
5	Italy	7	5.0
6	Japan	7	5.0
7	Australia	6	4.3
8	Canada	5	3.5
9	Ghana	5	3.5
10	Pakistan	5	3.5
11	Belgium	4	2.8
12	England	4	2.8
13	South Korea	4	2.8
14	Switzerland	4	2.8
15	Thailand	4	2.8
16	Germany	3	2.1
17	Greece	3	2.1
18	Netherlands	3	2.1
19	Portugal	3	2.1
20	Spain	3	2.1
21	Turkey	3	2.1
22	Vietnam	3	2.1
23	Algeria	2	1.4
24	Bangladesh	2	1.4
25	Denmark	2	1.4
26	France	2	1.4
27	Israel	2	1.4
28	Malaysia	2	1.4
29	Mexico	2	1.4
30	Nigeria	2	1.4
31	Norway	2	1.4
32	Romania	2	1.4
33	Saudi Arabia	2	1.4
34	Serbia	2	1.4
35	Sweden	2	1.4
36	Benin	1	0.7
37	Estonia	1	0.7
38	Iran	1	0.7
39	Ireland	1	0.7
40	Lithuania	1	0.7
41	Luxembourg	1	0.7
42	Morocco	1	0.7
43	New Zealand	1	0.7
44	Poland	1	0.7
45	Singapore	1	0.7
46	South Africa	1	0.7
47	Taiwan	1	0.7
48	United Arab Emirates	1	0.7

The citation and h-index analysis

The number of citations is the main factor to reflect the quality of a paper (Tahamtan *et al.*, 2016). According to the analysis of the data from Web of Science, all articles were cited 5290 times. These articles were cited in 110 countries, with four records not containing data in the field being analysed. The retrieved research studies have an h-index of 39. The h-index of 39 means that of the 141 research articles, 39 have received 39 citations. Based on

Table 4: Top 10 most occurring keywords

No.	Keyword	Occurrence	Link	Total link strength
1	Level	74	74	1085
2	Health	62	68	745
3	Soil	61	51	1274
4	Concentration	59	45	1353
5	Electronic equipment	57	57	872
6	Site	53	59	986
7	Sample	52	55	1120
8	Material	50	61	716
9	Area	48	64	742
10	System	45	61	644

the results of the citation report applied in the Web of Science database, the citation performance is summarised in the following indicators: citing articles – 4048; citing articles – 3959 (without self-citations); times cited – 5513; times cited – 5290 (without self-citations); and H-index – 39.

The keywords analysis of research hotspots

Analysis of e-waste and the environment research based on the frequency of the keywords used in the title and abstracts of the articles can achieve a conceptual image of the content of these studies and reflect research hotspots. A total of 4358 co-occurrence keywords were extracted from 141 articles. The minimum occurrence of each keyword was set to nine times, and 126 co-occurrence keywords were finally presented. The top three keywords ranked by the number of occurrences were as follows: level (n = 74), health (n = 68), and soil (n = 61). Table 4 shows the top ten most occurring keywords, links, and the total link strength. The link strength between two nodes refers to the frequency of co-occurrence. It can be used as a quantitative index to depict the relationship between two nodes (Pinto *et al.*, 2014).

Network visualisation graph

For each of the 126 keywords, VOSviewer calculated a relevance score and selected the 76 (60%) most relevant keywords that were mapped into four clusters representing four research themes. Fig. 2 shows the keyword co-occurrence network map. The distance between two nodes reflects their associative strength. A shorter distance generally reveals a more substantial relationship. The line between two keywords represents that they have appeared together. Nodes with a similar colour belong to the same cluster (Wiendartun *et al.*, 2022). Cluster 1 (red) is the largest cluster related to e-waste recycling, policies, strategies, technology, and environmental impact. Cluster 2 (green) shows the concentration levels of heavy metals and other chemicals in soil, water, plants and humans in the areas or region studied. Cluster 3 (blue) depicts the effect of e-waste management practices on health. Keywords include health, product, e-waste management, and information. The yellow cluster is the smallest, showing the level of knowledge on the generation of e-waste and its impact on the environment. The red cluster relates to e-waste recycling, policies, strategies, technology, and environmental impact.

Developed countries have the infrastructure and equipment to recycle electrical and electronic waste (WEEE) to recover valuable materials in an environmentally friendly manner (Maphosa and Maphosa, 2020). Developing countries lack policies, infrastructure and systems to recover precious materials, repair for reuse, and improper disposal of electronic equipment has a detrimental effect on the environment (Lebbie *et al.*, 2021). The green cluster shows the concentration levels of heavy metals and other chemicals in soil, water, plants and humans in the areas or regions studied. Studies reveal that a large area of farmland in China is contaminated with heavy metals such as pahs and phosphodiesterase (PDE) from e-waste recycling initiatives, thus reducing arable land, which has enormous consequences on sustainability (Wang *et al.*, 2020). Soil samples around e-waste dumpsites in Ghana have high levels of heavy metals, sometimes 50 times higher than the World Health Organisations' (WHO) threshold levels (Asante *et al.*, 2011). Crops and plants around dumpsites and

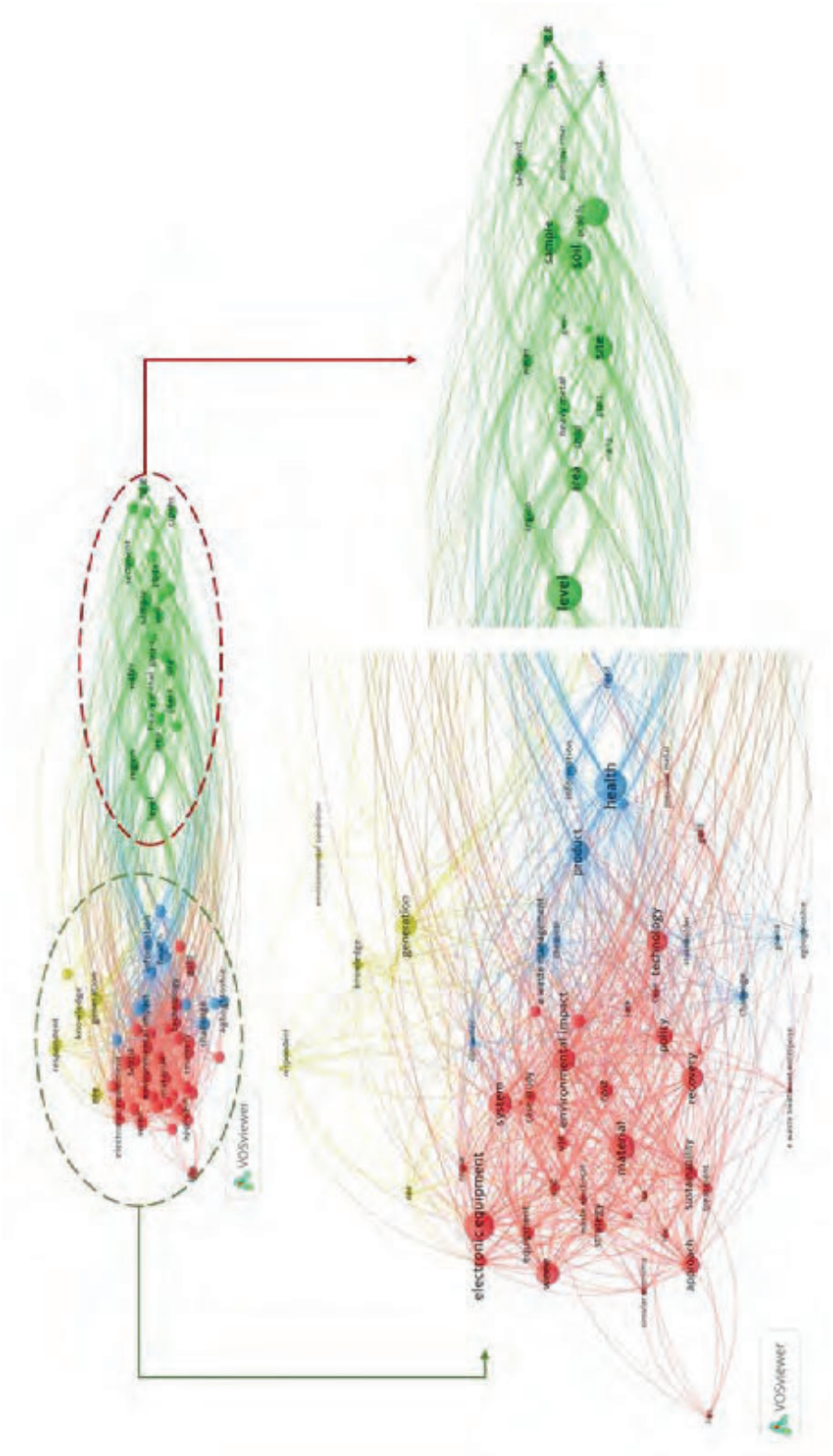

Fig. 2: The: Keywords co-occurrence network map

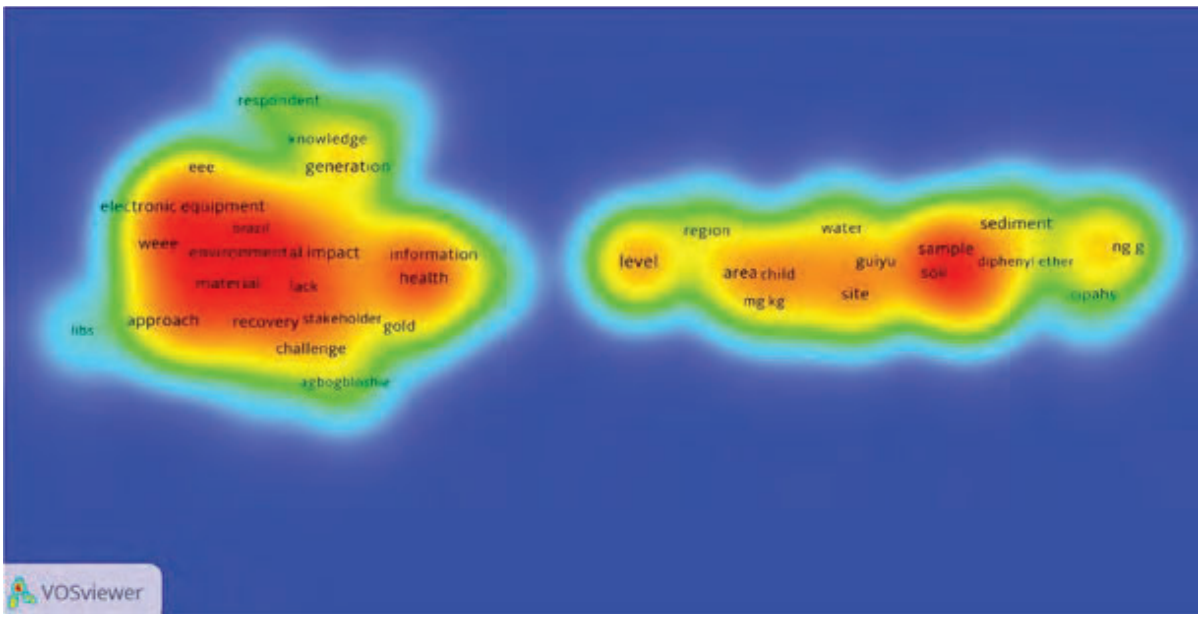

Fig. 3: Keywords density visualisation map

landfills are contaminated and toxic to humans and animals (Kiddee *et al.*, 2013). The blue cluster depicts the effect of e-waste management practices on health. Keywords include health, product, e-waste management, and information. The Agbogoloshie in Ghana is the largest landfill in Africa (Feldt *et al.*, 2014). Informal workers lack information on e-waste management and use rudimentary methods to extract rare earth metals through leaching, which causes health challenges (Huang *et al.*, 2014). The yellow cluster shows the level of knowledge on the generation of e-waste and its impact on the environment. The lack of e-waste policies, laws and legislation in most developing countries affects the awareness and knowledge levels of the community (Mutsau *et al.*, 2015). VOSviewer can make density visualisation (Fig. 3). Each node in the keyword's density visualisation map has a colour that relies on the density of items at that node. In other words, the colour of a node depends on the number of items in the node's neighbourhood.

The keywords in the red colour area appear more frequently; on the contrary, the keywords in the green colour area appear less frequently. From Fig. 3, we can see the core keywords in the e-waste and the environment field. These are: 'soil', 'sample', 'health', 'environmental impact', 'material', 'recovery', 'electronic equipment and 'WEEE'. In emerging economies, e-waste is collected together with municipal waste. Careless disposal and non-separation from solid waste lead to environmental pollution through illegal dumping and the recovery of precious minerals through rudimentary methods, polluting the air, soil, and water bodies (Kayes, 2019). Studies show that soils around e-waste dumpsites have high levels of toxic minerals such as lead, chromium, and cadmium. In some instances, these were 50 times higher than the permissible exposure levels set by WHO (Asante *et al.*, 2011). E-waste plants in Nigeria and China recorded high levels of lead, copper, manganese, cadmium in plants and the soils (Alabi *et al.*, 2012). Exposure to cadmium pollution during pregnancy may be a risk factor for shortened placental telomere length known to be related to cancer development and ageing (Lin *et al.*, 2013). The overlay network of keyword co-occurrence visualisation analysis is widely accepted to identify research hotspots (Chen, 2004). VOSviewer software was used to generate an overlay visualisation network of keyword co-occurrence to explore the changes of research hotspots over the last ten years. Fig. 4 shows the keywords overlay visualisation map. The results indicated that the keywords "LIBS" (laser-induced breakdown

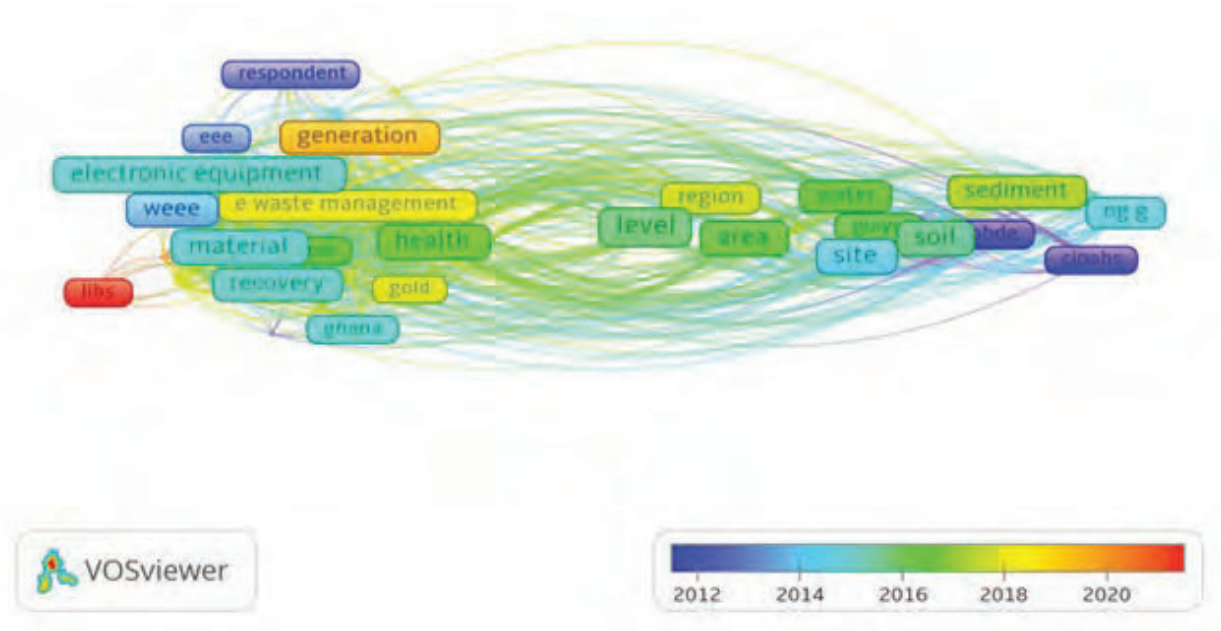

Fig. 4: Keywords overlay visualisation map (2012 – 2021)

spectroscopy) and "circular economy" emerged in 2021. LIBS is a tool for industrial process control that can be used to control the copper leaching process (Garcia *et al.*, 2021). Besides e-waste, LIBS also analyses soil, rocks, sediments, waters, landfill leachates, lubricating oils, and aerosols (Gonçalves *et al.*, 2021). A circular economy is an approach that avoids waste through the design of optimised cycles of products, components, and materials (Ellen MacArthur Foundation, 2013). More recently, the circular economy concept has been applied to e-waste. As a solution to the e-waste problem, a circular economy is an urban mining procedure of recovering and classifying mineral material (Xavier *et al.*, 2021). Gautam *et al.* (2021) explored how the disposal of solar photovoltaic e-waste could contribute to the circular economy in India. Islam *et al.* (2021) suggest a consumer-centric circular economy framework to advance knowledge and implementation strategies around e-waste.

The UN reported that e-waste recycling activities generated over USD 62.5 billion annually and reiterated the need to establish a circular economy based on e-waste management (IISD, 2019). Industry experts predict that e-waste revenue will surpass USD143 billion by 2028 (Allied Research Market, 2021). About 7% of the world's gold is contained in e-waste; low recycling rates have seen up to USD 22 billion worth of gold and platinum being dumped yearly (Globenewswire, 2018). Europe leads with about 40 collection and recycling rates, while less than 1% of e-waste generated in Africa is recycled (Forti *et al.*, 2020). China is currently recycling 30% of its generated e-waste (Chen *et al.*, 2019). Another study revealed that less than 1% of e-waste produced in Brazil was recycled in line with environmental and public health considerations (Caiado *et al.*, 2017). Proper recycling can reduce the release of greenhouse gas emissions, and the recovery of precious and rare earth metals from e-waste minimises the demand for pure minerals (Foelster *et al.*, 2016). Although informal e-waste recycling has created many jobs for the informal sector, rudimentary methods used to recover precious minerals are a threat to the environment and the health of the surrounding communities. The number of people dependent on e-waste activities continues to grow, and in 2010 over 200,000 people's livelihoods were supported by e-waste activities in Ghana (Prakash *et al.*, 2010). Annual income from e-waste activities in Ghana is estimated to be USD268 million (Oteng-Ababio *et al.*, 2014). The government of Ghana has organised seminars and workshops for the public to raise awareness of

the environmental and health impact of e-waste (Daum *et al.*, 2017). Based on the economic potential, e-waste management must be prioritised against other financial needs. The keywords such as "water", "soil", "health", "sediment", and "level" frequently appeared in the last six years, indicating that the impact of e-waste on the soil, water, and environment will continue to be researched hotspots in the near future. This is in line with findings of a study by Ackah (2017) that the major transport pathways in the e-waste recycling environment were: dust, air, water, soil, and biota. E-waste is dumped in landfills in most developing countries where informal workers attempt to recover precious materials using subsistence tools (Yohannessen *et al.*, 2019). Thus, hazardous chemicals contaminate water bodies, soils, and ozone-depleting gases are released into the atmosphere, contributing to climate change. Rare earth metals such as gold and copper, and other valuable materials are salvaged through burning and acid leaching, causing environmental damage and affecting the health of those living in the vicinity (Sun *et al.*, 2017; Tsydenova and Bengtsson, 2011). Informal workers in the e-waste value chain are often illiterate and cannot comprehend the environmental and health risks associated with their practices in recovering valuable materials (Singh *et al*., 2020). An earlier study by Harayama and Rekacewicz (2004) revealed that only 50% of the computer components were recyclable. The remaining 505 contained about 2kg of lead and other harmful materials, often dumped in landfills. About 20% of the farmland in China is contaminated with polycyclic aromatic hydrocarbons (pahs) from e-waste recycling initiatives, thus reducing arable land, which has enormous consequences on sustainability (Sun *et al*., 2018). Lakes, rivers and other water bodies in Guiyu, China, are contaminated with high lead levels due to indiscriminate burning and leaching of e-waste during the recovery of precious minerals (Li *et al.*, 2011). During recycling, released chemicals contaminate the dust, soils and water sources near dumpsites affecting the plants and fruits (Daum *et al.*, 2017). In a study in Japan, it was observed that rice and wheat irrigated with water from the Jinstu river were contaminated with cadmium and caused about 150 human deaths (Generowicz and Iwanejko, 2017). Research revealed that soils around informal e-waste recycling sites in Nigeria had high levels of zinc, nickel, chromium and cadmium compared to other sites (Isimekhai *et al.*, 2017). A study conducted in Ghana revealed that water bodies near dumpsites were contaminated as informal workers used leaching of acid to extract rare earth metals such as gold and copper from e-waste (Tue *et al.*, 2019). Thus toxic fumes, ashes, slag and harmful chemicals are released into the environment. E-waste recycling has contaminated large portions of underground water around landfills and dumpsites in Nigeria, making it unsuitable for human and animal consumption (Ewuim *et al.*, 2014;) explained that plants and crops are close to dumpsites are contaminated and are toxic to humans and animals. The UN's SDG 12 notes the rising e-waste problem and specifically addresses e-waste management. It highlights a recycling rate of 22.9%, while close to 80% of e-waste is unaccounted for and improperly disposed of, thereby polluting the environment (Ohajinwa *et al.*, 2017). Over 1000 substances are used in the manufacture of electronic equipment. These include precious minerals such as platinum, palladium, gold and copper, and toxic elements such as lead, mercury, cadmium, arsenic, etc. E-waste recycling is a lucrative industry; over USD 62.5 billion is realised annually, and over USD 22 billion worth of gold and platinum is dumped yearly. About 40% of e-waste generated in Europe is recycled, while less than 1% generated in Africa is recycled.

Looking forward

E-waste recycling is a lucrative industry; over USD 62.5 billion is realised annually, and over USD 22 billion worth of gold and platinum is dumped yearly. There is a need to establish a circular economy for the management of e-waste from the collection, separation, and recycling of e-waste. E-waste management will be improved by raising awareness of socio-economic and environmental benefits such as repairing, reusing, remanufacturing, and reducing. Funding is required to set up infrastructure that improves e-waste recycling and harnessing technology for e-waste management (Ellen Macarthur Foundation, 2021).

CONCLUSION

E-waste has become an environmental and epidemiological crisis requiring consented effort to

protect the environment from improper disposal. Many emerging economies do not have e-waste policies to protect the environment and public health. Less than 20% of African countries have an e-waste policy, legislation or regulation. In most developing countries, e-waste is collected together with municipal waste. Its management is informal, and workers with no environmental awareness use rudimentary tools to recover precious materials and release toxic elements that contaminate water bodies, the soils, and the release of ozone-depleting gases. Countries such as China, Nigeria and Ghana revealed that up to 20% of farmland and grazing land is polluted due to e-waste recycling. Lakes, rivers and other water bodies near landfills and dumpsites are contaminated, affecting marine life and plants. Human fatalities are reported from consuming plants and aquatic animals near landfills and dumpsites. Bibliometric analysis and review of the environmental impact of e-waste were conducted. No studies were found chronicling the environmental effects of e-waste using bibliometric analysis. This study aims to provide a comprehensive insight into e-waste and the environment through bibliometric and network analysis. From the initial 667 661 articles, 141 articles on e-waste and the environment published between 2003 and 2021 were selected for the study. The results show considerable growth in publications on e-waste and the environment. The number of articles published increased from one in 2003 to 25 in 2021, and citations rose from zero to 1049. This study highlights publication trends, citation trends, and articles' distribution by journals and geography. A third of the articles were published by Chinese authors, followed by India 13.5% and the United States with 12.8%. Developing countries contributed about 17% of the publications. It is observed that the research hotspots in the field are: soil, health, environmental impact, recovery, electronic equipment and waste electrical and electronic equipment. By tracing the evolutionary research pathway, it is clear that the research hotspots have shifted focus to e-waste generation, laser-induced breakdown spectroscopy, and circular economy. The red cluster from the density maps shows the strategies employed in recovering minerals from e-waste. The green cluster shows the concentration levels of the heavy minerals found in e-waste. The blue cluster visualises the impact of e-waste on health, and finally, the yellow cluster highlights the effects of e-waste on the environment. The study adds valuable insights to the body of literature in hazardous and toxic substances management. Scholars from developing countries are being encouraged to contribute more research as their countries are affected by the environmental impact of improper e-waste management. The knowledge gained from this research serves as a baseline for policymakers and scholars as more policies need to be enacted, and further research needs to be undertaken in light of the sustainable development goals (SDGs).

AUTHOR CONTRIBUTIONS

M. Maphosa was responsible for defining the bibliographic search, searching the bibliography, selecting the relevant references, synthesising the manuscript, revising the final version. V. Maphosa was responsible for conceptualising the draft, analysing the references' coding, and reviewing the whole manuscript.

ACKNOWLEDGEMENTS

The authors would like to thank the anonymous reviewers for their insightful suggestions, comments and careful reading of the manuscript.

CONFLICT OF INTEREST

The authors declare no potential conflict of interest regarding the publication of this work. In addition, ethical issues including plagiarism, informed consent, misconduct, data fabrication and, or falsification, double publication and, or submission, and redundancy have been completely witnessed by the authors.

PUBLISHER'S NOTE

GJESM Publisher remains neutral with regard to jurisdictional claims in published maps and institutional affiliations.

ABBREVIATIONS

%	Per cent
4IR	Fourth Industrial Revolution
CIPAHs	Chlorinated polycyclic aromatic hydrocarbons
EEE	Electrical and electronic equipment
E-waste	Electronic waste
Fig.	Figure
h-Index	Hirsch index
LCA	Life Cycle Assessment
ICT	Information Communications Technology
LIBS	Laser-Induced Breakdown Spectroscopy
mg/kg	milligrams per kilogram
ng/ g	nanogram per gram
PAHs	Polycyclic Aromatic Hydrocarbons
Pb	Lead
PCDD fs	Polychlorinated Dibenzo-p-Dioxins and Polychlorinated Dibenzofurans
PDE	Phosphodiesterase
SDG	Sustainable Development Goal
TI	Title
UN	United Nations
USD	United States Dollar
VOSviewer	A software tool for constructing and visualising bibliometric networks
WEEE	Waste Electrical and Electronic Equipment
WHO	World Health Organisation

REFERENCES

Abdul, K.; Muhammad, R.; Geoffrey, B.; Syed, M., (2014). Metal extraction processes for electronic waste and existing industrial routes: A Rev. Aust. Perspect. Resour., 3(1): 152–179 **(28 pages).**

Ackah, M., (2017). Informal e-waste recycling in developing countries: review of metal (loid) s pollution, environmental impacts and transport pathways. Environ. Sci. Pollut. Res., 24(31): 24092-24101 **(10 pages).**

Aimin, C.; Kim, N.; Xia, H.; Shuk-Mei, H., (2011). Developmental neurotoxicants in e-waste: an emerging health concern. Environ. Health Perspect., 119(4): 431-438 **(8 pages).**

Akon-Yamga, G.; Daniels, C.U.; Quaye, W.; Ting, B.M.; Asante, A.A., (2021). Transformative innovation policy approach to e-waste management in Ghana: perspectives of actors on transformative changes. Sci. Public Policy, 48(3): 387–397 **(11 pages).**

Alabi, O. A.; Bakare, A. A.; Xu, X.; Li, B., Zhang, Y.; Huo, X., (2012). Comparative evaluation of environmental contamination and DNA damage induced by electronic waste in Nigeria and China. Sci. Total Environ., 423: 62–72 **(11 pages).**

Allied Research Market, (2021). E-waste management market by application (trashed and recycled), processed material type (metal, plastic, glass, and others), and source type (household appliance, consumer electronics, and industrial electronics). Global Opportunity Analysis and Industry.

Amankwah-Amoah, J., (2016). Global business and emerging economies: towards a new perspective on the effects of e-waste. Technol. Forecasting Soc. Change, 105: 20-26 **(7 pages).**

Andrade, D.F.; Romanelli, J.P; Pereira-Filho, E.R., (2019). Past and emerging topics related to electronic waste management: top countries, trends, and perspectives. Environ. Sci. Pollut. Res., 26(17): 17135-17151 **(17 pages).**

Ardolino, F.; Cardamone, G.; Arena, U., (2021). About the environmental sustainability of the European management of WEEE plastics. Waste Manage., 126: 119–132 **(14 pages).**

Asante, K.; Adu-Kumi, S.; Nakahiro, K., (2011). Human exposure to PCBs, PBDEs and HBCDs in Ghana: temporal variation, sources of exposure and estimation of daily intakes by infants. Environ. Int., 37(5) : 921–928 **(8 pages).**

Avis, W., (2021). Drivers, barriers and opportunities of e-waste management in Africa.

Awasthi, A.K.; Zeng, X.; Li, J., (2016). Environmental pollution of electronic waste recycling in India: a critical review. Environ. Pollut., 211: 259-270 **(12 pages).**

Babu, B. R.; Parande, A. K.; Basha, C. A., (2007). Electrical and electronic waste: a global environmental problem. Waste Manage. Res., 25(4): 307-318 **(11 pages).**

Baldé, C.P.; Forti, V.; Gray, V.; Kuehr, R.; Stegmann, P., 2017. The global e-waste monitor 2017: quantities, flows and resources. United Nations University, International Telecommunication Union and International Solid Waste

Association.
Barba-Gutiérrez, Y.; Adenso-Diaz, B.; Hopp, M., (2008). An analysis of some environmental consequences of European electrical and electronic waste regulation. Resour. Conserv. Recycl., 52(3): 481-495 **(15 pages).**
Caiado, N.; Guarnieri, P.; Xavier, L.; Chaves, G., (2017). A characterisation of the Brazilian market of reverse logistic credits (RLC) and an analogy with the existing carbon credit market. Resour. Conserv. Recycl., 118: 47–59 **(13 pages).**
Chen, C., (2004). Searching for intellectual turning points: progressive knowledge domain visualisation. PNAS, 101(1): 5303-5310 **(8 pages).**
Chen, F.; Li, X.; Yang, Y.; Hou, H.; Liu, G.; Zhang, S., (2019). Storing e-waste in green infrastructure to reduce perceived value loss through landfill siting and landscaping: a case study in Nanjing, China. Sustain., 11(1829): 1-15 **(15 pages).**
Chitotombe, W., (2013). Globalisation of information communication technology (ICT) and consumerism in developing countries: confronting the challenges of e-waste disposal in Harare urban, Zimbabwe. Int. J. Environ. Sci., 3(6): 2172-2185 **(14 pages).**
Daum, K.; Stoler, J.; Grant, R., (2017). Toward a more sustainable trajectory for e-waste policy: a review of a decade of e-waste research in Accra, Ghana. Int. J. Environ. Res. Public Health, 14: 135-142 **(8 pages).**
de Albuquerque, C.A.; Mello, C.H.P.; de Freitas Gomes, J.H.; Dos Santos, V.C., (2021). Bibliometric analysis of studies involving e-waste: a critical review. Environ. Sci. Pollut. Res., 28(35): 47773-47784 **(12 pages).**
Deubzer, O.; Herreras, L.; Hajosi, E.; Hilbert, I.; Buchert, M.; Wuisan, L.; Zonneveld, N., (2019). Baseline and gap/obstacle analysis of standards and regulations – CEWASTE Voluntary Certification Scheme for Waste Treatment **(171 pages).**
Ellen Macarthur Foundation, (2021). Circular economy in Africa: examples and opportunities:
electronics and e-waste. Ellen Macarthur Foundation.
Ewuim, S.; Akkune, C.; Abajue, M.; Nwanko, E.; Faniran, O., (2014). Challenges of e-waste pollution to soil environments in Nigeria - a review. Animal Res. Int., 11(2): 1976–1981 **(6 pages).**
Feldt, T.; Fobil, J.N.; Wittsiepe, J.; Wilhelm, M.; Till, H.; Zoufaly, A.; Burchard, G.; Göen, T., (2014). High levels of pah-metabolites in urine of e-waste recycling workers from Agbogbloshie, Ghana. Sci. Total Environ., 466-467:369-376 **(8 pages).**
Foelster, A.; Andrew, S.; Kroeger, L.; Bohr, P.; Dettmer, T.; Boehme, S.; Herrmann, C., (2016). Electronics recycling as an energy efficiency measure – a life cycle assessment (LCA) study on refrigerator recycling in Brazil. J. Cleaner Prod., 129: 30-42 **(13 pages).**
Forti, V.; Balde, C.; Kuehr, R.; Bel, G., (2020). The global e-waste monitor 2020 **(120 pages).**
Gao, Y.; Ge, L.; Shi, S.; Sun, Y.; Liu, M.; Wang, B.; Shang, Y.; Wu, J.; Tian, J., (2019). Global trends and future prospects of e-waste research: a bibliometric analysis. Environ. Sci. Pollut. Res., 26(17): 17809-17820 **(12 pages).**
Garcia, J.A.; da Silva, J.R.A.; Pereira-Filho, E.R., (2021). LIBS as an alternative method to control an industrial hydrometallurgical process for the recovery of Cu in waste from electro-electronic equipment (WEEE). Microchem. J., 164: 1 -7 **(7 pages).**
Gautam, A.; Shankar, R.; Vrat, P., (2021). End-of-life solar photovoltaic e-waste assessment in India: a step towards a circular economy. Sustainable Prod. Consumption, 26: 65-77 **(13 pages).**
Generowicz, A.; Iwanejko, R., (2017). Environmental risks related to the recovery and recycling processes of waste electrical and electronic equipment (WEEE). Problemy Ekorozwofu/ Problems. Sustainable Dev., 12(2): 181-192 **(12 pages).**
Georgiadis, P.; Besiou, M., (2008). Sustainability in electrical and electronic equipment closed-loop supply chains: a system dynamics approach. J. Cleaner Prod., 16(15): 1665-1678 **(14 pages).**
Ghasem, A.M.H.; Khoramnejadian, S., (2015). The extraction of gold from e-waste by hydrometallurgy. Orient. J. Chem., 31(1): 113-120 **(8 pages).**
Globenewswire. (2018). Gold in e-waste valued at $22 billion thrown away in 2016, new study shows. GlobeNewswire.
Gonçalves, D.A.; Senesi, G.S.; Nicolodelli, G., (2021). Laser-induced breakdown spectroscopy applied to environmental systems and their potential contaminants. an overview of advances achieved in the last few years. Trends Environ. Anal. Chem., 30 :1-12 **(12 pages).**
Grant, K.; Goldizen, F.C.; Sly, F. D; Brune, M.N.; Neira, M.; van den Berg, M.; Norman, R.E., (2013). Health consequences of exposure to e-waste: a systematic review. The Lancet Global Health, 1(6): e350-e361 **(12 pages).**
Hischier, R.; Wäger, P.; Gauglhofer, J., (2005). Does WEEE recycling make sense from an environmental perspective?: the environmental impacts of the Swiss take-back and recycling systems for waste electrical and electronic equipment (WEEE). Environ. Impact Assess. Rev., 25(5): 525-539 **(15 pages).**
Hossain, M.S.; Al-Hamadani, S.M.; Rahman, M.T., (2015). E-waste: a challenge for sustainable development. J. Health Pollut., 5(9): 3-11 **(9 pages).**
Huang, J.; Nkrumah, P.; Anim, D.; Mensah, E., (2014). E-waste disposal effects on the aquatic environment: Accra, Ghana. Rev. Environ. Contam. Toxicol., 229: 19–34 **(16 pages).**
Ikhlayel, M., (2018). An integrated approach to establish e-waste management systems for developing countries. J. Cleaner Prod., 170: 119-130 **(12 pages).**
IISD, (2019). UN report highlights environmental, health risks from e-waste, urges circular economy shift.
Isimekhai, K.; Garelick, H.; Watt, J.; Purchase, D., (2017). Heavy metals distribution and risk assessment in soil from an informal e-waste recycling site in Lagos State, Nigeria. Environ. Sci. Pollut. Res. Int., 24: 17206–17219 **(14 pages).**
Islam, M.T.; Huda, N.; Baumber, A.; Shumon, R.; Zaman, A.; Ali, F.; Hossain, R.; Sahajwalla, V., (2021). A global review of consumer behavior towards e-waste and implications for

the circular economy. J. Cleaner Prod., 316: 1-36 **(36 pages).**

Kang, D. H.; Chen, M.; Ogunseitan, O. A., (2013). Potential environmental and human health impacts of rechargeable lithium batteries in electronic waste. Environ. Sci. Technol., 47(10): 5495-5503 **(9 pages).**

Kayes, I; Shahriar, SA; Hasan, K.; Akhtar, M.; Kabir, M.M.; Salam, M.A., (2019). The relationships between meteorological parameters and air pollutants in an urban environment. Global J. Environ. Sci. Manage., 5(3): 265-278 **(14 pages).**

Kiddee, P.; Naidu, R.; Wong, M., (2013). Electronic waste management approaches an overview. Waste Manage., 33(5): 1237–1250 **(14 pages).**

Kumar, A.; Holuszko, M.; Espinosa, D.C.R., (2017). E-waste: an overview on generation, collection, legislation and recycling practices. Resour. Conserv. Recycl., 122: 32-42 **(11 pages).**

Lambrechts, D., (2016). Environmental crime in Sub-Saharan Africa – a review and future challenges. Politikon, 43(2): 155–158 **(4 pages).**

Lebbie, T.; Moyebi, O.; Asante, K.; Fobil, J.; Brune-Drisse, M.; Suk, W.K; Sly, P.D.; Gorman, J.; Carpenter, D., (2021). E-waste in Africa: a serious threat to the health of children. Int. J. Environ. Res. Public Health, 18: 1- 25 **(25 pages).**

Li, B.; Hu, H. Z.; Ding, H. J.; Shi, M. Y., (2011). E-waste recycling and related social issues in China. Energy Procedia, 5: 2527–2531 **(5 pages).**

Li, K.; Xu, Z., (2019). A review of current progress of supercritical fluid technologies for e-waste treatment. J. Cleaner Prod., 227: 794-809 **(16 pages).**

Lin, S.; Ali, U.H.; Zheng, C.; Cai, Z.; Wong, M.H., (2022). Toxic chemicals from uncontrolled e-waste recycling: exposure, body burden, health impact. J. Hazard. Mater., 426: 1 - 12 **(8 pages).**

Lin, S.; Huo, X.; Zhang, Q.; Fan, X.; Du, L.; Xu, X., (2013). Short placental telomere was associated with cadmium pollution in an electronic waste recycling town in China. PLoS One, 8(4): 1-8 **(8 pages).**

Liu, H.; Zhou, Q.; Wang, Y.; Zhang, Q.; Cai, Z.; Jiang, G., (2008). E-waste recycling induced polybrominated diphenyl ethers, polychlorinated biphenyls, polychlorinated dibenzo-p-dioxins and dibenzo-furans pollution in the ambient environment. Environ. Int., 34(1): 67-72 **(6 pages).**

Lundgren, K., (2012). The global impact of e-waste: addressing the challenge. Geneva: International Labour Office **(72 pages).**

Maphosa, V., (2021). Students' awareness and attitudinal dispositions to e-waste: management practices at a Zimbabwean university. J. Inf. Policy, 11: 1-24 **(24 pages).**

Maphosa, V.; Maphosa, M., (2020). E-waste management in Sub-Saharan Africa: a systematic literature review. Cogent Bus. Manage., 1(7): 1-19 **(19 pages).**

Matsukami, H.; Tue, N. M.; Suzuki, G.; Someya, M.; Tuyen, L. H.; Viet, P. H.; Takahashi, S.; Tanabe., S.; Takigami, H., (2015). Flame retardant emission from e-waste recycling operation in northern Vietnam: environmental occurrence of emerging organophosphorus esters used as alternatives for PBDEs. Sci. Total Environ., 514: 492-499 **(8 pages).**

Mureithi, M.; Waema, T., (2008). E-waste management in Kenya **(67 pages).**

Mutsau, S.; Billiat, E.; Musingafi, M., (2015). Electronic waste management in Zimbabwe: a slow onset public health disaster. Civ. Environ. Res., 7(19): 84-87 **(4 pages).**

Needhidasan, S.; Samuel, M.; Chidambaram, R., (2014). Electronic waste – an emerging threat to the environment of urban India. J. Environ. Health Sci. Eng., 12(1): 1-9 **(9 pages).**

Nwagwu, W.E.; Okuneye, M., (2016). Awareness and attitudes of small-scale information technology business operators in Lagos, Nigeria, toward e-waste hazards. J. Global Inf. Technol. Manage., 19(4): 267-282 **(16 pages).**

Ohajinwa, C.M.; Van Bodegom, P.M.; Vijver, M.G.; Peijnenburg, W.G.J.M., (2017). Health risks awareness of electronic waste workers in the informal sector in Nigeria. Int. J. Environ. Res. Public Health, 14(8): 1-16 **(16 pages).**

Omobowale, A.O., (2013). The Tokunbo phenomenon and the second-hand economy in Nigeria. In: Onyeje, I. (Ed), Confronting the challenge of e-waste in Nigeria. Peter Lang., Oxford **(190 pages).**

Ongondo, F.; Williams, I.; Cherrett, T., (2011). How are WEEE doing? a global review of the management of electrical and electronic wastes. Waste Manage., 31: 714–730 **(17 pages).**

Oteng-Ababio, M.; Amankwaa, E.F.; Chama, M.A. (2014). The local contours of scavenging for e-waste and higher-valued constituent parts in Accra, Ghana. Habitat Int., 43: 163–71 **(9 pages).**

Patil, R.A.; Ramakrishna, S., (2020). A comprehensive analysis of e-waste legislation worldwide. Environ. Sci. Pollut. Res., 27(13): 14412-14431 **(20 pages).**

Pathak, P.; Srivastava, R.R., (2019). Environmental management of e-waste, in Prasad, M.N.V.; Vithanage, M. (Eds.), Electronic waste management and treatment technology. Butterworth-Heinemann, 103-132 **(30 pages).**

Perkins, D.; Drisse, B.; Nxele, T.; Sly, P., (2014). E-waste: a global hazard. Ann. Global Health, 80(4): 286–295 **(10 pages).**

Pinto, M.; Pulgarín, A.; Escalona, M. I., (2014). Viewing information literacy concepts: a comparison of two branches of knowledge. Scientometrics, 98: 2311–2329 **(19 pages).**

Prakash, S.; Manhart, A.; Amoyaw-Osie, Y.; Agyekum, O., (2010). Socio-economic assessment and feasibility study on sustainable e-waste management in Ghana. Oko-Institute Publications, Freiburg. **(118 pages).**

Premalatha, M.; Tabassum-Abbasi; Abbasi, T.; Abbasi, S.A., (2014). The generation, impact, and management of e-waste: state of the art. Crit. Rev. Env. Sci. Technol., 44(14): 1577-1678 **(2 pages).**

Rautela, R.; Arya, S.; Vishwakarma, S.; Lee, J.; Kim, K.H.; Kumar, S., (2021). E-waste management and its effects on the environment and human health. Sci. Total Environ., 773: 1-16 **(16 pages).**

Robinson, B. H., (2009). E-waste: An assessment of global production and environmental impacts. Sci. Total Environ.,

408(2): 183-191 **(9 pages).**

Sabra, S.; Malmqvist, E.; Saborit, A.; Gratacós, E.; Gomez, R., (2017). Heavy metals exposure levels and their correlation with different clinical forms of fetal growth restriction. PLoS One, 12(10): 1 -19 **(19 pages).**

Saphores, J. D.; Ogunseitan, O. A.; Shapiro, A. A., (2012). Willingness to engage in a pro-environmental behavior: an analysis of e-waste recycling based on a national survey of US households. Resour. Conserv. Recycl., 60: 49-63 **(15 pages).**

Schulz, H. J.; Schumann, H., (2006). Visualising graphs – a generalised view. In Tenth International Conference on Information Visualisation (IV'06). London, United Kingdom 5 – 7 July.

Singh, N.; Duan, H.; Tang, Y., (2020). Toxicity evaluation of e-waste plastics and potential repercussions for human health, Environ. Int., 137: 1-8 **(8 pages).**

Singh, S.; Trivedi, B.; Dasgupta, M.S.; Routroy, S., (2021). A bibliometric analysis of circular economy concept in e-waste research during the period 2008–2020. Mater. Today: Proc., 46: 8519-8524 **(6 pages).**

Sthiannopkao, S.; Wong, M., (2013). Handling e-waste in developed and developing countries: initiatives, practices, and consequences. Sci. Total Environ., 1147(53): 463–464 **(2 pages).**

Song, Q.; Li, J., (2014). Environmental effects of heavy metals derived from the e-waste recycling activities in China: a systematic review. Waste Manage., 34(12): 2587-2594 **(8 pages).**

Sun, J.; Pan, L.; Tsang, D.; Zhan, Y.; Zhu, L.; Li, X., (2018). Organic contamination and remediation in the agricultural soils of China: a critical review. Sci. Total Environ., 615: 724–740 **(17 pages).**

Sun, Z.H.; Cao, H.; Xiao, Y.; Sietsma, J.; Jin, W.; Agterhuis, H.; Yang, Y., (2017). Toward sustainability for recovery of critical metals from electronic waste: the hydrochemistry processes. ACS Sustainable Chem. Eng., 5(1): 21-40 **(20 pages).**

Sweileh, W., (2021). Bibliometric analysis of peer-reviewed literature on antimicrobial stewardship from 1990 to 2019. Globalisation Health, 17(1): 1-14 **(14 pages).**

Sztumski, W., (2014). Sustainable development — unbalanced devastation of the environment and its consequences. Probl. Sustain. Dev., 9: 89–96 **(8 pages).**

Tahamtan, I.; Afshar, A.S.; Ahamdzadeh, K., (2016). Factors affecting number of citations: a comprehensive review of the literature. Scientometrics, 107: 1195–1225 **(31 pages).**

Tue, N.M.; Matsushita, T.; Goto, A.; Itai, T.; Asante, K.A.; Obiri, S.; Mohammed, S.; Tanabe, S.; Kunisue, T., (2019) Complex mixtures of brominated/chlorinated diphenyl ethers and dibenzofurans in soils from the Agbogbloshie e-waste site (Ghana): occurrence, formation, and exposure implications. Environ. Sci. Technol., 53(6): 3010–3017 **(8 pages).**

Tsydenova, O.; Bengtsson, M., (2011). Chemical hazardous associated with the treatment of waste electrical and electronic equipment. Waste Manage., 31: 45-58 **(14 pages).**

UN, (2021). Ensure sustainable consumption and production patterns. United Nations.

van Eck, N.; Waltman, L., (2010). Software survey: VOSviewer, a computer program for bibliometric mapping. Scientometrics, 84(2): 523–538 **(16 pages).**

Vi, K.S.; Matthew, D., (2014). Recycling mobile phone impact on life cycle assessment. Procedia CIRP, 15: 263-271 **(9 pages).**

Wäger, P. A.; Hischier , R.; Eugster, M., (2011). Environmental impacts of the Swiss collection and recovery systems for waste electrical and electronic equipment (WEEE): a follow-up. Sci. Total Environ., 409(10): 1746-1756 **(11 pages).**

Wang, K.; Qian, J.; Liu, L., (2020). Understanding environmental pollutions of informal e-waste clustering in global south via multi-scalar regulatory frameworks: a case study of Guiyu Town, China. Int. J. Environ. Res. Public Health, 17: 1-18 **(18 pages).**

Wang, R.; Xu, Z., (2014). Recycling of non-metallic fractions from waste electrical and electronic equipment (WEEE): A review. Waste Manage., 34(8):1455–1469 **(15 pages).**

Wiendartun, W.; Wulandari, C.; Fauzan, N.; Hasanah, L.; Nugroho, H.; Pawinanto, E.; Mulyanti, B., (2022). Trends in research related to photonic crystal (PHC) from 2009 to 2019: a bibliometric and knowledge mapping analysis. J. Eng. Sci. Technol., 17(1): 343-360 **(18 pages).**

Xavier, L.H.; Giese, E.C.; Ribeiro-Duthie, A.C.; Lins, F.A.F., (2021). Sustainability and the circular economy: a theoretical approach focused on e-waste urban mining. Resour. Polic., 74: 1-9 **(9 pages).**

Xing, G. H.; Chan, J. K.; Leung, A. O.; Wu, S. C.; Wong, M. H., (2009). Environmental impact and human exposure to PCBs in Guiyu, an electronic waste recycling site in China. Environ. Int., 35(1): 76-82 **(7 pages).**

Ye, F.; Liu, Z.; Xia, L., (2021). Materials and energy balance of e-waste smelting—an industrial case study in China. Met., 11(11): 1-14 **(14 pages).**

Yohannessen, K.; Pinto-Galleguillos, D.; Parra-Giordano, D.; Agost, A., Valdés, M.; Smith, L., (2019). Health assessment of electronic waste workers in Chile: participant characterisation. Int. J. Environ. Res. Public Health, 16(3): 386-393 **(8 pages).**

Zeng, X.; Li, J., (2016). Measuring the recyclability of e-waste: an innovative method and its implications. J. Cleaner Prod., 131: 156-162 **(7 pages).**

Zhang, L.; Geng, Y.; Zhong, Y.; Dong, H.; Liu, Z., (2019). A bibliometric analysis on waste electrical and electronic equipment research. Environ. Sci. Pollut. Res., 26(21): 21098-21108 **(11 pages).**

Zheng, X.; Huo, X.; Zhang, Y.; Wang, Q.; Zhang, Y.; Xu, X., (2019). Cardiovascular endothelial inflammation by chronic coexposure to lead (Pb) and polycyclic aromatic hydrocarbons from preschool children in an e-waste recycling area. Environ. Pollut., 246: 587–596 **(10 pages).**

AUTHOR (S) BIOSKETCHES

Maphosa, M., Ph.D. Candidate, Researcher, School of Information Technology, Varsity College, Independent Institute of Education, Sandton, South Africa.

- Email: *mfowabo@gmail.com / mmfowabo@varsitycollege.co.za*
- ORCID: 0000-0003-3702-6821
- Web of Science ResearcherID: NA
- Scopus Author ID: NA
- Homepage: https://www.varsitycollege.co.za/

Maphosa, V.., Ph.D., Director, Information Communication and Technology Services Department, Lupane State University, Bulawayo, Zimbabwe.

- Email: *v.maphosa@gmail.com / vmaphosa@lsu.ac.zw*
- ORCID: 0000-0002-2595-3890
- Web of Science ResearcherID: NA
- Scopus Author ID: NA
- Homepage: http://www.lsu.ac.zw/

HOW TO CITE THIS ARTICLE

Maphosa, M.; Maphosa, V. (2022). A bibliometric analysis of the effects of electronic waste on the environment. Global J. Environ. Sci.Manage., 8(4): 589-606.

DOI: 10.22034/gjesm.2022.04.10

url: https://www.gjesm.net/article_251174.html

PUBLICATION ETHICS

The ethical policy of GJESM is based on the Committee on Publication Ethics (COPE) guidelines and complies with International Committee of GJESM Editorial Board codes of conduct. Readers, authors, reviewers and editors should follow these ethical policies once working with GJESM. The ethical policy of GJESM is liable to determine which of the typical research papers or articles submitted to the journal should be published in the concerned issue. For information on this matter in publishing and ethical guidelines please visit http://publicationethics.org

Duties and Responsibilities of Publishers

1. GJESM is committing to ensure that editorial decisions on manuscript submissions are the final.
2. GJESM is promising to ensure that the decision on manuscript submissions is only made based on professional judgment and will not be affected by any commercial interests.
3. GJESM is committing to maintain the integrity of academic and research records.
4. GJESM is monitoring the ethics by Editor-in-Chief, Associate Editors, Editorial Board Members, Reviewers, Authors, and Readers.
5. GJESM is always checking the plagiarism and fraudulent data issues involving in the submitted manuscript.
6. GJESM is always willing to publish corrections, clarifications and retractions involving its publications as and when needed.

Duties and Responsibilities of Editors

1. The Editors of the journal should have the full authority to reject/accept a manuscript.
2. The Editors of the journal should maintain the confidentiality of submitted manuscripts under review or until they are published.
3. The Editor-in-Chief should take a decision on submitted manuscripts, whether to be published or not with other editors and reviewers
4. The Editors of the journal should preserve the anonymity of reviewers.
5. The Editors of the journal should disclose and try to avoid any conflict of interest.
6. The Editors of the journal should maintain academic integrity and strive to meet the needs of readers and authors.
7. The Editors of the journal should be willing to investigate plagiarism and fraudulent data issues and willing to publish corrections, clarifications, retractions, and apologies when needed.
8. The Editors of the journal should have the limit themselves only to the intellectual content.
9. The Editors of the journal must not disclose any information about submitted manuscripts to anyone other than the corresponding author, reviewers, potential reviewers, other editorial advisers, and the publisher, as appropriate.
10. Unpublished materials disclosed in a submitted paper will not be used by the editor or the members of the editorial board for their own research purposes without the author's explicit written consent.

Duties and Responsibilities of Reviewers

1. The Reviewers of the journal should assist the Editors in taking the decision for publishing the submitted manuscripts.
2. The Reviewers should maintain the confidentiality of manuscripts, which they are invited to review.
3. The Reviewers should provide comments in time that will help editors to make decision on the submitted manuscript to be published or not.
4. The Reviewers are bound to treat the manuscript received for peer reviewing as confidential, and must not use the information obtained through peer review for personal advantage.
5. The Reviewers comments against each invited manuscript should be technical, professional and objective.
6. The Reviewers should not review the manuscripts in which they have found conflicts of interest with any of the authors, companies, or institutions.
7. The Reviewers should disclose and try to avoid any conflict of interest.

Duties and Responsibilities of Authors

1. Manuscripts must be submitted only in English and should be written according to sound grammar and proper terminology.
2. Manuscripts must be submitted with the understanding that they have not been published elsewhere (except in the form of an abstract or as part of a published lecture, review, or thesis) and are not currently under consideration by another journal published by or any other publisher.
3. The submitting (corresponding) author is responsible for ensuring that the manuscript article's publication has been approved by all the other coauthors.
4. In order to sustain the peer review system, authors have an obligation to participate in peer review process to evaluate manuscripts from others.
5. It is also the authors' responsibility to ensure that the manuscripts emanating from a particular institution are submitted with the approval of the necessary institution.
6. It is a condition for submission of a manuscript that the authors permit editing of the paper for readability.
7. Authors are requested to clearly identify who provided financial support for the conduct of research and/or preparation of the manuscript and briefly describe the role of the funder/sponsor in any part of the work.
8. A copy right release and conflict of interest disclosure form must be signed by the corresponding author in case of multiple authorships, prior to the acceptation of the

manuscript, by all authors, for publication to be legally responsible towards the Journal ethics and privacy policy.

9. Under open access license, authors retain ownership of the copyright for their content, but allow anyone to download, reuse, reprint, modify, distribute, and/ or copy the content as long as the original authors and source are cited properly.
10. All authors have agreed to allow the corresponding author to serve as the primary correspondent with the editorial office, to review the edited manuscript and proof.
11. When author(s) discovers a significant error or inaccuracy in his/her own published work, it is the author's obligation to promptly notify the journal editor or publisher to retract or correct the manuscript.
12. All authors must know that that the submitted manuscripts under review or published with GJESM are subject to screening using Plagiarism Prevention Software. Plagiarism is a serious violation of publication ethics.

Violation of Publication Ethics

1. **Plagiarism:** Plagiarism is intentionally using someone else's ideas or other original material as if they are one's own. Copying even one sentence from someone else's manuscript, or even one of your own that has previously been published, without proper citation is considered by GJESM Journals as plagiarism. All manuscripts under review or published with GJESM are subject to screening using plagiarism prevention software. Thus, plagiarism is a serious violation of publication ethics. The development of CrossCheck is a service that helps editors to verify the originality of papers. CrossCheck is powered by the Ithenticate software from iParadigms, known in the academic community as providers of Turnitin. For a searchable list of all journals in the CrossCheck database, please visit: www.ithenticate.com/search
2. **Data Fabrication and Falsification:** Data fabrication and falsification means the researcher did not really carry out the study, but made up data or results and had recorded or reported the fabricated information. Data falsification means the researcher did the experiment, but manipulated, changed, or omitted data or results from the research findings.
3. **Simultaneous Submission:** Simultaneous submission occurs when a manuscript (or substantial sections from a manuscript) is submitted to a journal when it is already under consideration by another journal.
4. **Duplicate Publication:** Duplicate publication occurs when two or more papers, without full cross referencing, share essentially the same hypotheses, data, discussion points, and conclusions.
5. **Redundant Publications:** Redundant publications involve the inappropriate division of study outcomes into several articles, most often consequent to the desire to plump academic vitae.
6. **Improper Author Contribution or Attribution:** All listed authors must have made a significant scientific contribution to the research in the manuscript and approved all its claims. Don't forget to list everyone who made a significant scientific contribution, including students and laboratory technicians.
7. **Citation Manipulation:** Citation Manipulation is including excessive citations, in the submitted manuscript, that do not contribute to the scholarly content of the article and have been included solely for the purpose of increasing citations to a given author's work, or to articles published in a particular journal. This leads to misrepresenting the importance of the specific work and journal in which it appears and is thus a form of scientific misconduct.

Handling Cases of Misconduct

Once GJESM confirms a violation against GJESM's publication ethics, GJESM addresses ethical concerns diligently following an issue-specific standard practice as summarized below.

1. The first action of the journal Editor is to inform the Editorial Office of GJESM by supplying copies of the relevant material and a draft letter to the corresponding author asking for an explanation in a nonjudgmental manner.
2. If the author's explanation is unacceptable and it seems that serious unethical conduct has taken place, the matter is referred to the Publication Committee via Editorial Office. After deliberation, the Committee will decide whether the case is sufficiently serious to warrant a ban on future submissions.
3. If the infraction is less severe, the Editor, upon the advice of the Publication Committee, sends the author a letter of reprimand and reminds the author of GJESM publication policies; if the manuscript has been published, the Editor may request the author to publish an apology in the journal to correct the record.
4. Notification will be sent to corresponding author and any work by the author responsible for the violation or any work these persons coauthored that is under review by GJESM journal will be rejected immediately.
5. The authors are prohibited from serving on GJESM editorial board and serving as a reviewer for GJESM Journal. GJESM reserves the right to take more actions.
6. In extreme cases, notifications will be sent to the affiliations of the authors and the authors are prohibited from submitting their work to GJESM for 5 years.
7. In serious cases of fraud that result in retraction of the article, a retraction notice will be published in the journal and will be linked to the article in the online version. The online version will also be marked "retracted" with the retraction date.

GUIDE FOR AUTHORS

"Global Journal of Environmental Science and Management" (GJESM) is a double blind peer reviewed electronic and print quarterly publication concerned with all aspects of environmental science and management. GJESM publishes original research papers, review papers, case reports and short communications, letters to editor and authors' response about letters to editor across the broad field of environment. These include but are not limited to environmental science, environmental management, environmental engineering, environmental planning and design, urban and regional landscape design and industrial ecology. Environmentalist disciplines are invited to contribute their knowledge and experience. The publication appears at regular intervals time quarterly. The Journal database is fully open access and full text of published articles are available for everyone who can get access to the Journal website free of cost. The authors never pay any charges for submission, article processing and publication.

Guide for Authors: More details on guide for authors refer: http://gjesm.net/journal/authors.note

GENERAL

1. Authors should submit their contributions electronically through the GJESM website submission system to the Editorial Office.

2. Manuscripts must be submitted only in English and should be written according to sound grammar and proper terminology. Manuscripts should be typed in Times New Roman of 11 pt. font and in MS-Word format in one column with 2.5 cm margin at each side. Manuscript submission must be applied once in order to obtain only one submission ID number. More than one submission for a single manuscript can lose the chance of the manuscript consideration. Manuscript must be accompanied by a covering letter including title and author(s) name.

3. There are no strict formatting requirements but all manuscripts must contain the essential elements needed to convey your manuscript, for example Abstract, Keywords, Introduction, Materials and Methods, Results, Conclusions, Artwork and Tables with Captions. Please ensure the figures and the tables included in the single file are placed next to the relevant text in the manuscript, rather than at the bottom or the top of the file. There are no strict requirements on reference formatting at submission. References can be in any style or format as long as the style is consistent.

BEFORE YOU BEGIN

1. Peer-Review Process: In order to sustain the peer review system, authors have an obligation to participate in peer review process to evaluate manuscripts from others. When appropriate, authors are obliged to provide retractions and/or corrections of errors to the editors and the Publisher. All papers submitted to GJESM journal will be peer reviewed for at least one round. GJESM journal adopts a double-blinded review policy: authors are blind to reviewers, but reviewers are not blind to authors. After receiving reviewers' comments, the editorial team member makes a decision. Because reviewers sometimes do not agree with each other, the final decision sent to the author may not exactly reflect recommendations by any of the reviewers. The decision after each round of peer review may include (a) Accept without any further changes, (b) Accept with minor revision, (c) Major changes are necessary for resubmission and (d) Decline without encouraging resubmission.

2. Post-Publication Evaluation: In addition to rapid Peer Review Process, the GJESM Journal has Post-Publication Evaluation by the scientific community. Post-Publication Evaluation is concentrated to ensure that the quality of published research, review and case report meets certain standards and the conclusions that are presented are justified. The post-publication evaluation includes online comments and citations on published papers. Authors may respond to the comments of the scientific community and may revise their manuscript. The Post-Publication Evaluation is described in such a way; it is allowing authors to publish quickly about Environmental science, management, engineering and technology concepts.

3. Publication Ethics: The ethical policy of GJESM is based on the Committee on Publication Ethics (COPE) guidelines and complies with International Committee of GJESM Editorial Board codes of conduct. Readers, authors, reviewers and editors should follow these ethical policies once working with GJESM. The ethical policy of GJESM is liable to determine which of the typical research papers or articles submitted to the journal should be published in the concerned issue. The ethical policy insisted the Editor-in-Chief, may confer with other editors or reviewers in making the decision. Visit at: http://publicationethics.org

4. Conflict of Interest: Authors are requested to evident whether impending conflicts do or do not exist. A copyright transfer agreement is signed by the corresponding author, upon the acceptance of the manuscript, on behalf of all authors, for publication to be legally responsible towards the journal ethics and privacy policy. Authors will be notified as soon as possible of decisions concerning the suitability of their manuscripts for publication in the journal. The submitted materials may be considered for inclusion but cannot be returned and Editors of the journal reserve the right to accept or reject any article in any stage, if necessary. Conflict of Interest Disclosure form can be found at: www.gjesm.org/conflict_of_interest_discloure_form.docx

5. Submission Declaration and Verification: While submitting a manuscript to GJESM, all contributing author(s) must verify that the manuscript represents authentic and valid work and that neither this manuscript nor one with significantly similar content under their authorship has been published or is being considered for publication elsewhere including electronically in the same form, in English or in other language, without the written consent the copy right holder.

6. Authorship: All contributing authors should qualify for authorship and corresponding author should sign the authorship form while submitting the manuscript. It can be found at:
(http://www.gjesm.net/data/gjesm/news/authorship_form.docx).

7. Changes to Authorship: After the manuscript is submitted or accepted for publication, the corresponding author is required to send a request to add or remove an author or to rearrange the author names of the submitted/accepted manuscript by sending the change of authorship form to editorial office. No authorship change is allowed after publication of manuscript. More details may be found at:
(http://www.gjesm.net/data/gjesm/news/change_of_authorship_form.docx)

8. Retained Author Rights: As an author, author or authors' employer or institution retains certain rights. For more information on author rights, found at:
www.gjesm.org/retained_authors_right.docx.

9. Copy Right: Journals should make clear the type of copyright under which authors' work will be published. For open access articles the publisher uses an exclusive licensing agreement in which authors retain copyright in their manuscript. More details may be found at: (www.gjesm.org/copyright_form.docx)

10. User license Agreement: GJESM provides access to archived material through GJESM archives. Manuscripts are the parts of an open archive are made freely available from GJESM website after certain period, which begins from the final publication date of the manuscript. All articles published open access will be immediately and permanently free for everyone to read and download. Permitted reuse is defined by Creative Commons user license called ***Creative Commons Attribution***. Visit at: **(**Creative Commons Attribution 4.0 International (CC BY 4.0)**)**

11. Plagiarism Prevention and Violation of Publication Ethics: All manuscripts under review or published with GJESM are subject to screening using Plagiarism Prevention Software. Plagiarism is a serious violation of publication ethics. Other violations include duplicate publication, data fabrication and falsification, and improper credit of author contribution. Thus, the Plagiarism or Fraudulent or knowingly inaccurate statements constitute unethical behavior are unacceptable and submitting the same manuscript to more than one journal concurrently constitutes unethical publishing behavior and is unacceptable. The development of CrossCheck is a service that helps editors to verify the originality of papers. CrossCheck is powered by the Ithenticate software from iParadigms, known in the academic community as providers of Turnitin. For more details visit at: www.ithenticate.com/search

12. Handling Cases of Misconduct: Once GJESM confirms a violation against GJESM's publication ethics, the following actions will be taken.

a. The work is rejected / retracted immediately. Notification will be sent to corresponding authors. In extreme cases, notifications will be sent to the affiliations of the authors.
b. The authors are prohibited from submitting their work to GJESM for 5 years.
c. Any work by the authors responsible for the violation or any work these persons coauthored that is under review by any GJESM journal will be rejected immediately.
d. The authors are prohibited from serving on GJESM editorial board. GJESM reserves the right to take more actions.

MANUSCRIPT PREPARATION

1. Title Page: The title page should include: the name(s) of the author(s), a concise and informative title, the affiliation(s) and address (es) of the author(s), and e-mail address, telephone and fax numbers of the corresponding author.

2. Manuscript Title: Title of up to 17 words should not contain the name of locations, countries or cities of the research as well as abbreviations. The title should be oriented to Environmental issues while not being obscure or meaningless.

3. Abstract: An abstract of 150 to 250 words that sketches the purpose of the study; basic procedures; main findings its novelty; discussions and the principal conclusions, should not contain any undefined abbreviations or references.

4. Keywords: Provide 5 to 7 keywords which can be used for indexing purposes. Keywords should not repeat the words of the manuscript title or contain abbreviations and shall be written in alphabetical order as separated by semicolon.

5. Introduction: The Introduction should state the purpose of the investigation and identify clearly the gap of knowledge that will be filled in the Literature review study. Date and location of the research carried out throughout the study must be mentioned at the end of this section.

6. Materials and methods: The Materials and Methods section should provide enough information to permit repetition of the experimental work. It should include clear descriptions and explanations of sampling procedures, experimental design, and essential sample characteristics and descriptive statistics, hypothesis tested, exact references to literature describing the tests used in the manuscript, number of data involved in statistical tests, etc.

7. Results and Discussion: The Results section should describe the outcome of the study. Data should be presented as concisely as possible - if appropriate in the form of tables or figures, although very large tables should be avoided. The Discussion should be an interpretation of the results and their significance with reference to work by other authors. Please note that the policy of the Journal with respect to units and symbols is that of SI symbols.

8. Tables: Do not submit tables and graphs as photograph. Place explanatory matters in footnotes, not in the heading. Do not use internal horizontal and vertical rules. Tables should be called out in the text and should have a clear and rational structure and consecutive numerical order. All tables should be numbered 1, 2, 3, etc. Give enough information in subtitles so that each table is understandable without reference to the text. Footnotes to tables should be indicated by superscript lower-case letters (or asterisks for significance values and other statistical data) and included beneath the table body.

9. Figures: Figures/ illustrations should be in high quality art work, within 200-300 dpi and separately provided in Excel format. Ensure that figures are clear, labeled, and of a size that can be reproduced legibly in the journal. Each figure should have a concise caption describing accurately what the figure depicts. Figure captions begin with the term Fig. Figures should be with the captions placed below in limited numbers. No punctuation is to be placed at the end of the caption.

10. Conclusion: This section should highlight the major, firm discoveries, and state what the added value of the main finding is, without literature references.

11. Acknowledgements: Acknowledgments of people, grants, funds, etc. should be placed in a separate section before the reference list. The names of funding organizations should be written in full. Financial support affiliation of the study, if exists, must be mentioned in this section. Thereby, the Grant number of financial support must be included.

12. References: All the references should be cited throughout the manuscript text as well as in the Reference section organized in accordance with Harvard system. Groups of references should be listed first alphabetically, then chronologically. The number of references extracted from each journal should not exceed 3 to 5 citations, which is the average acceptable amount. The number of references should not be less than 30 for original paper, less than 100 for review paper. It is substantially recommended to the authors to refer to more recent references rather than old and out of date ones. Volume, issue and pages of the whole references must be specified according to the GJESM format.

Citing and listing of Web references: As a minimum, the full URL should be given. Any further information, if known (Author names, dates, reference to a source publication, etc.), should also be given.

Text: All citations in the text should refer to: 1. Single author: the author's name (without initials, unless there is ambiguity) and the year of publication; 2. Two authors: both authors' names and the year of publication; and 3. Three or more authors: first author's name followed by "et al." and the year of publication. Citations may be made directly (or parenthetically). Groups of references should be listed first alphabetically, then chronologically. Examples: "as demonstrated (Allan, 1996a, 1996b, 1999; Allan and Jones, 1995). Kramer *et al.,* (2000) have recently shown …".

List: References should be arranged first alphabetically and then further sorted chronologically if necessary. More than one reference from the same Author(s) in the same year must be identified by the letters "a", "b", "c", etc., placed after the year of publication.

Journal article: Nouri J.; Lorestani B.; Yousefi N.; Khorasani N.; Hassani A. H.; Seif, F.; Cheraghi M., (2011). Phytoremediation potential of native plants grown in the vicinity of Ahangaran lead-zinc mine. Environ. Earth Sci., 62(3): 639-644.

Book: Davis, M. L., (2005). Introduction to Environmental Engineering, 3rd. Ed. McGraw Hill Inc.

Book chapter: Mettam, G. R.; Adams, L. B., (1999). How to prepare an electronic version of your article, in: Jones, B. S., Smith, R. Z. (Eds.), Introduction to the electronic age. E-Publishing Inc., New York.

Conference paper: Brown, J., (2005). Evaluating surveys of transparent governance. In UNDESA, 6th. Global forum on reinventing government: towards participatory and transparent governance. Seoul, Republic of Korea 24-27 May. United Nations: New York.

Dissertation: Trent, J. W., (1975). Experimental acute renal failure. Ph.D. Dissertation, University of California. USA.

Online document: Cartwright, J., (2007). Big stars have weather too. IOP Publishing Physics Web.
http://physicsworld.com/cws/article/news/2007/jun/26/big-stars-have-weather-too

AFTER ACCEPTANCE

1. Online Proof Correction: Corresponding authors will receive an e-mail with a link to our online proofing system, allowing annotation and correction of proofs online. Use this proof only for checking the typesetting, editing, completeness and correctness of the text, tables and figures. Significant changes to the article as accepted for publication will only be considered at this stage with permission from the Editor-in-Chief. It is important to ensure that all corrections are sent back to us in one communication. Please check carefully before replying, as inclusion of any subsequent corrections cannot be guaranteed. Proofreading is solely the corresponding author responsibility.

2. Offprints: The offprints can be downloading from the GJESM website once the final corrected manuscripts are disseminated.

AUTHORS INQUIRIES

Authors can track their submitted article through GJESM website on author's login section at: http://gjesm.net/contacts?_action=login

Global Journal of Environmental Science and Management (GJESM)

Copyright Transfer Agreement

1. Parties of the agreement

Author (s):

Manuscript Title:

Manuscript ID:

(Herewith referred to as the "materials"),

Journal Title: Global Journal of Environmental Science and Management (GJESM)

2. Subject of the agreement

A) Copyright
1- The Author and each co-authors shall transfer and sell to the Publisher for the length of the copyright starting from the moment the present agreement comes into force the exclusive rights to the materials, including the rights to translate, reproduce, transfer, distribute or otherwise use the materials or parts (fragments) contained therein, for publication in scientific, academic, technical or professional journals or other periodicals and in derivative works thereof, worldwide, in English, in print or in electronic editions of such journals, periodicals and derivative works in all media or formats now existing or that may exist in future, as well as the right to license (or give permission to) third parties to use the materials for publication in such journals, periodicals and derivative works worldwide. The transfer under this agreement includes the right to adapt the presentation of the materials for use in conjunction with computer systems and programs, reproduction or publication in machine-readable format and incorporation into retrieval systems.
2- Reproduction, placement, transfer or any other distribution or use of the materials, or any parts of the materials contained therein, in any way permitted under this Agreement, shall be accompanied by reference to the Journal and mentioning of the Publisher, namely: the title of the article, the name of the Author (Co-authors), the name of the Journal, volume/number, copyright of the publisher.

B) Reserved Rights
The Author (Co-authors) or the employer of the Author (Co-authors) of the materials shall retain all proprietary rights (with the exception of the rights transferred to the Publisher under the present Agreement).

C) Author Guarantee
The Author (Co-authors) guarantees that the materials are an original work, submitted only to GJESM, and have not been published previously.
In case the materials were written jointly with co-authors, the Author guarantees that he/she has informed them of the terms of this Agreement and obtained their signatures or written permission to singe on their behalf.
The Author guarantees as well that:
The materials do not contain libelous statements.
The materials do not infringe on other persons' rights (including without limitation copyrights, patent rights and the trademark right).
The materials do not contain facts or instructions that can cause damage or injury to third parties and their publication does not cause the disclosure of any secret or confidential information

---

Author (Corresponding Author):

Correspondence Address:

Phone:

Fax:

Email:

Corresponding Author Name: Signature Date

On Behalf of the Publisher:

Iran Solid Waste Association,
Faculty of Environment, University of Tehran,
Postal Code: 1417854511, Tehran,
Iran

Telefax: (+9821) 2610 5110

Email: *editor@gjesm.net*
Gjesm.publication@gmail.com

Website: www.gjesm.net

Accepted for publication ☑ Signature Date

PLEASE NOTE: The accepted manuscript cannot be processed for publication until the publisher has received this signed form. The form MUST be signed by the Corresponding Author and then scanned and sent through the system or email. If the manuscript is not published in the Journal, this release will not take effect.

The sole responsibility for the whole content (s) of the article remains only with the corresponding author. However, Editor would reserve the right to adjust the style to certain standards of uniformity before publication.

CONFLICT OF INTEREST DISCLOSURE FORM

Conflict of Interest is defined as a set of conditions in which professional judgment concerning a primary interest, such as the validity of research, may be influenced by a secondary interest, such as financial gain. A Conflict of Interest Disclosure is an agreement or notification from the authors that they have not been paid for the work, or if they have, stating the source of their payment. The purpose of Conflict of Interest Disclosure form is to provide readers of authors' manuscript with information about authors' interests that could influence how the authors receive the work. The corresponding author (on behalf of all co-authors) should submit a conflict of interest disclosure form and is responsible for the accuracy and completeness of the submitted manuscript. Conflict of Interest Disclosure form can be signed by the corresponding author on behalf of all co-authors and stating that the submitted manuscript is the authors' original work, has not received prior publication and is not under consideration for publication elsewhere, permission has been received to use any material in the manuscript much as tables, figures etc. or no permissions have necessary to publish the authors' work.

1. Name of the corresponding author

2. Affiliation including e-mail and phone number

3. Manuscript Title

4. Do the authors or authors' institution at any time receive payment or services from a third party (government, commercial, private foundation, etc.) for any aspect of the submitted manuscript (including but not limited to grants, data monitoring board, study design, manuscript preparation, statistical analysis, etc.)?

   Are there any relevant conflicts of interest? Yes / No

5. Do the authors have any patents, whether planned, pending or issued, broadly relevant to the work?

   Are there any relevant conflicts of interest? Yes / No

6. Are there other relationships or activities that readers could perceive to have influenced, or that give the appearance of potentially influencing, what the authors' information in the submitted manuscript?

   Are there any relevant conflicts of interest? Yes / No

7. Are there any aspect of the work covered in this manuscript that has involved either experimental animals or human patients has been conducted with the ethical approval of all relevant bodies or not.

   Are there any relevant conflicts of interest? Yes / No

Corresponding Author Signature | Print Name | Date

AUTHORSHIP FORM

By completing and signing the following statements, the corresponding author acknowledges and accepts the responsibility on behalf of all contributing authors, if any, concerning Authorship Responsibility.

Manuscript title:

Corresponding author:

Affiliation:

Email:

Phone No:

By signing and filling this form, the corresponding author certifies that each author has met all criteria below (A, B, C, and D) and indicates each author general and specific contributions by listing his or her name next to the relevant section.

A. I certify that

- The manuscript is authentic and valid and that neither this manuscript nor one with considerably similar content under my authorship has been published or is being considered for publication elsewhere, except as described in an attachment, nor copies of closely related manuscripts are provided.
- I will provide the data or will contribute fully in providing and obtaining the data on which the manuscript is based for examination by the editors or their assignees, if requested.
- Every author has agreed to allow the corresponding author to serve as the primary correspondent with the editorial office, to review the edited manuscript and proof.

B. Each author has given final approval of the submitted manuscript.

C. Each author has participated sufficiently in the work to take public responsibility for the whole content.

D. Each author qualifies for authorship by listing his or her name on the appropriate line of the categories of contributions listed below. List appropriate author next to each section – each author must be listed in at least 1 field. More than 1 author can be listed in each field.

- conception and design
- acquisition of data
- analysis and interpretation of data
- drafting of the manuscript
- critical revision of the manuscript for important intellectual content
- statistical analysis
- obtaining funding
- administrative, technical, or material support
- supervision
- no additional contributions
- other (specify)

Corresponding Author Signature **Print Name** **Date**

CHANGE OF AUTHORSHIP FORM

Manuscript Title:

Corresponding Author:

Please check all that apply.

☐ New author(s) have been added.

☐ There is a change in the order of authorship.

☐ An author wishes to remove his/her name. An author's name may only be removed at his/her own request in writing.

ORIGINAL AUTHORSHIP

List ALL AUTHORS in the same order as the original (first) submission.

Print Name	Print Name
Name (1)	Name (6)
Name (2)	Name (7)
Name (3)	Name (8)
Name (4)	Name (9)
Name (5)	Name (10)

NEW AUTHORSHIP

List the ALL AUTHORS in same order as the new version.

Print Name	Print Name
Name (1)	Name (6)
Name (2)	Name (7)
Name (3)	Name (8)
Name (4)	Name (9)
Name (5)	Name (10)

I attest that:

1. The manuscript is not currently under consideration, in press, or published elsewhere, and the research reported will not be submitted for publication elsewhere until a final decision has been made as to its acceptability by the journal (posting of submitted material on a web site may be considered prior publication-note this in your cover letter).
2. The manuscript is truthfully original work without fabrication, fraud, or plagiarism.
3. I have made an important scientific contribution to the study and am thoroughly familiar with the primary data.
4. I have read the complete manuscript and take responsibility for the content and completeness of the manuscript and understand that I share responsibility if the paper, or part of the paper, is found to be faulty or fraudulent.

Corresponding Author Signature Name Date

SUBSCRIPTION FORM

Subscription form

Global Journal of Environmental Science and Management

Please enter my annual subscription to the Global Journal of Environmental Science and Management (GJESM), including 4 quarterly issues for the Year ..... Vol. ..... Nos.....

	Domestic (Rials)	International (USD)
▪ Institutional	3,000,000	150
▪ Individual	2,000,000	100
▪ Student	1,000,000	80
▪ Single Copy	500,000	50

Name: **Tel.:** **Email:**

Mailing Address:

Payment method: Check or money order must be made in order of:
Account #. 0101834143005, Account name: J. Nouri
Bank Melli Iran, IAU Branch, Code 1017, Tehran, Iran

□ Bank receipt enclosed

* *Please allow 3 to 5 weeks for delivery*

Please send this filled in order form along with the Bank receipt payment to:

Global Journal of Environmental Science
and Management
No. 2, Kouhestan Deadend, Janpour Street,
Darabad, Tehran 1956934461 Iran

Global

Journal of Environmental Science and Management

CONTENTS

Volume 8, Number 4, Autumn 2022

(Serial # 32)